Illinois U Library

The American Mineralogist

Journal of the Mineralogical Society of America

Vol. 37 NOVEMBER-DECEMBER, 1952 Nos. 11 and 12

Contents

Phosphate mineralization at Bomi Hill and Bambuta, Liberia, West Africa .... J. M. Axelrod, M. K. Carron, C. Milton and T. P. Thayer 883

Variations in chemical and physical properties of fluorite.... Robert D. Allen 910

Hurlbutite, $CaBe_2(PO_4)_2$, a new mineral.................... Mary E. Mrose 931

Effect of heavy charged particle and fast neutron irradiation on diamonds... ..... Joseph G. Hamilton, Thomas M. Putnam, and Martin L. Ehrmann 941

Studies of uranium minerals (X): Uranopilite.............. Clifford Frondel 950

Zunyite from Postmasburg, South Africa................. F. H. S. Vermaas 960

Relationship between density and composition in mol per cent for some solid solution series.................................. F. Donald Bloss 966

Stibiconite and cervantite........... Charles J. Vitaliano and Brian Mason 982

Chemical compositions of hypersthene and pigeonite in equilibrium in magma .... Hisashi Kuno and Kōzō Nagashima 1000

Cone-axis diffraction patterns.......................... D. Jerome Fisher 1007

X-ray precession techniques.......................... D. Jerome Fisher 1036

Notes and News: Stability of chrysotile asbestos.......................... .... Bartholomew Nagy and Thomas F. Bates 1055

Second occurrence of bayleyite in the United States................. .... T. W. Stern and Alice Dowse Weeks 1058

Guadarramite discredited.............................. George Switzer 1061

Mineralogical Society (London).. 1064

Book reviews.. 1066

New mineral names... 1070

Index to volume 37; Title page; Table of contents..................... 1075

EDITOR: WALTER F. HUNT
ASSISTANT EDITOR: LEWIS S. RAMSDELL

BOARD OF ASSOCIATE EDITORS: MICHAEL FLEISCHER, ESPER S. LARSEN, JR., ELBURT F. OSBORN, AUSTIN F. ROGERS, AND GEORGE TUNELL

Published bi-monthly by the Society

Mineralogical Society of America

ASSOCIATED WITH THE GEOLOGICAL SOCIETY OF AMERICA

President: Michael Fleischer, U. S. Geological Survey, Washington 25, D. C.
Vice President: J. D. H. Donnay, The Johns Hopkins University, Baltimore, Maryland.
Secretary: C. S. Hurlbut, Jr., Harvard University, Cambridge, Massachusetts.
Treasurer: Earl Ingerson, U. S. Geological Survey, Washington 25, D. C.
Editor: Walter F. Hunt, University of Michigan, Ann Arbor, Michigan.
Councillors: Lewis S. Ramsdell, University of Michigan, Ann Arbor, Michigan.
E. F. Osborn, School of Mineral Industries, Pennsylvania State College, Pennsylvania.
George T. Faust, U. S. Geological Survey, Washington 25, D. C.
Victor T. Allen, Institute of Geophysical Technology, St. Louis, Missouri.
Adolf Pabst, University of California, Berkeley, California

The enlarged issues of this journal for 1952 are made possible by a grant from the Penrose Fund of the Geological Society of America.

The American Mineralogist—Journal of the Mineralogical Society of America

A journal containing articles on mineralogy, crystallography, petrography, and allied sciences, is issued every two months. Contributions are invited from everyone.

Office of Publication, Mineralogical Laboratory, Ann Arbor, Mich.

The general conduct of the journal is in the hands of the editor, **Walter F. Hunt,** Ann Arbor, Michigan, to whom all manuscripts should be submitted. To assist the editor the council of the Mineralogical Society has appointed **Lewis S. Ramsdell,** Ann Arbor, Michigan, assistant editor, and the following board of associate editors:

Michael Fleischer, U. S. Geological Survey, Washington, D. C.
Esper S. Larsen, Jr., U. S. Geological Survey, Washington, D. C.
Elburt F. Osborn, Pennsylvania State College, State College, Pa.
Austin F. Rogers, 2412 Durant Ave., Berkeley, California.
George Tunell, University of California at Los Angeles, California.

Contributors of leading articles are given without charge 100 reprints (without covers) of their article. If additional reprints are desired these can be purchased at the following rates:

Pages	*1–4*	*5–8*	*9–12*	*13–16*	*17–20*	*21–24*	*25–28*	*29–32*	*Covers*
Copies									
25	$3.50	$5.00	$ 8.00	$ 9.50	$11.00	$13.00	$15.00	$16.00	$4.90
50	3.80	5.55	8.80	10.40	12.10	14.20	16.40	17.50	5.50
75	4.10	6.10	9.60	11.30	13.20	15.40	17.80	19.00	6.10
100	4.00	6.65	10.40	12.20	14.30	16.60	19.20	20.50	6.70
Addl. C's	1.20	2.20	3.20	3.60	4.40	4.80	5.60	6.00	2.40

Cover Composition $1.55.

Sent to all members and fellows of the Mineralogical Society of America. Subscription price, $4.00 per year (single copies of normal issues, $1.00 plus postage).

Entered as second class matter at the post office at Menasha, Wis., under Act of March 3, 1879. Acceptance for mailing at the special rate of postage provided for in section 1103, Act of Oct. 3, 1917, paragraph 4 section 429 P. L. & R. authorized March 13, 1922.

Notice of change of address, orders, and remittances should be sent to Dr. Earl Ingerson, U. S. Geological Survey, Washington 25, D. C.

Printed by the George Banta Publishing Company, Menasha, Wisconsin
Printed in the United States of America

THE AMERICAN MINERALOGIST

JOURNAL OF THE MINERALOGICAL SOCIETY OF AMERICA

Vol. 37 NOVEMBER-DECEMBER, 1952 Nos. 11 and 12

PHOSPHATE MINERALIZATION AT BOMI HILL AND BAMBUTA, LIBERIA, WEST AFRICA*

J. M. AXELROD, M. K. CARRON, C. MILTON, AND T. P. THAYER

ABSTRACT

An interesting suite of iron phosphate minerals formed by biogeochemical processes occurs at Bomi Hill and Bambuta in western Liberia. The phosphates at Bomi Hill form bouldery aprons on the slopes below two prominent cliffs and occur in place in caves and open fissures in cliffs of high-grade iron ore. They were formed by the interaction of bat dung, or substances derived from it, with exposed iron oxide. The minerals thus formed include strengite and its dimorph, phosphosiderite; a member of the rockbridgeite group (formerly included with dufrenite); and, most noteworthy, leucophosphite, hitherto known only from Western Australia. From chemical, optical, and *x*-ray data, together with a recent synthetic study, leucophosphite is established as a valid and well-defined mineral species and, so far, the only known alkali-iron phosphate mineral of sedimentary origin. Chemical studies by soils chemists have been correlated with natural occurrences, giving a better understanding of the geochemistry of phosphatic fertilizers and of phosphate minerals.

The phosphates from Bambuta differ from those at Bomi Hill; the differences, however, may reflect incomplete knowledge of the two deposits rather than any significant difference of origin. In both, the source of the phosphorus is believed to be the dung of bats.

CONTENTS

Abstract 883
Occurrence—locality and field relations 884
General character of specimens studied 888
Description of specimens from Bomi Hill (and Australia)
  A. Breccia of iron oxide in phosphate matrix 890
  B. Hematitic granitic gneiss 893
  C. Leucophosphite from Liberia and Australia 893
Description of specimens from Bambuta
  A. Magnetite—phosphosiderite—strengite 895
  B. Strengite (rock) 898
Investigation of leucophosphite
  X-ray data for natural and synthetic leucophosphite 899
  Spectrographic analysis of leucophosphite 901
  Chemical analysis 902

---

* Publication authorized by the Director, U. S. Geological Survey.

Discussion of analyses . . . 902
Synthesis of leucophosphite . . . 903
Morphology and optical data for synthetic leucophosphite . . . 903
Minerals related to leucophosphite . . . 903
Geochemistry of leucophosphite and related phosphates
Sources of constituent elements . . . 905
Physical chemistry of alkali iron-aluminum phosphates . . . 907
Acknowledgments . . . 908
References . . . 908

OCCURRENCE—LOCALITY AND FIELD RELATIONS

At the request of the Liberian government the iron ore deposits at Bomi Hill, 40 miles north of Monrovia, were mapped in 1943–44 by the U. S. Geological Survey. Limited exposures of a gray to cream-colored rock superficially resembling calcareous tufa were noted near the bases of two cliffs of massive magnetite-hematite ore. It was not until 1949, however, after the jungle growth had been cleared away, and analysis of some of the material showed it to be essentially ferric phosphate, that the significance of these deposits was appreciated.

The field relations of the phosphate rock were studied briefly by T. P. Thayer and G. G. Lill while on furlough with the Liberia Mining Com-

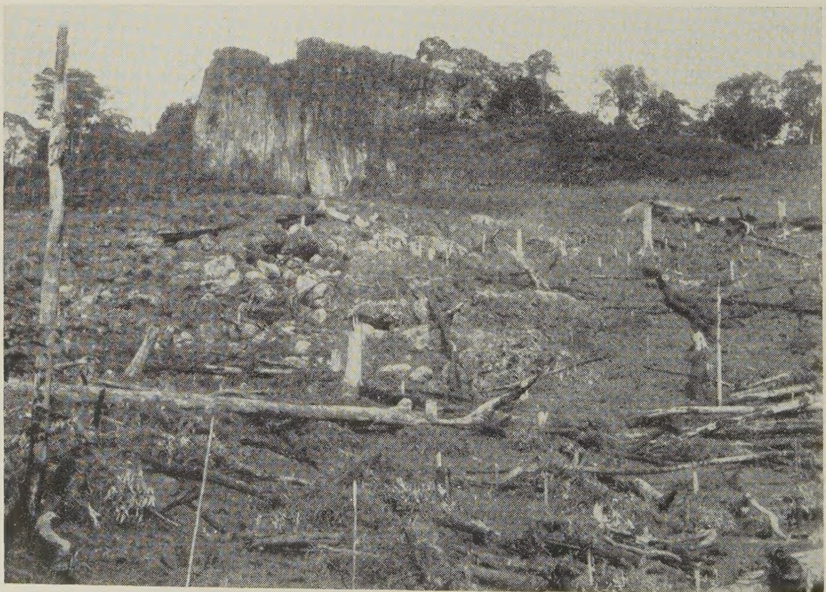

FIG. 1. Phosphate-cemented talus down slope from cliff at west end of Ore Body #1 (Monkey Hill). Note absence below lower iron ore exposures to right, and the cave at base of the 120-foot high cliff. Bomi Hill, Liberia.

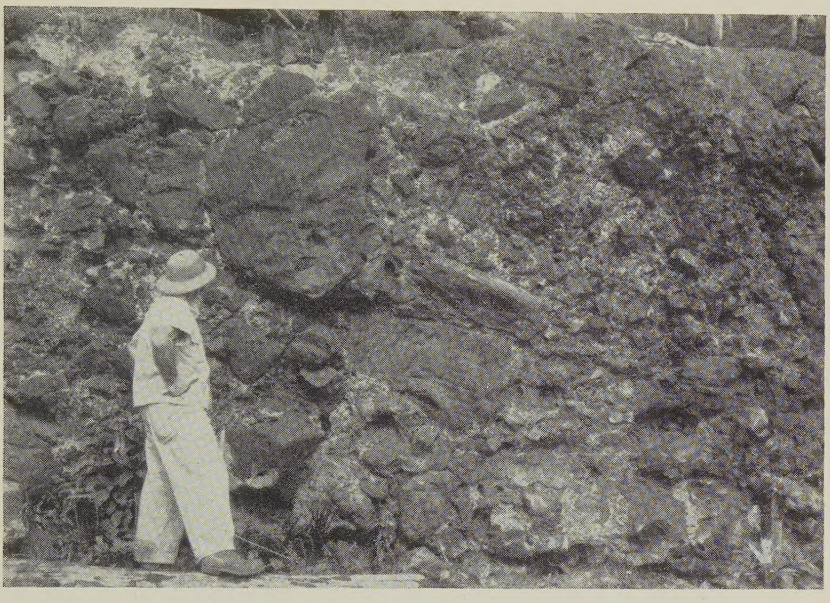

FIG. 2. Massive talus ore cemented by iron phosphate, on south slope of Bomi Hill. Blocks are massive magnetite-hematite. Bomi Hill, Liberia.

pany, Ltd., and they discovered a second occurrence near Bambuta, about 22 miles east of Bomi Hill. The mining company was interested in the high phosphorus content of the material primarily as a contaminant of several tens of thousands of tons of otherwise premium-grade float iron ore, and also because the presence of this phosphate suggested that parts of the main ore bodies might be high in phosphate.

The largest high-grade deposits are on the south slope of Bomi Hill, where they form two prominent cliffs. The phosphate forms bouldery talus aprons on the slopes below the cliffs (Fig. 1), fills joint cracks in massive ore, and replaces some layers of medium-grade ore at the base of the cliffs. The talus consists of fragments of massive iron ore in a matrix of light-colored phosphate (Fig. 2). At the margins of the phosphatic talus, the matrix grades into normal limonite. Accumulations of talus cemented with phosphate extend up into wide joints in the iron ore cliffs below the roosting places of numerous bats (Fig. 3). The talus overlies 50 feet or more of thoroughly weathered residual soil on which, in places, benches have been formed by landsliding. The phosphate is absent below low exposures of iron ore between the two cliffs.

Similar iron phosphate minerals were found on the summit of the second body of massive iron ore, about $1\frac{1}{2}$ miles west of the Boporo-Suehn trail and about a mile southwest of Bambuta. The phosphate there forms pink and white cavity fillings in medium-to coarse-grained magnetite, fills narrow fractures, and cements small masses of iron ore fragments. The largest exposure of the breccia noted was about 2 feet across and lay 20 to 25 feet away from the topmost outcrop of massive ore.

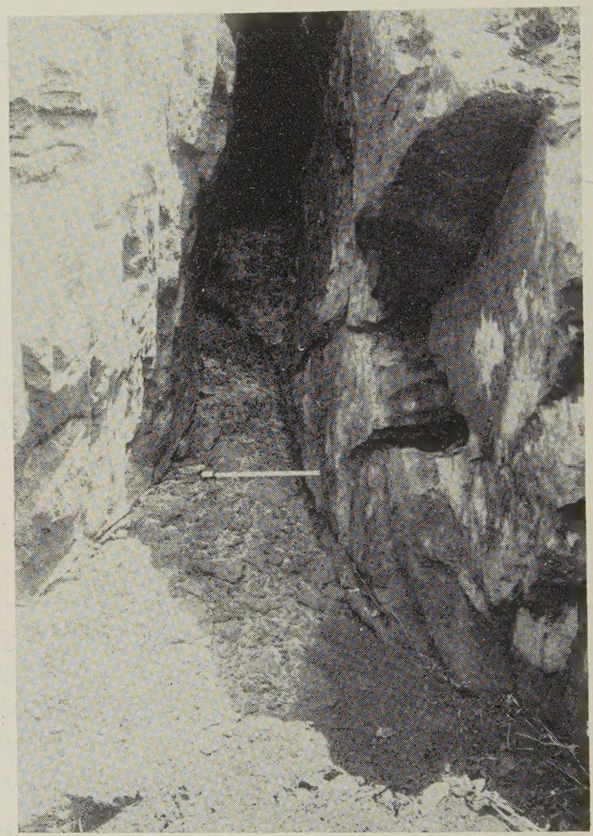

FIG. 3. Iron phosphates cementing iron ore fragments in joint in base of cliff of massive iron ore. (12 inch scale). Bomi Hill, Liberia.

The relations at Bomi Hill indicate that the phosphates form by the reaction of bat excreta with iron oxides under the extreme conditions of the rain-forest climate. Solution cavities in talus boulders of massive ore and in two caves in the highest cliff give eloquent testimony of solution of iron oxides by rain water and organic acid. Abundance of bat guano in the caves and open joints in the cliffs and markedly low phosphorus content in the massive ore itself clearly indicate that bats are the source of the phosphorus. The extent of the accumulations on the slopes below the cliffs is explained by soil creep or minor landsliding, combined with insolubility of the phosphate. The occurrence of massive strengite on the summit of the hill southwest of Bambuta shows that the strengite, at least, must compare with magnetite and hematite in resistance to solution.

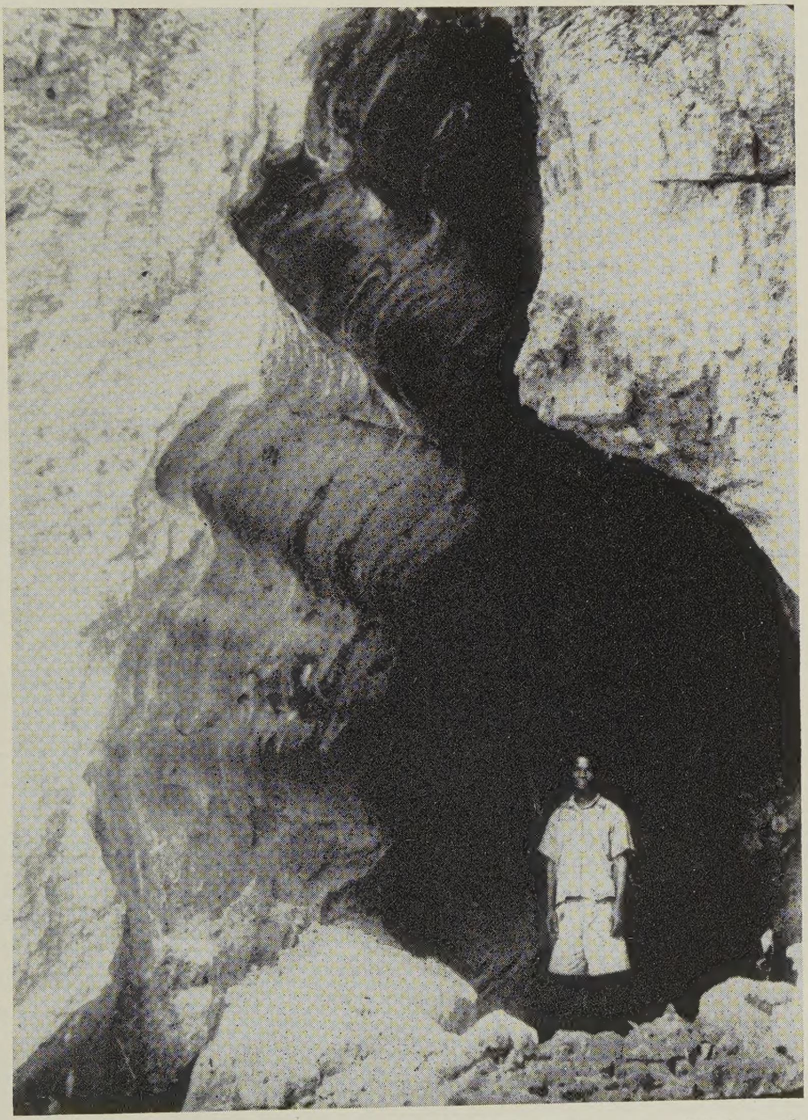

FIG. 4. Cave in massive iron ore at Bomi Hill, inhabited by bats responsible for surficial phosphatization of ore. Note solution flutings in iron ore.

Figures 1, 2, and 3 show typical field relations of the iron phosphates. Figure 4 shows one of the caves, home of the bats responsible for the remarkable phosphatization.

In describing weathering of the iron ores at Bomi Hill, E. F. Fitzhugh, Jr. (1951) stated "The ore and siliceous iron formation at Bomi Hill, Liberia, are similar in character and occurrence to the better-known deposits of Venezuela and Brazil. Iron formation forms a hanging wall and granite gneiss a footwall of the massive, high-grade ore. Ore outcrops and float show induration and recrystallization to a fine-grained, steely hematite. Similar transformations by tropical meteoric waters in Venezuela are noted. Canga capping is confined to the hanging-wall side of the Bomi Hill ore. This, together with comparable occurrences in Venezuela, suggest that the iron in porous limonitic canga is derived from iron-rich, siliceous rocks rather than from high-grade iron ore."

A general account of the Liberian iron ore deposits, by Thayer, Newhouse, and Butler (1952), is in preparation.

General Character of Specimens Studied

Nine specimens of phosphatized rock and ore were available for this study; no two were alike in appearance, and almost all of them were loose float and obviously heterogeneous. For this reason conclusions as to paragenesis must rest on interpretation of the mineralogy. Figures 5*A*, *B*, *C*, *D*, and 6*A*, *B*, *C*, illustrate the variety of the material.

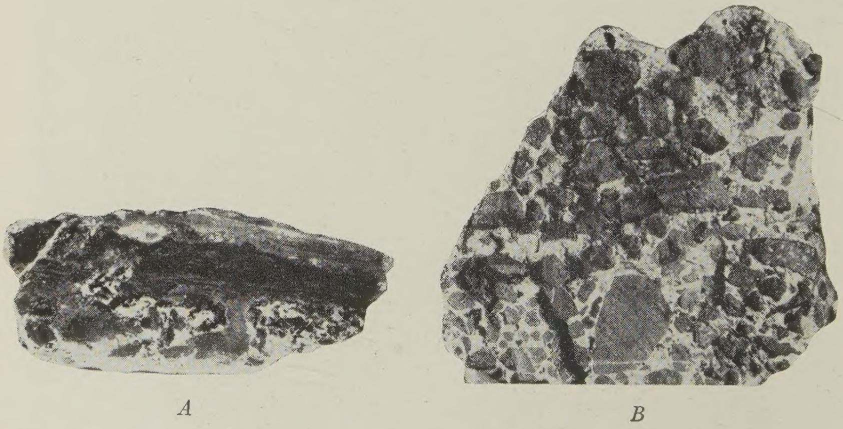
A

B

Fig. 5*A*. "Bomi 1 TPT" shows complex structure of phosphatized ore. The dark band across the middle is essentially limonite. The white areas are largely phosphosiderite and strengite; the black granular areas rockbridgeite; and the gray areas are leucophosphite.

Fig. 5*B*. "Bomi 6 TPT." Hematite-limonite fragments in phosphosiderite-strengite matrix.

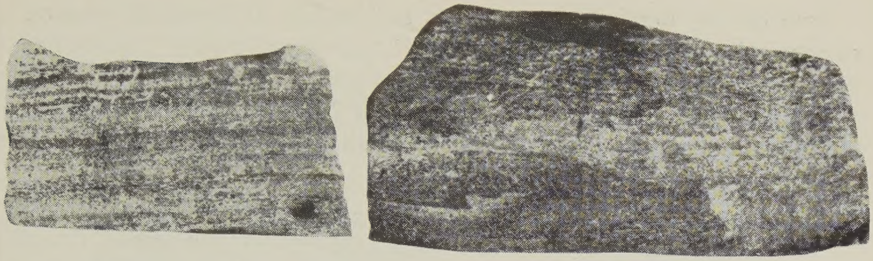

FIG. 5*C*. "Bomi 4 TPT." Hematite-quartz-phosphosiderite/strengite; replacement of granitic gneiss.

FIG. 5*D*. "Sta. 27 WHN." Strengite and hematite replacing granitic gneiss. Goethite (?) at lower right corner.

All figures are $\frac{2}{3}$ natural size.

Seven of the specimens are from the Bomi Hill locality, and two are from Bambuta. At Bomi Hill the phosphates include leucophosphite, phosphosiderite, and strengite, associated with hematite-limonite. At Bambuta, there are phosphosiderite, strengite, and (in the two specimens studied) no leucophosphite; the iron oxide is magnetite. This difference in mineralogy may indicate deeper erosion of the ore at Bambuta than at Bomi Hill.

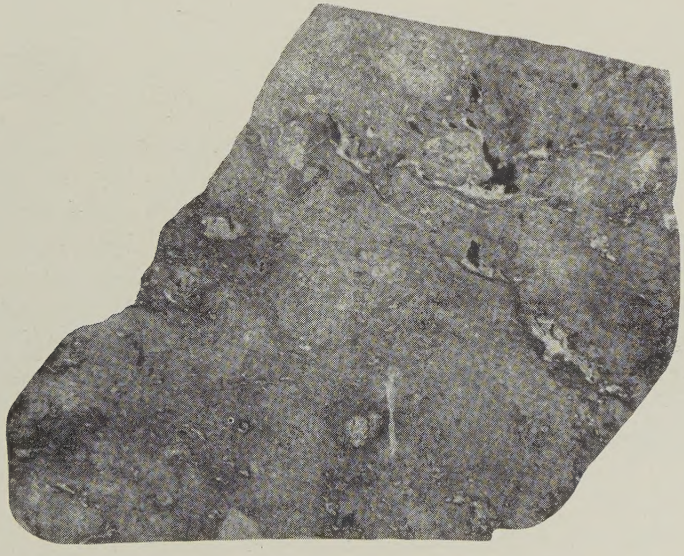

FIG. 6A. Leucophosphite, Bomi Hill. Shows open cavitites and meta-colloid structure. Six x-ray samples were studied from the face of this specimen.

Two of the Bomi Hill specimens are breccia of hematite-limonite cemented by phosphate ("Bomi 1 TPT" and "Bomi 6 TPT"), three are hematitic granitic gneiss, with iron oxide and other minerals partially replaced by phosphate ("Bomi 4 TPT," "ST 27 WHN" and "SA 34 C"), and two are massive leucophosphite ("SP 35 Ore Body IIIC"), and the two others (from Bambuta) massive microcrystalline strengite ("SP 34"), and magnetite with phosphosiderite-strengite ("SP 35").

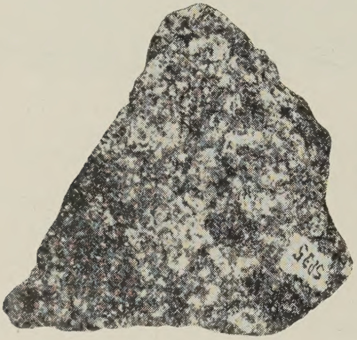

B

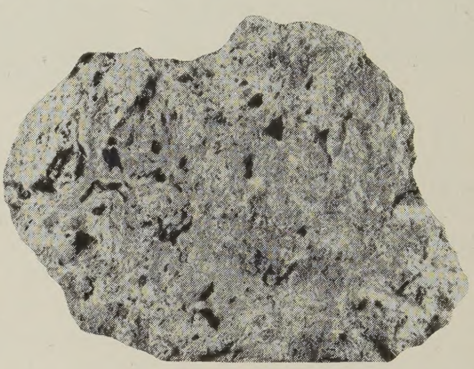

C

Fig. 6*B*. "SP 35 Ore body III C" Bambuta. Magnetite, with vugs of phosphosiderite and strengite.

Fig. 6*C*. Bambuta "SP 34." Massive strengite. Shows shrinkage openings and meta-colloid structure.

All figures are $\frac{2}{3}$ natural size.

Description of Specimens from Bomi Hill

A. Breccia of iron oxide in phosphate matrix

"Bomi 1 TPT." This is a rather small specimen a few inches across, and is shown in Fig. 5*A*. It was broken from rock in place at the base of the high cliff, and probably represents material formed by replacement along a fracture in magnetite-bearing gneiss. A very rough separation may be made into light brownish layers, largely phosphatic, and dark mahogany brown pebbly layers, essentially limonitic. Both layers include quartz and hematite particles. Typical areas were sectioned, and, by careful picking of the specimen under a binocular microscope, more or less apparently homogeneous phases were isolated (to correspond to individual minerals or substances perceived in thin section). The picked materials were analyzed by *x*-ray diffraction patterns and thereby, despite their apparent homogeneity, shown to be in general inhomogeneous aggregates of two or more compounds. Four such samples of *x*-rayed material, selected by color, had the following compositions:

X-ray film 5385 (brick red and black)	Hematite, strengite, trace of unidentified
X-ray film 5386 (black)	Rockbridgeite group
X-ray film 5387 (brown and black)	Leucophosphite, goethite, trace of unidentified
X-ray film 5388 (light reddish crust)	Strengite with traces of quartz and of unidentified.

Applying these data to the interpretation of the thin sections (Figs. 7 and 8) it appears that the light brown areas of the hand specimen (pale yellow in section) consist essentially of apparently isotropic leucophosphite and crystalline colorless strengite. The specific characters and relationships of these minerals will be considered further on. Here it may be noted that leucophosphite varies from optically isotropic to weakly birefringent, resembling chert in this respect, and that strengite and phosphosiderite are so similar optically that in fine-grained mixtures their differentiation is impractical microscopically. There are also present with these phosphate minerals quartz grains which show strikingly corroded outlines (see Figs. 7 and 8), and brown to black masses of limonite with outlines suggesting original magnetite.

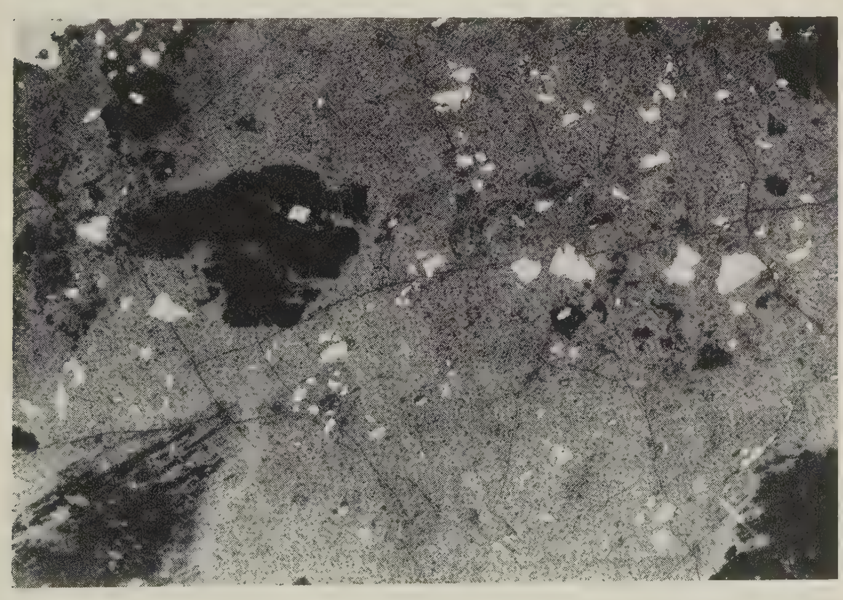

Fig. 7. "Bomi 1 TPT." Bomi Hill, Liberia. ×8 Thin section. Hematite-limonite (black), quartz (white) and leucophosphite (gray). Around the larger quartz particles right of center, instead of leucophosphite there is strengite (which has about the same relief and hence does not show up under ordinary light); at the lower left corner is a fragment of hematite almost completely replaced by phosphate.

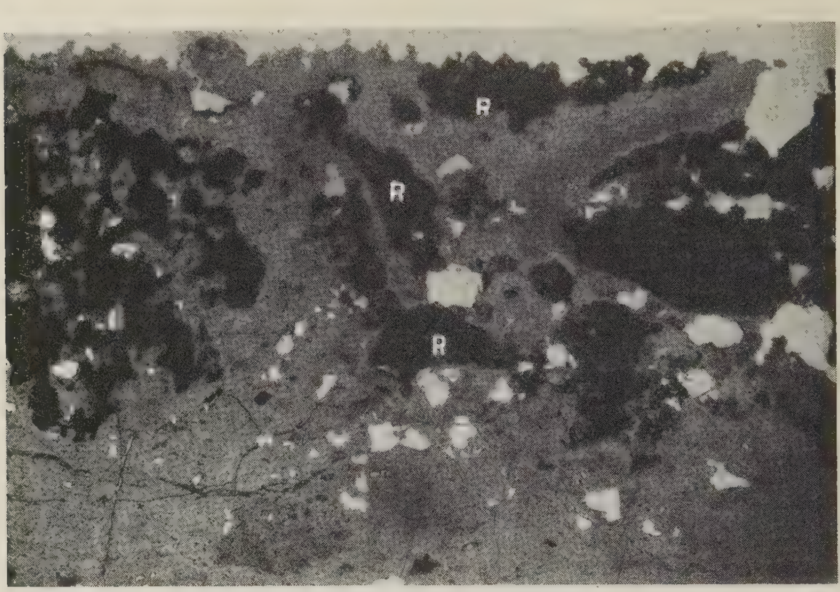

FIG. 8. "Bomi 1 TPT." Bomi Hill, Liberia. ×8 Thin section. Hematite (most of the black areas), quartz (white) and rockbridgeite (very dark or black—indicated by R) in a groundmass of strengite (gray areas).

The darker bands are mainly brown-black limonite, with much light brown iron phosphate (?) and colorless phosphate. Some, at least, of the "limonite" may be hematite.

Where the colorless crystalline strengite is abundant, there is seen a mineral of the rockbridgeite group (Frondel, 1949) which is well crystallized, sometimes in radial aggregates. It is black in the hand specimen, and characteristically pleochroic in reddish brown and bluish green in thin section. Its optics resemble those of dufrenite, with which it was formerly included. As shown by Frondel, dufrenite and rockbridgeite differ crystallographically, as well as chemically: dufrenite being best represented by $Fe''Fe_4'''(PO_4)_3(OH)_5 \cdot 2H_2O$, whereas rockbridgeite may be $Fe''Fe_4'''(PO_4)_3(OH)_5$.

"Bomi 6 TPT." This is a breccia consisting of slightly rounded hematite fragments up to 2 cm. across (some partly altered to limonite) in a flesh-colored dense phosphate matrix.

Microscopically, the flesh colored matrix is mostly isotropic (leucophosphite) where it adjoins the ore fragments it is definitely crystalline, and x-ray analysis shows the crystalline material to be phosphosiderite and strengite, with a little unidentified substance, and a trace of quartz (x-ray film 5301).

The rock is illustrated in Fig. 5*B;* a typical thin section is shown in Fig. 9.

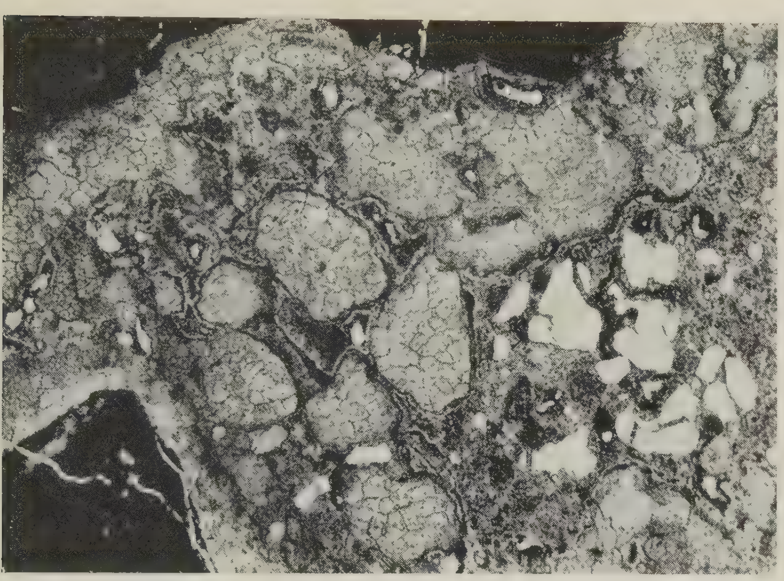

FIG. 9. "Bomi 6 TPT." Bomi Hill, Liberia. ×8. The rounded masses are apparently homogeneous and isotropic, and are referred to leucophosphite; their matrix however is anisotropic and is shown to be phosphosiderite-strengite. The white areas are quartz, showing characteristic corroded outlines; the black is hematite-limonite (the thin white lines are cracks). Note shrinkage (?) cracks in the leucophosphite.

B. Hematitic granitic gneiss

"Bomi 4 TPT." This specimen (Fig. 5*C*) superficially resembles a sandstone, although it is a granitic gneiss containing iron ore with the original structure emphasized by the banding of dark hematite and light quartz and phosphate. The microstructure is similar to that of "Sta. 27 WHN" and "Sta. 34 c" described in detail below.

"Sta. 27 WHN." This is a banded rock consisting of alternate streaks of minute grains of black hematite and pinkish strengite. At one end of the specimen is a deep red-brown translucent substance, probably goethite. Its appearance is shown in Fig. 5*D*.

In thin section, granular quartz and hematite are abundant in an obscurely crystallized or isotropic matrix identified by *x*-rays as strengite. Figures 10 and 11 show the microscopic character of this rock.

C. Leucophosphite from Liberia and Australia

Presumably the least changed material from the original phosphatized ore is that represented by a buff to liver-brown stony mass, generally dense and taking a high polish, but containing numerous open cavities. It is shown in Fig. 6*A*. Inspection of the polished surface shows a hetero-

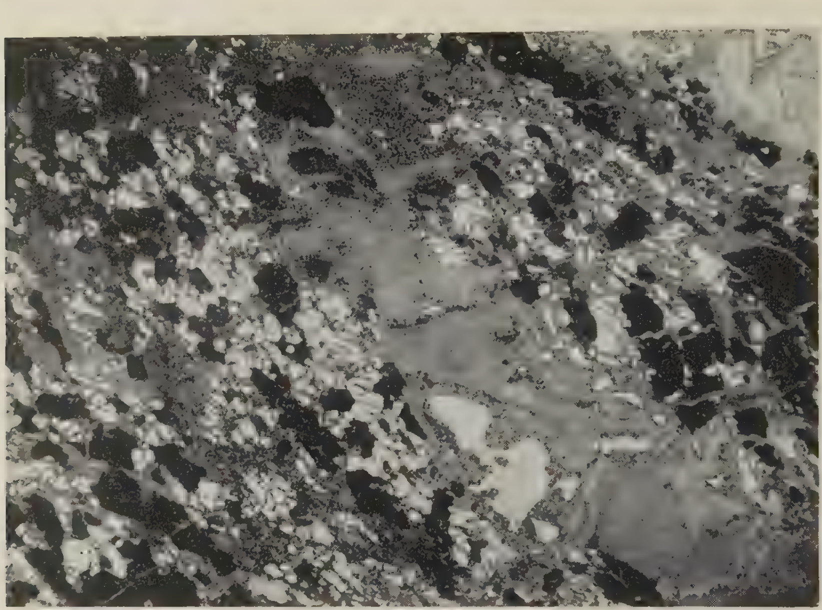

Fig. 10. "Sta. 27 WHN." Bomi Hill, Liberia. ×8 Thin section. Ore-bearing granite gneiss partly replaced by strengite. The largest white area (lower center) is a void; the others are quartz grains.

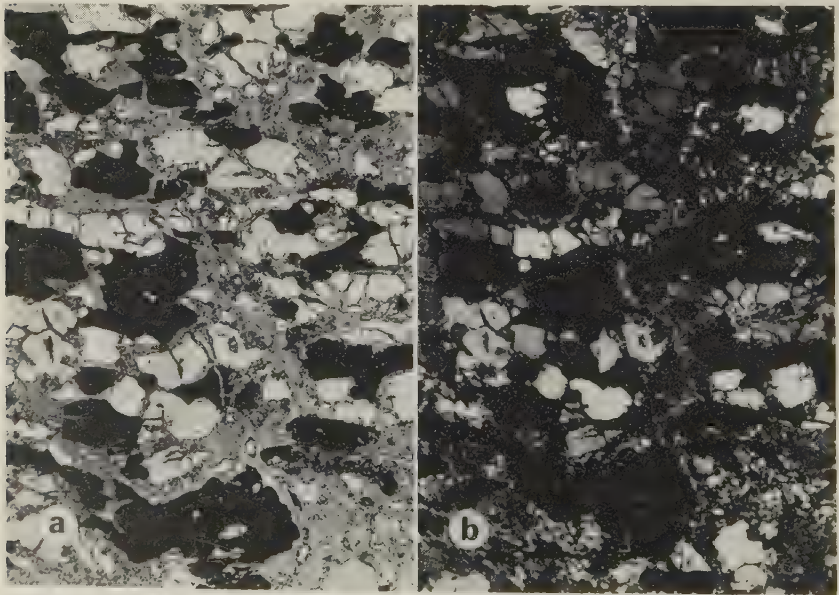

Fig. 11. (*a*) ordinary light. (*b*) crossed nicols. "Liberia Sta. 27 WHN." Bomi Hill, Liberia. ×12½. Hematite-quartz in phosphosiderite-strengite matrix. Under crossed nicols the anisotropy of the matrix is clearly seen.

geneous metacolloid structure suggesting brecciation of an original gel-structure, with marked contrast in depth of the color of successive zones and of matrix and fragments. Small irregular grains of quartz and hematite are strewn through the mass. The microstructure of the Liberian leucophosphite is shown in Fig. 12.

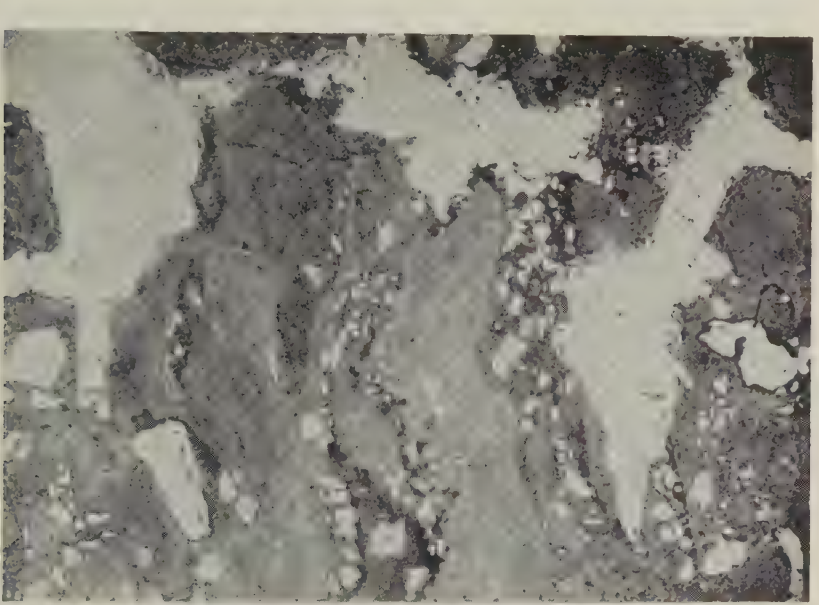

FIG. 12. Leucophosphite. Bomi Hill, Liberia. ×8. Shows meta colloid structure. The clear large white areas are voids in the specimen probably caused by shrinkage. The smaller white areas are mostly quartz grains. The varying shades of gray correspond to minor variations in texture and possibly composition.

The Australian leucophosphite is markedly different in appearance. It is far more obviously heterogeneous with bright green (talc?) areas and hematitic streaks. It is soft and friable, and has a distinct, by no means unpleasant aromatic odor. The freshly scratched surface is white, but in time turns to a light purplish brown. The microstructure is shown in Fig. 13. At a casual glance, and even with chemical analyses available, there would be nothing to suggest the essential identity of the African and Australian material, but the *x*-ray data demonstrate this beyond question.

DESCRIPTION OF SPECIMENS FROM BAMBUTA

A. Magnetite with Phosphosiderite, etc.

Specimen "SP 35 Ore body III C Bambuta" is massive magnetite with its grains peripherally martitized (Fig. 16) and with countless vugs filled

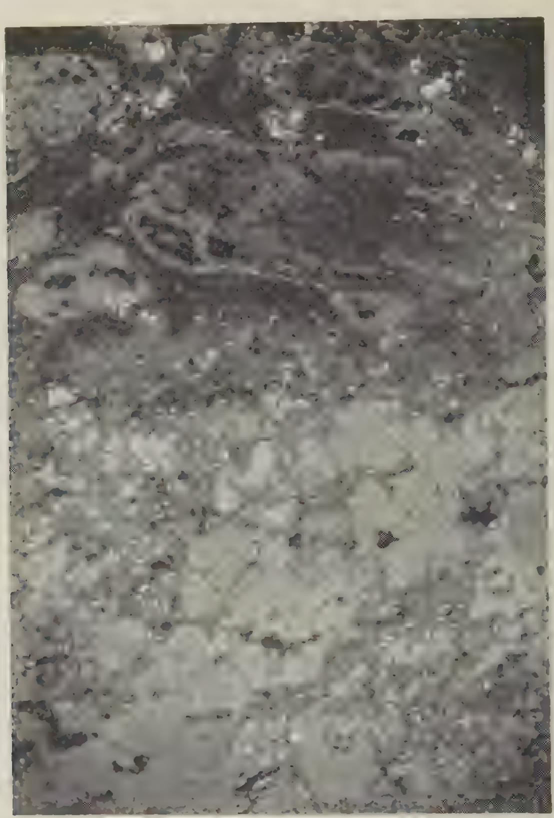

FIG. 13. Leucophosphite. U.S.N.M. 96772. Australia. ×8 Thin section. Shows highly irregular variation in texture and, no doubt, composition. The black areas are opaque grains probably hematitic; the rest of the section, different kinds of fine grained material, much of which, however, yields a characteristic *x*-ray diffraction pattern.

with excellently developed rose-colored clear crystals of phosphosiderite and colorless crusts of strengite (illustrated in Fig. 6*B*, 14, and 15).

The association of the dimorphous phosphates, phosphosiderite and strengite, appears to be fairly common. The crystallographic relations of these minerals, their isodimorphous aluminum homologues, metavariscite and variscite, and the mixed iron-aluminum dimorphs, barrandite and clinobarrandite have been summarized by Strunz and Sztrokay (1939).

Hutchinson (1950) points out that these minerals presumably "represent the normal products of phosphatization of igneous and other aluminosilicate rocks in tropical and subtropical regions of markedly seasonal rainfall." He cites Lacroix who compared this process to lateritization, involving loss of silica and soluble bases, which occurs

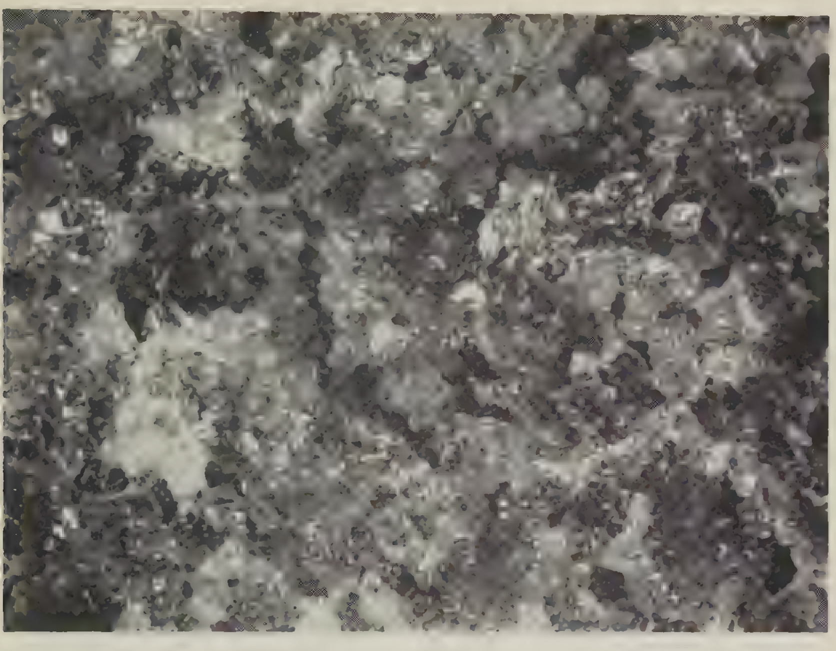

FIG. 14. "SP 35 Ore Body III C Bambuta." ×7. Bambuta, Liberia. Vugs in magnetite lined with sharp-edged red crystals of phosphosiderite.

when phosphate is absent. Phosphosiderite, however, has been reported (six localities) only from Europe (Laubmann and Steinmetz, 1920).

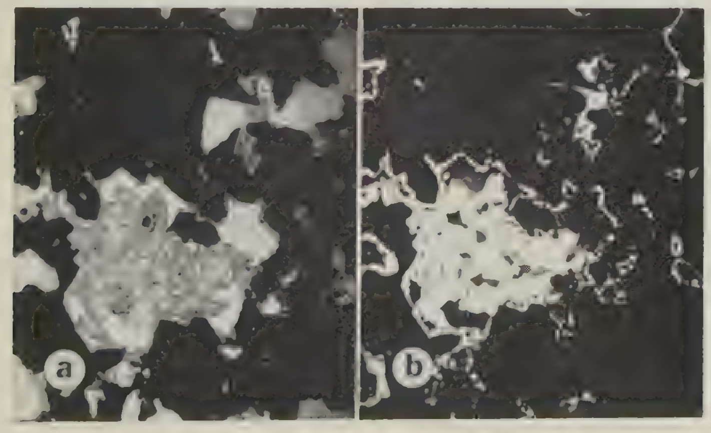

FIG. 15. (*a*) Ordinary Light. ×6. (*b*) Crossed nicols. "SP 35 Ore body III C Bambuta." Bambuta, Liberia. Magnetite ore with phosphosiderite. The clear areas (left) are open cavities. Phosphosiderite (gray) lines and partly fills the vugs. Some strengite is also present, but cannot be distinguished in the figures. Crossed nicols shows twinning in phosphosiderite.

B. *Strengite (rock)*

A second massive phosphate, with merest traces of iron oxide minerals and very little quartz, is represented by "SP 34 Ore body III C Bambuta" and is illustrated in Fig. 6C. This is a light brownish, rather porous, but firmly coherent aggregate, more or less stony in texture, and, with a hand lens, clearly shows colloform structure like that of the leucophosphite. Very rarely, in the numerous open cavities, extremely minute crystals are visible. Both crystals and the main mass give the *x*-ray pattern of strengite, $FePO_4 \cdot 2H_2O$ (*x*-ray film 5299). It will be noted that this is simply the formula of leucophosphite after deduction of (K, $NH_4)_2O$ and part of the water. The work of Cole and Jackson (1950), cited in detail below, shows that the related mineral minyulite dissociates at a pH near 7 to produce variscite as a stable phase, and thus throws light on the relations of leucophosphite to phosphosiderite-strengite.

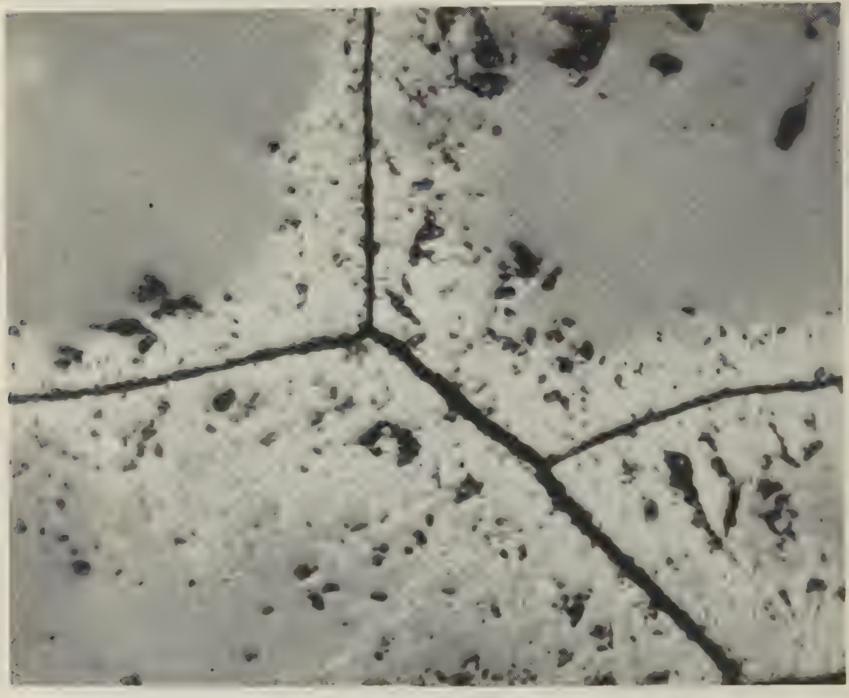

FIG. 16. "SP 35 Ore Body III C Bambuta." ×200. Bambuta, Liberia. (Polished section.) Magnetite oxidized to hematite along grain boundaries. The hematite follows octahedral planes in the magnetite (martitization) as is clearly seen in the lower right corner. This ore is porous, and the pores are more or less lined with pink to red phosphosiderite, accompanied by minor strengite. (Figs. 6*B*, 14, and 15.)

INVESTIGATION OF LEUCOPHOSPHITE

X-ray data for natural and synthetic leucophosphite

Numerous *x*-ray diffraction patterns, made of variously-appearing particles of this substance, were the same with insignificant variations. Table 1 gives the *x*-ray data for the Liberian mineral, for the type Australian leucophosphite (which likewise shows a varied degree of crystallinity from "statistically isotropic to barely visible crystals"), and for synthetic leucophosphite (Haseman, Lehr and Smith, 1950). It will be seen that these three patterns are substantially the same, the minor discrepancies being assignable to impurities in the natural compounds and to variation in isomorphous replacement of NH_4 and K, and of Al and Fe.

It was suspected that the better crystallized material might be fine-grained strengite or phosphosiderite, but careful examination of eight

TABLE 1. *X*-RAY DATA FOR LEUCOPHOSPHITES FROM LAKE WEELHAMBY, S.W. AUSTRALIA AND BOMI HILL, LIBERIA, AND FOR SYNTHETIC LEUCOPHOSPHITE. FILTERED IRON RADIATION, $\lambda = 1.937$Å

Australia		Africa		Synthetic "*I*"[1]	
d	*I*	*d*	*I*	*d*	I/I_1
7.5	5½	7.6	6	7.50	.31
6.73	10	6.78	10	6.77	1.00
		6.11	5		
5.93	8	5.96	9	5.92	.76
4.71	5	4.78	5½	4.73	.28
4.26	4	4.30	5	4.23	.21
4.17	6	4.23	5	4.20	.28
4.05	5	4.08	5	4.05	.14
3.90*	3				
3.76	5	3.80	4	3.78	.21
3.68*H*	3				
3.51	5	3.55	2		
3.35	6½	3.38 3.35	5	3.34	.35
3.19	6*b*	3.23	4*b*	3.20	.14
				3.09	.14

H = wholly or partly hematite.

* = probably an unidentified impurity.

b, *vb* = broad, very broad.

[1] Haseman, Lehr, and Smith (1950)

Intensities, by comparison with a scale based on log $\sqrt{2}$ so that $I_{10}/I_2 = 16$, approximate the integrated rather than the peak intensities. Weaker lines have been omitted.

(*Table continued on next page*)

TABLE 1—(*continued*)

Australia		Africa		Synthetic "*I*"[1]	
d	*I*	*d*	*I*	*d*	I/I_1
3.03	7	3.06	7	3.03	.59
				3.00	.28
2.95	5	2.98	4	2.97	.28
2.88	6	2.91	6	2.90	.37
2.79	6*b*	2.83	6	2.81	.41
2.70*H*	6				
2.64	6*b*	2.68	4	2.66	.35
		2.66	6	2.64	.37
		2.58	4		
2.52*H*	7			2.53	.17
		2.54	2		
2.47*	5			2.48	.17
		2.49	3½		
		2.446	3		
2.358	5	2.382	2	2.38	.17
2.318		2.343	4	2.33	.21
2.210*H*	4*b*				
		2.279	2*b*		
2.130	5*b*	2.154	2½	2.14	.21
1.995	2	2.000	5*b*		
		1.966	3*b*		
1.920	1	1.928	4*b*		
1.907*	1*b*	1.896	4*b*		
1.842*H*	2*b*				
		1.819	4		
1.758	2*b*	1.786	4*b*		
		1.706	3*b*		
1.692*H*	6*b*				
1.645	4*b*	1.658	4*b*		
1.598	4*b*	1.588	2		
		1.570	2		
1.532	3	1.526	2		
1.503					
1.490*H*	6	1.498	4*b*		
1.479		1.454	3*b*		
		1.259	3*b*		
		1.228	2*b*		
		1.130	2*b*		
		1.081	3*vb*		
		1.067	2*vb*	2*vb*	
		1.020	3*vb*		
		1.009	3*vb*		

x-ray patterns of various parts of the specimens failed to show the strongest line of either of these minerals.

The smaller cell size of the Australian mineral is in accord with the presumed substitution of aluminum for some of the iron. Some of the leucophosphite powder patterns were spotty, which confirms the observation that all of it is not cryptocrystalline.

Hutchinson (1950) mentions Bannister as having proved by x-ray diffraction that the Australian leucophosphite is amorphous, which is not in accord with our findings. However, this seeming conflict was resolved on further investigation of the type specimen (U. S. National Museum 96772). The visible heterogeneity of this material persists in the microscopic range; that is to say, it is impossible to take a small x-ray sample of seemingly uniform material and say in advance whether it will be "amorphous" or give a definite crystalline pattern. Of three trials, one was amorphous, two gave good or poor, but consistent, x-ray patterns of leucophosphite.

It should also be noted in this connection that Haseman, Lehr and Smith expressly note that their synthetic "*I*" (leucophosphite), unlike most of their other preparations, "gave a weak pattern"; although this is rather surprising in view of the relatively large size of crystals illustrated in their paper (some 200 microns in length).

Spectrographic analysis of leucophosphite

Spectrographic analysis by K. J. Murata of the Liberian leucophosphite showed:

%	
>1	Fe, P
.X	Si, Al, Ti
.0X	Ca
.00X	Mg, Ba, Mn, Cu, Zr
.000X	Sr, Cr

not found: B, Be, Sn, Zn, Cd, V, Ni, Co, Ag, Bi, Mo, W, Pb, Tl, Ge, In, Y, La, Na.

The material selected for spectrographic and chemical analysis was freed as much as possible from quartz. Also it should be noted that the alkali metals were not sought spectrographically; the wave-length range photographed did not include their most sensitive lines. Otherwise the agreement between the spectroscopic data and the analysis is good. Murata also noted the possible presence of ammonia, judging from the behavior of the sample during arcing. This was the first indication of its presence in the Liberian mineral.

Chemical analysis

TABLE 2. ANALYSES OF NATURAL AND SYNTHETIC LEUCOPHOSPHITE

	A	B	C	D
Insoluble	(4.92)			
SiO_2	4.32	.00		
Al_2O_3	.88	12.73		
Fe_2O_3	36.85	32.82	38.9	40.55
Cr_2O_3	—	.00		
FeO	.14	.00		
CaO	.16	tr		
MgO	.02	.73		
MnO	—	.22		
NiO	—	tr		
$(NH_4)_2O$	1.99	.09		
K_2O	7.86	7.88	12.2	11.96
Na_2O	.22	.13		
H_2O+	11.67	12.28		
H_2O-	1.23	6.59		
TiO_2	.41	—		
P_2O_5	33.46	26.69	37.4	36.07
CO_2	—	.17		
C (organic)	.30	tr		
Cl	—	—		
SO_3	—	—		
Ignition loss	—	—	11.6	11.42
	99.51	100.33	(100.1)	100.00
Sp. gr.	2.6	2.45	2.93	
Ratios				
$Fe_2O_3+Al_2O_3$	1.90	3.71		2
$(NH_4)_2O+K_2O+Na_2O$	1.00	1.00		1
P_2O_5	1.87	2.11		2
H_2O+	5.14	7.66		5

A. Leucophosphite, Bomi Hill, Liberia.
M. K. Carron, analyst.

B. Leucophosphite, Ninghanboun Hills, Lake Weelhamby, Southwest Australia.
D. G. Murray, analyst.

C. Leucophosphite, synthetic.
Haseman, Lehr, and Smith (1950).

D. Theoretical $K_2O \cdot 2Fe_2O_3 \cdot 2P_2O_5 \cdot 5H_2O$.

Discussion of analyses

Allowing for about 5% of siliceous impurity in the African material, and for replacement of K_2O by $(NH_4)_2O$ there appears to be a satisfactory agreement between the analysis of this leucophosphite and the theoretical $K_2O \cdot 2Fe_2O_3 \cdot 2P_2O_5 \cdot 5H_2O$. The Australian leucophosphite, although in general chemically comparable, contains hematite and other impurities, and a notable Al_2O_3 content probably, in part, in isomorphous replacement of Fe_2O_3. The similarity in composition and the common x-ray diffraction pattern indicate a species rank for the African and Australian minerals; comparison with the synthetic preparation shows that this is justified.

Synthesis of leucophosphite

If possible, a new mineral of complex composition should be synthesized as assurance of the validity of the formula proposed from the analysis. A formula obtained from a synthetic substance of known composition, homogeneity, and physical properties is much more acceptable than one inferred from analysis of a complex mixture. Happily, while the natural impure leucophosphite was being studied, Haseman, Lehr and Smith (1950) prepared and described in completely satisfying detail a substance whose properties establish it beyond question as artificial leucophosphite. In brief, they added to precipitated ferric phosphate (from ferric chloride and orthophosphoric acid) potassium hydroxide, to a pH of 3. The resulting precipitate, after washing, was suspended in KOH solutions of alkalinity up to pH 8, with concentrations of potassium phosphate from .001 to 3.5M. (PO_4 basis). After sealing, the suspensions were digested from 1 to 54 days at constant temperatures between 27° C. and 145° C.

Morphology and optical data for synthetic leucophosphite

The excellent synthetic study of Haseman, Lehr, and Smith gives satisfactory morphological and crystallographic data for this mineral species. They show photomicrographs of leucophosphite crystals with formula $K_2O \cdot 2Fe_2O_3 \cdot 2P_2O_5 \cdot 5H_2O$ (and of the homologous $(NH_4)_2O \cdot 2Fe_2O_3 \cdot 2P_2O_5 \cdot 6H_2O$). They report for the synthetic: pale yellow color; indices 1.706, 1.720, and 1.741; monoclinic symmetry; $Z \wedge c = 2° - 3°$; habit, stout prisms terminated by clinodomes. This color agrees with the yellowish brown of the Liberian mineral whose mean refractive index lies close to 1.723. The density of the Liberian mineral was 2.6, against 2.93 for the synthetic; the Liberian mineral however is porous and contains about 5% of quartz, and ammonium replaces part of the potassium.

MINERALS RELATED TO LEUCOPHOSPHITE

Leucophosphite is one of a genetically closely related group of naturally occurring alkali iron-aluminum phosphates, including the substances that have been named paratooite, taranakite, minervite, palmerite, and minyulite.

Paratooite is somewhat sketchily described from Elder Rock, in the desert about 160 miles north of Adelaide, South Australia, by Mawson and Cooke (1907). It is formed by the action of bird droppings on ferruginous (magnetite and hematite) quartzite. "Much" ammonium is mentioned in their account, although the two analyses given do not show any. Their analyses vary widely, with alkalies in one not mentioned and in the other determined by difference; both analyses sum to 100.00. In the latter 1.22% of "alkalies, etc." are cited. The refractive indices are not given, beyond a mention of "yellowish-brown birefringent globules" with double refraction about .023, and index (sic) much above quartz; this is for the substance without alkalies; the other is "isotropic, light yellow." These data are inadequate to define the substances. The analyses compute approximately to $2(Fe,Al)_2O_3 \cdot P_2O_5 \cdot 5H_2O$ and $(Al,Fe)_2O_3 \cdot P_2O_5 \cdot 4H_2O$, respectively. The paratooite minerals need further study.

L. R. Catalano (1933) described a deposit off the coast of Argentina, essentially potassium aluminum phosphate, formed by penguins nesting on an island composed of quartz porphyry and granite. No optical or *x*-ray data are given. He describes and gives an analysis of "whitish nodules, whose diameter varies from a few millimeters to 5 centimeters. They crumble in the fingers giving a white, unctuous powder in which are sandy particles. . . ." Catalano derives a different formula from that ascribed to palmerite, but his data are too vague for any definite characterization of the material.

A much more satisfactory situation exists with regard to taranakite, minervite, and palmerite, the recent work of Bannister and Hutchinson (1947) having shown their identity. Although the *x*-ray patterns and optical constants of the poorly crystallized natural minerals are identical, there is considerable variation in the reported analyses, which approximate $K_2O \cdot 3(Al, Fe)_2O_3 \cdot 3P_2O_5 \cdot 18H_2O$. The synthetic study of Haseman, Lehr, and Smith shows that the composition of taranakite is $2K_2O \cdot 3Al_2O_3 \cdot 5P_2O_5 \cdot 26H_2O$, and deviations from this in analyses of the natural substances may be referred to impure material.

Minyulite, $KAl_2(PO_4)_2(OH, F) \cdot 4H_2O$ is mentioned by Bannister and Hutchinson (1947) as being the only potassium aluminum phosphate defined precisely, chemically and crystallographically; with no potassium iron phosphate so defined. Leucophosphite and taranakite (Haseman, Lehr, and Smith, 1950) may also now be listed as well-defined species.

The taranakite minerals and minyulite, though containing essential K_2O, differ sharply from leucophosphite in morphology and optical character, as well as chemically.

GEOCHEMISTRY OF LEUCOPHOSPHITE AND RELATED PHOSPHATES

Within the last year three important papers have appeared which help elucidate the relationships of the Liberian phosphates: one by Haseman, Lehr, and Smith (1950), and two by Cole and Jackson (1950), all of which deal with the physical chemistry of the systems and minerals in question; but first, we should consider the source of the components that enter these systems—potassium, ammonium, phosphorus, and iron (aluminum).

Sources of constituent elements

The potassium has two obvious sources—one organic and one inorganic. The former is the excreta of birds and mammals (bats, etc.). The latter is potassium feldspar, a common and abundant constituent of many igneous, metamorphic, and sedimentary rocks.

Analyses of fresh guano from both birds and bats show notable quantities of K_2O. In Table 3, taken from Hutchinson (1950) three analyses, one of bird, two of bat guano, show respectively 2.51, 3.85, and 1.57% K_2O. (In the bird guano cited, there is also 3.51% Na_2O.

TABLE 3. ANALYSES OF FECES AND GUANO

	A	B	C	D	E	F
H_2O	9.40	43.96	29.40	22.28	83.65	82.63
Organic matter	81.75	18.94	17.74	56.03		
Total N	21.66	2.33	2.86	17.41	10.25	11.73
P_2O_5	4.30	16.34	16.80	7.14	6.95	7.42
Alkalies, etc.	3.70	20.36	27.84			
Sand	.85	.40	8.22			
Insol.				1.47	.16	1.39
Na_2O				3.51		
K_2O				2.51	3.85	1.57
CaO				3.67	2.36	4.56
MgO				.50	1.40	1.03
Al_2O_3					.00	.49
Fe_2O_3					.38	.78
SO_3					3.00	3.80

A. Excrement of *Pelecanus occidentalis thagus* (pelicans), air dried apparently.
B. Feces of *Otaria byronica* (sea lion).
C. Guano from seal feces, Peru.
D. Guano (bird) Peru.
E. Fresh bat guano, Lares, Puerto Rico.
F. Fresh bat guano, San German, Puerto Rico.

The data in Table 3 also show a nitrogen content varying from 2.33% to 21.66%. (It should be noted that the low figures are for feces of sea-mammals; were the nitrogen content of their liquid urine added, the figure would be far higher.) The analyses of bat guano, presumably including solid and liquid excreta, run over 10% N, while the two analyses of bird guano, in which all of the excreta are solid, run twice as high.

No attempt will be made to unravel the complicated chemistry whereby this nitrogen is converted, in part or wholly, into ammonium. That this does occur cannot be questioned, nor that some of the other strong base, K_2O, is likewise liberated or made available for fixation in inorganic phosphate compounds. An abundance of phosphorus is at hand in the guano.

The commonly present additional source of K_2O in the phosphatized country rock has already been mentioned. It is not probable that such a source of K_2O is of any great significance in the formation of complex potassium phosphates. Iron and aluminum, however, are practically absent in feces and guano, and must be derived wholly from the country rock, whatever it may be, on which the guano was deposited. On destruction of the (felspathic) rock, some potash may be released along with the alumina.

One aspect of the geochemistry of the nitrogen should be mentioned. In birds the semisolid urine consists, more or less, of relatively stable and insoluble uric acid. The liquid urine of mammals, however, is characterized by urea, unstable and soluble. This changes first to ammonia, which in turn oxidizes to nitric acid. This explains the nitrate often found in caves frequented by bats. The intense alteration of original rock or ore shown in Liberia and elsewhere, effected by bat excreta, may in part be explained by a secondary action of nitric acid, as well as the first-formed alkaline ammonia and potash solutions.

Replacement of siliceous (and carbonate) rocks by phosphatizing solutions has been described by many writers. The extensive phosphate deposits of oceanic coral islands need only be mentioned; less familiar is phosphatization of igneous rocks, as described by McConnell (1943), where augite-andesite has been replaced by phosphosiderite-strengite. An analysis gave:

Phosphosiderite and strengite	87.2
Ilmenite (Ti-magnetite)	3.0
Quartz and opaline silica	4.3
Leucoxene (TiO_2)	3.9
H_2O-, H_2O+(opal), organic	1.6
	100.0

On the same island, an amygdaloidal scoria has been partially replaced, most of the feldspar laths being replaced by either clear quartz or variscite with metavariscite (both $AlPO_4 \cdot 2H_2O$). The source of the phosphate was guano from sea birds (masked booby, Sula dactylotra). Similarly, Willemse (1949) described a South African occurrence in which a dolerite has been converted to aluminum-iron phosphate (77–89 per cent, the balance essentially SiO_2). The source of the phosphate is droppings from birds and dassies (i.e. rabbits). A laterite derived from the unphosphatized dolerite contained only 0.4% P_2O_5.

In these occurrences, it will be noted that the phosphate formed is nonpotassic. However, Lacroix (1936) described lava changed to taranakite in a bat cave in basalt; and further that minervite (taranakite) has changed to redondite (barrandite) by loss of alkalies. Very likely then, the occurrences described by McConnell and Willemse were originally potassic (or ammoniac) but have altered by loss of alkali.

Physical chemistry of alkali iron-aluminum phosphates

Haseman, Lehr, and Smith (1950) have shown that taranakite, leucophosphite (and homologous aluminum and ammonium compounds), and minyulite, can form under soil conditions. Other possible compounds of the same constituents may be synthesized, but are not known to form under ordinary, natural conditions. Their observations in reference to the role of potassium and ammonium are noteworthy: "The digestion of precipitated phosphates of iron and aluminum in solutions of potassium or ammonium phosphate invariably resulted in the absorption of potassium or ammonium by the solid to form a complex phosphate of the respective uni- and ter-valent cations. Similar digestions in solutions of the phosphates of lithium, cesium, calcium or magnesium phosphates yielded variscite, strengite, or berlinite" ($AlPO_4 \cdot 2H_2O$, $FePO_4 \cdot 2H_2O$, and $AlPO_4$, respectively). That is, complex alkali compounds of the leucophosphite-taranakite-minyulite type form when the proper alkali is available; any simple iron-aluminum phosphates changing into the alkali compounds. At first glance, this might seem to be opposed to the findings of Cole and Jackson (1950) who investigated the solubility behavior of minyulite $K[Al(OH)_2H_2PO_4]_2OH$ and variscite $Al(OH)_2H_2PO_4$. They found that minyulite transforms to variscite, which is the reverse of the reaction indicated above. However, in the reaction variscite (strengite)→ taranakite (minyulite, leucophosphite) an excess of K or NH_4 ion was present, whereas in the reverse reaction minyulite→variscite, an aqueous suspension of minyulite was treated with dilute NaCl solution containing HCl or NaOH to establish a pH of 2, 3, 4 . . . 9. Thus, removal of K or NH_4 ion, regardless of other alkali or alkali-earth ions present, would result in the formation of variscite, etc., in agreement with the findings of both groups of workers. Cole and Jackson note that suspensions of minyulite in $N/_{20}$NaCl are nearly neutral (pH 6.5 after one day). However, in two weeks the pH changes to 4.6, corresponding to the formation of a second solid phase in the suspension, namely variscite. In suspensions more acid than pH 4.0, solution of variscite occurs, the excess hydrogen ion going into water perhaps according to a reaction such as $Al(OH)_2H_2PO_4 + 2H^+ \rightleftarrows Al^{3+} + H_2PO_4^- + 2H_2O$. On the other hand, in suspensions more alkaline than pH 4.0 hydroxyl ions are removed perhaps in the reaction $Al(OH)_2H_2PO_4 + (OH)^- \rightleftarrows Al(OH)_3 + H_2PO_4^-$. In other words, variscite is amphoteric, with pH 4 the neutral (isoelectric) point.

From this summary of Cole and Jackson's data, it is seen that the initial (metastable) equilibria in suspensions of minyulite at varying pH in the absence of K, reach a final stable equilibrium at a pH corresponding to the existence of variscite as the solid phase present. Extrapolating from the experimental relations of minyulite and variscite, to the analogous iron-bearing system, a similar formation of strengite $Fe(OH(OH)_2H_2PO_4$ is proposed by these writers, who point out in this connection the well-known isomorphism in the variscite-barrandite-strengite crystal series, and, also, the similar isoelectric pH values of 4.0 for variscite and 3.4 for strengite (Swenson, Cole, and Seiling, 1949).

From this, it is to be concluded that the complex alkali compounds found in nature (leucophosphite, taranakite, minyulite) form in the presence of an excess of the proper alkali (K, NH_4) ion; and that such compounds are unstable in water free of K and NH_4 passing by loss of alkali into the far more commonly-found variscite-barrandite-strengite minerals.

ACKNOWLEDGMENTS

Without the wholehearted cooperation of Mr. L. K. Christie, President of the Liberia Mining Company, Ltd., in providing the opportunity to collect the specimens and in encouraging publication of the results, this study would not have been undertaken. Dr. Michael Fleischer of the U. S. Geological Survey gave most helpful advice in writing the paper.

REFERENCES

1. BANNISTER, F. A., AND HUTCHINSON, G. E., The identity of minervite and palmerite with taranakite: *Mineral. Mag.*, **28,** 31–35 (1947).
2. CATALANO, LUCIANO R., Informes sobre depositos de guano en dos islas de la costa Atlantica: depositos de guano en la isla Leones (Territorio del Chubut): *Argentina Direccion Minas y Geol.*, No. **100,** 1–19 (1933).
3. COLE, C. V., AND JACKSON, M. L., Solubility equilibrium constant of dihydroxy aluminum dihydrogen phosphate relating to a mechanism of phosphate fixation in soils: *Soil Sci. Proc.*, **15,** 84–89 (1950).
4. COLE, C. V. AND JACKSON, M. L. Colloidal dihydroxy dihydrogen phosphates of

aluminum and iron with crystalline character by electron and x-ray diffraction: *Jour. Physical and Colloid Chem.*, **54**, 128–142 (1950).

5. Fitzhugh, E. F. Jr., *Soc. Econ. Geol.*, Annual Meeting, Detroit, Michigan, Nov. 1951 (published abstract).
6. Frondel, Clifford, The dufrenite problem: *Am. Mineral.*, **34**, 513–540 (1949).
7. Haseman, J. F., Lehr, J. R., Jr., and Smith, J. P., Mineralogical character of some iron and aluminum phosphates containing potassium and ammonium: *Soil Science Soc. Am.* Proceedings 1950, **15**, 76–84.
8. Hutchinson, G. E., The biogeochemistry of vertebrate excretion: *Bull. Am. Mus. Nat. Hist.*, **96**, 275 (1950).
9. Lacroix, A., Le Volcan actif de l'Ile de la Reunion et ses produits. Paris (1931).
10. Laubmann, H., and Steinmetz, H., Phosphatführende Pegmatite des Oberpfalzer and Bayerischen Waldes: *Zeit. Kryst.*, **55**, 522–586 (1920).
11. Mawson, D., and Cooke, W. T., The phosphate minerals from Elder Rock: *Trans. Roy. Soc. Southern Australia*, **31**, 65–70 (1907).
12. McConnell, Duncan, Phosphatization at Malpelo Island, Colombia: *Bull. Geol. Soc. Am.*, **54**, 701–716 (1943).
13. Simpson, E. S., Contributions to the mineralogy of Western Australia: *Jour. Roy. Soc. Western Australia Sec.*, **7**, 18, 61–74 (1932).
14. Strunz, H., and Sztrokay, K. V., Isodimorphie zwischen Metavariscit, Variscit, Phosphosiderit und Strengit: *Zentrallblatt Min.*, 272–277 (1939A).
15. Swenson, R. M., Cole, C. V., and Seiling, D. H., Fixation of phosphate by iron and aluminum and replacement by organic and inorganic ions: *Soil Science*, **67**, 3–22 (1949).
16. Thayer, T. P., Newhouse, W. H., and Butler, A. P. Jr., The iron ore deposits of Western Liberia. (in preparation).
17. Willemse, J., Die Fosfaat—afsetting op Zoetendalesvley 889, Potgietersrustse. Distrik: *Trans. and Proc. Geol. Soc. S. Africa*, **52**, 385–402 (1949).

Manuscript received May 1, 1952.

VARIATIONS IN CHEMICAL AND PHYSICAL PROPERTIES OF FLUORITE*

Robert D. Allen, *332 Villanova Drive, Claremont, California*

Abstract

In a laboratory study of 39 fluorite specimens the following properties were considered: color, index of refraction, unit cell dimension, chemical composition, x-radiation effects, ultra microscopic appearance and luminescence. Spectrographic analyses revealed the following minor elements: Be, Na, Mg, Al, Si, Mn, Fe, Cu, Sr, Y, Zr, Ag, Ba, La, Eu, Yb, and Pb. A high percentage of strontium is almost always present: 0.05–0.5%. Other elements which occur in practically all fluorites are Mg, Al, Mn, and Y. Minor elements are sometimes found as major constituents in minerals associated with fluorite. The total range of variation in refractive index (Na, 20° C.) was 0.00111. Fluorites with principal light absorption at long wave lengths are characterized by abnormally low refractive indices unless minor constituents obscure the effect; fluorites with principal absorption at short wave lengths are characterized by abnormally high refractive indices. Abnormally low refractive indices are explained by a fluorine deficiency which is electrostatically compensated by colloidal calcium; abnormally high indices are attributed to excess calcium in structural holes. The value a_0 for synthetic fluorite of optical grade is 5.46295 Å ± 0.00010 at 28° C. No significant variations in unit cell dimension were found. Calculations based upon the lattice constant support the hypothesis that the short wave length absorption maximum of fluorite is produced by "color centers." Fluorite colors are correlated with size of light scattering centers as follows: green-small, blue-medium and violet-large. Light is scattered by aggregates of neutral calcium atoms. The color most commonly produced by x-rays is blue; yellow or brown fluorites usually become colored intense blue-black. Atomic calcium, which causes "F centers" in yellow-brown fluorite, is believed to coagulate into colloidal particles which in turn produce the blue color.

Table of Contents

I. Historical Review 911
  Refractive Index 911
  Luminescence 911
  Color 911
  Minor Elements 913
II. Experimental Observations 913
  General Tabulation of Descriptive and Experimental Information 913
  Refractive Index and Dispersion 915
  Unit Cell Dimension 919
  Semi-Quantitative Spectrographic Analyses 920
  Irradiation Experiments 921
  Dark-Field Observations 922
  Luminescence 923
III. Correlation and Integration of Data 923
  The Relation of Refractive Index to Chemical Composition 923
  Dependence of Color Centers upon the Lattice Constant 925
  A Theory of Color 925
  References 929

---

* Condensation from a doctoral thesis submitted to the Department of Mineralogy, Harvard University, Cambridge, Massachusetts, May, 1950. Contribution from the Department of Mineralogy and Petrography, Harvard University, No. 336.

I. HISTORICAL REVIEW

Refractive Index

Accurate measurements on optical quality fluorite have been reported by Gifford (1902; 1910) and Merwin (1911). Gifford's measurements were obtained through the method of minimum deviation while Merwin's represent data compiled from refractometer determinations. Both men concur in the following: $n_{\mathrm{Na}} = 1.43385$ at 20° C. The premise that refractive index variations accompany color variations in fluorite is supported by several publications. Hlawatsch (1897) reported $n_{\mathrm{Na}} = 1.43342$ to 1.43328 in dark violet blue fluorites. Morgante (1939) found $n_{\mathrm{Na}} = 1.4335$ to 1.4330 in green fluorites; the index dropped progressively with increasing depth of color. Dudenhausen (1904) reported abnormally low indices for three blue, one violet and three yellow fluorites. Two violet fluorites from Weardale gave slightly high values. Hlawatsch (1897) found abnormally high indices in Weardale material.

Luminescence

Haberlandt (1934; 1938) has shown that rare earths frequently cause fluorescence in fluorite. Fluorescence is characteristic of the trivalent positive ions of the rare earth metals europium, terbium, samarium and gadolinium (Pringsheim, p. 76, 1943). In contrast to this rare earth-induced "line fluorescence," band fluorescence spectra are produced by the bivalent rare earth ions as follows: europium, blue; ytterbium, yellowish green; samarium, red; thulium, red (Přzibram, 1937). Gunnell (1933) and Haberlandt (1940) have independently reported that included hydrocarbons cause a yellowish fluorescence. Iwase (1933; 1934), Haberlandt (1935) and Wick (1937) have established the fact that fluorite thermoluminescence spectra commonly contain abundant rare earth lines.

Color

Wyrouboff (1866) was an early advocate of the organic coloring theory. Blount and Sequeira (1919) and Garnett (1920) demonstrated the presence of hydrocarbons in fluorite. Recently Morrison (1935) has attributed the yellow to brown color of Clay Center, Ohio, fluorite to a bituminous impurity. The inspection (Přzibram, 1936) of a large number of fluorite absorption spectra between 660 and 350 mμ shows two principal absorption maxima: (1) 380 to 405 mμ; (2) 575 to 650 mμ. The organic theory of color has declined in importance since the discovery that the absorption maxima of fluorite can be artificially induced by various physical techniques.

Přzibram (1938) ascribed the short wave length absorption maximum to bivalent europium and samarium. However, Yoshimira (1933), Eysank (1936) and Mukherjee (1948) have concluded that the natural color of fluorite is not related to the varieties of rare earths contained in it.

Doelter (1925) expressed the belief that fluorite is colored by colloidal calcium. Göbel (1931) gave support to the colloidal theory through observations with the ultramicroscope. The smallest Ca particles give green, while an increase in size causes blue, violet and colorless. Yoshimura (1933) has proposed a colloidal mechanism to explain variations in the absorption spectrum of fluorite. Mollwo attributes the long wave length absorption maximum to colloidal calcium (Přzibram, 1936).

Pohl has developed a new approach (Hughes, 1936) to the problem of color in alkali halides. Color is interpreted as being caused by "F centers" (color centers). These are associated with surplus metal atoms in the crystal. The surplus atoms are thought to occur as positive metal ions and electrons dissociated from each other. The behavior of "F centers" suggests that they are electrons bound to internal surfaces in the crystal, the positive ions serving to offset the negative space charge which would result from electrons alone. The wave length of the corresponding absorption maximum, is determined by the unit cell dimension, not by the nature of the excess metal. Natural crystals may contain "F centers," but the latter can also be artificially induced in the following ways: (1) by irradiation with ultraviolet light or *x*-rays; (2) by exposure of the crystal at high temperature to a metal vapor; (3) by introducing electrons into a warmed crystal from a pointed cathode.

Mollwo colored fluorite by introducing electrons from a pointed cathode. At 1500° C. the concentration of color centers reached 10^{22} per cc. Crystals with such concentrations were less dense than normal, a result which is consistent with the view that incoming electrons displace fluorine ions. Other workers have artificially produced absorption maxima in fluorite. Kellermann (1937) produced yellow coloration in fluorite by radium irradiation at low temperatures. Leitmeier (1925) explains the cobalt blue color of radium-treated fluorite as the result of separation of electrons from fluorine ions. Cathode rays (Doelter and Leitmeier, 1931) and deuteron bombardment (Cork, 1942) may also be used to produce the long wave length absorption maximum.

Wöhler and Kasarnowski (Doelter and Leitmeier, 1931) colored a colorless fluorite deep blue with calcium vapor. This proved to be a stable color. The calcium excess was found by analysis to be 2.4%. In contrast, Mollwo (1934) showed that quenching an additively colored crystal produces the short wave length absorption maximum. Existing natural or artificial absorption maxima in fluorite may be transformed by physical influences. Thus, pressure causes a blue or green fluorite to become violet (Přzibram, 1929). In general, the long wave length absorption maximum is shifted toward shorter wave lengths by pressure, heat and radiations of various wave lengths.

The artificial production of color in fluorite by radium suggests that natural colors may have developed in response to hard radiation. Hoffman (1937) believes beta- and gamma-radiation partially break fluorite down into elemental fluorine and calcium. This belief is supported by the presence of fluorine gas in fluorite associated with radioactive minerals. Schilling (1926) cites the presence of radioactive haloes in fluorite from Wölsendorf. Both he and Göbel attribute the formation of colloidal calcium to a partial destruction of the fluorite structure; radiation splits off electrons from fluorine ions and fluorine gas is released, the electrons being captured by calcium ions. Přzibram (1947) has stated that in naturally colored fluorites the uranium content is great enough to account for color formation. Evidence also exists which points to a primary crystal structural interpretation of color. Barnes and Holroyd (Mellor, vol. III, p. 692, 1923) claim to have synthesized crystals of fluorspar exhibiting all natural colors. They conclude that color is an optical phenomenon dependent on the crystallization and physical state of the substance. Haberlandt and Schiener (1935) have described in detail relations between color and crystallographic orientation in fluorite.

Minor Elements

The literature of trace elements is summarized in Table 1. After every element capital letters indicate the means of analysis while arabic numerals indicate the appropriate references at the end of this paper.

II. EXPERIMENTAL OBSERVATIONS

General Tabulation of Descriptive and Experimental Information

Table 2 summarizes descriptive and experimental information pertaining to the 39 fluorite specimens examined in this investigation. In the first column are given reference numbers by which the specimens have been identified throughout the investigation. The second and third columns contain respectively the localities and colors (as seen in hand specimens). Except in the case of synthetic fluorite these are natural colors. In the fourth column the forms on specimens which exhibit crystal faces are listed. In column five type of occurrence is designated by Roman numerals in the manner prescribed below: I, Deposits associated with igneous rocks to which they are presumed genetically related; II, Deposits associated with typically hydrothermal minerals,

TABLE 1. MINOR ELEMENTS REPORTED IN FLUORITE

Letters refer to methods of analysis:
A—absorption spectrum analysis.
B—chemical analysis.
C—cathodo-luminescence spectrum analysis.
D—emission spectrum analysis.
E—radio-fluorescence spectrum analysis.
F—thermoluminescence spectrum analysis.
G—triboluminescence spectrum analysis.
H—ultraviolet fluorescence spectrum analysis.
I—*x*-ray fluorescence spectrum analysis.
Numbers refer to references at the end of the paper.

Element	Methods of Analysis	References
Aluminum	B D	1, 2, 3, 7, 56, 58
Argon	B	2
Barium	B D	3, 7
Beryllium	B D	1, 3
Carbon	B D	2, 7, 43, 61
Cerium	B D	3, 4
Chlorine	B	66
Chromium	D	3
Copper	B D	1, 3
Dysprosium	B C D F G H I	4, 19, 21, 34, 44, 59, 60, 63, 64, 65, 69
Erbium	B C D H I	4, 19, 21, 34, 44, 60, 69
Europium	C E F H I	23, 34, 38, 44, 50, 60, 63, 65, 69
Gadolinium	B C D F	4, 32, 44, 59, 60, 63, 69
Helium	B	7
Hydrogen	B D	2, 7, 43, 61
Iron	B D	1, 2, 3, 7, 41, 45, 56, 58
Lanthanum	B D	3, 4
Lead	B D	3, 45, 58, 66
Lithium	B D	1
Magnesium	B D	2, 3, 7, 41, 45, 56, 58
Manganese	B D F G	3, 7, 18, 19, 41, 45, 56, 58, 65
Neodymium	A B C D	3, 4, 19, 30, 44, 69
Nitrogen	B	2, 7
Oxygen	B D	2, 7, 8, 43, 61
Phosphorus	B	2, 7
Potassium	B D	1, 3
Praseodymium	A C D I	4, 30, 34, 69
Samarium	A B C D E F H I	4, 19, 21, 34, 38, 44, 49, 52, 54, 59, 60, 63, 64, 65, 69
Scandium	D	3
Silicon	B D	3, 7, 8, 41, 45, 58
Silver	B D	3, 66
Sodium	B D	1, 3, 7, 56
Strontium	B D	1, 3, 42, 58
Sulphur	B	1, 2
Terbium	C D F G H I	19, 21, 32, 34, 44, 49, 59, 60, 63, 64, 65, 69
Thorium	B	7, 58
Tin	D	45
Uranium	B H	7, 22
Vanadium	D	3
Ytterbium	B D E F H	4, 19, 21, 28, 29, 38, 50
Yttrium	B D F H	3, 4, 19, 21, 28, 29, 38, 58

but not known to be near igneous rocks; III, Deposits in sedimentary rock with evidence for magmatic origin lacking. In column six refractive indices for sodium light (20° C.) are given. The unit cell dimension was measured on about one half of the suite and is recorded in column seven. Information pertaining to trace elements appears in column eight. Only elements in quantity greater than 0.005% are listed. X-ray-induced color data are presented in column nine. In every case the induced color is followed by a Roman numeral which designates the degree of coloration as follows: I, very strong; II, strong; III, moderate; IV, weak; V, none observed.

Refractive Index and Dispersion

In order to attempt the detection of slight but significant variations in the refractive index of fluorite a method of refractometry of the highest accuracy had to be selected. The method of minimum deviation was the logical choice. The maximum usable prism angle for fluorite is 87°40′ and maximum accuracy in refractive index determinations is achieved when the prism angle approaches this value. Indices of refraction were corrected to 20° C. according to the formula $n(20)=n(T)+(0.00001)(T\text{-}20)$, where T equals the temperature at which measurement was made.

The magnitude of determinate error in this group of measurements is small. The average of five separate determinations on a perfect prism of optical fluorite (cut from specimen No. 38) was 1.43385 (20° C.). This is in exact agreement with the findings of Gifford (1902) and Merwin (1911). Indeterminate error is subject to treatment under the theory of probable error. Five separate prisms were prepared from specimen No. 38 with varying quality of signal reflections. These prisms were measured and the resulting indices of refraction were employed to calculate probable errors for the various wave lengths of light utilized. These were as follows: 6550 Å, ±0.00002; 5893 Å*, ±0.00001; 5780 Å, ±0.00002; 5461 Å, ±0.00002; 4359 Å, ±0.00003. According to convention the limit of error is taken to be three times the probable error.

In Table 3 the results of this investigation are presented. Specimens No. 2, 33, and 34 have been omitted from the tabulation; several unsuccessful attempts were made to cut transparent prisms from them. In some cases readings could not be obtained using one or more wave lengths of light due to inefficiency of light transmission.

* Average wave length of the sodium doublet.

TABLE 2. DESCRIPTIVE AND EXPERIMENTAL INFORMATION

Ref. No.	Locality	Color	Form	Type Occurrence	n_{Na} (20° C.)	a_0 (Å units)	Minor Elements (>0.005%)	X-ray Induced Color and Intensity	
1	Göschener Alp, Switzerland	pale rose	{111}	III	1.43385	—	Al, Sr, Y, Yb	violet	II
2	Mt. Antero, Colorado	deep violet (outer portion)*	{111}	I	—	—	Sr	—	V
3	Mt Antero, Colorado	colorless (inner portion)*	{111}	I	1.43373	—	Be, Sr	blue	III
4	Striegau, Silesia	very pale violet	{111}	I	1.43359	5.46324	Al, Sr	—	IV
5	Cave-in-Rock, Illinois	pale blue (outer portion)	{010}	II	1.43433	5.46304	Mn, Sr	blue	III
6	Cave-in-rock, Illinois	pale violet (central portion)	{010}	II	1.43361	5.46342	Sr	blue	III
7	Cave-in-rock Illinois	amber (inner portion)	{010}	II	1.43393	—	Sr	blue	II
8	Brienz, Tyrol	pale green	{010}	III	1.43363	5.46281	Sr, Y	bluish green	III
9	Grand View Mine, Black Range, Grant Co., New Mexico	colorless	{111} and {110}	I	1.43387	—	Sr	blue	IV
10	Macomb, New York	pale green	{010} and subordinate {111}	II	1.43365	5.46286	Sr, Y	blue	II
11	Near Rossie, New York	colorless (outer portion)	{010}	II	1.43376	—	Sr, Y, Zr	blue	II
12	Near Rossie, New York	pale green (inner portion)	{010} and subordinate {111}	II	1.43349	5.46326	Sr, Y, La	green	III
13	East Pool Mine, Cornwall	very pale blue	{010}	I	1.43366	—	Sr, Y	blue	III
14	St. Agnes Mine, Cornwall	very pale blue	{010}	I	1.43360	5.46336	Sr, Y	blue, green and violet	III
15	Stolberg, Germany	colorless	(Conchoidal fracture)	II	1.43379	—	Sr, Y	blue	II
16	Hessenbach Mine, Baden	pale bluish green	{010}	I	1.43415	5.46321	Na, Fe, Sr, Y	blue	II
17	Livingston Co., Kentucky	yellow	{010}	I	1.43405	—	Sr	blue-black	I
18	Livingston Co., Kentucky	pale blue	—	I	1.43407	—	Sr	blue	IV
19	Livingston Co., Kentucky	violet (color zoned)	{010}	I	1.43358	5.46321	Sr	—	V
20	Weardale, England	green	{010}	II	1.43440	5.46329	Sr, Y, La, Eu, Yb	bluish green	III
21	Weardale, England	pale brown	{010}	II	1.43460	5.46321	Sr, Y, Eu	gray	III
22	Weardale, England	colorless	{010}	II	1.43420	5.46274	Sr, Y, Eu	gray-blue	II
23	Madoc, Ontario	very faint lavender (outer portion)	—	I	1.43390	—	Sr, Y, Ba	green	III
24	Madoc, Ontario	green (inner portion)	—	I	1.43417	5.46343	Sr, Y, Ba, La	green and blue	II
25	Marienberg, Saxony	pale brown	{010}	I	1.43402	—	Al, Sr, Y	blue-black	I
26	Cornwall	pale olive	{010}	I	1.43393	—	Sr, Y, Pb	blue-black	I

† Made from Illinois fluorite.

‡ Made from Mexican fluorite.

* Numbers 2 and 3 are the same mineral specimen; this usage is followed throughout the table.

TABLE 2—(*Continued*)

Ref. No.	Locality	Color	Form	Type Occurrence	n_{Na} (20° C.)	a_0 (Å units)	Minor Elements (>0.005%)	X-ray Induced Color and Intensity	
27	Wölsendorf, Bavaria	golden brown	{010}	I	1.43426	5.46313	Al, Sr, Y	blue-black	I
28	Přibram, Bohemia	pale brown	{010}	I	1.43402	—	Al, Si, Sr, Y	blue-black	I
29	Rabenstein, Tyrol	colorless	—	II	1.43392	—	Na, Al, Sr, Y, Pb	blue	II
30	Cornwall	blue (color zoned)	—	I	1.43359	5.46343	Al, Sr, Y	blue	II
31	Clay Center, Ohio	brown	{010}	II	1.43460	5.46277	Sr, Y, Ba	brown	III
32	Westmoreland, New Hampshire	green	{111}	I	1.43420	5.46315	Al, Sr, Y, Yb	deep green	III
33	Greenleaf #1 Mine, Luna Co., New Mexico	faint green (inner portion)	—	I	—	—	Al, Si, Sr, Y	blue	II
34	Greenleaf #1 Mine, Luna Co., New Mexico	pale pinkish violet (outer portion)	—	I	—	—	Al, Si, Sr, Y, Ba, Yb	blue	II
35	(Synthetic)†	colorless	—	—	1.43388	—	Sr	violet	II
36	(Synthetic)†	orange	—	—	1.43388	—	Sr	mauve	IV
37	(Synthetic)†	very faint green	—	—	1.43375	—	Sr	blue	III
38	(Synthetic)†	colorless (optical)	—	—	1.43385	5.46295	Al, Sr	blue	IV
39	(Synthetic)‡	pale lavender	—	—	1.43409	—	Sr	violet	II

The total range of variation in the index of refraction for sodium light (20°) is 0.00111 ± 0.00002, where the error limit indicated is equal to twice the probable error of a single measurement. The lowest value reported is 1.43349 (green fluorite from Rossie); the highest value reported is 1.43460 (brown fluorite from (1) Weardale and (2) Clay Center).

An attempt was made to correlate refractive index with occurrence. No obvious relation exists between sodium index and mode of occurrence. Even in different colored specimens from the same locality, index measurements usually have very little in common. Three blue fluorites from Cornwall gave the following values: 1.43359, 1.43360 and 1.43362. A yellow fluorite and a blue fluorite from Livingston Co., Kentucky, gave 1.43405 and 1.43407, respectively. Weardale measurements are unique: colorless—1.43420; green—1.43440; brown—1.43460.

Refractivity bears a striking relation to color in fluorite.

All natural violet specimens have indices below normal. Yellow and brown specimens have indices above normal. In general, blue and green fluorites have indices which are either considerably above or considerably below normal. The rose specimen has an index of 1.43385, the optical value; the lavender specimen's index exceeds this value by 0.00005. Colorless specimens rarely show great abnormality.

A green synthetic fluorite shows a relatively low index; a violet one gives a relatively high measurement.

Table 3. Indices of Refraction

Spec. No.	n(6550 Å)	n(5893 Å)	n(5780 Å)	n(5461 Å)	n(4359 Å)	n(4359) $-n$(6550 Å)
1	1.43266	1.43385	1.43424	1.43499	1.43965	0.00699
3	—	1.43373	—	—	—	—
4	1.43229	1.43359	1.43381	1.43473	1.43958	0.00729
5	1.43317	1.43433	1.43466	1.43552	1.44025	0.00708
6	1.43220	1.43361	1.43386	1.43472	1.43928	0.00708
7	1.43248	1.43393	1.43420	1.43501	1.43966	0.00718
8	1.43235	1.43363	1.43396	1.43484	—	—
9	1.43262	1.43387	1.43421	1.43505	1.43969	0.00707
10	1.43241	1.43365	1.43392	1.43474	1.43941	0.00700
11	1.43248	1.43376	1.43404	1.43491	1.43971	0.00723
12	1.43203	1.43349	1.43376	1.43459	1.43905	0.00702
13	1.43231	1.43366	—	1.43484	—	—
14	1.43235	1.43360	1.43393	1.43480	1.43942	0.00707
15	1.43243	1.43379	1.43412	1.43495	1.43950	0.00707
16	1.43273	1.43415	1.43440	1.43526	1.43995	0.00722
17	1.43274	1.43405	1.43432	1.43516	1.43995	0.00722
18	1.43272	1.43407	1.43441	1.43531	1.43991	0.00719
19	1.43230	1.43358	1.43387	1.43475	1.43937	0.00707
20	1.43310	1.43440	1.43473	1.43553	1.44023	0.00713
21	1.43332	1.43460	1.43490	1.43575	1.44055	0.00723
22	1.43304	1.43420	1.43460	1.43551	1.44015	0.00711
23	1.43263	1.43390	1.43414	1.43508	1.43968	0.00705
24	1.43281	1.43417	1.43441	1.43531	1.44004	0.00723
25	1.43275	1.43402	1.43426	1.43534	—	—
26	1.43260	1.43393	1.43424	1.43508	1.43971	0.00711
27	1.43298	1.43426	1.43454	1.43543	1.44019	0.00721
28	1.43277	1.43402	1.43435	1.43517	1.43989	0.00712
29	1.43290	1.43392	1.43439	1.43521	1.43988	0.00698
30	1.43238	1.43359	1.43393	1.43491	1.43937	0.00699
31	1.43331	1.43460	1.43481	1.43591	1.44050	0.00719
32	1.43276	1.43420	1.43448	1.43539	1.43998	0.00722
35	1.43257	1.43388	1.43416	1.43508	1.43956	0.00699
36	1.43277	1.43388	1.43415	1.43498	1.43979	0.00702
37	1.43239	1.43375	1.43404	1.43482	—	—
38	1.43252	1.43385	1.43423	1.43507	1.43970	0.00718
39	1.43281	1.43409	1.43435	1.43523	1.43982	0.00701

The writer is of the opinion that significant variations in dispersion have not been found. The probable error in every dispersion measurement is equal to the sum of the probable errors of the two boundary indices. These are ±0.00002 for n(6550 Å) and ±0.00003 for n(4359 Å). The sum is thus ±0.00005. The range of dispersion variation reported is ±0.00015. This is equal to three times the probable error, i.e., the quantity which is generally considered to be the limit of error.

Unit Cell Dimension

High precision measurements of the fluorite unit cell edge are practically nonexistent. Most experimental values in the literature lack accuracy beyond the second decimal place. The best experimental value appears to be the one given in the *Strukturbericht* (*Zeits. Krist.*, pp. 185–186, 1913–1928): $a_0 = 5.451$ kX units). The calculated a_0, assuming a specific gravity of 3.181, is 5.452 (kX units). This calculated value is in good agreement with the experimental results obtained by the writer. The "back reflection" technique coupled with analytical extrapolation to $\theta = 90°$ has been employed (Cohen, 1935; 1936).

Determinations of a_0 have been carried out on only about one-half of the fluorite specimens. Synthetic fluorite (No. 38)* has been adopted as the standard of reference. Seventeen other specimens have been selected for measurement on the basis of their indices of refraction (Na). Eight of these had the lowest refractive indices; nine had the highest refractive indices. It was believed that in this manner any measurable variation of unit cell dimension with refractive index would be detected. The assumption is made that variation in the unit cell dimension would be reflected by the refractive index; thus, measurement was needed on only those specimens which had the most abnormal indices to ascertain whether or not cell dimension variations could be detected.

A symmetrical focusing back-reflection camera was used with copper *x*-radiation. The camera diameter was found by micrometer measurement to be 99.85 mm. at 28° C. The temperature at which fluorite specimens were *x*-rayed was 28° C. ± 1° C.

Before commencing film calculation it was necessary to index a fluorite film to determine *hkl* values corresponding to the three predominant reflections. These indices were found to be 444, 533 and 620, respectively.

As a check on the absolute accuracy of the technique, a photograph of Leadville pyrite was taken. A value of 5.4067 kX units (25° C.) was found by measurement of two reflections and extrapolation to $\sin^2\theta = 1$. This value checks very well with one reported by Wasserstein (1949). To test the relative accuracy of the back-reflection technique five photographs were taken of synthetic optical fluorite. The range of possible error indicated was ±0.00038 Å. The calculated probable error was ±0.0001 Å.

Experimental results have previously been tabulated in Table 2.

Measurements on (1) optical fluorite, and (2) seventeen other fluorites yielded the following ranges of variation:

Optical fluorite	±0.00038 Å
Other fluorites	±0.00035 Å

---

* Supplied by Harshaw Chemical Co., Cleveland, Ohio.

It appears that the limits of possible random error obtained from five photographs of optical fluorite are qualitatively comparable with the limits of variation as obtained from photographs of the seventeen test specimens. Furthermore, the latter seventeen values lie within the absolute range of variation (due to random error) as determined from specimen No. 38.

A second point of importance is this: no obvious correlation can be made between variations in index of refraction and the variable measurements of cell edge. Since the latter determinations apparently lie within the limits of possible error it must be concluded that no significant differences among the specimens have been uncovered.

The value of a_0 for optical fluorite (average of five measurements) is 5.46295 Å ± 0.00010 Å at 28° C.

Semi-Quantitative Spectrographic Analyses

Analysis of fluorite specimens for minor elements was accomplished by emission spectrography using the cathode glow method. Use is made of the very high sensitivity of excitation that exists in the small region of the electric arc near the negative electrode when this is used to hold the sample. The arc is so adjusted that radiation from just above the cathode passes through the optical system of the spectrograph. Samples were mixed with an equal weight of purest graphite. A direct current carbon arc and grating spectrograph were employed. Semi-quantitative determinations were accomplished by comparison of unknown spectra with standard spectra taken with seven groups of standard samples. The findings are summarized in Table 4.

Elements which occur in practically all fluorites are magnesium, aluminum, manganese, strontium, and yttrium. An amazingly high percentage of strontium is almost always present: 0.05–0.5%. Fairly common in trace amounts are beryllium, silver, barium, ytterbium, and lead.

Mt. Antero beryllium-containing fluorite is associated with beryl, phenakite, and bertrandite. Quartz accompanies silicon-bearing fluorite from (1) Přzibram, and (2) Greenleaf Mine. The iron-rich fluorite from Hessenbach Mine is found encrusted by limonite. Celestite accompanies strontium-rich Clay Center fluorite. A barium-bearing fluorite from Madoc is found associated with barite. Thus, minor elements are sometimes found as major constituents in minerals associated with fluorite.

It has not been possible to assign any particular color to a given impurity or group of impurities. The only observation that can be made is this: all three fluorite specimens containing lanthanum are green. In general, the violet fluorites are the purest; they are notably free from rare earths.

TABLE 4. SPECTROGRAPHIC ANALYSES

Symbol meanings:
A 0.5–5.0%
B 0.05–0.5%
C 0.005–0.05%
D 0.0005–0.005%
E less than 0.0005%
F not found

Specimen No. 40: a control run of purest graphite

	Be	Na	Mg	Al	Si	Mn	Fe	Cu	Sr	Y	Zr	Ag	Ba	La	Eu	Yb	Pb
1	F	F	E	C	F	E	F	F	B	C+	F	E	D	F	F	C	F
2	D	F	E	D	F	E	F	F	B	E	F	E	F	F	F	F	F
3	C	F	E	E	D	E	F	F	B	D	F	F	F	F	F	F	F
4	D	F	E	C	F	E	F	F	C	E	F	F	F	F	F	F	F
5	F	F	E	D	F	B−	F	F	B	E	F	F	F	F	F	F	F
6	E	F	E	D	F	E	F	F	C	E	F	F	F	F	F	F	F
7	E	F	E	D	F	F	F	D	B	D	F	E	F	F	F	F	F
8	F	F	E	D	F	D	F	F	B	C	F	F	D	F	F	F	E
9	F	F	D	D	F	D	F	F	B	E	F	F	F	F	F	F	E
10	F	F	E	D	F	D	F	F	B	C+	F	F	F	F	F	F	F
11	F	F	E	D	F	E	F	F	B	C+	C	F	F	F	F	F	E
12	F	F	E	D	F	E	F	F	B	C	D	F	F	C	F	F	E
13	F	F	E	D	F	E	F	F	B	C	F	F	F	F	F	F	F
14	E	F	E	D	F	E	F	F	B	C	F	F	F	F	F	F	F
15	F	F	E	D	F	F	F	F	B	C+	F	F	F	F	F	F	E
16	F	C	D	D	D	E	B	F	B	C+	F	F	D	F	F	F	E
17	F	F	E	D	F	F	F	F	B	E	F	F	F	F	F	F	F
18	F	F	E	D	F	E	F	F	B	E	F	F	F	F	F	F	E
19	F	F	E	D	F	F	F	F	B	E	F	F	F	F	F	F	F
20	E	F	E	D	D	E	F	F	B	C+	F	E	F	C	C	C	F
21	D	F	E	D	F	E	F	F	B	C+	F	F	F	F	C	E	F
22	D	F	E	D	F	D	F	F	B	C+	F	E	F	F	C	E	F
23	F	F	E	E	F	F	F	F	B	C+	F	F	B	F	F	E	F
24	F	F	E	E	F	E	F	F	B	C+	F	E	B	C	F	E	F
25	F	F	E	C+	F	D	F	F	B	C	F	D	F	F	F	E	F
26	F	F	E	E	E	D	F	F	B	C+	F	D−	F	F	F	D	C−
27	F	F	E	C	F	E	F	F	B	C+	F	E	F	F	F	E	E
28	F	F	E	C	B	E	F	E	B	C+	F	F	F	F	F	E	E
29	F	C	E	C+	F	E	F	F	B	C−	F	F	F	F	F	F	C−
30	F	F	E	C	F	E	F	F	B	C+	F	F	F	F	F	E	E
31	F	F	D	D	F	F	F	F	A−	C−	F	F	B	F	F	F	F
32	F	F	E	C	F	F	F	F	B	C+	F	F	F	F	F	C	D
33	F	F	E	C+	C	F	F	F	B	C+	F	D	F	F	F	D	F
34	F	F	E	C	C	F	F	F	B	B−	F	F	B	F	F	C	F
35	F	F	E	D	F	F	F	F	B	D	F	F	F	F	F	F	F
36	F	F	E	D	F	F	F	F	B	D	F	F	F	F	F	F	F
37	F	F	E	D	F	F	F	F	B	D	F	F	F	F	F	F	F
38	F	F	E	C	E	F	F	F	B	D	F	F	F	F	F	F	E
39	E	F	E	D	F	F	F	F	A−	D+	F	F	F	F	F	F	F
40	E−	E	E−	E−	E−	E−	D	E−	C−	F	E	E−	E−	F	F	F	F

Irradiation Experiments

It is well known that radiation can produce colors in fluorite. To study this variable property, samples from the entire suite of specimens were irradiated 24 hours with unfiltered copper *x*-radiation. Data have been summarized in Table 2. Five yellow-brown specimens showed extraordinarily intense blue-black coloration. In specimen No. 17 the induced color penetrated to a depth exceeding one centimeter. The induced color in 24 of 39 specimens was blue. Some specimens showed what was probably a mixture of induced blue and the initial body color of the specimen: orange specimen No. 36 became mauve. This may also be the case in green fluorites which show a deeper green after irradiation. In other cases the induced color is definitely not blue, i.e., in specimens No. 35 and 39. Of especial interest are specimens in which more than one color is induced (Nos. 14 and 24). The association of this phenomenon with cleavage in specimen No. 14 suggests that a relation exists between color and structural disturbance.

To test the effect of x-radiation on refractive index, seven fluorite prisms were irradiated: Nos. 1, 14, 17, 21, 26, 36, and 38. An exposure time of only a few hours was needed on specimens 17 and 26. The technique employed was to irradiate prisms at one end of the prism edge only. A given prism was oriented on the goniometer head and brought to the position of minimum deviation for sodium light. Then the prism was moved vertically on the goniometer head so that refracted light passed first through an unirradiated portion and then through an irradiated portion of the fluorite. In no case did the signal show any displacement from its original position. It must be concluded that no change in refractive index as a result of x-radiation has been proved.

Dark-Field Observations

Dark-field observations were carried out on the fluorite prisms used in making refractive index determinations. A petrographic microscope with high power objective and diaphragmed light source were employed.

Scattering centers were mainly in green, blue, violet, and pink fluorites. Green fluorites showed individual tiny circular spots of light. These were most densely distributed in the deepest green specimens, i.e., Nos. 12, 20, and 32. In the deeper blue fluorites most of the scattering centers had a somewhat different appearance. Circular spots of light were frequently seen in roughly equidimensional aggregates. Violet and pink fluorites showed still larger aggregates. In violet specimens Nos. 2, 6, and 19 some of the scattering centers showed definite linear arrangement parallel to crystal faces. Less numerous scattering centers were also seen in some brown-yellow and colorless specimens; in these colors scattering was of the fine type seen in the green specimens. The scattering phenomenon was also seen in fluorite artificially colored by irradiation. No. 37 (artificial blue) showed coarse aggregates. For purposes of comparison a specimen of blue halite was examined. Scattering centers were very similar to those seen in violet fluorite, both with respect to size and density of distribution.

These observations could be interpreted as support for the colloidal calcium theory of color stated by Göbel.

Luminescence

Luminescence experiments in this investigation have been carried out in a qualitative fashion which is in sharp contrast to the rigorous luminescence spectral analyses made by Haberlandt and other workers. For this reason they have been of very restricted value in developing a general picture of structural variations in fluorite. Space does not permit a description of the experiments carried out or tabulation of data accumulated. In view of the limited applicability of emission spectrographic analysis to the detection of several rare earths, however, a very general use of luminescence phenomena to this end has been made. Luminescence phenomena in calcium fluoride, with the exception of excitation by manganese or hydrocarbons, are caused by trivalent rare earth ions (line spectra) and four bivalent rare earth ions (band spectra), i.e., europium, ytterbium, samarium, and thulium. In relating luminescence (and therefore rare earth content in most cases) and color the following observations seem pertinent: (1) Ultraviolet fluorescence and phosphorescence are usually absent in violet and pink varieties; (2) the prevalence of strong thermoluminescence in green fluorites suggests the universal presence of rare earth activators; (3) blue fluorites are second to the green in thermoluminescent power while violet, brown and colorless specimens show the effect only occasionally; (4) yellowish-white fluorescence, seen in yellow-brown specimens from Cave-in-Rock and Clay Center, is probably due to included organic material. The thermoluminescence data strongly suggest that green fluorites always contain abundant rare earths. Other fluorites which exhibit strong thermoluminescence presumably also contain rare earths. Luminescence experiments and spectrographic analyses both attest to the relative purity of violet fluorites.

Miscellaneous observations made in connection with thermoluminescence experiments are given below. As a result of heating, most fluorites lose their color. Violet specimens become pink. Some green and brown specimens fail to decolorize completely. Decrepitation and bleaching occur between 150° and 200° C. for most specimens. None of the synthetic specimens shows any thermoluminescence or decrepitation.

III. Correlation and Integration of Data

The Relation of Refractive Index to Chemical Composition

The optical properties of ionic crystals are to a first approximation those of the aggregate of ions. Ionic refractivities are additive. The refractivity of the individual ions is a measure of the deformability or polarization of the electronic structure by the electric vector of incident light, and is therefore largest for ions with a large and loosely bound electron configuration. Three general rules relating refractive index to the character of an ion can be applied in qualitative fashion: (1) refractive index is increased by an increase in ionic radius; (2) refractive index is raised by an increase in atomic weight; (3) increase in the positive charge of an ion depresses the refractive index.

The way in which a minor element occurs in fluorite must be known before any prediction can be made as to its effect on the refractive index. It is probable that the following reported impurities substitute for calcium in the ionic structure: Na, Mn″, Fe″, Sr, Y, Zr, Ba, La, Eu, Yb, and Pb. Silver and copper may substitute for calcium in atomic form provided that a compensatory mechanism exists. (Neutral atoms could be compensated for by the presence of trivalent cations or by partial omission of anions, i.e., fluorine.) The small ions of Be, Mg, Al, and Si probably cannot substitute for the calcium ion. Perhaps they occur in structural holes or in microscopically included foreign matter.

TABLE 5. CORRELATION OF ELEVATED REFRACTIVE INDICES WITH IMPURITIES OF HIGHER REFRACTIVE POWER THAN CALCIUM

Specimen No.	n_{Na} (20° C.)	Minor Elements
5	1.43433	Mn
16	1.43415	Fe
20	1.43440	Eu, La, Yb
21	1.43460	Eu
22	1.43420	Eu
24	1.43417	Ba, La
31	1.43460	Ba, Sr
32	1.43420	Yb
39	1.43409	Sr

A limited number of fluorites, which exhibit abnormally high indices of refraction, contain minor elements which would be expected to increase the over-all refractivity of the fluorite structure (Table 5). Specimens No. 20, 21, and 22 contain europium and show abnormally high indices. Barium probably accounts for the high refractive indices of specimens No. 24 and 31. Other minor elements believed to increase total refractivity include manganese, iron, lanthanum, ytterbium, and strontium.

Specimens Nos. 26 and 29 have slightly high refractive indices; these may be caused by the presence of a trace of lead in each specimen. Elements which have no apparent effect upon the refractive index (in the concentration in which they are present) include the following: Be, Na, Mg, Al, Si, Cu, Y, Zr, and Ag.

More interesting than the refractive indices which are explained by the presence of impurities are those for which no apparent explanation exists. Most outstanding, nine specimens of green, blue and violet colors exhibit abnormally low indices of refraction. Four yellow-brown fluorites (Nos. 17, 25, 27, and 28) have abnormally high indices for no apparent reason. A blue fluorite (No. 18) has an unexplained high refractive index. Unaccounted for is the presence of rare earths (other than yttrium) in fluorites with normal or low indices, i.e., specimens Nos. 1 and 12. The heavy rare earths would be expected to increase the index. A comparison of results on green and brown Weardale fluorites reveals an anomaly. The green specimen with abundant rare earths has a lower refractive index than the brown specimen which contains only europium. Another anomalous situation is presented by specimens Nos. 23 and 24. Both contain about 0.1% Ba but show widely different indices. An interpretation of the facts brought out above will be reserved until color is discussed later.

Dependence of Color Centers Upon the Lattice Constant

The exceedingly constant value of a_0 has significance with regard to the theory of "F centers." It has been shown by Pohl (Hughes, 1936) that the location of the characteristic F band for a given alkali halide is a function of the interplaner spacing as follows:

$$(V_{\max})(d^2)=k,$$

where "$V_{\max}$" is the frequency at maximum absorption, "d" is the lattice spacing and "k" is a constant.

If this type of relation holds for alkaline earth halides, it can readily be seen that various colors of fluorite are not to be explained on the basis of an F band whose location is subject to variation. The very constancy of a_0 for calcium fluoride rules out this possibility.

Mollwo (1934) has attributed the short wave length absorption maximum of fluorite to the presence of "F centers." It is a simple matter to prove the validity of his assumption by mathematical means. The above equation is used to determine the constant, "k," for (1) NaCl and (2) CaF_2. In Table 6 the pertinent figures relating to these equations are given.

A Theory of Color

The writer proposes a theory of the color of fluorite which has much in common with proposals made by Mollwo (1934) and Göbel (1931).

TABLE 6. DATA PERTAINING TO F CENTERS IN CALCIUM FLUORIDE AND SODIUM CHLORIDE

Compound	Wave Length	Frequency	$(a_0)^2$	k
CaF_2	4000 Å	$.75\times10^{15}$	29.8	2.23×10^{16}
NaCl	4400 Å	$.68\times10^{15}$	32.0	2.18×10^{16}

The values for "k" are within 2.5% of each other.

The short wave length absorption maximum (380 to 405 mμ) is ascribed to "F centers" such as occur in alkali halides. The long wave length absorption maximum (575 to 650 mμ) is ascribed to colloidal calcium. The smallest colloidal particles cause absorption in the red region (green fluorite). An increase in size of colloids causes the absorption maximum to be displaced first into the orange range, then finally into the yellow causing blue and violet colors, respectively.

Evidence from this Investigation

Dark field observations, lattice constant determinations, spectrographic analyses, refractive index determinations, and x-radiation experiments have proved to be especially helpful in developing a theory of color.

Dark field observations made in the course of this investigation are in good agreement with those made earlier by Göbel. Light scattering centers were smallest in green fluorite, of intermediate size in blue fluorite and largest in violet fluorite. The long wave length absorption maximum is thus attributed to colloidal calcium by the writer. This view is strengthened (see below) by refractive index data and x-radiation results.

The short wave length absorption maximum (in most cases) is attributed to the presence of "F centers." Support for this stand is obtained by use of the formula $(V_{\max})(d^2)=k$, which Pohl has developed in studying "F centers" in alkali halides. The frequency corresponding to 4000 Å (the short wave length maximum) and the square of a_0 are substituted in the equation. The value obtained for k is within 2.5% of k for sodium chloride.

Spectrographic analyses fail to reveal any correlation between the color of fluorite and the content of rare earths or transition elements, noted coloring agents. The only observation which can be made is this: all three fluorites containing lanthanum are green. In general, the violet fluorites are the purest; they are remarkably free of rare earth elements. Thermoluminescence experiments indicate the prevalence of rare earths in green fluorites.

A further line of evidence supports the conclusions drawn by the writer. It has been pointed out that colored fluorites are characterized by refractive indices which are either considerably higher or remarkably lower than the value for optical fluorite. All fluorites in which the short wave length absorption maximum is prominent, i.e., yellow or brown specimens, have indices which are higher than normal. Fluorites in which the long wave length maximum is prominent have refractive indices which are either higher (eight specimens) or lower (ten specimens) than normal. It has been shown that in some cases elevated indices can be traced to highly refractive impurities. Of the eight long wave length maximum specimens seven contain such minor elements. But of the eight yellow-brown specimens only two contain such impurities. We are now in a position to make a generalization: Fluorites with principal absorption at long wave lengths are usually characterized by abnormally low refractive indices unless minor constituents obscure the effect; fluorites with principal absorption at short wave lengths are characterized by abnormally high refractive indices. Anomalous indices of refraction would be accounted for by departure from the stoichiometric ratio of the calcium fluoride formula. Thus, fluorine deficiency compensated for by colloidal calcium would explain abnormally low refractive indices; and a calcium excess, present as elemental calcium in structural holes, would account for elevated indices. In short, the charge requirement in each case is satisfied by partial neutralization of calcium. Omission of fluorine satisfies the space requirements for formation of colloidal calcium in the one case. In the other case it must be pointed out that it is rather difficult to imagine the large calcium *atom* fitting into a structural hole. The calcium atom has nearly twice the radius of the divalent calcium ion. But the separation of the calcium atom and its valence electrons, i.e., formation of an "F center," makes the picture easy to visualize. A hole in the fluorite structure could easily contain a divalent calcium ion.

The striking effect of x-radiation on five yellow and brown fluorites is readily explained by the writer's theory. Atomic calcium, which causes "F centers" in yellow-brown fluorite, is believed to coagulate into colloidal aggregates which produce the blue color of irradiated fluorite. Presumably fluorine must migrate in the crystal to permit this coagulation. Mollwo's experiment of electron introduction into fluorite has proved that fluorine migration is a feasible process.

However, not all brown and yellow fluorites can be considered to contain "F centers." Specimens from Clay Center and Cave-in-Rock do not show striking color change when irradiated. Their yellowish white ultraviolet fluorescence suggests that color may be the result of enclosed hydrocarbons. Brown Weardale fluorite also fails to exhibit the irradiation effect. Perhaps as suggested by Přzibram (1938) the color is due to bivalent europium which is known to be present.

Blue material from Livingston Co., Kentucky, is unusual in that it has an unusually high refractive index without the presence of an impurity to explain the index. Associated with the blue fluorite is yellow fluorite whose index of refraction is identical within the limits of experimental error. It is suggested that colloidal calcium in the blue specimen resulted from coagulation of "F centers" formerly present.

The fact that artificial irradiation does not change the index of refraction is regarded as support for the present hypothesis. If x-radiation merely causes a coarsening of pigment particle size it would not be expected to effect a change in index. No change in density would be experienced by the irradiated substance.

The Mechanism of Color Origin

Two opposite points of view have been taken on the question of the mechanism of color origin. According to the prevalent school of thought color in fluorite is caused by radioactivity. We have seen that Schilling (1926) and Göbel (1931) attribute the formation of colloidal calcium to a partial destruction of the fluorite structure by radioactive influences. It is also possible that color is of primary origin. Evidence has been cited above which points to such an explanation. Přzibram (1934) concludes that the size of colloidal sodium particles in halite varies directly with the rate of growth. Macroscopic structural features in fluorite suggest that color is a primary property of the mineral. Color-zoning is commonly observed, especially in violet fluorite. Perhaps, as Přzibram suggests for halite, a relation exists between rate of crystal growth and size of colloidal particles.

The writer believes it is possible that color in fluorite is not infrequently produced by a defect structure. Omission of fluorine ions could result in the presence of colloidal calcium. Alternately, if excess calcium ions were caught in structural holes they would have to become neutral. In this manner F centers could come about—a natural form of additive coloring. This explanation is in agreement with refractive index findings reported in an earlier section.

The presence of large amounts of rare earths in green fluorites is capable of an explanation without invoking any particular rare earth ion to perform the work of pigment. Přzibram (1938) has demonstrated that europium exists in the bivalent state at 300–400° C. whereas at lower temperatures it assumes the trivalent form. A fluorite crystallizing at a high temperature could take up bivalent rare earth ions in its structure. Upon cooling the rare earths might oxidize to the trivalent state reducing adjacent calcium ions. Reduced calcium might then coagulate into small particles which characterize green fluorite.

REFERENCES

1. ALIMARIN, I. P., AND AREST-YAKUBOWICH, R. E., *Bull. Soc. Naturalists, Moscou*, ser. 2, **42**, 575–583 (1934).
2. BLOUNT, B., AND SEQUEIRA, J. H., *Jour. Chem. Soc. London, Trans.*, **115**, 705–709 (1919).
3. BRAY, J. M., *Am. Mineral.*, **27**, 769–775 (1942).
4. CHANG, TING-CHAO, *J. Shanghai Sci. Inst.*, no. 2, 115–155 (1943).
5. CORK, J. M., *Phys. Rev.*, **62**, 80–81 (1942).
6. DOELTER, C., *Tschermaks Min., Petr. Mitt.*, **38**, 456–463 (1925).
7. DOELTER AND LEITMEIER, Handbuch der Mineralchemie, **4**, pt. 3, 193–269 (1931.)
8. DOMANGE, L., *Compt. Rend. Acad. Sci.*, Paris, **194**, 1667–1669 (1932).
9. DUDENHAUSEN, H., *Neues Jahrb. für Min.*, **i**, 8–29 (1904).
10. EYSANK, E., *Sitz.-ber. Akad. Wiss. Wien, Math.-naturw. Kl.*, Abt. IIa, **145**, 387–406 (1936).
11. GARNETT, C. S., *J. Chem. Soc. London, Trans.*, **117**, 620–622 (1920).
12. GIFFORD, W. J., *Proc. Royal Soc. London*, **70**, 329–340 (1902).
13. GIFFORD, W. J., *Proc. Royal Soc. London*, Ser. A, **84** (1910).
14. GÖBEL, L., *Zeits. Krist.*, **76**, 457 (1931).
15. GUNNELL, E. M., *Am. Mineral.*, **18**, 68–73 (1933).
16. HABERLANDT, H., *Sitz.-ber. Akad. Wiss. Wien, Math.-naturw. Kl.*, Abt. II*a*, **143**, 591–596 (1934).
17. HABERLANDT, H., *Sitz.-ber. Akad. Wiss. Wien, Math.-naturw. Kl.*, Abt. II*a*, **144**, 663–666 (1935).
18. HABERLANDT, H., *Sitz.-ber. Akad. Wiss. Wien, Math.-naturw. Kl.*, Abt. II*a*, **146**, 1–10 (1937).
19. HABERLANDT, H., *Sitz.-ber. Akad. Wiss. Wien, Math.-naturw. Kl.*, Abt. II*a*, **147**, 137–150 (1938).
20. HABERLANDT, H., *Chemie der Erde*, **13**, 212–230 (1940).
21. HABERLANDT, H., KARLIK, B., AND PŘZIBRAM, K., *Sitz.-ber. Akad. Wiss. Wien, Math.-naturw. Kl.*, Abt. II*a*, **144**, 77–83 (1935).
22. HABERLANDT, H., KARLIK, B., AND PŘZIBRAM, K., *Sitz.-ber. Akad. Wiss. Wien, Math.-naturw. Kl.*, Abt. II*a*, **144**, 135–140 (1935).
23. HABERLANDT, H., KARLIK, B., AND PŘZIBRAM, K., *Sitz.-ber. Akad. Wiss. Wien, Math.-naturw. Kl.*, Abt. II*a*, **144**, 141–149 (1935).
24. HABERLANDT, H., AND SCHIENER, A., *Zeits. Krist.*, **90**, 193–214 (1935).
25. HLAWATSCH, C., *Zeits. Krist.*, **27**, 605–607 (1897).
26. HOFFMANN, J., *Chemie der Erde*, **11**, 368–374 (1937).
27. HUGHES, A. L., *Review of Modern Physics*, **8**, 294–315 (1936).
28. HUMPHREYS, W. J., *Astrophys. Jour.*, **20**, 266–272 (1904).
29. HUMPHREYS, W. J., *Astrophys. Jour.*, **22**, 157 (1905).
30. IWASE, E., *Inst. Phys. and Chem. Research, Tokyo*, Scient. Papers, **22**, 233–241 (1933).
31. IWASE, E., *Inst. Phys. and Chem. Research, Tokyo*, Scient. Papers, **23**, 22–23 (1933)
32. IWASE, E., *Inst. Phys. and Chem. Research, Tokyo*, Scient. Papers, **23**, 153–161 (1934).
33. IWASE, E., *Inst. Phys. and Chem. Research, Tokyo*, Scient. Papers, **23**, 212–223 (1934).
34. IWASE, E., *Bull. Inst. Phys. and Chem. Research, Tokyo*, **21**, 61–65 (1942).

35. KELLERMANN, E. W., *Sitz.-ber. Akad. Wiss. Wien, Math.-naturw. Kl.*, Abt. II*a*, **146,** 115–144 (1937).
36. LEITMEIER, H., *Tschermaks Min., Petr. Mitt.*, **38,** 591–598 (1925).
37. MELLOR, J. W., A Comprehensive Treatise on Inorganic and Theoretical Chemistry, **II,** 538; **III,** 688–696 (1923).
38. MERKADER, S., *Sitz.-ber. Akad. Wiss. Wien, Math.-naturw. Kl.*, Abt. II*a*, **149,** 349–365 (1940).
39. MERWIN, H. E., *Am. Jour. Sci.*, **32,** 429–432 (1911).
40. MOLLWO, E., *Nachr. Ges. Wiss. Göttingen*, Fachgruppe 2, **1,** 79–89, (1934).
41. MORGANTE, S., *Periodico Min. Roma*, **10,** 379–396 (1939).
42. MORRISON, R. B., *Am. Mineral.*, **20,** 780–790 (1935).
43. MORSE, H. W., *Proc. Am. Acad. Arts, Sci.*, **41,** 587–613 (1905).
44. MUKHERJEE, B., *Indian J. Physics*, **22,** 221–228 (1948).
45. NORTHUP, M. A., AND LEE, I. O., *Jour. Opt. Soc. Am.*, **30,** 206–223 (1904).
46. PRINGSHEIM, P., AND VOGEL, M., Luminescence of Liquids and Solids, Interscience Publishers (1943).
47. PŘZIBRAM, K., *Sitz.-ber. Akad. Wiss. Wien, Math.-naturw. Kl.*, Abt. II*a*, **138,** 263–269 (1929).
48. PŘZIBRAM, K., *Sitz.-ber. Akad. Wiss. Wien, Math.-naturw. Kl.*, Abt. II*a*, **143,** 489–496 (1934).
49. PŘZIBRAM, K., *Zeits. Physik,* **102,** 331–352 (1936).
50. PŘZIBRAM, K., *Zeits. Physik,* **107,** 709–712 (1937).
51. PŘZIBRAM, K., *Nature,* **139,** 329 (1937).
52. PŘZIBRAM, K., *Neues Jahrl. Mineral., Geol.*, Ref. **I,** 356–357 (1937).
53. PŘZIBRAM, K., *Nature,* **141,** 970 (1938).
54. PŘZIBRAM, K., *Sitz.-ber. Akad. Wiss. Wien, Math.-naturw. Kl.*, Abt. II*a*, **147,** 261–270 (1938).
55. PŘZIBRAM, K., *Acta Phys. Austriaca,* **I,** 131–136 (1947).
56. ROLL, K. H., *Yale Sci. Mag.*, **19,** no. 2, 10–11, 26, 32 (1944).
57. SCHILLING, A., *Neues Jahrb. Min., Abt. A.*, **53,** 241–265 (1926).
58. STARIK, I. E., KRAVCHENKO, L. L., AND MELIKOVA, O. S., *Comptes Rendus de l'Acad. des Sciences de l'URSS*, **32,** no. 4, 254–255 (1941).
59. URBAIN, G., *Comptes Rendus de l'Acad. des Sciences, Paris*, **143,** 825–827 (1906).
60. URBAIN, G., *Annales de Chimie et Physique*, **18,** 222–386 (1909).
61. VAN DER LINGEN, S., *Zeits. Physik*, **53,** 581–586 (1929).
62. WICK, F. G., *Phys. Rev.*, **24,** 272–282 (1924).
63. WICK, F. G., *Jour. Opt. Soc. Am.*, **21,** 223–231 (1931).
64. WICK, F. G., *Jour. Opt. Soc. Am.*, **27,** 275–285 (1937).
65. WÜLFING, E. A., *Neues Jahrb. für Mineralogie*, **ii,** 166–169 (1907).
66. WYROUBOFF, G., *Bull. de la Soc. Chim. de Paris*, 16 (1866).
67. YOSHIMURA, J., *Inst. of Phys. and Chem. Research, Tokyo*, Scient. Papers, **20,** 170–177 (1933).
68. YOSHIMURA, J., *Inst. of Phys. and Chem. Research, Tokyo*, Scient. Papers, **23,** 224–247 (1934).

Manuscript received March 3, 1952.

HURLBUTITE, $CaBe_2(PO_4)_2$, A NEW MINERAL

MARY E. MROSE, *State Teachers College, Salem, and Harvard University, Cambridge, Massachusetts**

ABSTRACT

Hurlbutite, $CaBe_2(PO_4)_2$, is a new mineral from the Smith mine, Chandler's Mill, Newport, New Hampshire. Crystals are orthorhombic and stout prismatic [001] in habit with {001}, {010}, {110}, {101}, {201}, and {311} doubtful. Faces often delicately etched with striations on {110}. Unit cell dimensions: $a_0 = 8.29$ Å, $b_0 = 8.80$, $c_0 = 7.81$ ($a_0 : b_0 : c_0 = 0.9420 : 1 : 0.8875$), with the space group $D_{2h}^1 - Pmmm$. Colorless to greenish white. Hardness 6. Specific gravity 2.877 (meas.), 2.88 (calc. for four formula-units per cell). Cleavage not observed. Optically biaxial negative (−) with $nX = 1.595$, $nY = 1.601$, $nZ = 1.604$; $2V = 70°$; $r > v$, weak; $X = b$, $Y = c$. Analysis gave: CaO 21.84, BeO 21.30, P_2O_5 56.19, insol. 0.76; total 100.09. The strongest *x*-ray powder lines are 3.67 Å (10), 3.03 (9), 2.78 (9), and 2.21 (9). The name *hurlbutite* is proposed for the mineral in honor of Cornelius S. Hurlbut, Jr., Professor of Mineralogy, Harvard University.

INTRODUCTION

The mineral here described as hurlbutite was first found as a large broken crystal on the dump at the pegmatite known as the Smith mine, Chandler's Mill, Newport, New Hampshire by Dr. Judith Weiss-Frondel in August, 1949. Within five minutes of the original find the writer picked up a matrix specimen containing two crystals of hurlbutite embedded in light-smoky quartz in the same general section of the dump. It is very probable that these original specimens would have been overlooked had it not been for the yellow stain on the surface of the crystals. Successive visits to the same locality were not fruitful until the spring and summer of 1951 when nineteen additional crystals were collected by various members of the mineralogy department at Harvard. Other than the aforementioned crystals the only other specimens of hurlbutite known to have been found were by Gunnar Bjareby of Boston and Curt G. Segeler of Brooklyn, New York.

OCCURRENCE AND PARAGENESIS

The pegmatite at which hurlbutite was found is located at Chandler's Mill, Sullivan County, in the township of Newport, New Hampshire (43°21′27″ North and 72°15′00″ West). It was originally opened for the production of mica and is known locally as the Smith mine, being on the land owned by George and Agnes Smith. The mine is easily reached by a dirt road on the south side of Sugar River, about 4½ miles west of the center of Newport. It lies at the boundary of the Claremont and Sunapee,

---

* Contribution from the Department of Mineralogy and Petrography, Harvard University, No. 335.

N. H. quadrangles. The pegmatite is an easterly dipping, tabular body with a maximum exposed thickness of approximately 20 feet and a length of at least 300 feet parallel to the strike.

The pegmatite is of the complex type with distinct lithium and phosphate phases. Quartz and albite constitute most of the mass; potash feldspar is noticeably absent. Muscovite and black tourmaline are present in smaller quantities and with albite form a zone extending a few inches from the contact of the pegmatite into the surrounding schist. Large magnesia-rich triphylite crystals for which this locality is noted (Chapman, 1943) occur most characteristically in euhedral crystals up to four inches in length. The triphylite crystals have been found to occur only locally. The pegmatite appears to have been locally traversed by late-stage relatively low-temperature hydrothermal solutions, resulting in the formation of secondary minerals which occur as drusy crystals in small solution cavities—beryllonite, albite, brazilianite in composite growths as well as single crystals, twinned amblygonite crystals, tiny colorless and purple hexagonal prisms of apatite, and siderite.

Observations and conclusions concerning the paragenetic sequence of hurlbutite are made with reservations since no specimens of the mineral have as yet been found *in situ* in the pegmatite. Hurlbutite appears to belong to the early stage hydrothermal period of formation since no crystals have been found in cavities or in such relationship to other minerals in the hand specimens to suggest otherwise. The relationships observed in those specimens collected to date suggest that hurlbutite is later than triphylite but earlier than quartz. The minerals with which hurlbutite has been found directly associated include muscovite, albite, triphylite, massive, light-smoky quartz, and siderite. The sequence of formation appears to have been muscovite-albite-triphylite-hurlbutite-quartz. The best crystals of hurlbutite are those found embedded in the smoky quartz, and when not stained could easily be mistaken for feldspar crystals. Several interesting pseudomorphs of siderite after hurlbutite have been found.

CRYSTALLOGRAPHY

Hurlbutite crystals occur embedded for the most part in a matrix of massive, light-smoky quartz and feldspar. Hurlbutite is orthorhombic. The crystals are stout prismatic [001] in habit, with relatively large development of $c\{001\}$ and $m\{110\}$. They range in size from 4 to 25 millimeters along [110]. The faces are delicately etched and exhibit striations or what may actually be fibration on $\{110\}$. The crystals appear to have grown attached to the matrix by one end of the [100] axis. Two doubly terminated crystals were freed from the embedding material.

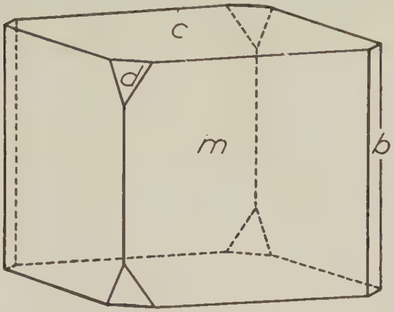

FIG. 1. Hurlbutite crystal of typical habit.

The crystals are rather simple in habit. The forms *c*{001} and *m*{110} are dominant and are truncated by *d*{201} and *b*{010}. On one crystal the form *e*{101} occurred, but only as a very small face. The form to which the symbol *r*(311) has been assigned is uncertain since measurements were possible only on the Goldschmidt two-circle contact goniometer. Because the faces of this form were rounded, the ϕ and ρ angle measurements were found to spread over as much as from 2° to 4° and therefore were not considered reliable enough for angle table calculations. It is without question an {*hkl*} form and its presence is indicative of holohedral symmetry.

Two of the larger crystals were measured on the Goldschmidt two-circle contact goniometer; one small doubly terminated crystal was measured on the reflecting goniometer. An average of the measured angles tabulated below gives the ratio $a:b:c=0.9420:1:0.9017$ which is in fairly good agreement with that derived from *x*-ray study ($a_0:b_0:c_0=0.9420:1:0.8875$).

Forms	*Measured*		*Calculated* (*x*-ray cell)	
	ϕ	ρ	ϕ	ρ
c 001	——	0°00′	——	0°00′
b 010	0°00′	90 00	0°00′	90 00
m 110	46 35	90 00	46 42½	90 00
e 101	90 00	43 15	90 00	43 17½
d 201	90 00	61 59	90 00	62 02½
(?)*r* 311	72 40	71 43	72 34	71 21

An angle table based on the elements derived from *x*-ray study for forms observed on hurlbutite crystals is given in Table 1.

PHYSICAL AND OPTICAL PROPERTIES

Crystals of hurlbutite are colorless to greenish white; when stained, yellow. Transparent to translucent. Cleavage not observed. Fracture conchoidal. Brittle. Hardness 6. Specific gravity 2.877 ± 0.005 (an

TABLE 1. HURLBUTITE: ANGLE TABLE

Orthorhombic; dipyramidal—$2/m\ 2/m\ 2/m$

$a:b:c=0.9420:1:0.8875$ $p_0:q_0:r_0=0.9421:0.8875:1$

$q_1:r_1:p_1=0.9420:1.0615:1$ $r_2:p_2:q_2=1.1268:1.0616:1$

Forms	ϕ	ρ	ϕ_1	$\rho_1=A$	ϕ_2	$\rho_2=B$
c 001	——	0°00′	0°00′	90°00′	90°00′	90°00′
b 010	0°00′	90 00	90 00	90 00	——	0 00
m 110	46 42½	90 00	90 00	42 17½	0 00	46 42½
e 101	90 00	43 17½	0 00	46 42½	46 42½	90 00
d 201	90 00	62 02½	0 00	27 57½	27 57½	90 00
(?)*r* 311	72 34	71 21	41 35½	25 19	19 29	73 30½

average of measurements on 8 different fragments on the Berman microbalance); 2.88 (calculated). Luster vitreous to greasy. Streak white. Difficult to fuse. Very slowly soluble in acids. Not fluorescent in either short-wave or long-wave ultraviolet radiation.

The optical properties of hurlbutite are cited in Table 2 in comparison with those of beryllonite and herderite.

CHEMICAL COMPOSITION

A chemical analysis of one of the original matrix crystals, cited in column 2 of Table 3, proves the mineral to be $CaBe_2(PO_4)_2$. A comparison with the reported analyses of beryllonite and herderite shows that hurlbutite has a higher BeO and P_2O_5 content than either of these beryllium phosphates. *X*-ray studies discussed later in this paper indicate that hurlbutite is not a possible end-member of a series with beryllonite or herderite.

A spectrographic analysis on the same material in the spectral range between 2200 Å and 4300 Å showed that the minor constituents and traces included Si, Al, Na, and Sr.

The cell volume 570 Å and the measured specific gravity, 2.877, give the molecular weight of the cell contents, $M_0=994$. Multiplying this value by the atomic quotients, the experimental cell contents are derived. Assuming the integers given under the theoretical cell contents in Table 3 as correct, the unit cell contents are $Ca_4Be_8(PO_4)_8$ or $4[CaBe_2(PO_4)_2]$.

X-RAY STUDY DATA

Single-crystal work on hurlbutite was done using a fragment of known orientation drilled out from the original crystal found by Dr. Judith Weiss-Frondel. This fragment contained what was assumed to be (001)

TABLE 2. COMPARISON OF SOME PHYSICAL AND OPTICAL PROPERTIES OF HURLBUTITE, BERYLLONITE, AND HERDERITE

	Hurlbutite (Mrose, 1951)	Beryllonite				Herderite		
		(Dana and Wells 1889)			(Palache and Shannon, 1928)	Hydroxyl-herderite (Penfield, 1894)	Herderite (?) (Yatsevitch, 1935)	Herderite (?) (Bertrand in Des Cloizeaux, 1886)
Locality:	Newport, N. H.	Stoneham, Maine			Newry, Maine	Paris, Maine	Topsham, Maine	Stoneham, Maine
Color:	colorless to greenish white	colorless to snow white or pale yellowish				colorless to pale yellowish or greenish white		
Opt. sign:	(−)	(−)			(−)	(−)	(−)	(−)
Indices:								
nX	1.595±0.003	$1.5492_{(\text{Li})}$	$1.5520_{(\text{Na})}$	$1.5544_{(\text{Tl})}$			1.591±0.003	$1.592_{(\text{Na})}$
nY	1.601±0.003	1.5550	1.5579	1.5604	1.558	$1.632_{(\text{Na})}$	1.611±0.003	1.612
nZ	1.604±0.003	1.5604	1.5608	1.5636	1.562		1.619±0.003	1.621
Opt. orient.:	$X=b$, $Y=c$	$X=b$, $Y=a$, $Z=c$				$X\wedge c\sim+87°$, $Y=b$, $Z\wedge c\sim-3°$		
Dispersion:	$r>v$,weak	$r<v$, weak				$r>v$, inclined		
2V (meas.):	70°				medium	72°	75°±5°	66°59′34″
2V (calc.):	70°18′	67°51′	67°56′	67°57′				
Cleavage:	not observed	{010} perfect, {100} good but interrupted, {101} distinct, {001} in traces				{110} interrupted		
Hardness	6	5½-6				5-5½		
G. (meas.)	2.877		2.845		2.806 (Berman)	2.952; 2.95 (hydroxyl-herderite) to 3.01 (hydroxyl-herderite with OH:F=1.5:1)		
G. (calc.)	2.88				2.81	2.94 (hydroxyl-herderite)		
Composition	CaBe$_2$(PO$_4$)$_2$	NaBe(PO$_4$)				CaBe(PO$_4$)(OH, F)		CaBePO$_4$(F, OH)

Table 3. Chemical Analysis and Unit Cell Contents of Hurlbutite

	Weight per cent		Molecular quotients	Atomic quotients	Experimental cell contents (×994/100)	Theoretical cell contents
	1	2				
CaO	21.84	21.99	0.3921	(Ca) 0.392	3.90	4
BeO	21.30	21.44	0.8569	(Be) 0.857	8.52	8
P_2O_5	56.19	56.57	0.3983	(P) 0.797	7.92	8
Insol.	0.76			(O) 3.210	31.92	32
Total	100.09	100.00				

1. Gonyer analysis, 1951.
2. Recalculated to 100% after deducting insoluble.

because of the importance of the form development. Rotation and Weissenberg photographs were taken using copper radiation and nickel filter, and rotating about the *c*, *b*, and *a* axes of the fragment. The axes were located by the oscillating technique on the Weissenberg unit. The Laue symmetry D_{2h} was clearly observed for the 0- and *n*-level Weissenberg photographs and the orthorhombic character of the mineral hence confirmed. No space group extinctions were found on any of the Weissenberg photographs. If the crystal class is taken to be dipyramidal as is indicated by the form development and absence of piezoelectricity, the space group is definitely established by the diffraction effects as $D_{2h}^1 - Pmmm$.

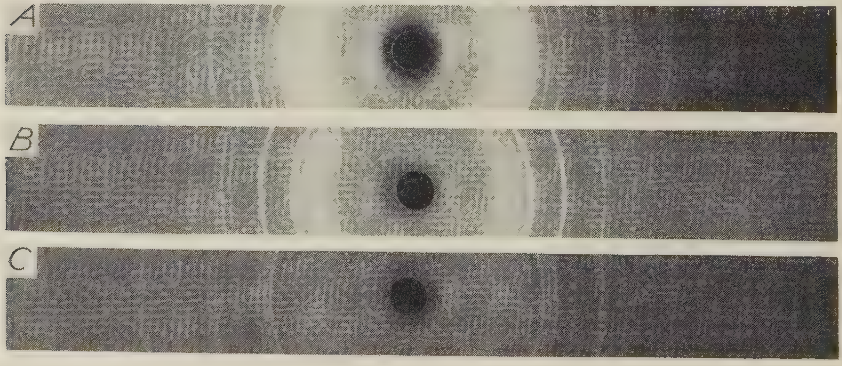

Fig. 2. *X*-ray powder photographs taken with Cu/Ni radiation. A. Hurlbutite. Smith mine, Newport, New Hampshire. B. Beryllonite. Stoneham, Maine. C. Herderite. Palermo mine, North Groton, New Hampshire.

The powder photograph taken with copper radiation was indexed in terms of the dimensions of the cell found by single-crystal study. Because of the large number of solutions possible for the lines of high sin θ, the *hkl*'s for lines with *d*-spacings less than 1.969 Å were not determined. The indices thus obtained are listed in Table 4 and are consistent with the space group $D_{2h}^1 - Pmmm$.

TABLE 4. POSSIBLE INDICES FOR REFLECTIONS OCCURRING ON POWDER PHOTOGRAPH OF HURLBUTITE—$CaBe_2(PO_4)_2$

Copper radiation ($\lambda = 1.5418$ Å), nickel filter
(Indices for *d* values below 1.969 have been omitted.)

Line	*d* (meas.)	*hkl*	*d* (calc.)	Line	*d* (meas.)	*hkl*	*d* (calc.)
1	5.83	011	5.84			311	2.498
2	3.91	002	3.906	12	2.50	013	2.496
		120	3.887			103	2.484
3	3.67	201	3.662			230	2.395
4	3.50	102	3.510	13	2.40	113	2.390
		121	3.480			222	2.388
5	3.39	211	3.381	14	2.29	231	2.291
6	3.28	112	3.279			203	2.205
7	3.03	220	3.018	15	2.21	040	2.200
8	2.93	030	2.933	16	2.17	312	2.185
		022	2.921			123	2.163
9	2.86	202	2.848	17	2.10	140	2.127
		221	2.815			041	2.117
10	2.78	130	2.766	18	2.06	400	2.072
		300	2.765			410	2.018
		310	2.636	19	2.02	330	2.011
11	2.64	131	2.607			401	2.003
		003	2.604	20	1.969	223	1.970

In Table 5 are listed the *x*-ray powder spacing data for hurlbutite, beryllonite, and herderite; the powder photographs of these minerals are shown in Fig. 2. The *d*-spacings and intensities of hurlbutite are distinct from those of beryllonite and herderite. The unit cell dimensions of hurlbutite, beryllonite, and herderite are cited in Table 6. The *x*-ray, chemical, and optical data all confirm hurlbutite as a new and distinctive mineral species.

A structural resemblance may exist between hurlbutite and beryllonite. It may be noted that the unit cell volumes are nearly in the ratio of 2 to 3, and that in equal volumes in arbitrary units the numbers of Be, O, and P atoms are identical with $Ca^{+2} = 2\ Na^{+1}$.

TABLE 5. *X*-RAY POWDER SPACING DATA FOR HURLBUTITE, BERYLLONITE, AND HERDERITE

Copper radiation (λ=1.5418 Å), nickel filter

Hurlbutite $CaBe_2(PO_4)_2$		Beryllonite $NaBe(PO_4)$		Herderite $CaBe(PO_4)(OH,F)$	
Intensity	*d* (meas.)	Intensity	*d* (meas.)	Intensity	*d* (meas.)
2	5.83	4	4.44	2	5.99
5	3.91	2	4.11	2	4.77
10	3.67	6	3.92	3	3.79
7	3.50	9	3.65	1	3.65
2	3.39	2	3.52	5	3.43
6	3.28	½	3.40	½	3.33
9	3.03	1	3.25	10	3.14
1	2.93	1	3.04	6	3.00
1	2.86	½	2.91	8	2.86
9	2.78	10	2.84	½	2.75
1	2.64	3	2.70	6	2.55
7	2.50	1	2.64	2	2.46
6	2.40	½	2.56	1	2.40
1	2.29	2	2.44	3	2.34
9	2.21	6	2.37	5	2.26
6	2.17	7	2.28	7	2.20
½	2.10	1	2.22	1	2.11
5	2.06	1	2.19	1	2.05
5	2.02	3	2.11	4	2.00
5	1.969	2	2.05	½	1.957
1	1.951	4	1.965	½	1.922
1	1.833	4	1.910	4	1.881
1	1.792	2	1.821	4	1.781
5 broad	1.729	2	1.755	1	1.749
4	1.691	½	1.719	3	1.722
3	1.635	1	1.675	1	1.684
2	1.596	2 diffuse	1.593	5	1.650
½	1.572	3	1.526	½	1.573
3	1.523	2	1.508	½	1.547
1	1.496	4 diffuse	1.443	½	1.506
6	1.462	1	1.328	½	1.465
4	1.428	2	1.218	½	1.443
6	1.387			½	1.419

(16 additional lines with *d* values below 1.387 have been omitted.)

TABLE 6. UNIT CELL DIMENSIONS OF HURLBUTITE, BERYLLONITE, AND HERDERITE

	Hurlbutite (Newport, N. H.) (Mrose, 1951)	Beryllonite (Locality unknown) (Gossner and Besslein, 1934)	Herderite (Topsham, Me.) (Strunz, 1936)
Cryst.	Orthorhombic; dipyramidal (2/*m* 2/*m* 2/*m*)	Monoclinic; prismatic (2/*m*) (marked ortho. pseudo-symmetry)	Monoclinic; prismatic (2/*m*)
a_0	8.29 Å	8.15 Å	4.81 Å
b_0	8.80	7.78	7.70
c_0	7.81	14.28	9.82
$a_0:b_0:c_0$	0.9420:1:0.8875	1.0477:1:1.8260	0.625:1:1.276
β		90°00′	90°06′
Cell volume	570 Å	894 Å	361 Å
Cell contents	$Ca_4Be_8(PO_4)_8$	$Na_{12}Be_{12}(PO_4)_{12}$	$Ca_4Be_4(PO_4)_4(OH, F)_4$
Space group	D_{2h}^1-Pmmm	$C_{2h}^5-P2_1/c$	$C_{2h}^5-P2_1/c$

NAME

This mineral is named *hurlbutite* after Professor Cornelius S. Hurlbut, Jr., of the Department of Mineralogy and Petrography, Harvard University. The name is particularly appropriate in view of Prof. Hurlbut's interest and studies in the beryllium-bearing minerals. The name hurlbutite has already appeared in the literature, having been given gratuitously by Gagarin and Cuomo (1949) to the species wurtzite-4H described by Frondel and Palache (1948, 1950). The prior usage is unnecessary and unjustifiable and is not here recognized. Fleischer (1951) in commenting on the mineral names proposed by Gagarin and Cuomo in their paper, and also in private communication (1951) with the writer on the proposed naming of this new mineral states: "It seems to me that mineralogists should not feel bound by any names proposed in this paper." Professor Frondel concurs in this opinion.

ACKNOWLEDGMENTS

The writer is indebted to Dr. Judith Weiss-Frondel for the use of a fragment from her crystal for the single-crystal *x*-ray work, Mr. Gunnar Bjareby for the loan of his single crystal for goniometric measurements, Dr. Harold R. Harrison of Harvard University and the University of Rhode Island for the spectrographic analysis, and Dr. Clifford Frondel for helpful suggestions and aid during the progress of this investigation and for critical reading of the manuscript.

REFERENCES

CHAPMAN, C. A., Large magnesia-rich triphylite crystals in pegmatite: *Am. Mineral.*, **28,** 90–98 (1943).

DANA, E. S., AND WELLS, H. L., Description of the new mineral, beryllonite: *Am. J. Sci.*, **37,** 23–32 (1889).

DES CLOIZEAUX, A., Note sur la véritable valeur de l'indice moyen de la Herdérite de Stoneham: *Bull. soc. min.*, **9,** 141–143 (1886).

Fleischer, M., New mineral names: *Am. Mineral.*, **36**, 638–641 (1951).

Frondel, C., and Palache, C., Three new polymorphs of zinc sulphide: *Science*, **107**, 602 (1948); *Am. Mineral.*, **35**, 29–42 (1950).

Gagarin, G., and Cuomo, J. R., Algunas proposiciones sobre nomenclatur mineralogica: *Comun. Inst. Nacal. Invest. Cienc. Naturales, Museo Argentino Cienc. Naturales "Bernardino Rivadavia," Cienc. Geol.*, **1**, No. 5 (1949).

Gossner, B., and Besslein, J., Ein Beitrag sur Kenntnis des Beryllonites: *Cbl. Min., Abt.* **A**, 144–150 (1934).

Penfield, S. J., On the crystallization of herderite: *Am. J. Sci.*, **47**, 329–339 (1894).

Strunz, H., Datolith und herderit: *Zeits. Krist.*, **93**, 146–150 (1936).

Yatsevitch, G. M., The crystallography of herderite from Topsham, Maine: *Am. Mineral.*, **20**, 426–437 (1935).

Manuscript received April 30, 1952.

EFFECT OF HEAVY CHARGED PARTICLE AND FAST NEUTRON IRRADIATION ON DIAMONDS

Joseph G. Hamilton, Thomas M. Putnam, and Martin L. Ehrmann,* *Crocker Laboratory, University of California, Berkeley*

Abstract

The color changes in diamonds produced by irradiation with high energy nuclear particles, neutrons, deuterons and alpha particles have been studied. The bombarding deuterons and alpha particles were accelerated to energies of 20 and 40 Mev, respectively, in the Crocker Laboratory 60-inch Cyclotron at the University of California. The permanence of the color under various conditions and the depth of the changes within the stone have been investigated. A summary of the work in this field together with a discussion of the results of this series of experiments will be presented.

Changes in color of a large variety of crystals have been reported as a result of exposing them to ultraviolet light, x-rays, cathode rays, and the radiations of radon and its decay products, which, of course, include alpha particles.[1,2,3] The information available from these sources is somewhat conflicting in character, particularly with reference to the variations in permanence of color changes produced in crystals of the alkali halides. This communication is primarily concerned with color changes produced in the diamond and accordingly color effects produced by ionizing radiation on other substances will be referred to but briefly.

The first report of induced color changes in crystals by irradiation with artificially accelerated, positively charged nuclear particles has been given by Cork.[4] His experiments included the bombardment of alkali halides, fluorite, quartz, beryl, and diamond, with 10 Mev deuterons produced by the cyclotron at the University of Michigan. The color changes produced in the alkali halides were similar to those reported by Bayley, though no comment was made in Cork's communication as to the degree of permanence of these changes. However, the observation was made that the color changes in the alkali halides disappeared upon heating to about 220° C. In the case of the diamond he made the observation that stones of an amber tint assumed a green coloration equivalent to that of the rare naturally occurring green diamond. It was stated that heating to approximately 900° C. for an unspecified period of time caused the green diamonds to revert to their original color. Interestingly, a comment is made concerning the production of a color change in some of the stones which was bluish in character. No statement was made as to the number of stones irradiated or the specific conditions of the experiment, namely, the duration and intensity of the deuteron bombardment, or whether or not these bombardments were performed *in vacuo* or in the presence of air or some inert gas. A final statement is made that this transformation of color in the irradiated diamonds is presumed to be permanent at room temperature.

---

* Martin L. Ehrmann Co., Los Angeles, California.

[1] Goldstein, *Stiz. d.K. Akad. Wiss.*, Berlin, p. 937 (1894).

[2] Doelter, Das Radium und die Farben (1910).

[3] Bayley, P. L., *Phys. Rev.*, **24**, 495 (1924).

[4] Cork, J. N., *Phys. Rev.*, **62**, 80 (1942).

Green diamonds are known to occur naturally; however, diamonds of such a color which are of gem quality are extremely rare. For this reason, over a number of years, many attempts have been made to artificially produce this effect, usually employing radon as the source of irradiation. This procedure in the main was never very satisfactory for several reasons. First, such stones remained radioactive due to the presence of radium-D (Pb^{210}) which has a half-life of 22 years and which is a radioactive descendant of radon. In addition, radium-D has two radioactive daughters, namely radium-E (Bi^{210}) and radium-F (Po^{210}). It was a frequent misunderstanding that the stones themselves were made radioactive by treatment with radon, but actually the radioactivity was due to the deposition on the surface of the exposed stones of radium-D and its decay products. Inasmuch as the depth of penetration of the alpha particles from radon and its descendants was of the order of 2 microns, attempts to polish off the deposited radioactivity frequently resulted in the removal of the extremely thin superficial layer which had been subjected to alpha particle irradiation. Due to the fact that the associated beta particles and gamma radiation were not only less energetic but had far less specific ionization, their action was negligible in most instances.

Prior to the first reported irradiation of diamonds by high energy deuterons, some preliminary experiments of this character were carried on in 1941, using the cyclotron in the Department of Physics at Harvard University.[5] In these experiments small stones were used, again ranging in color from yellow to brown, which are commonly described as Cape stones. In these experiments 12 Mev deuterons were employed and the radiation was for three minutes with a beam intensity of 5 microamperes. At this point it is appropriate to indicate that deuterons in the energy range of 10 to 12 Mev can penetrate to a maximum depth of approximately 0.2 mm. or 200 microns, which is far greater than can be employed by using alpha particles from naturally occurring radioactive elements. In addition, the only appreciable residual radioactivity produced in stones by this type of irradiation was due to the presence of radioisotopes of nitrogen, the principal one being N^{13} with a half-life of 10 minutes. Obviously this radioactivity will diminish to the vanishing point after an interval of only a few hours. The question was raised as to the production of artificial radioactivity by this type of irradiation from the transmutation of elements other than carbon present in such diamonds. This is an insignificant factor for three reasons. First, these contaminating elements are present in very minute amounts, whose total is of the order of 0.01 per cent or less in stones which might be suitable for treatment by this process. Second, the volume of material irradiated was so small that only an extremely minute amount of foreign material would be exposed to the possibility of undergoing transmutation. Third, an investigation by spectrographic analysis at the Massachusetts Institute of Technology, revealed the presence of thirteen different elements. These were usually found in the following order of abundance: aluminum, silicon, calcium, magnesium, copper, barium, iron, sodium, silver, titanium, chromium, and lead. Aluminum, silicon and calcium were apparently present in almost all of the diamonds subjected to spectrographic analysis. Those diamonds which showed strong yellowish tints were observed to contain iron and titanium. The significance of the spectrographic analysis from the point of view of induced radioactivity is the fact that the two most commonly found foreign elements would result in the production of practically undetectable amounts of long-lived radioactivity as the result of the deuteron bombardment.

---

[5] Ehrmann, M. L., Unpublished data.

After it was discovered that the effect reported by Cork could be duplicated, larger diamonds were bombarded and in this instance a few white stones of gem quality, as well as stones possessing varying degrees of yellow coloration were included. In most instances all of the stones changed to the same tint of green except those that were initially of a fine white gem quality, and they became bluish green; those of a brown-color, became a dirty olive-green. It would seem probable that the last effect mentioned might be due to the combination of the original color of the diamond and having superimposed upon it the green changes produced by irradiation.

The diamonds which had been bombarded appeared to permanently retain their change in color, even when exposed for prolonged intervals to the sun or to artificial light at room temperatures. At this time it was also demonstrated that if the bombarded stones were re-cut to a depth greater than the range of the deuterons the green coloration was lost and the stone resumed its original color.

Recently at the University of California a series of detailed and more systematic experiments were conducted using the 60-inch Cyclotron at the Crocker Laboratory. Diamonds of varying sizes, ranging from $\frac{1}{2}$

carat to 30 carats, were employed. The majority of these were cut stones with either a brilliant or emerald cut. The colors ranged from small white stones of gem quality to those of quite dark brown. The bombarding particles were 40 Mev alpha particles, 20 Mev deuterons, and fast neutrons. A significant proportion of the fast neutrons possessed energies ranging from 10 to 20 Mev, the source being a deuteron bombarded beryllium target. A few of the diamonds were bombarded with deuterons and alpha particles within the evacuated target chamber; however, the majority of the stones which were exposed to alpha particles were mounted within a small chamber through which was passed a stream of helium. In this case the alpha particles entered the chamber after passing through a 0.001 inch aluminum foil which was used to maintain the vacuum within the cyclotron itself. The purpose of using alpha particles rather than deuterons arose from the fact that the amount of induced radioactivity in the aluminum mounts used to support the diamonds was very small as compared to that which would have been present if deuterons had been employed as the bombarding particles. This procedure made it possible to handle the aluminum mounts with safety a few minutes after the diamonds had been bombarded, thus permitting the treatment of a larger number of stones in the same length of time and the occasional re-irradiation of a stone necessary to achieve the desired degree of green coloration. The target mount which contained the diamonds was covered with a 0.00025 inch sheet of tantalum foil, the purpose being primarily to hold the stones in place during the irradiation.

The presence of an atmosphere of helium was found to be mandatory; otherwise, the diamonds would not turn green but rather appeared burned. It was observed that they turned golden, very dark yellowish, or brown in color. This was found to be superficial in character and usually corresponded to the maximum range of the alpha particles at this energy in the diamonds. The depth of penetration varied from 0.3 mm. to less than 0.1 mm. depending upon the orientation of the stone with respect to the alpha particle beam. This apparent burned appearance was interpreted as being due to the combined effects of (a) the stones were raised to a considerable temperature during the period of bombardment, (b) the presence of oxygen and nitrogen in the air, and (c) the oxidation of the tantalum foil.

After considerable preliminary experimentation it was found that the best results were achieved if the stones were bombarded for approximately 0.5 microampere hours with a beam current ranging from 5 to 10 microamperes. Inasmuch as the helium provided relatively little cooling, it was feared that the use of higher beam currents would be destructive, since the energy from the beam which would have to be dissipated as heat was considerable. The amount of heat varied depending on the size of the stone and since the intensity of the beam was not uniform, it also varied with respect to the position of the stone in the target mount.

As a first approximation, the energy dissipated from the beam was of the order of several watts per square centimeter. This may seem like a small amount but consideration must be given to the fact that the range of penetration was quite small. Thus this value of energy dissipation must be expressed in terms of watts per unit volume rather than watts per unit area. In this case the value is increased by nearly a factor of 100.

Most of the stones subjected to alpha particle bombardment were brilliant cut. They were usually irradiated only on the culet, since it was noted that this gave essentially the same results as stones irradiated both on the culet and table. Stones irradiated on the table alone showed a smaller color change, resulting in a very pale green. The effect of irradiating the stone on the culet alone is undoubtedly due to the many internal reflections within the diamond.

The effect of alpha particle irradiation did not appear to be significantly different whether the stones were large or small. The major difficulty encountered, apart from the accidental entry of air into the bombardment chamber, was that occasionally a stone appeared to have received an inadequate amount of bombardment. Under these circumstances, after allowing time for the decay of the short-lived radioisotopes of nitrogen and oxygen produced by the bombardment of the diamond, such a stone was re-irradiated.

As has been noted previously, these stones appeared to retain their color permanently, even under exposure to the sun as well as artificial light. Over a year has elapsed since the first stones were irradiated and these do not appear to have lost any of the original color. Heating the bombarded stones to 1000° C. for one hour in the absence of air will completely remove all of the green color and the diamond resumes its original color, with the exception that under such treatment the stone was usually slightly darker than before irradiation. Re-cutting the stones to a depth greater than the range of the alpha particle penetration completely returns them to the original color and none of the green tinge remains. This is a conclusive test for determining whether a green diamond has been artificially produced by heavy charged particle irradiation. In the case of neutron irradiation, as will be indicated later, the penetration is through the entire stone and re-cutting would not affect the color significantly. Since natural green diamonds have not been heated to a high temperature, the effect of this on the color is unknown, and hence, heating a green diamond might not be conclusive proof as regards its origin of color. Uncut stones likewise turn green in color. This color is retained if the stone is cut in such fashion as not to remove too much of the area into which the alpha particles had penetrated.

On one occasion a number of cut stones were subjected to a prolonged fast neutron irradiation and turned a very pale green. This is assumed to be due to the fact that an insufficient amount of neutron exposure was achieved, since the total neutron flux integrated over the period of irradiation approximated 5×10^{16} neutrons per square centimeter.

The results described here, particularly the effects observed following the alpha particle irradiation of diamond, have demonstrated several facts. First, alpha particles, deuterons, and neutrons are capable of producing a greenish coloration of diamonds. Second, this effect is presumably permanent at room temperatures, even including circumstances under which such stones are directly exposed to sunlight.

Coloration of crystals, which has been alluded to briefly earlier, is believed to be due to the fact that under the conditions of exposure to appropriate irradiation, electrons are displaced from the lattice positions and lie in the space between. These isolated electrons possess the property of absorbing energy from visible light and this energy is then re-emitted at a fixed frequency from these electrons. The intensity of this re-emitted light will vary, depending upon the number of electrons displaced. For example, the irradiation of potassium chloride produces a characteristic bluish-purple color with either deuterons or alpha particles.[6] If the irradiation is sufficiently prolonged, the sample will appear almost black, whereas a pale bluish-purple color results with a relatively small amount of bombardment. In other words, the apparent effect of color change is not due to the difference in the frequency of light emitted but rather to an ever-increasing intensity due to more and more electrons being displaced which can absorb energy from other electrons which have received energy and are re-emitting it in the color characteristic for the particular crystal in question. In the case of the diamond, the same effect has likewise been observed, namely, if too much irradiation is given, the desired green color may become so dark as to give the stone a dark green appearance.

In the past it has been frequently thought that this green coloration was due to the interaction of the radiation with the contaminants within the diamond rather than to a change within the diamond structure itself. However, the available evidence strongly rules out the possibility that the green color is due to contaminants. A number of arguments

---

[6] Unpublished data.

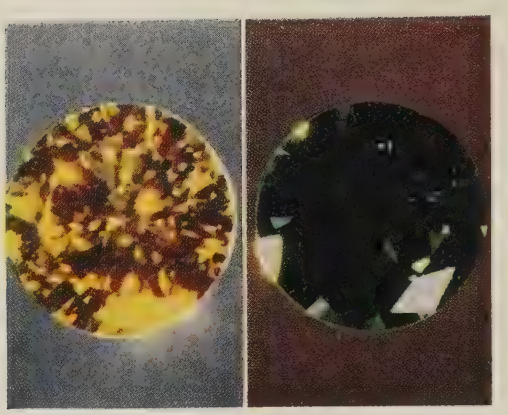

Plate 1. A color photograph of a brilliant-cut diamond, weighing approximately 10 carats, before and after irradiation with alpha particles at an energy of approximately 40 Mev. The picture on the left indicates the appearance of the stone prior to irradiation, showing the characteristic yellow color of the gem. On the right may be seen the same stone after the alpha-particle irradiation.

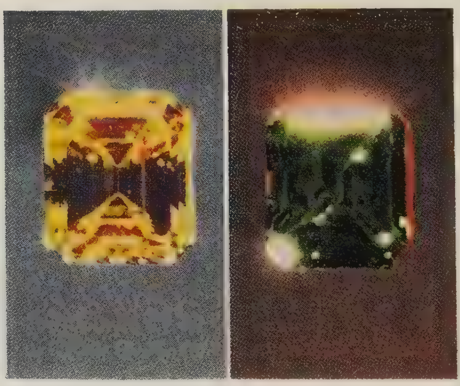

Plate 2. An emerald-cut yellow diamond weighing approximately 8 carats before and after alpha-particle irradiation. As in Plate 1, the photograph on the left shows the stone prior to irradiation and that on the right, the same gem following irradiation, showing the characteristic green color associated with exposure of the diamonds to high energy alpha particles.

may be presented to support this conclusion. The color change in stones ranging from pure white to the Cape stones of a relatively light yellow tint was always the same. Moreover, the amount of radiation required to produce this color effect at a level judged by visual observation did not vary by more than a factor of two. This variability lay within the range of experimental error, due to unhomogeneity of the beam intensity within the area in which the diamonds were bombarded. It is apparent that the amount or relative abundance of the foreign elements present will vary from diamond to diamond. This is a known fact, since these diamonds came from different regions in Africa and Brazil. Since over 200 diamonds were subjected to alpha particle bombardment and the regularities mentioned have prevailed, the possibility of the color change being due to foreign elements present seems exceedingly remote. Another consideration is the fact that these foreign contaminants are present in some instances in exceedingly minute amounts, this being particularly true of the white stones of gem quality. Upon this assumption the observed effect would be far too great to be accounted for on the basis of such minute amounts of other elements within the diamond. Finally, if the foreign elements had been a factor, then it would have been obvious that there would have been an extremely high degree of variability in response, both as to color and amount of radiation required to produce this effect. Representative illustrations of the effect produced by alpha particle irradiation are shown in Plates 1 and 2. The gem shown in Plate 1 was a brilliant-cut diamond weighing approximately 10 carats and the stone in Plate 2 was an 8 carat emerald-cut diamond. In both plates the photograph to the left shows the appearance of the gem prior to irradiation and to the right can be seen the effect of irradiation.

It has been suggested that effects of this character under the circumstances described above might be due to the physical displacement of carbon atoms within the lattice structure of the diamond. This concept does not appear to be reasonable on the basis of several lines of thought. The fact that heating to a relatively low temperature will destroy the green coloration of the diamond without destroying the diamond itself is a most cogent argument that the characteristic green color arises from electron displacement rather than displacement of carbon atom from the lattice structure. Another consideration is the fact that the number of electrons displaced either by direct ion bombardment or by the secondary effect produced by fast neutrons is presumably many thousand times greater than the number of carbon atoms displaced.

The effect of fast neutrons upon the diamonds is of interest, inasmuch as their range of penetration is far greater than the dimensions of not only the largest diamond irradiated in this series of experiments but any known diamond. In the case of the neutron irradiation the direct mechanism for change in color is presumed to be somewhat different. The primary loss of energy when charged particles are employed, notably deuterons or alpha particles, is affected by the interaction of the charged particles with the electrons surrounding the carbon nuclei within the diamond. The neutron is an uncharged particle and does not interact with the electrons directly. The principal process by which the neutron dissipates its energy under these circumstances is the elastic collisions made with the carbon nuclei. Under such circumstances, for each collision approximately one-fifth of the energy of a neutron making such a collision will be imparted to the carbon nucleus. The carbon nucleus in turn will frequently then have imparted to it a kinetic energy of several million volts. When a carbon nucleus has received this amount of kinetic energy it will be knocked out of its position in the crystal lattice structure of the diamond and in the process will lose several of its orbital electrons. Thus, there is created within the diamond an ionizing particle, namely a moving, charged atom of carbon which in turn will dissipate its energy primarily by interacting with electrons of other carbon atoms until it comes to rest. Even though its range within the diamond will be less than 0.1 micron, it still passes by many billion carbon atoms. In short, the direct bombardment with charged particles such as deuterons or alpha particles or neutron irradiation produce the same effect, though in the case of the neutron it is of a secondary nature rather than primary; also it must be kept in mind that in the case of deuterons or alpha particles, the effect is superficial. While protons were not used it is predictable that such particles, where energy is of the order of 5 Mev or greater, would produce comparable effects. A review of the effects of radiation on various materials has been compiled by Slater.[7] A number of the factors that relate to the possible mechanism responsible for the green coloration of the diamond have been discussed in greater detail in his paper.

The use of deuterons, or alpha particles of sufficient energy to produce these color changes in the diamond which have been described may well produce various color changes in other precious and semi-precious stones. In this respect there is a limitation imposed upon most stones. It would be anticipated that stones which contain even minute amounts of water would be completely disintegrated, since there is an appreciable depth of penetration of these charged particles and the heat released within the range of penetration would be sufficient to disrupt the physical structure of the gem. A more attractive possibility in the case of stones other than the diamond is neutron irradiation, since this can be conducted under conditions in which the heating effect can be reduced to a point where physical damage to the gem would not be anticipated.

---

[7] Slater, J. C., *Jour. Appl. Phys.*, **22**, 237 (1951).

Another limitation to the radiation of other precious and semi-precious gems by either charged particles or neutrons arises from the fact that there may be produced radioisotopes of quite an appreciable half-life and thus subject the stone to hazard. An example that might be cited is zircon, a semi-precious stone which contains a large amount of zirconium and a variable but appreciable amount of hafnium. The neutron irradiation of such stones would produce detectable amounts of radioisotopes of zirconium and hafnium which might prove troublesome. For example, Zr^{95} which is formed by the neutron capture of Zr^{94}, has a half-life of 65 days. Moreover, it decays to niobium-95 which has a half-life of 35 days. In the case of hafnium, the neutron capture of Hf^{180} results in the production of Hf^{181} with a half-life of 46 days. The problem becomes more complex with the use of charged particle bombardment as, for example, in the case of the alpha particle bombardment of zircon, radioisotopes of niobium, molybdenum and zirconium will be formed as well as radioisotopes of hafnium, tantalum and tungsten from the hafnium present. Before serious thought is given to a detailed study of affecting radiation charges for practical purposes in precious and semi-precious stones, the physical properties and chemical components, including foreign elements, should be known, for in a number of instances work of this character would be rendered impractical as has been described above. The use of very high energy accelerators in which protons, deuterons, or alpha particles may be accelerated to energy levels ranging from 200 to 400 Mev does not sound attractive, inasmuch as the beam currently available is relatively small, even though the energy is sufficient to penetrate large gems.

Acknowledgments

The assistance of Mr. G. B. Rossi and the staff of the 60-inch Cyclotron at the Crocker Laboratory in setting up the equipment necessary for the irradiation of the diamonds and the operation of the cyclotron is gratefully acknowledged. The photographs in Plates 1 and 2 were taken by Mr. Mason Weymouth of San Francisco, California.

Manuscript received May 18, 1952.

STUDIES OF URANIUM MINERALS (X): URANOPILITE*

Clifford Frondel, *Harvard University, Cambridge, Massachusetts*

Abstract

The status of the many natural uranium sulfates that have been reported is reviewed. Only three appear to be valid species: uranopilite, zippeite and johannite. New optical, chemical and dehydration data are given for uranopilite together with x-ray powder data for uranopilite, zippeite and johannite. New localities for uranopilite are Great Bear Lake and Hottah Lake, N.W.T., Canada. Beta-uranopilite of Novacek (1935) probably is not a dehydration product of uranopilite and is a doubtful species.

Introduction

The descriptive mineralogy and nomenclature of the natural uranium sulfates presents many difficulties. Nineteen different names, tabulated below, have already been given as species or generic designations for uranium sulfates, but only three of these substances, *johannite*, *zippeite* and *uranopilite*, can be said to be adequately defined and recognizable on the basis of existing data.

Alpha-uranopilite
Basisches Schwefelsaures Uranoxyd
Basisches Uransulphat
Beta-uranopilite
Calciouraconite
Cuprozippeite
Dauberite
Johannite
Medjidite
Uraconise
Uraconite
Uranblüthe
Urangrün
Uranochalcite
Uranocker
Uranopilite
Uranvitriol
Voglianite
Zippeite

Further, descriptions have been given in the literature of unnamed sulfates whose properties do not correspond to any of these minerals so far as known. Johannite is a relatively well-established species, whose x-ray crystallography has been described by Hurlbut (1950) in a preceding paper of this series. The species rank of uranopilite and of zippeite was first put on adequate grounds by the careful study of Novacek (1935), and a further description of uranopilite is given in the present paper. X-ray powder data for zippeite, obtained from a study of both natural specimens and analyzed synthetic material, and for johannite also are given here. Some of the localities cited for zippeite in the literature are not well authenticated and may refer to uranopilite or some other uranium sulfate.

Very little is known of the other reported uranium sulfates. Many were set forth as distinct species on the basis of chemical analyses which were made by faulty analytical procedures, or which were made on mixtures. The status of *uranochalcite* and of *voglianite* has been discussed by Novacek. The original descriptions by Vogl (1857) of these substances and later notices by others of minerals ascribed thereto are inadequate to establish their species validity and a complete re-examination of the type materials is needed. Such material does not appear to be extant. Novacek, however, examined all of the specimens reputedly of uranochalcite and voglianite that were available in various museum collections in Czechoslovakia and Austria. He found that these specimens were not of uranium sulfate at all but for the most part were composed of the copper-uranium silicate cuprosklodowskite. One specimen was a uranium phosphate and another proved to be langite or herrengrundite. Of the material here available, two specimens supposedly of voglianite proved to be identical with liebigite, and five specimens supposedly of uranochalcite variously were metatorbernite, cuprosklodowskite and uranospinite.

---

* Contribution from the Department of Mineralogy and Petrography, Harvard University, No. 334.

The substances called *uraconise* (uraconite) by Beudant (1832) and *medjidite* by J. L. Smith (1848) are only names on paper. Beudant's uraconise is classed with the uranium sulfates by most modern authors. His description states only that the substance is a yellow powder and a specific locality is not given. The composition is given as a hydrated oxide of uranium, on the basis of a recalculated analysis affording oxygen 5.24 per cent, uranium 94.76, and an unknown amount of water. This scant information together with a statement that the mineral sometimes contains carbonic acid is repeated in the 3rd (1850) edition of Dana's *System of Mineralogy*, where the name is given as a synonym of zippeite, and in the 4th (1854) edition where it is given as a synonym of uranochre. In the 5th (1868) edition, Dana applied the name *uraconite* to an ill-defined uranium sulfate from Joachimsthal analyzed poorly by Lindacker (1857) and called uranocker by Vogl (1857). The 6th (1892) edition contains the same account. Uraconite has the same meaning as uraconise, and since Dana condemned Beudant's practice of ending mineral names in *ise*, it appears that uraconite was intended as a substitute for that name. Nevertheless, Dana cites Beudant's uraconise as a doubtful synonym of uraconite, and remarks that the composition of uraconise is unknown. In any case, the substance analyzed by Lindacker, and on which the name uraconite is based by Dana, is according to Novacek (1935) only zippeite. Uraconite is essentially a name without a mineral and should be abandoned. It is a common designation on museum labels; the specimens usually turn out to be zippeite or uranopilite.

Occurrences of uranium sulfates whose true identity is quite unknown have been mentioned under the name uraconite by Gordon (1922)

[Avondale, Chester and Leiperville in Delaware Co. and Fairmount Park in Philadelphia, all in Pennsylvania], Johnston (1915) [Madoc, Hastings Co., and Snowdon, Haliburton Co. in Ontario, Canada], Luquer (1904) [Bedford, Westchester Co., New York], James (1947) [Cornwall, England], and Sohon (1951) [Branchville and Middletown, Conn.] Larsen (1921) gives an optical description of an unanalyzed but apparently distinct sulfate from Gilpin County, Colorado, which he refers to as uraconite, and Koritnig (1939) refers to an undetermined sulfate from Schwag near Trahütten, Styria, Austria, as uraconite or zippeite. Rickard (1895) mentions yellow uranium ocher in an oxidized gold quartz vein containing uraninite [?] in the Rathgeb Mine, San Andreas, Calaveras Co., California, and some later authors have cited this occurrence as of uraconite.

Elsewhere in his book, Beudant mentions a *sulfate verte d'urane* (later to become known as johannite) and a yellow, earthy *sous-sulfate d'urane* whose true identity is not now known. *Medjidite* of Smith (1848) is an amber-brown massive material that was said on the basis of qualitative tests to be a hydrated sulfate of uranium and calcium, and other characterizing data are lacking. Two specimens of uncertain authenticity labelled medjidite that were examined in the course of this study proved to contain only uraninite and liebigite. The *uranocker* of Vogl (1857) from Joachimsthal, which has also been classed by some under the name uraconite, is an earthy or scaly, lemon-yellow substance which from the evidence of two discordant analyses appears to be identical with zippeite. *Dauberite* of Adam (1869) is a synonym of zippeite and *alpha-uranopilite* of Foshag (1935) is a synonym of beta-uranopilite. The names *uranvitriol*, *urangrün* and *uranblüthe* have been used more or less as generic terms for uranium sulfates in the German literature.

All of the above-mentioned names are devoid of any exact meaning and can hardly be applied to new occurrences of specific uranium sulfates in lack of a definitive re-description of the original materials. It seems desirable and justifiable to completely abandon these names, and to relieve any future investigator of the responsibility of resolving the earlier nomenclature before proposing a new species that differs from the three well-established species that are presently known.

Several additional uranium sulfates have been reported that may have a real existence. Novacek (1935) briefly described a natural fibrous sulfate close in composition to uranopilite under the name *beta-uranopilite* (meta-uranopilite). The status of this mineral is discussed beyond in connection with a dehydration study of uranopilite. Boldyrev (1935), in a publication not available to the writer, has used the names *cuprozippeite* and *calciouraconite* for minerals said to be near $Cu(UO_2)_3$

$(SO_4)_3(OH)_2.11H_2O$ and $Ca(UO_2)_4(SO_4)_2(OH)_6.20H_2O$, respectively. These names recall the old analyses of zippeite and uranopilite that contain CaO and CuO due to admixture.

URANOPILITE

The identification of the mineral here described as uranopilite is based principally on the definition of this species given by Novacek (1935), to whose excellent paper reference should be made both for a history of the name and for a summary of earlier recorded optical and chemical data.

Uranopilite is a secondary mineral and in part at least is of recent formation as an efflorescence on the walls of mine workings. It commonly occurs as a coating on oxidized vein material in which uraninite and sulfides were primary constituents. Gypsum and zippeite are common associates. The mineral forms fragile, small-botryoidal crusts or isolated, globular to reniform incrusting masses of small size. These are composed of tiny and sometimes microscopic lath- or needle-like crystals that form felted aggregates. The measured specific gravity is 3.96 (Wheal Owles, Cornwall). The hardness cannot be determined accurately because of the fibrous nature of the material but apparently is quite low. The color is bright lemon yellow, sometimes straw yellow in compact crusts, and the luster is faintly silky due to the fibrous character. Uranopilite shows the bright yellow-green fluorescence characteristic of uranyl compounds in both long- and short-wave ultraviolet light. In the hand specimen, the fine-fibrous and silky appearance of uranopilite contrasts with the fine-granular to earthy and rather dull appearance of zippeite. The color of the two minerals often is quite similar, but zippeite tends more toward deep yellow to orange-yellow tones. A distinction between uranopilite and zippeite is easily made by either optical or *x*-ray diffraction tests. Fluorescence is not a reliable means of discrimination between the two minerals. Uranopilite uniformly fluoresces a bright yellow-green, but zippeite varies from yellow-green (especially in fresh synthetic material obtained by adding very dilute NH_4OH to a dilute water solution of uranyl sulfate until a precipitate barely forms and then allowing to stand) through dull yellow green and dull yellowish olive green, and some material apparently fluoresces only weakly, if at all. Uranopilite is insoluble in cold water. It is easily soluble in dilute acids.

Under the microscope the mineral appears as elongated laths and needles with the optical orientation shown in Fig. 1. The laths sometimes are seen to be doubly terminated by oblique faces. The mineral appears to be monoclinic, with the elongation along [001] and the flattening on {010}. There is a good cleavage on {010}. Sections parallel {100} show parallel extinction with abnormal blue interference colors. The dispersion is rather strong, with $r>v$. The indices of refraction are tabulated below. They represent the range of numerous values here measured on air-dried, Museum specimens. Concordant optical data are given by Novacek (1935) and Buttgenbach (1935, 1947). The optical data given in the tables of Larsen and Berman (1934) for zippeite actually refer to uranopilite; the source of this error has here been traced back to a borrowed specimen that was erroneously labelled. It is shown beyond that the optical properties of uranopilite vary widely accompanying loss of water by heating or desiccation.

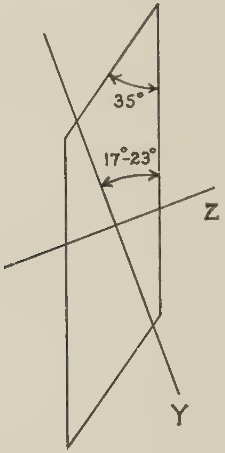

FIG. 1. Optical Orientation of Uranopilite.

Optical Properties of Uranopilite

Indices	Pleochroism	
$nX=1.621$ to 1.623	Colorless	Biaxial positive (+)
$nY=1.623$ to 1.625	Yellow	$r>v$, strong
$nZ=1.632$ to 1.634	Yellow	$Y \wedge c=17°$ to $23°$

The x-ray powder spacings of uranopilite, zippeite, and johannite are listed in Table 1.

Chemistry. Uranopilite is a hydrated basic uranyl sulfate. Novacek (1935) derived the ratios $6UO_3 \cdot SO_3 \cdot 16$ or $17H_2O$, corresponding to $(UO_2)_6(SO_4)(OH)_{10} \cdot 11$ or $12H_2O$, from the six new analyses reported by him. The three earlier analyses of Schulze (1882) and Dauber (1854) are of inferior quality. A later analysis by Buttgenbach (1935) of material from the Belgian Congo is close to $(UO_2)_5(SO_4)(OH)_8 \cdot 10H_2O$, and a recent analysis of uranopilite from France reported by Branche, Chervet and Guillemin (1952) approximates to $(UO_2)_6(SO_4)(OH)_{10}$

TABLE 1. *X*-RAY POWDER SPACING DATA FOR URANOPILITE, ZIPPEITE AND JOHANNITE

Copper radiation, nickel filter, in Å($\lambda=1.5418$)

Uranopilite		Zippeite		Johannite	
d	*I*	*d*	*I*	*d*	*I*
9.18	8	8.60	3	7.81	10
8.21	2	7.06	10	6.24	9
7.12	10	6.42	1	5.61	3
5.99	2	5.45	4	4.89	1
5.51	4	4.29	3	4.42	3
5.13	1	3.89	2	4.22	1
4.76	1	3.66	3	3.89	4
4.61	1	3.51	9	3.74	3
4.28	8	3.12	8	3.53	2
4.02	1	2.87	4	3.42	5
3.86	2	2.72	2	3.24	1
3.65	5	2.65	4	3.13	4
3.48	2	2.478	3	3.06	4
3.31	4	2.340	2	2.93	2
3.08	1	2.216	5	2.806	3
2.99	3	2.143	3	2.687	3
2.90	3	2.096	2	2.588	3
2.75	1	2.050	4	2.455	2
2.69	2	1.944	3	2.385	1
2.585	2	1.879	1	2.321	1
2.417	1	1.865	1	2.245	2
2.356	1	1.835	3	2.199	1
2.275	1	1.749	5	2.143	2
2.243	1	1.698	5	2.096	2
2.190	3	1.668	1	2.048	1
2.126	1	1.632	1	2.013	2
2.075	1	1.601	1	1.929	3
2.040	1	1.565	4	1.895	3
2.013	1	1.523	2	1.852	4
1.932	2	1.496	2	1.803	1
1.880	2	1.463	1	1.770	2
1.826	3	1.426	2	1.711	2
1.757	3	1.402	3	1.678	1
1.732	1	1.371	2	1.599	2
1.700	2	1.329	2	1.571	1
1.674	1			1.554	1
1.638	1			1.531	3
1.604	1			1.490	3
				1.463	2
				1.439	1

$\cdot 13H_2O$. A new analysis of uranopilite from the Wheal Owles, Cornwall, is cited below. This analysis, made on a 200 mg. sample, agrees well with earlier analyses in content of UO_3 but contains somewhat less SO_3 and has a slightly greater content of H_2O, being comparable to one of the analyses of Schulze (1882) in this regard. The ratios of the analysis are closer to $(UO_3)_7(SO_4)(OH)_{12}\cdot 15H_2O$ than to the formula of Novacek. The divergence among the reported analyses in the $UO_3\cdot SO_3$ ratio probably is due to analytical error. The water of crystallization is in part loosely held, as discussed beyond, and its variation probably reflects the temperature and humidity at which the sample was held prior to analysis. The CaO reported in some of the analyses is due to admixed gypsum. The formula advanced by Novacek and cited above probably best represents the composition of the mineral, although the ideal water content may be slightly higher.

URANOPILITE. WHEAL OWLES, ST. JUST, CORNWALL

UO_3	Fe_2O_3	Al_2O_3	CaO	SO_3	H_2O	Insol.	Total	G
79.44	0.05	nil	nil	3.30	15.68	1.72	100.19	3.96

Analyst: R. Meyerowitz, U. S. Geological Survey, 1949.

Localities. The following localities for uranopilite were established by Novacek on optical and analytical evidence: Johanngeorgenstadt, Saxony; Příbram, Bohemia; Joachimsthal, Saxony, St. Just, Cornwall. Specimens from all of these localities were examined in the present study and the identification was verified by optical and x-ray study. One very fine specimen from the Wheal Owles, St. Just, Cornwall, comprised a deeply altered mass of uraninite-bearing vein material the size and almost the color of an orange that was incrusted by uranopilite. The original handwritten label of this specimen reads: *Uraconite, Uran-ochre. From Wheal Owles, nr. St. Just, Cornwall. Evidently a secondary product on Pitchblende. Hydrous oxide of uranium with variable proportion of sulfuric acid. An indefinite mixture. This is a very fine specimen. Bought of Gregory, December 19, 1885. £1.10. J.P.*[*James Percy*] *December 20, 1885.* James (1947) mentions zippeite as occurring at the Wheal Owles among other places in Cornwall, and Greg and Lettsom (1858) mention several localities for zippeite (which they consider an oxide) in Cornwall; probably both zippeite and uranopilite were included by these authors under the single name. Uranopilite also has been identified by George (1949) in ore samples from the Urgeirica mine, Canas de Senhorim parish, Viseu district, Portugal. An optical description and analysis of the uranopilite from Shinkolobwe in the Belgian Congo has been given by Buttgenbach (1935–1947). Two occurrences in France, at La Crouzille, Haute-Vienne, and Grury, Saône-et-Loire (with analysis) are cited by Branche, Chervet and Guillemin (1952). Two new occurrences of uranopilite were found during the present study. At Great Bear Lake, Canada, it occurs very sparsely as thin, felt-like crusts and films, locally small botryoidal, on massive pitchblende. The mineral is relatively dense and fine-grained, with a straw-yellow to pale yellow color and a dull-silky luster. It is associated with minor amounts of zippeite as golden-yellow crusts, tiny radial-fibrous globules of johannite, fourmarierite, and erythrite. Uranopilite also has been identified as thin coatings on altered pitchblende from Hottah Lake, N.W.T., Canada. This material, like that from Great Bear Lake, is relatively fine-grained with a pale yellow color and a felt-like structure.

Dehydration. In the course of his study of uranopilite, Novacek (1935) observed that laths of this substance when kept embedded in Canada balsam for some time changed in color from yellow to grayish brown. The extinction also became parallel and the birefringence decreased almost to zero. These changes were ascribed to dehydration. Later, Novacek (1942) made a dehydration study of analyzed uranopilite from Joachimsthal. His data show that of the (total) $16H_2O$ present in this material, $6H_2O$ are lost sharply between 60°–70° and the remainder is lost gradually up to about 250°–300°. Over about 250°–270° the SO_3 begins to be lost as well. The divergent results of Buttgenbach (1935) were explained by Novacek as due to confusion in the temperature scales employed, Centigrade and Reamur.

Further observations were made here on the dehydration of the analyzed Wheal Owles material. When heated in air at 72°, 112° or 152°, water is lost rapidly. The loss at 72° was found to be 5.2 weight per cent, corresponding to the loss found by Novacek at 60–70°. When heated to bright redness the mineral decomposes completely leaving U_3O_8. The color of the mineral changes during dehydration from the original lemon-yellow to orange or, at higher temperatures, to deep orange and reddish orange. The mineral simultaneously loses its property of fluorescing in long- and short-wave ultraviolet radiation. There are marked accompanying optical changes. The extinction becomes parallel, the pleochroism is less marked and the indices of refraction increase to values depending on the temperature: $nY = nZ \sim 1.71$ at 72°, $nY = nZ \sim 1.84$ at 112°, $nY = nZ \sim 1.89$ at 152°. The birefringence also decreases from the initial value of 0.011 and some grains become almost isotropic at higher temperatures. There is a small but noticeable variation in both birefringence and indices between different grains in the heated samples, due to lack of attainment of equilibrium, and it is not possible to measure all of the indices on any single grain. The heated samples give weak and very diffuse *x*-ray powder patterns.

When the heated samples are held at room temperature in air or are immersed in cold water the original water content is very quickly restored. The original color and fluorescence are simultaneously regained, and the rehydrated material gives a sharp *x*-ray pattern of uranopilite. The original optical properties, including inclined extinction, also are restored.

Meta-uranopilite. The name beta-uranopilite* was given by Novacek (1935) to a needle-to lath-like mineral of a grayish, dirty green or brownish tint which he considered to have probably formed by the natural dehydration of uranopilite. An analysis in which Ca and Cu could not be determined for lack of sufficient material gave UO_3 82.40, Fe_2O_3 2.03, SO_3 4.17, H_2O 9.40; total 98.00. The iron oxide presumably is due to admixture of limonite. From this analysis was derived the tentative formula $6UO_3 \cdot SO_3 \cdot 10H_2O$ or $(UO_2)_6(SO_4)(OH)_{10} \cdot 5H_2O$. Only a single specimen from Joachimsthal, Bohemia, is known. The mineral is biaxial negative with parallel extinction with Y parallel to the elongation and X perpendicular to the flattening of the laths. The indices of refraction are $nX=1.72$, $nY=1.76$, $nZ=1.76$, and pleochroism is not perceptible.

No mineral corresponding to meta-uranopilite was found among the numerous specimens of fibrous uranium sulfates here examined. One of the studied specimens from Joachimsthal, however, shows a yellow, coarsely fibrous mineral, admixed with uranopilite, which has optical properties close to those reported for meta-uranopilite. This material is biaxial negative, with $nX=1.685$ (colorless), $nY=nZ=1.754$ to 1.764 (yellow). Extinction parallel with X perpendicular to the elongation. The *x*-ray pattern, however, is identical with that of becquerelite although the optical properties diverge considerably from those of crystallized becquerelite from the Belgian Congo. The material may be a pseudomorph after a fibrous sulfate. It may be noted in this connection that becquerelite, a mixture of becquerelite with zippeite, or zippeite alone is formed, depending on the pH, when uranyl sulfate solution is partly neutralized by NH_4OH and allowed to stand.†

The status of meta-uranopilite is uncertain, and further work on the mineral is desirable. It now appears very unlikely that it is a dehydration product of uranopilite as suggested by Novacek. Uranopilite, as shown above, can be dehydrated to a point where the indices of refraction are much higher than those of meta-uranopilite and the water content considerably less. This material, however, differs from meta-uranopilite in having a much lower birefringence and in rehydrating immediately to normal uranopilite when exposed to air at room temperature.

---

* The name meta-uranopilite is preferable, since the prefix beta is generally applied to designate instances of polymorphism, as in uranophane and beta-uranophane, and meta to cases of alteration or dehydration, as in torbernite and meta-torbernite.

† Private communication from Prof. J. W. Gruner, University of Minnesota, 1950.

References

Adam, G. J., Tableau Minéralogique, Paris, 64 (1869).

Beudant, F. S., Traité élémentaire de Minéralogie, 2nd ed., Paris, **2**, 672 (1832).

Boldyrev, A. K., Course of Descriptive Mineralogy, Leningrad and Moscow, **3**, 83 (1935) [cited by Hey, M. H.: Chemical Index of Minerals, London, 256, 257 (1950)].

Branche, G., Chervet, J., and Guillemin, C., *Bull. Soc. Min.*, **74**, 457 (1952).

Buttgenbach, H., Les Minéraux de Belgique et du Congo Belge, Liège, 515 (1947); *Mém. Inst. roy. colon. belge*, **6**, 449 (1935).

Dauber, H., *Ann. Phys. Chem.*, ser. 4, **92**, 237 (1854).

Foshag, W. F., *Am. Mineral.*, **20**, 813 (1935).

George, d'A., *U. S. Atomic Energy Comm. Rept.* **RMO-563,173** (1949).

Gordon, S. G., Mineralogy of Pennsylvania: *Acad. Nat. Sci. Philadelphia, Spec. Publ.* no. **1**, 148 (1922).

Greg, R. P., and Lettsom, W. G., Manual of the Mineralogy of Great Britain and Ireland, London, 382 (1858).

Hurlbut, C. S., *Am. Mineral.*, **35**, 531 (1950).

James, C. C., *Trans. Royal Geol. Soc. Cornwall*, **17**, Pt. 5, 256 (1947).

Johnston, R. A. A., *Canada Dept. Mines, Geol. Survey, Mem.*, **74**, 230 (1915).

Koritnig, S., *Zbl. Min.*, 116 (1939A).

Larsen, E. S., *U. S. Geol. Surv., Bull.*, **679**, 159 (1921).

Larsen, E. S., and Berman, H., *U. S. Geol. Surv., Bull.* **848**, 112, 113 (1934).

Luquer, L. M., *Am. Geol.*, **33**, 17 (1904).

Novacek, R., *České Spol. Nauk, Třída Mat.-Příro., Vêstník* no. **7**, (1935); *ibid.*, no. **17** (1941).

Rickard, T. A., *Colorado Sci. Soc. Proc.*, **4**, 329 (1895).

Schulze analysis cited in Weisbach, A., *Jb. Min.*, **II**, 249 (1882).

Smith, J. L., *Am. J. Sci.*, **5**, 337 (1848).

Sohon, J. A., Connecticut Minerals, Their Properties and Occurrence: *Conn. Geol. and Nat. Hist. Survey, Bull.* **77**, (1951).

Vogl, J. F., Gangverhältnisse und Mineralreichthum Joachimsthals, Teplitz (1857).

Manuscript received April 10, 1952.

ZUNYITE FROM POSTMASBURG, SOUTH AFRICA

F. H. S. Vermaas, *Geological Survey of the Union of South Africa, Pretoria**

Abstract

New determinations of the cube edge, refractive index, dispersion and disintegration on heat treatment combined with existing chemical analysis of zunyite are given. This mineral has a face-centered cubic lattice and a cube edge of 14.034 (0.003) Å. The refractive index for Na-light is 1.600 (±0.001) and dispersion $n_F - n_C = 0.009$ (±0.001). Its determined specific gravity of 2.87 is in good agreement with the calculated value of 2.85. On heating zunyite to 1100° C. the structure breaks down to form mullite, indicating a Si:Al ratio of 1:3 in the zunyite itself. The mineral contains less fluorine but more chlorine than the American variety from Zuni-mine.

Introduction

The occurrence of the very rare aluminum silicate, zunyite, in the highly aluminous shales and flagstones at Postmasburg, was first described by Nel (1, pp. 207–216). The zunyite crystals vary in size from about 3 mm. to less than 1 mm. (measured along the edges). They are usually perfectly crystallized octahedrons which often show twinning. The crystals have a flesh color, some having reddish nuclei. The latter type was never used for examination. Pure material was obtained by hand picking from the soft country rock in which it occurs.

As described by Nel (1, p. 211), zunyite occurs in two ways; "either it forms curious patches in the coarse diaspore-rock or its crystals are roughly arranged in layers or disseminated through a rock in which diaspore is only of microscopic dimensions." The zunyite occurring in the latter manner is also larger and only these have been used for the investigations. The matrix of this rock was identified as consisting of intimately intergrown pyrophyllite and kaolinite.

Specific Gravity

The specific gravity was determined in two ways: (*a*) according to the method of Jahns (2, pp. 216–222) in which fragments are suspended in Clerici solution. The mean of three determinations yielded G_4^{16} 2.87^1 (±0.005), and (*b*) by the pyknometer method. The results obtained by this method were corrected for the difference in the displacement of air by the volume of the contents of the bottle and the volume of the weights used with the balance. For this correction the density of air was calculated as 0.0010296 gr./cc. at Pretoria where the atmospheric pressure is 65 cms. Hg at a temperature of 25° C. (3. p. 1694). The mean of three determinations was found to be G_4^{25} 2.877 (±0.005). The final specific gravity was taken as 2.874 (±0.005). Taking the molecular weight of zunyite as 4736 (i.e. when the unit-cell contains the following atoms, 19 Si, 53 Al, 1 Fe, 2 Na, 64 OH, 7 Cl, 1 F and 82 oxygen) its specific gravity can be calculated as 2.845 (4, pp. 109–110), which is in good agreement with the experimental value.

---

* Published with the consent of the Department of Mines.

OPTICAL PROPERTIES

Zunyite is optically isotropic and its refractive index and dispersion were determined according to a single variation method at room temperature (20° C.) using a monochromator. Its index of refraction was found to be:

$$n_{\mathrm{Na}} = 1.600\ (\pm 0.001)$$

Dispersion: $n_F - n_C = 0.009\ (\pm 0.001)$.

TABLE 1. QUALITATIVE SPECTROGRAPHIC ANALYSIS OF ZUNYITE

Present: Si, Al, Fe, Na.
Trace: Mg, Ca, K, Ti, Cr, V.
Absent: Be, Sr, Bb, Cs, Li, Mn, Mo, Ba.

TABLE 2. CHEMICAL ANALYSIS

a		*b*	*c*		*d*		
SiO_2	24.10	0.4016	Si	0.4016	19.18	Si	(19)
Al_2O_3	56.85	0.5573	Al	1.1146	53.23 0.87	Al	(54)
Fe_2O_3	1.45	0.0091	Fe	0.0182			
MgO	0.30	0.0075	Mg	0.0075	0.35		
CaO	0.20	0.0036	Ca	0.0036	0.17		
Na_2O	1.45	0.0232	Na	0.0464	2.24	Na	(2)
K_2O	tr.	tr.	P	0.0036	0.17		
Cl_2	4.80	0.1352	Cl	0.1352	6.56 1.01 63.73	Cl, F+OH	(72)
F_2	0.40	0.0211	F	0.0211			
P_2O_5	0.25	0.0018	H	1.3334			
H_2O H_2O	11.65 0.35	0.6667	O−(F+Cl)	3.0563	146.00*	O	(82)
Less O for F, Cl	1.30						
	100.50						

* After an equivalent amount of O has been subtracted for (F+Cl).

a. Chemical analysis by H. G. Weall.

b. Molecular proportions.

c. Atomic ratios.

d. Unit-cell contents.

CHEMICAL COMPOSITION

The chemical analysis listed is the one given by Nel (1, p. 216) and the spectrographic analysis was carried out on a large Hilger Littrow-type spectrograph; samples were arced in hollowed copper anodes (the cathodes were slightly pointed) for 20 seconds at 5 amps.

The unit-cell contents were determined by the following equation:

$$\text{Number of ions of each element in the unit-cell} = \frac{\text{Unit-cell volume} \times \text{Avogadro's number} \times \text{atomic ratio} \times \text{density}}{\text{Sum total of the chemical analysis}}$$

where $a = 14.03$Å and Avogadro's number $= (6.0597 \pm 0.0016)\ 10^{23}$ (4, p. 110).

X-RAY EXAMINATION

X-ray powder diffraction patterns were obtained by using 114 cms. diameter cameras in which the film is mounted according to the Straumanis method (5, p. 726). The temperature during the exposures remained reasonably constant and did not vary more than 1° C. above room temperature of 20° C. The time of exposure was $2\frac{1}{4}$ hours using unfiltered Cu-radiation at 35 K.V. and 20 ma. Shrinkage correction factors were determined and the measuring carried out as described by Wasserstein (6, p. 106).

The final value for a_0 was determined using Bradley and Jay's graphical extrapolation method (7, p. 563) and represents the mean of three determinations. X-ray diffraction angles were converted to interplanar spacings by using suitable tables. The wavelengths used were:

$CuK\alpha_1$ 1.537395 KXu. or 1.540501 Å
$CuK\alpha_2$ 1.541232 KXu. or 1.544345 Å

Pauling (9, pp. 442 452) determined the cube edge of zunyite from Zuni-mine, Colorado, U.S.A., as 13.830 (±0.005)Å. He suggested that it has a face-centered lattice and a space-group symmetry T_d^2. The powder photographs of the Postmasburg zunyite also indicate a face-centered cubic lattice.

The South African variety contains more chlorine and less fluorine than that from the Zuni-mine. As the water content is more or less the same in the two samples, chlorine replaces fluorine in the Postmasburg zunyite. The ionic radius of chlorine is much larger than that of fluorine viz: Cl^- 1.81 Å and F^- 1.33 Å (10, p. 1314) and this causes an expansion of the unit-cell.

Pauling also suggested that the unit-cell contains four molecules of composition $Al_{13}Si_5O_{20}(OH, F)_{18}Cl$. If the unit-cell contents as calculated in Table 2 (*d*) are divided by 4 the results shown in Table 4 are obtained.

TABLE 3. *X*-RAY DATA FOR POSTMASBURG ZUNYITE

$\alpha_o = 14.034\ (\pm 0.003)$ Å

No.	Int(obs.)	2θ (Cu)	d Å	(*hkl*)
1	2	9.98	β-line	
2	10	11.08	7.99	(111)
3	3	19.19	β-line	
4	10	21.24	4.18	(311)
5	8	22.23	4.00	(222)
6	1	25.25	β-line	
7	4	28.02	3.18	(331)
8	6	30.26	β-line	
9	7	31.63	2.83	(422)
10	10	33.59	2.67	(333) (511)
11	5	36.61	2.45	(440)
12	5	38.41	2.34	(531)
13	4	40.72	2.22	(620)
14	7	42.75	2.12	(622)
15	8	45.32	2.00	(444)
16	4	46.77	1.942	(711) (551)
17	6	49.14	1.854	(642)
18	6	50.47	1.808	(731) (553)
19	5	54.55	1.682	(820) (644)
20	9	56.23	1.636	(555)
21	4	57.76	1.600	(662)
22	2	59.80	1.547	(840)
23	5	60.87	1.522	(842)
24	1	62.62	1.484	(664)
25	4	64.00	1.455	(931)
26	4	65.89	1.418	(844)
27	6	67.16	1.394	(933)
28	2	68.96	1.362	(10, 2, 0) (862)
29	5	70.17	1.341	(666), (10, 2, 2)
30	5	74.94	1.267	(10, 42)
31	2	76.15	1.251	(11, 1, 1) (775)
32	5	77.85	1.227	(880)
33	3	79.18	1.210	(10, 4, 4) (882)
34	6	81.91	1.176	(10, 6, 2)
35	5	93.16	1.0606	(12, 4, 4)
36	6	96.19	1.0347	(12, 6, 2)
37	2	98.84	1.0149	(888)
38	1	101.64	0.9937	(14, 2, 0)
39	4	105.01	0.9708	(12, 8, 0)
40	1	107.76	0.9535	(14, 4, 2) (12, 6, 6)
41	7	109.29	0.9444	(12, 8, 4)
42	2	112.55	0.9261	(14, 4, 4)
43	2	113.94	0.9187	(14, 6, 0)
44	1	116.81	0.9043	(999) (13, 7, 5) (11, 11, 1)
45	3	120.08	0.8891	(12, 10, 2)
46	3	123.22	0.8756	(16, 0, 0)
47	4	126.89	0.8611	(13, 7, 7)
48	4	128.75	0.8543	
49	4	130.18	0.8493	(15, 5, 5)
50	6	133.99	0.8368	(12, 10, 6)
51	2	140.60	0.8181	(16, 4, 2)
52	3	145.27	0.8093	(16, 8, 2)
53	1	152.79	0.7925	(17, 5, 1)
54	1	157.07	0.7858	(16, 8, 4)
55	6	159.76	0.7824	(17, 5, 3)

TABLE 4. COMPARISON OF EMPERICAL FORMULA OF THE SOUTH AFRICAN AND AMERICAN ZUNYITES

Atom	S.A. Zunyite	American Zunyite (9, p. 445)
Si	4.80	4.63
Al	13.31	13.17
Fe	0.22	0.03
P	0.04	0.09
Ca	0.04	—
Mg	0.09	—
Na	0.56	0.12
K	—	0.04
Cl	1.64	0.96
F	0.20	3.17
OH	15.94	14.37
O	20.50	20.08
(OH+F+Cl)	17.78	18.50

TABLE 5. *X*-RAY DIFFRACTION DATA FOR MULLITE EX. ZUNYITE COMPARED TO THAT FOR MULLITE EX. KAOLINITE AND NATURAL MULLITE

Mullite ex. zunyite			Mullite ex. Kaolinite[1]		Natural mullite[2]	
No.	Int(*est*)	*d* Å	Int(*est*)	*d* Å	Int(*est*)	*d* Å
1	8	5.40	7	5.40		
2	4	3.77	3	3.76		
3	10	3.41	10	3.39	10	3.44
4	1	2.87	3	2.88	4	2.90
5	7	2.70	6	2.70	5	2.70
6	7	2.54	7	2.54	6	2.56
7	3	2.43	4	2.42	3	2.43
8	3	2.29	3	2.28	4	2.30
9	8	2.20	7	2.20	7	2.21
10	3	2.12	5	2.11	5	2.13
11	3	2.03	2	2.00		
12	4	1.694	5	1.699	6	1.70
13	4	1.595	5	1.600	4	1.60
14	7	1.524	7	1.520.	7	1.53
15	4	1.436	5	1.444	4	1.45

[1] McVay and Thompson, *Jour. Am. Cer. Soc.*, **11**, 834 (1928).

[2] Norton, *Jour. Am. Cer. Soc.*, **8**, 637 (1925).

There is a close agreement in Si, Al, oxygen, and the minor constituents. The Cl, F and OH values vary antipathetically but the (Cl+F+OH) totals for both are about the same, and its emperical formula can therefore be written as: $Al_{13}Si_5O_{20}(OH, F, Cl)_{19}$. The Postmasburg zunyite also contains more sodium.

PACKING INDEX

The packing index of zunyite calculated from the formula

$$P.I.=\frac{\text{volume of ions}}{\text{volume of cell}}\times 10 \text{ (10, p. 1310) is } \mathit{6.4}.$$

For this calculation the volumes of the ions given by Fairbairn (10, p. 1314) were used.

HEAT TREATMENT

Grosner and Musgnug (11, p. 153) published data on the dehydration of zunyite for temperatures ranging from 300° C. to 810° C. When the Postmasburg zunyite, pulverized to −200 mesh, was heated in an electric furnace to 1100° C., mullite was formed. No fluorine could be detected spectrographically in this mullite and all the volatile constituents OH, F and Cl, were probably completely driven off below 1100° C.

Mullite, with a chemical formula of $3Al_2O_3\cdot 2SiO_2$ (orthorhombic) reveals the primary Al:Si ratio of 3:1 in the zunyite as suggested by Grosner and Musgnug (11, p. 154). This 3:1 ratio is also indicated in Table 4. The Postmasburg zunyite has (Al, Fe):Si=2.82:1 and the American zunyite Al:Si=2.82:1.

ACKNOWLEDGMENTS

Appreciation is expressed to Dr. L. T. Nel, Director of the Geological Survey, Pretoria, who kindly contributed the samples of zunyite described in this work.

REFERENCES

1. NEL, L. T., *Min. Mag.*, **23** (1931).
2. JAHNS, R. W., *Am. Mineral.*, **24** (1939).
3. Handbook for Chemistry and Physics. 30th Edition (1949).
4. SCHLECHT, W. G., *Am. Mineral.*, **29** (1944).
5. STRAUMANIS, M. E., *Jour. App. Physics*, **20** (1949).
6. WASSERSTEIN, B., *Am. Mineral.*, **36** (1951).
7. BRADLEY, A. J., AND JAY, A. H., *Proc. Phys. Soc.*, **44** (1932).
8. Tables of *d*-Spacings for Angle 2, *U. S. Dept. of the Interior, Circular* **29** (Aug. 1948).
9. PAULING, L., *Zeit. Krist., Min.*, **84** (1933).
10. FAIRBAIRN, W. H., *Bull. Geol. Soc. Am.*, **54** (1943).
11. GROSNER, B., AND MUSGNUG, F., *Centb. Min. Geol. Pal., Abt.* **A** (1926).

Manuscript received Feb. 9, 1952.

RELATIONSHIP BETWEEN DENSITY AND COMPOSITION IN MOL PER CENT FOR SOME SOLID SOLUTION SERIES

F. Donald Bloss,* *University of Chicago, Chicago, Illinois.*

Abstract

A general equation relating density to composition in mol per cent is derived for all two component solid solution series wherein volume is an additive property. Dependent upon K, which is defined as the ratio of the molar volume of the end member of higher molecular weight to the molar volume of the remaining component, i.e. $K = V_a/V_b$, the general equation may be graphically represented (density along ordinate) by a concave upward quadratic ($K<1$), a straight line ($K=1$), or a convex upward quadratic ($K>1$). For convenience these three types are labelled type I, II, and III, respectively. Examples of all three types are presented. All ideal solutions should exactly follow one of these types of ideal curves.

Deviation of the empirical data from the theoretical relationship between density and composition is presented as proof for the non-ideality of a solution, since additivity of volume is a necessary property of thermodynamically ideal solutions.

The statistically-fitted curve for the forsterite-fayalite series, previously determined as ideal by the heat of solution measurements of Sahama and Torgeson, proved practically identical to the theoretical curve. The straight line generally used to relate density to composition in mol per cent for this series is definitely erroneous.

Introduction

A linear relationship between density and mol per cent composition has frequently been assumed in published articles on solid solution series, especially when few data are available. The situation is commonly not so simple; rather a quadratic relationship generally lies closer to the truth. This is particularly true when the molar volumes of the end members differ considerably.

Theoretical Relationship Between Density and Composition In Mol Per Cent

If molar volume can be considered as an additive† property in a solid solution series between two components A and B (as it is for an ideal solution: Lewis and Randall, 1923, p. 222) then

$$V = \frac{N_a}{100} V_a + \left(1 - \frac{N_a}{100}\right) V_b \tag{1}$$

where N_a represents the mol per cent of end member A in the mixed crystal, and where V, V_a, and V_b represent the molar volume of the mixed crystal, of pure A, and of pure B, respectively. Gram molecular weight for this series is undoubtedly an additive property (MacDougall, 1943, p. 194) and therefore

---

* Present address: Department of Geology, University of Tennessee, Knoxville, Tennessee.

† In effect any property which varies linearly with mol per cent composition. For further discussion see any physical chemistry text, for example, that by MacDougall (1943, p. 194).

$$M = \frac{N_a}{100} M_a + \left(1 - \frac{N_a}{100}\right) M_b \tag{2}$$

where M, M_a and M_b represent the gram molecular weights of the mixed crystal, of pure A, and of pure B, respectively.

The general relationship between density, ρ, and mol per cent composition, N_a, is theoretically given by division of eq. (2) by eq. (1) thus

$$\rho = \frac{(M_a - M_b)N_a + 100M_b}{(V_a - V_b)N_a + 100V_b}. \tag{3}$$

This relationship, in agreement with that developed by Retgers (1889, p. 509), becomes increasingly rigorous as volume approaches additivity for the series.

Where composition is to be calculated from a density measurement, the following form of eq. (3) will be found more convenient:

$$N_a = \frac{100}{1 + K\dfrac{(\rho_a - \rho)}{(\rho - \rho_b)}} \tag{3a}$$

where

$$K = \frac{V_a}{V_b} = \frac{M_a \rho_b}{\rho_a M_b}$$

and V_a represents the molar volume of the end member with the larger molecular weight. Dependent upon the value of K, eq. (3*a*) may be graphically represented (density along ordinate) by three types of curves (Table 1).

TABLE 1. THE RELATIONSHIP BETWEEN THE VALUE OF K AND THE TYPE OF THEORETICAL CURVE

Value of K	Type	Description of curve
<1	I	Concave-upward quadratic
1	II	Straight line
>1	III	Convex-upward quadratic

Table 2 presents solutions of eq. (3*a*) at five selected mixed crystal densities

$$\left(\frac{\rho_a + 3\rho_b}{4}, \quad \frac{\rho_a + 2\rho_b}{3}, \quad \text{etc.}\right)$$

for 31 solid solution series in which K ranges from 0.85 to 1.15 in steps of 0.01. The utility of Table 2 may be illustrated by considering a hypo-

TABLE 2. COMPOSITION IN MOL. PER CENT, N_a, FOR CRYSTALS OF FIVE INTERMEDIATE DENSITIES BELONGING TO SOLUTION SERIES WITH K VALUES RANGING FROM 0.85 TO 1.15

Value of K* for the series	Density, ρ, of mixed crystals				
	$\frac{\rho_a+3\rho_b}{4}$	$\frac{\rho_a+2\rho_b}{3}$	$\frac{\rho_a+\rho_b}{2}$	$\frac{2\rho_a+\rho_b}{3}$	$\frac{3\rho_a+\rho_b}{4}$
.85	28.17	37.04	54.05	70.18	77.92
.86	27.93	36.76	53.76	69.93	77.72
.87	27.70	36.50	53.48	69.69	77.52
.88	27.47	36.23	53.19	69.44	77.32
.89	27.25	35.97	52.91	69.20	77.12
.90	27.03	35.71	52.63	68.97	76.92
.91	26.81	35.46	52.36	68.73	76.73
.92	26.60	35.21	52.08	68.49	76.53
.93	26.39	34.97	51.81	68.26	76.34
.94	26.18	34.72	51.55	68.03	76.14
.95	25.97	34.48	51.28	67.80	75.95
.96	25.77	34.25	51.02	67.57	75.76
.97	25.58	34.01	50.76	67.34	75.57
.98	25.38	33.78	50.51	67.11	75.38
.99	25.19	33.56	50.25	66.89	75.19
1.00	25.00	33.33	50.00	66.67	75.00
1.01	24.81	33.11	49.75	66.45	74.81
1.02	24.63	32.89	49.50	66.23	74.62
1.03	24.45	32.68	49.26	66.01	74.44
1.04	24.27	32.47	49.02	65.79	74.26
1.05	24.10	32.26	48.78	65.67	74.07
1.06	23.92	32.05	48.54	65.36	73.89
1.07	23.75	31.85	48.31	65.15	73.71
1.08	23.58	31.65	48.08	64.94	73.53
1.09	23.42	31.45	47.85	64.73	73.35
1.10	23.26	31.25	47.62	64.52	73.17
1.11	23.09	31.06	47.39	64.31	72.99
1.12	22.94	30.86	47.17	64.10	72.82
1.13	22.78	30.67	46.95	63.90	72.64
1.14	22.62	30.49	46.73	63.69	72.46
1.15	22.47	30.30	46.51	63.49	72.30

* K is defined as the ratio of the molar volume of the denser end member, A, to that of the lighter end member, B, i.e. V_a/V_b or $M_a\rho_b/\rho_a M_b$.

thetical solid solution series for which $\rho_a = 2.000$, $\rho_b = 1.000$, and $K = 0.895$. By interpolation from Table 2, five intermediate points (1.250, 27.14%; 1.333, 35.84%; 1.500, 52.77%; 1.667, 69.09%; and 1.750, 77.02%) on the theoretical curve for this series may be quickly secured. These plus the two end points permit an accurate graphical presentation of eq. (3*a*) for this particular series. The five points also show the deviation of the theoretical curve from linearity (by comparison with the corresponding values for the series where $K = 1$); for example, in this series the deviation from linearity in the $\rho_a + \rho_b/2$ region is +2.77%. The accuracy of the interpolation is high; substituting 2.000, 1.000, 1.500 and 0.895 into eq. (3*a*) for ρ_a, ρ_b, ρ, and K, respectively, yields 52.77% when the function is solved for N_a.

EXAMPLES

A Series with K<1

Complete solid solution exists between $Ni(NH_4)_2(SO_4)_2 \cdot 6H_2O$ and $Mg(NH_4)_2(SO_4)_2 \cdot 6H_2O$. From their respective gram-molecular weights, 394.99 and 360.62, and from the writer's density measurements of 1.9225 and 1.7209, respectively, K can be calculated to be 0.980 for this series. Thus, consulting Tables 1 and 2, one sees that the theoretical curve is concave-upward (Type I) and that it deviates from linearity about 0.51 mol per cent in the 50 mol per cent region.

Crystals of this series were grown from aqueous solutions, their densities measured, then carefully analyzed. Full details of growth, chemical analysis, and density measurements are given by Bloss (1951); results are summarized in Table 3. Densities are believed accurate to ±0.0005, composition to within ±0.5 mol per cent; the empirical values were not rounded off, however, for statistical reasons. The writer's end point values, 1.7209 and 1.9225, which were the results of several determinations on each of several specimens, agree closely with those in the literature which are for the magnesium member 1.721, 1.7225 (Tutton, 1905, p. 1136), and 1.721 (Perrot's value cited by Tutton, 1905, p. 1136) and for the nickel member 1.9227 (Tutton, 1916, p. 6). From Hofmann's (1931, p. 288) *x*-ray data, density is calculated to be 1.722 for the

TABLE 3. EMPIRICAL DENSITY-COMPOSITION DATA FOR THE (Ni, Mg) $(NH_4)_2(SO_4)_2 \cdot 6H_2O$ SERIES

Mol Per Cent Nickel Member	0.00	21.03	21.20	30.45	42.40	55.46	56.34	65.97	66.18	81.09	81.22	100.00
Density	1.7209	1.7611	1.7626	1.7810	1.8065	1.8304	1.8336	1.8525	1.8543	1.8831	1.8855	1.9225

magnesium end member; from Mukherjee's (1935, p. 504) x-ray data, density is calculated to be 2.038 for the nickel end member.

The data of Table 3 were next analyzed statistically. All regressions[1] were carried out in terms of composition upon density (i.e., the lines were calculated which minimized the deviations in composition of the data from them), since the calculated density-composition curves were intended for use in predicting composition from measured density values. Both linear and quadratic equations were fitted to the data by the standard method of least squares (described in Rider, 1939, pp. 27–32); their relative goodness of fit was then compared by means of calculating their t value.[2] This process was performed twice, once double weighting[3] the end points and once giving them infinite weight.[4] Extra weighting of the end points was deemed justifiable since for them composition was known absolutely and, in addition, their density values could be compared with those in the literature. For the assumption of infinitely weighted end points the quadratic

$$g(\rho) = (\rho - 1.7209)(602.76264 - 55.51659\rho) \tag{4}$$

and the straight line

$$f(\rho) = 496.032(\rho - 1.7209) \tag{5}$$

represent the equations of best fit. If the end points are only double weighted, the quadratic

$$h(\rho) = -1028.0653 + 689.6492\rho - 53.5518\rho^2 \tag{6}$$

and the straight line

$$k(\rho) = 494.6053\rho - 850.6854 \tag{7}$$

are the equations of best fit. The functions $g(\rho)$, $f(\rho)$, $h(\rho)$, and $k(\rho)$ represent composition in mol per cent of nickel ammonium sulfate. The proper values for nickel ammonium sulfate and magnesium ammonium sulfate may be substituted into eq. (3*a*) to get the theoretical relationship for this series, namely,

---

[1] In statistical terminology regression signifies the process of fitting a line to the data which accurately follows their trend yet, at least in part, lacks their chance errors.

[2] The statistical quantity t refers to "Student's" t distribution (Mood, 1950, p. 206; Rider, 1939, pp. 88–98). It was here used to compare the linear regression function with the quadratic one developed under similar weighting assumptions; in effect the calculated value of t permits a determination of the probability of the data having by chance favored a quadratic distribution even though the relationship investigated was actually linear.

[3] Each end member observation was counted twice in making the least square computations.

[4] Each end member observation was considered to have been made an infinite number of times, mixed crystal observations but once. Under this assumption the statistically derived curves must perforce pass through the end points.

$$N_{ni} = \frac{100}{1 + K \dfrac{(\rho_{ni} - \rho)}{(\rho - \rho_{mg})}}, \tag{8}$$

where

$$K = \frac{M_{ni}\rho_{mg}}{M_{mg}\rho_{ni}} = 0.98044839.$$

Table 4 indicates the relative accuracies of the various equations in predicting the composition of a mixed crystal from its measured density. Table 5 summarizes the results of statistical tests of the equations and

TABLE 4. COMPARISON OF CURVES RELATING DENSITY TO MOL PER CENT OF NICKEL AMMONIUM SULFATE IN MIXED CRYSTALS OF THE $(Mg, Ni)(NH_4)_2(SO_4)_2 \cdot 6H_2O$ SERIES

Empirical Results		End Points Given Infinite Weight				End Points Double Weighted				Theoretical Curve	
		Quadratic		Straight Line		Quadratic		Straight Line			
Density (1)	Composition by Analysis (2)	Predicted Composition (3)	Deviation* (4)	Predicted Composition (5)	Deviation* (6)	Predicted Composition (7)	Deviation* (8)	Predicted Composition (9)	Deviation* (10)	Predicted Composition (11)	Deviation* (12)
1.7209	0.00	0.00	0.00	0.00	0.00	0.16	0.16	0.48	0.48	0.00	0.00
1.7611	21.03	20.30	−0.73	19.94	−1.09	20.39	−0.64	20.36	−0.67	20.25	−0.78
1.7626	21.20	21.05	−0.15	20.68	−0.52	21.13	−0.07	21.10	−0.10	21.01	−0.19
1.7810	30.45	30.28	−0.17	29.81	−0.64	30.33	−0.12	30.21	−0.24	30.22	−0.22
1.8065	42.40	43.01	0.61	42.46	0.06	43.02	0.62	42.82	0.42	42.94	0.54
1.8304	55.46	54.88	−0.58	54.32	−1.14	54.86	−0.60	54.64	−0.82	54.80	−0.66
1.8336	56.34	56.46	0.12	55.90	−0.44	56.43	0.09	56.22	−0.12	56.39	0.05
1.8525	65.97	65.79	−0.18	65.28	−0.69	65.74	−0.23	65.57	−0.40	65.72	−0.25
1.8543	66.18	66.68	0.50	66.17	−0.01	66.62	0.44	66.46	0.28	66.61	0.43
1.8831	81.09	80.80	−0.29	80.46	−0.63	80.72	−0.37	80.71	−0.38	80.76	−0.33
1.8855	81.22	81.99	0.77	81.65	0.43	81.89	0.67	81.90	0.68	81.94	0.72
1.9225	100.00	100.00	0.00	100.00	0.00	99.86	−0.14	100.19	0.19	100.00	0.00

* From empirical data.

TABLE 5. COMPUTED STATISTICAL VALUES FOR EQUATIONS (4)–(8)

Number of Equation in Text	(4)	(5)	(6)	(7)	(8)
Residual Sum of Squares	2.250	4.423	2.169	2.744	2.297
Degrees of Freedom	9	9	9	9	
Value of t	2.948		1.707		
Probability of a Larger Value of t Arising by Chance	0.01		0.10		

indicates that, for the same method of end point weighting, the quadratic function always fitted the data significantly better than did the linear function. Moreover, calculated values of the standard statistical quantity, *t*, indicate small likelihood that this occurred by chance. Interestingly, the theoretical equation, as judged by its residual sum of squares, fits the data almost equally as well as either of the two statistically fitted quadratics. This statistical analysis leads to the following conclusions for this series:

(1) the distribution of the empirical data on density and composition in mol per cent is more likely quadratic than linear.

(2) this distribution coincides almost precisely with that predicted by theoretical eq. (8).

The latter conclusion was further checked. The average density (1.8063 ± 0.0005) and, by chemical analysis, the average composition (42.71 ± 0.5 mol per cent nickel ammonium sulfate) was determined for a group of mixed crystals grown from the same solution. Using the theoretical equation the composition was calculated from the density value to be 42.84 mol per cent.

Series with $K \cong 1$

When the value of *K* is very close to one, the density—mol per cent composition relationship may be indistinguishably close to linearity. For example, magnesium ammonium chromate, $Mg(NH_4)_2(CrO_4)_2 \cdot 6H_2O$, and magnesium rubidium chromate, $MgRb_2(CrO_4)_2 \cdot 6H_2O$, have molar volumes*of 218.3 and 217.4 cc, respectively. Since the rubidium salt has the larger molecular weight, these volumes correspond to V_b and V_a, respectively. Thus for this series *K* equals 0.996. Tables 1 and 2 indicate that, for this value of *K* the theoretical curve is an almost linear, very slightly concave-upward quadratic. Table 6 indicates that the empirical data follow the predicted theoretical distribution rather precisely; the densities predicted for the intermediate compositions on the basis of a linear relationship are slightly higher around the 50 mol per cent region than those empirically determined, an indication that the empirical curve is slightly concave upward. Furthermore, Table 2 indicates the deviation from linearity in the 50 mol per cent region to be 0.1 mol per cent or 1 part in 1,000. In terms of density, therefore, this deviation from linearity is −0.0006. As shown by Table 6, the empirical densities in the 50 mol per cent region, also differ from linearity in the same direction and by approximately the same amount.

---

* Calculated from Porter's (1925, p. 92) data.

TABLE 6. COMPARISON OF EMPIRICAL DENSITIES OF $(NH_4, Rb)_2Mg(CrO_4)_2 \cdot 6H_2O$ MIXED CRYSTALS WITH THOSE CALCULATED ON BASIS OF A STRAIGHT LINE THROUGH THE END POINTS

Empirical Data[a]		Intermediate densities calculated from end values on basis of linearity
Mol % Ammonium Magnesium Chromate[b]	Density	
0	2.463	
4.1273	2.437	2.437
14.1170	2.374	2.374
23.8121	2.313	2.313
35.2616	2.241	2.242−
45.9248	2.174	2.175−
54.1927	2.122	2.123−
60.8866	2.080	2.081−
73.9891	1.998	1.998
84.4436	1.932	1.933−
94.5609	1.869	1.869
100.0000	1.835	

[a] Porter (1925, p. 92).

[b] Recalculated from weight per cent by the writer. The third and fourth decimal places were retained for computational purposes only.

A Series Where $K>1$

An example of this type is the forsterite-fayalite solid solution series. Unfortunately, reported densities for forsterite range from 3.19 to 3.22, those for fayalite from 4.07 to 4.34, the low determinations being generally derived from artificial crystals. The data of Table 7, collected from the literature, were therefore restricted to fairly recent determinations on natural crystals.

A quadratic equation was fitted to the data by the method of least squares; the curve which best fit the data (minimized the sum of the squares of the deviations of the empirical points from it) was determined to be,

$$q(\rho) = -207.754 + 47.68521\rho + 5.25529\rho^2 \tag{9}$$

where $q(\rho)$ represents mol per cent fayalite as a function of the density, ρ, of mixed crystals of the forsterite-fayalite series.

Solution of the equation for ρ, when $q(\rho)$ is set equal to 0.00 and 100.00 mol per cent, respectively, yields the density values 3.217 ± 0.005 for forsterite and 4.36 ± 0.01 for fayalite. These values, in effect based upon the work of several investigators on 30 crystals of differing fayalite content, are assumed to be the most reliable available although they

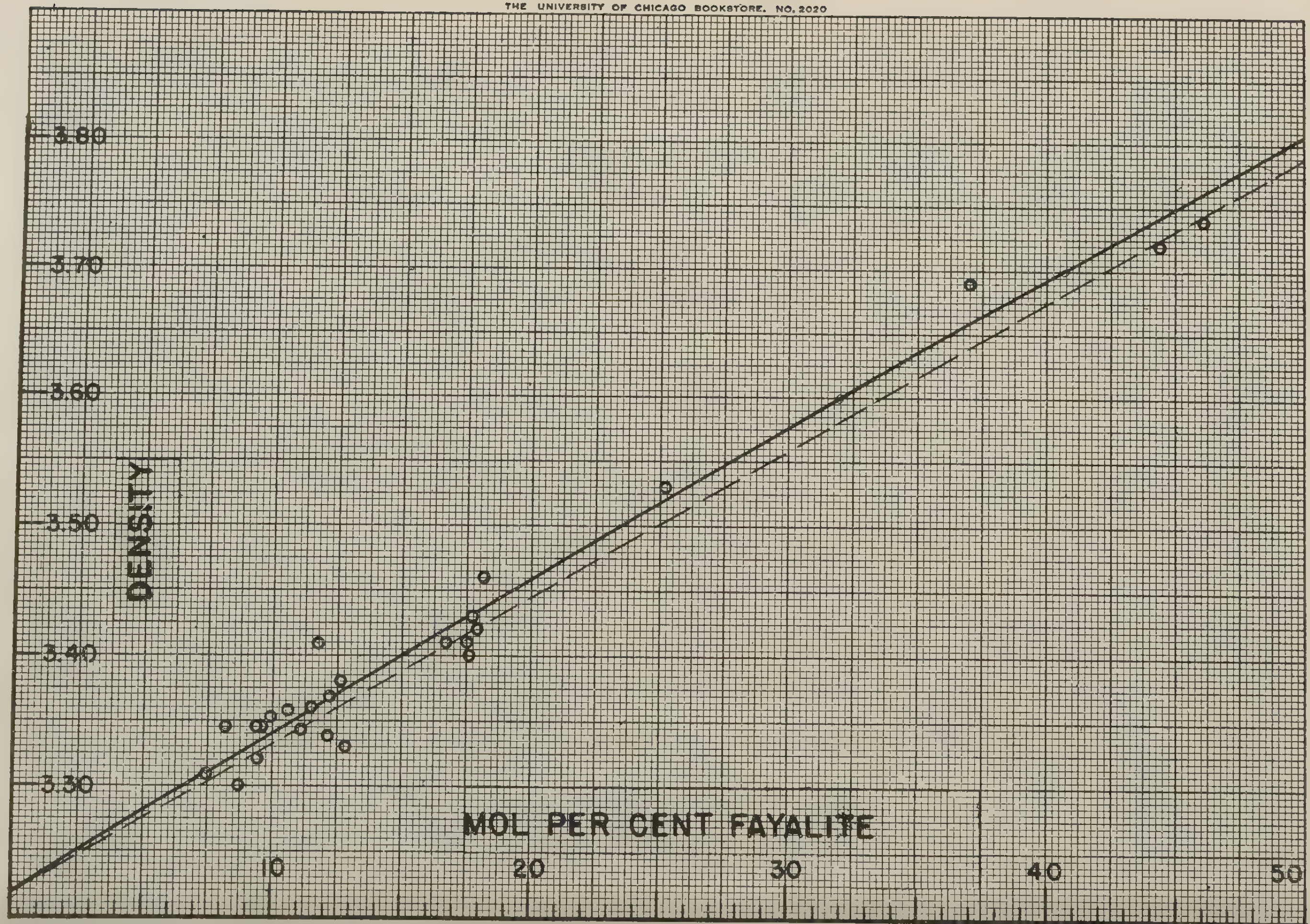
THE UNIVERSITY OF CHICAGO BOOKSTORE. NO. 2020
DENSITY
3.80
3.70
3.60
3.50
3.40
3.30
MOL PER CENT FAYALITE
10
20
30
40
50

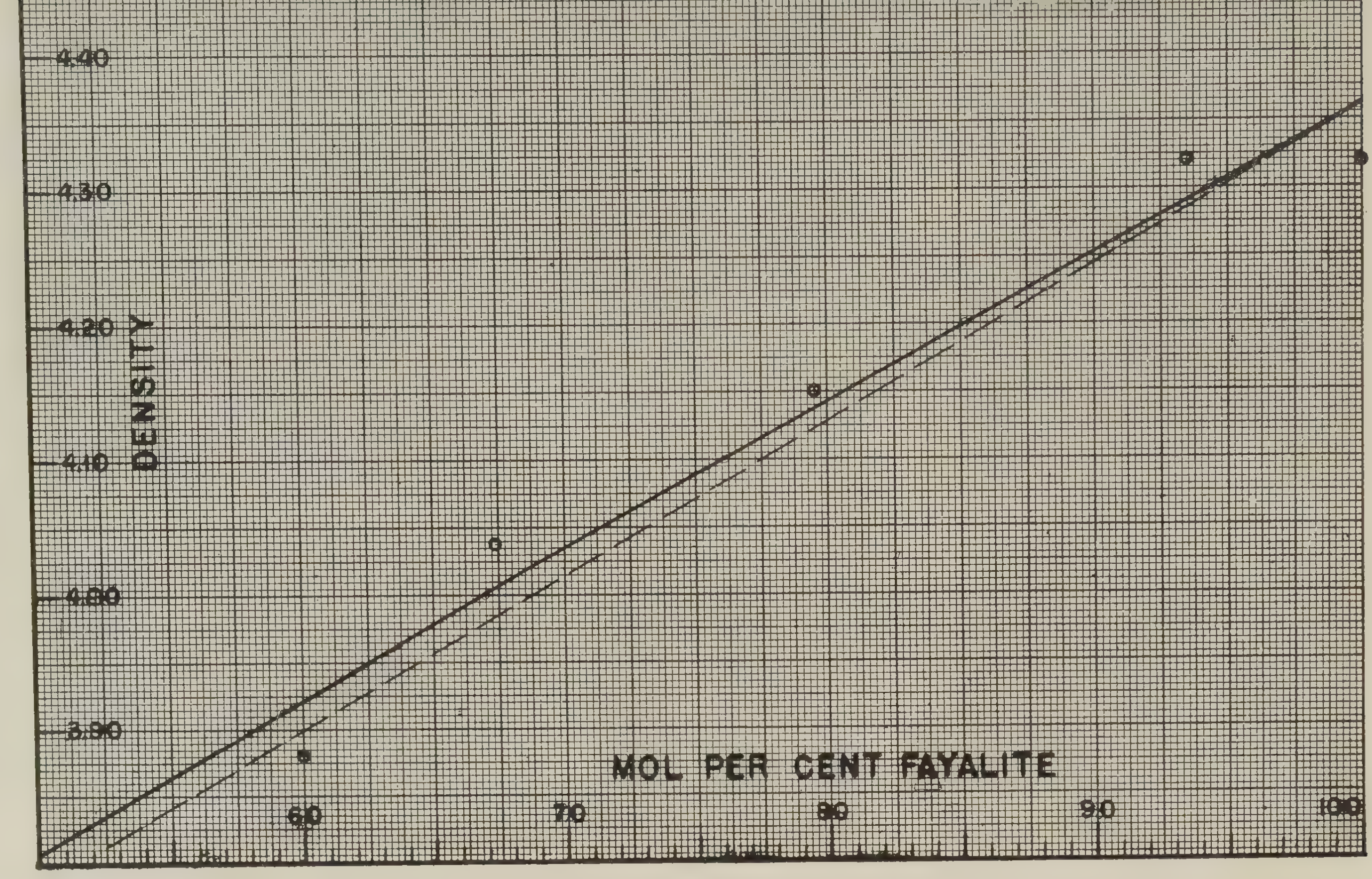

FIG. 1. The relationship between density and composition for natural crystals of the forsterite-fayalite series. The open circles represent the data of Table 7. The solid line curve indicates both the statistically derived quadratic of best fit as well as the theoretical equation secured by substituting the fitted quadratic's end points into the general theoretical equation. Only 37% of the assembled mixed crystal data plot below the dashed straight line joining the quadratic's end points; if the fayalite end point is assumed to represent a density of less than 4.36, this discrepancy

Table 7. Collected Density Data on Natural Crystals of the Forsterite-Fayalite Series

Mol % Fayalite[a]	Sp. G.	Source
7.4	3.309	Sandell and Goldich (1943, p. 177)
8.2	3.346	Gossner (1929, p. 177)
8.7	3.30	Hawkes (1946, p. 281)
9.3	3.347	Lauro (1940) [M.A. 10, p. 420]
9.4	3.321	Sandell and Goldich (1943, p. 177)
9.6	3.345	Sahama and Torgeson (1949, p. 3–5)
9.9	3.353	Sahama and Torgeson (1949, p. 3–5)
10.6	3.357	Gossner (1929, p. 177)
11.1	3.343	Ernst (1925, p. 138–9)
11.4	3.360	Aurousseau and Merwin (1928, p. 560)
11.7	3.409	Gossner, (1929, p. 177)
12.1	3.338	Sahama and Torgeson (1949, p. 3–5)
12.2	3.369	Aurousseau and Merwin (1928, p. 560)
12.6	3.38	Aurousseau and Merwin (1928, p. 560)
12.8	3.33	Mathias (1949, p. 488)
16.7	3.410	Carobbi (1928) [M.A. 4, p. 138]
17.5	3.41	Spencer (1932, p. 40)
17.6	3.40	Harada (1936, p. 294)
17.7	3.43	Esenwein (1929, p. 126)
17.9	3.42	Harada (1936, p. 294)
18.1	3.462	Carobbi (1928) [M.A. 4, p. 138]
25.2	3.53	Mathias (1949, p. 489)
37.0	3.69	Deer and Wager (1939, p. 19–20)
44.4	3.72	Sahama and Torgeson (1943, p. 5–6)
46.1	3.74	Sahama and Torgeson (1949, p. 5–7)
60.0	3.88	Deer and Wager (1939, p. 19–20)
67.4	4.038	Penfield and Forbes (1896, p. 131–2)
79.5	4.15	Deer and Wager (1939, p. 19–20)
93.5	4.32	Palmgren (1916, p. 117)
100.0	4.318	Penfield and Forbes (1896, p. 130)

[a] Since the density of tephroite is very close to that of fayalite, mol per cent tephroite was included as mol per cent fayalite.

vary somewhat from those generally cited in the literature (Table 8).

K for this series is calculated from the newly calculated density values to be approximately 1.069. On this basis the theoretical relationship between mol per cent fayalite, N_{fa}, and density, ρ, is for the series

TABLE 8. DENSITY VALUES OF OLIVINE END MEMBERS CITED IN LITERATURE

Substance	Density	Source
Forsterite (artificial)	3.223	Aurousseau and Merwin, (1928, p. 563)
Forsterite (artificial)	3.216	Bowen and Anderson, (1914, p. 498)
Forsterite (pure)	3.19	Handbook of Physical Constants, (1942, p. 10)
Fayalite (pure)	4.14	Handbook of Physical Constants, (1942, p. 10)
Fayalite (artificial)	4.068	Handbook of Physical Constants, (1942, p. 15)
Fayalite (natural)	4.318	Penfield and Forbes (1896, p. 130)

$$N_{\mathrm{fa}} = \frac{100}{1 + 1.0685366\left(\dfrac{4.36 - \rho}{\rho - 3.217}\right)} \tag{10}$$

which is graphically represented by a convex upward curve.

In Table 9 compositions predicted from density by the fitted quadratic eq. (9) are compared with those predicted by theoretical eq. (10). Since the end member densities used in the theoretical equation were derived from the fitted quadratic, the close agreement of the two near the end compositions was anticipated. Their exceedingly close agreement for intermediate compositions, however, strongly suggests that the forsterite-

TABLE 9. FORSTERITE-FAYALITE SERIES. COMPOSITIONS PREDICTED BY SUBSTITUTING DENSITY VALUES INTO THE STATISTICALLY FITTED EMPIRICAL QUADRATIC EQUATION AND INTO THE THEORETICAL EQUATION

Density	Predicted Composition (in Mol Per Cent Fayalite)	
	By Fitted Quadratic	By Theoretical Equation
3.217	0	0
3.300	6.84	6.83
3.400	15.13	15.14
3.500	23.52	23.55
3.600	32.02	32.05
3.700	40.63	40.65
3.800	49.34	49.35
3.900	58.15	58.15
4.000	67.07	67.06
4.100	76.10	76.07
4.200	85.23	85.18
4.300	94.46	94.41
4.360	100.00	100.00

fayalite data closely adhere to the theoretical curve and are not linearly distributed as commonly assumed. Figure 1 shows a plot of the collected data, of the theoretical curve (for all purposes identical to the fitted quadratic), and of the commonly accepted straight line joining the end points.

Further corroboration of the close adherence of the forsterite-fayalite density-composition data to the theoretical curve may be derived from thermodynamic considerations. Since volume is necessarily an additive property for all ideal solutions (Lewis and Randall, 1923, p. 222) and since deviations from the theoretical equation can be expected only when volume is not additive, theoretical eq. (3) should be valid for all ideal solid solutions. In particular, since the heat of solution measurements of Sahama and Torgeson (1949) established the forsterite-fayalite series as a thermodynamically ideal solid solution, the density-composition relationships for this series should therefore follow the theoretical equation.

Where the density-composition relationships do not follow theoretical equation (3), even in the face of accurate data on the density and molecular weight of the end points, the solid solution being investigated may be assumed to be non-ideal.

CONCLUSIONS

1. For all ideal solid solution series the following equation accurately expresses the relationship between density, ρ, and composition for mixed crystals of the series:

$$\rho = \frac{(M_a - M_b)N_a + 100M_b}{(V_a - V_b)N_a + 100V_b} \tag{3}$$

where N, M, and V refer by subscript to mol per cent, gram-molecular weight, and molar volume, respectively, of the two end members, A and B. The equation is numbered as in the text.

2. Solution of eq. (3) for N_a, the mol per cent of A in the mixed crystal, yields the more useful equation:

$$N_a = \frac{100}{1 + K\left(\frac{\rho_a - \rho}{\rho - \rho_b}\right)} \tag{3a}$$

where

$$K = \frac{V_a}{V_b} = \frac{M_a \rho_b}{\rho_a M_b};$$

and where substance A, by definition, has the larger molecular weight.

Thus, if the densities and molecular weights of the end members are known, the composition of an ideal mixed crystal may be calculated from its measured density.

3. Both equations are non-linear in general; only in the special case where $K=1$ do they become linear.

4. Graphically expressed with density along the ordinate, the theoretical relationship follows one of three types of curves dependent on the value of K for the series. (See Table 1 of text.)

5. The relationship between density and composition for non-ideal solutions will follow the theoretical relationship only to the extent that their molar volumes approach additivity. However, non-additivity of volume can hardly be expected to produce a relationship between density and composition more simple than that expressed by eqs. (3) or (*3a*).

6. Consequently, linear relationships between density and composition, especially where refined measurements are made, should be relatively rare. Statistically fitting a quadratic equation to the data is to be preferred over the practice of ruling a straight line through the plotted points. Where the data are too meager for statistical analysis, the theoretical equation should give better results than such a straight line, even for non-ideal solutions.

7. Where the densities are known only for analyzed crystals of intermediate compositions, the densities of the end members may be secured by either of two ways: (1) statistically fitting a quadratic to the density-composition data and solving it for the densities at 0 and 100 mol per cent compositions (as was done for the olivines in this paper), or (2) computing the molar volumes for the intermediate members and statistically fitting a linear equation to the data with subsequent solution of this equation to yield the molar volume of the end members (from which the densities may be calculated).

8. Deviation of empirical density-composition data from the theoretical relationship of eq. (3) or (*3a*) indicates the solution to be a non-ideal one.

9. The following solid-solutional series adhere to the theoretical relationship between density and composition:

(*a*) $Ni(NH_4)_2(SO_4)_2 \cdot 6H_2O - Mg(NH_4)_2(SO_4)_2 \cdot 6H_2O$ (Type I curve)
(*b*) $Mg(NH_4)_2(CrO_4)_2 \cdot 6H_2O - MgRb_2(CrO_4)_2 \cdot 6H_2O$ (Type II curve)
(*c*) Forsterite-fayalite (Type III curve)

10. Of particular interest, the forsterite-fayalite curve relating density to mol per cent is not linear as commonly assumed.

11. The density of pure natural forsterite is computed to be 3.217 ± 0.005; that of pure natural fayalite, 4.36 ± 0.01.

ACKNOWLEDGMENTS

The advice of Professors D. J. Fisher and Hans Ramberg of the Department of Geology of the University of Chicago was deeply appreciated.

I should like to thank Professor L. J. Savage of the Department of Mathematics and Mr. Harry Roberts of the School of Business (both of the University of Chicago) for their invaluable aid in designing the statistical treatment of data herein employed.

Sincere thanks are extended to Professor Fisher and to Dr. Morris W. Leighton of the Carter Oil Company for reading the manuscript. All views expressed, however, are the responsibility of the writer.

REFERENCES

AUROUSSEAU, M., AND MERWIN, H. E. (1928), Olivine: I. From the Hawaiian Islands. II. Pure forsterite: *Am. Mineral.*, **13,** 559–564.

BIRCH, FRANCIS, SCHAIRER, J. F., AND SPICER, H. CECIL (1942), Handbook of Physical Constants, *Special Paper No.* **36,** *Geol. Soc. Am.*

BLOSS, F. DONALD (1951), Relationship between light absorption and composition in the solid solutional series between $Ni(NH_4)_2(SO_4)_2 \cdot 6H_2O$ and $Mg(NH_4)_2(SO_4)_2 \cdot 6H_2O$: *Ph.D. thesis,* Department of Geology, University of Chicago.

BOWEN, N. L., AND ANDERSON, OLAF (1914), The binary system $MgO-SiO_2$: *Am. Jour. Sci.*, 4th Ser., **37,** 487–500.

CAROBBI, G. (1928), Ricerche chimiche sull' olivina di Linosa (Isole Pelagie): *Rend. Acad. Lincei, Cl. Sci. fis. mat. nat.*, Roma, ser. 6, vol. **7,** 654–660. (Not seen. Quoted from *Mineral. Abstracts*, **4,** p. 138).

DEER, W. A., AND WAGER, L. R. (1939), Olivines from the Skaergaard intrusion, Kangerdlugssuak, East Greenland: *Am. Mineral.*, **24,** 18–25.

ERNST, E. (1925), Über Olivin von Önundarfjord, N-W Island—Ein Beitrag zur Kenntnis der Olivingruppe: *Neues Jahrb. Mineral., Beilage Bd.* **52,** 113–156.

ESENWEIN, PAUL (1929), Zur Petrographie der Azoren: *Zeit. für Vulkanologie, Bd.* **12,** 108–227.

GOSSNER, B. (1929), Beitrag zur Stöchiometrie der Silicate: *Zeit. Angewandte Chem.*, **42,** 175–179.

HARADA, ZYUNPEI (1936), Chemische Analysenresultate von japanischen Mineralien: *Jour. Fac. Sci. Hokkaido Imperial Univ., Sapporo, Japan,* vol. **3,** ser. 4, 221–362.

HAWKES, H. E. JR. (1946), Olivine from northern California showing perfect cleavage: *Am. Mineral.*, **31,** 276–283.

HOFMANN, WILHELM (1931), Die Struktur der Tuttonschen Salze: *Zeit. Krist.*, **78,** 279–333.

LAURO, CARLO (1940), I minerali degli inclusi autigeni nel basalto di Conca de Janas (Orosei). I. L'olivina e lo spinello cromifero: *Atti (Rend.) R. Accad. Italia, Cl. Sci. fis. mat. nat.*, ser. 7, vol. **1,** 186–192, 290–294. (Not seen, quoted from *Mineral. Abst.*, **10,** 420).

LEWIS, G. N., AND RANDALL, MERLE (1923), Thermodynamics, McGraw-Hill Book Co., Inc., New York.

MACDOUGALL, FRANK H. (1943), Physical Chemistry, The Macmillan Company, New York.

Mathias, Morna (1949), Two olivines from S. African melilite-basalts: *Mineral. Mag.*, **28,** 486–491.

Mood, Alexander M. (1950), Introduction to the Theory of Statistics, McGraw-Hill Book Co., Inc., New York.

Mukherjee, P. L. (1935), On the isomorphism of the double fluoberyllates with the Tutton salts: *Zeit. Krist.*, **91,** 504.

Palmgren, John (1916), Die Eulysite von Södermanland: *Bull. Geol. Inst. Upsala*, **14,** 109–228.

Penfield, S. L., and Forbes, E. H. (1896), Fayalite from Rockport, Mass., and on the optical properties of the chrysolite-fayalite group and of monticellite: *Am. Jour. Sci.*, 4th Ser., **1,** 129–135.

Porter, Mary W. (1925), A contribution to the study of the optical properties of mixed crystals: *Proc. Royal Soc. London*, Series A, **109,** 78–98.

Retgers, J. W. (1889), Das Spezifische Gewicht isomorpher Mischungen: *Zeit. Phys. Chemie*, **3,** 497–561.

Rider, Paul R. (1939), An Introduction to Modern Statistical Methods, John Wiley and Sons, Inc., New York.

Sahama, Th.G., and Torgeson, D. R. (1949), Thermochemical study of the olivines and orthopyroxenes: *Report of Investigations No. 4408, U. S. Bureau of Mines.*

Sandell, Ernest B., and Goldich, Samuel S. (1943), The rarer metallic constituents of some American igneous rocks. II: *Jour. Geol.*, **51,** 167–189.

Spencer, L. J. (1932), A new pallasite from Alice Springs, Central Australia: *Mineral. Mag.*, **23,** 38–42.

Tutton, A. E. H. (1905), The relation of ammonia to the alkali metals. A study of ammonium magnesium and ammonium zinc sulphates and selenates: *Jour. Chem. Society (London), Trans.*, **87,** 1123–83.

———. (1916), The monoclinic double sulphates containing ammonium: *Philosophical Trans. Royal Society*, Series A, **216,** 1–62.

Manuscript received March 1, 1952.

STIBICONITE AND CERVANTITE

CHARLES J. VITALIANO AND BRIAN MASON, *Indiana University, Bloomington, Indiana*

ABSTRACT

The only anhydrous oxides of antimony known as minerals are senarmontite and valentinite, polymorphs of Sb_2O_3. The higher oxides of antimony occur in nature as a single phase, crystallizing in the isometric system with a structure of the pyrochlore type. This mineral has been referred to under two names, stibiconite and cervantite; as stibiconite has priority, we recommend that the name cervantite be dropped. Stibiconite always contains water in the structure, and generally some calcium also; its range in composition can be expressed by the formula: $(Sb^{3+}, Ca)_y Sb^{5+}_{2-x}(O, OH, H_2O)_{6-7}$, in which y is generally near 1, and x ranges from zero towards 1. This variability in composition is reflected in the physical properties; the density varies from 3.3 to 5.5, the refractive index from 1.62 to 2.05. Volgerite, stibianite, and hydroromeite are synonymous with stibiconite; arsenostibite is arsenian stibiconite; the names stibioferrite, rivotite, and barcenite apply to mixtures of minerals.

INTRODUCTION

The standard works on mineralogy, as for example volume 1 of the seventh edition of Dana's *System of Mineralogy*, list four antimony oxide minerals-senarmontite, valentinite, cervantite, and stibiconite. Senarmontite and valentinite, polymorphs of Sb_2O_3, are well characterized both as minerals and as laboratory products. Cervantite and stibiconite are less well defined, and material described under one or other of these names is exceedingly variable. We aim to show that cervantite and stibiconite are in fact synonymous, and that the higher oxides of antimony are represented as minerals by only one phase. During the greater part of this paper however, we will refer to this phase by the non-committal term "antimony ocher" which was in fact applied to it before the names stibiconite and cervantite were introduced.

HISTORICAL SURVEY

Both stibiconite and cervantite have been used as mineral names for over a century, but the material to which these names have been applied was known to mineralogists much earlier as antimony ocher, and this term is still current in German as "Antimonocker." The name stibiconite was introduced by Beudant in 1832 (in the form "Stibiconise") as synonymous with the material called "Antimonocker"; he described it as earthy, pale yellow to whitish yellow, found in association with stibnite. Beudant quoted no analysis, but gave the formula as $Sb_2O_4 \cdot xH_2O$, and stated that the mineral gives off water on heating. He gave no locality for it, so it is not possible to establish a type locality for stibiconite.

The name cervantite was introduced by J. D. Dana in 1850 for an antimony ocher described by Dufrenoy (1845) from Cervantes in the Spanish province of Galicia. Dufrenoy's analysis showed no water, and agreed fairly well with the formula Sb_2O_4. Hence the distinction between stibiconite and cervantite has been largely based on the presence or absence of water. Our experience indicates, however, that no anhydrous oxide of antimony other than Sb_2O_3 exists as a mineral.

Much pertinent information regarding the oxides of antimony is to be found in the literature of inorganic chemistry. This information is well summarized in the standard works of Mellor (1929) and Gmelin (1949). Even here, however, much confusion is apparent, and contradictory statements are not hard to find. Comprehensive investigations of the Sb-O system or the Sb-O-H_2O system have not yet been made. The two polymorphs of Sb_2O_3 corresponding to senarmontite and valentinite can readily be prepared in the laboratory; senarmontite is the stable form up to 570°, above which temperature valentinite is the stable form (although valentinite can be prepared even at room temperature). The most satisfactory data on the higher oxides of antimony have been obtained from researches carried out at the Department of Inorganic Chemistry of the University of Stockholm, and were summarized by Schrewelius (1943). Precipitates of hydrated Sb_2O_5 cannot be completely dehydrated without the loss of some oxygen, and it thus appears that anhydrous Sb_2O_5 is not a stable compound. The substance produced by heating hydrated Sb_2O_5 is generally not Sb_2O_4, as is stated in many places, but Sb_3O_6OH. This substance has a structure of the pyrochlore type, and is very stable; the hydroxyl group is tenaciously held, and can be removed only by heating the substance for many days or weeks at a high temperature. Such treatment produces Sb_2O_4, which thus appears to be the only anhydrous oxide of antimony besides Sb_2O_3. It is orthorhombic and is isomorphous with stibiotantalite ($SbTaO_4$). It has not been identified as a mineral. None of the so-called cervantite, nor any other material which we have examined, shows any trace of this phase.

The work of Schrewelius and others has shown that the many ways suggested for making the higher oxides of antimony all result in more or less hydrated products with a variable Sb:O ratio. These products are either non-crystalline or have a structure of the pyrochlore type. Our experience is in agreement with these results; apart from senarmontite and valentinite the only antimony oxide mineral is a phase of variable composition with the pyrochlore structure.

Methods of Investigation

This investigation began with what appeared to be a simple problem of the identification of the minerals present in pseudomorphs after stibnite from Milton Canyon, Nevada. The evident difficulty in deciding whether cervantite or stibiconite or both were present led us to undertake the examination of similar material from other localities. We are particularly indebted to the following institutions for the loan of valuable specimens: the Mineralogical Museum of Harvard University, the U. S. National Museum, the U. S. Geological Survey (through Dr. D. E. White) and the Department of Geology of the University of California. Without such a variety of material on which to work, we would have had much greater difficulty in arriving at valid conclusions. As it was, many specimens were unsatisfactory for one or another reason. The antimony ochers are usually earthy and fine-grained, and admixture with foreign matter is general. It is always difficult and often impossible to separate homogeneous material for analysis. Even material free from foreign matter may be variable in composition, as is shown by the variation in refractive index and density of pure grains taken from different parts of the same specimen.

Refractive indices were measured in white light by the immersion method; for indices greater than 1.81 P-S-CH_2I_2 liquids, standardized by the prism method, were used. Densities were determined on carefully selected grains by means of the Berman balance, carbon tetrachloride being used as the displacement liquid. *X*-ray powder photographs (Cu radiation, Ni filter) were made of material from all specimens, using 114.6 mm. diameter cameras. Spectrographic analyses were made of most specimens. We are indebted to the Indiana Geological Survey and to its spectrographer, Mr. R. K. Leininger, for the great amount of valuable data thereby obtained. Some specimens were selected for complete analyses, which were carried out by Mr. M. E. Coller, to whom we would express our appreciation for his careful work on a difficult problem. The differential thermal analyses were made on a standard type of apparatus.

CHEMICAL COMPOSITION

The first step in the investigation was the determination of refractive index and density and the taking of *x*-ray powder photographs of all the samples of antimony ocher available to us. The powder photographs all gave a similar pattern of lines, indicating that we were dealing with a single phase, but the variation in density and refractive index from one specimen to another showed that this phase must be exceedingly variable in composition. To obtain a picture of the variation in the composition chemical analyses for total antimony and H_2O (minus and plus 105°) were made on all reasonably pure specimens. The resulting data are given in Table 1.

Table 1. Data on Specimens of Antimony Ocher

No.	Sb[1]	H_2O-	H_2O+	n	D	a_0[2]	Valentinite	[3]
1	76.9	0.92	1.63	2.047	5.27		20–25%	*c*
2	75.4	1.27	3.15	1.865	5.12		15–20%	*c*
3	74.8	1.58	2.75	2.046	5.32		15–20%	*c*
4	73.8	0.61	1.98	1.993	5.54		10–15%	*c*
5	72.2	1.78	3.48	1.790	4.58		10–15%	*b*
6	69.4	3.28	5.08	1.785	4.52		10–15%	*b*
7	68.7	0.61	3.11	1.929	4.96		10–15%	*b*
8	68.2	0.72	3.10	1.735	4.68		10–15%	*a*
9	67.4	0.66	4.13	1.775	4.82		5–10%	*a*
10	67.4	1.17	4.82	1.795	4.70		5–10%	*b*
11	67.2	0.30	2.84	1.915	5.16		present?	*b*
12	66.4	0.34	3.00	1.762	5.00	10.266 Å	present?	*a*
13	65.5	0.36	3.27	1.908	4.89		5–10%	*b*
14	65.4	0.85	3.54	1.807	4.96		5–10%	*a*
15	65.4	0.14	2.85	1.795	4.76	10.275 Å	—	*a*
16	63.4	0.28	3.04	1.822	4.88		present?	*a*
17	63.4	1.78	4.61	1.775	4.23		—	*b*
18	62.9	0.77	3.67	1.728	4.43	10.264 Å	—	*a*
19	61.8	1.08	4.24	1.741	4.56	10.264 Å	present?	*a*
20	61.0	0.93	4.71	1.713	4.16		—	*b*
21	60.4	2.32	5.20	1.755	4.10	10.282 Å	—	*a*
22	59.4	1.28	5.68	1.748	4.06		—	*b*
23	56.7	0.96	5.65	1.743	4.01		—	*a*
24	56.3	1.77	5.83	1.698	3.74	10.261 Å	—	*a*
25	56.0	0.70	4.51	1.702	4.80		—	*a*
26	56.0	1.66	5.60	1.705	3.89	10.257 Å	—	*a*
27	55.8	1.51	8.68	1.705	3.72		—	*b*
28	53.7	0.72	4.99	1.731	3.96	10.269 Å	—	*a*
29	53.3	4.42	8.82	1.64	3.32		—	*b*
30	53.3	2.64	8.73	1.638	3.32		—	*b*
31	52.9	1.16	6.29	1.717	4.16	10.255 Å	—	*a*
32	52.7	3.57	9.20	1.698	3.73		—	*a*
33	52.6	0.71	4.77	1.765	4.18	10.262 Å	—	*a*

[1] Mean of two analyses; the difference between the figures given in this table and those for the same specimens in Table 2 is because the figures in this table are calculated on "dried at 105°" basis, those in table 2 on "as received" basis.

[2] ±0.005 Å.

[3] Quality of *x*-ray powder photograph: *a* = back reflections clear and sharp; *b* = back reflections diffuse; *c* = no back reflections.

Key to Tables 1, 2 and 3

1. Borneo. Harvard 95976.
2. Lugo, Spain (probably from Cervantes area).
3. Esmeralda County, Nevada. Harvard 80282.

(*Continued on next page*)

4. Yucunani Mine, Tejocotes, Oaxaca, Mexico.
5. 3¼ km. N.W. of Ateca, Zaragoza, Spain.
6. Mexico.
7. Mexico.
8. Sonora(?), Mexico. Harvard 96084.
9. Constantine, Algeria. Harvard 83283. Labelled volgerite.
10. Sonora, Mexico. Harvard 97270.
11. Argentina Mine, El Antimonio, Sonora, Mexico.
12. Ojuela Mine, Mapimi, Durango, Mexico.
13. Argentina Mine, El Antimonio, Sonoro, Mexico.
14. Empire district, Nevada. Harvard 83277.
15. China. Harvard 88887.
16. El Antimonio, Sonora, Mexico.
17. Mexico.
18. Palotes district, Durango, Mexico.
19. No locality. Univ. of California collection. Specimen is no. 4 of Larsen, *Geol. Surv. Bull.* 697, p. 136, (1921).
20. Sud Chichas, Bolivia.
21. Poggio Fuoco, Manciano, Italy (labelled hydroromeite).
22. Oaxaca, Mexico.
23. Pachecho, Zacatecas, Mexico.
24. El Antimonio, Sonora, Mexico.
25. El Antimonio, Sonora, Mexico.
26. El Antimonio, Sonora, Mexico.
27. Poggio Fuoco, Manciano, Italy (labelled hydroromeite).
28. Mexico.
29. Near San Jose Mines, Wadley, San Luis Potosi, Mexico.
30. Milton Canyon, Nevada.
31. Mexico.
32. Shia Ying Shan, near Shinkwan, North Kwangtung, China.
33. Near Taxco, Guerrero, Mexico.

Significant features of these results are the variability in total antimony, from 50% to nearly 80%, and the universal presence of combined water, its amount ranging from 1.63 to 9.20%. Significant too is the presence of valentinite as an impurity in all specimens containing more than about 67% of total antimony. This valentinite was revealed by extra lines on the powder photographs. It was seldom detected optically, and is evidently present in extremely small grains. Unfortunately the strong lines of valentinite coincide either with those of the major phase or with strong lines of quartz, which is often present as an impurity. As a result it is difficult to detect less than 10% of valentinite by means of powder photographs, so some samples labelled homogeneous may also contain this mineral.

Spectrographic analyses were also made of each of the specimens enumerated in Table 1. Besides antimony in major amounts, the spectrograms showed that calcium was omnipresent, ranging up to about 10% or more; silicon (ubiquitous as admixed quartz) occurred in amounts up to about 1% or a little more; minor amounts ($<1\%$) of Fe, Al, and Mg were present in most specimens; and occasional traces of Ag, Mn, Pb, Na, and Ti were observed.

The data showed that the antimony ochers with which we were working were essentially hydrated antimony oxides with a variable calcium content. From a consideration of the results of these initial investigations, some specimens were selected for complete chemical analysis. A major problem was the determination of the relative amounts of trivalent and quinquivalent antimony. The antimony ochers are remarkably insoluble in all the common reagents, and our experience is that they can only be dissolved in the presence of a reducing agent, which of course immediately alters the relative amounts of the two forms of antimony. We did not find a suitable reducing agent insensitive to air, so abandoned methods based on solution. The procedure finally adopted was to determine the oxygen as water removed when the antimony ocher was heated at 850° in a stream of purified hydrogen. The water given off included of course the water content of the mineral and had to be corrected for this; the remainder represented the oxygen combined with antimony plus that combined as Fe_2O_3. We are not entirely satisfied with the reliability of the procedure for samples with a high water content, since the correction involved is then considerable. Total antimony was determined by dissolving a sample in concentrated HCl containing KI as a reducing agent, under refluxing conditions in an Erlenmeyer flask. The antimony was precipitated with H_2S, and the precipitate filtered off and digested in a Kjeldahl flask with concentrated H_2SO_4 and Na_2SO_4. Upon complete solution the antimony was reduced with Na_2SO_3 and the reduced antimony then titrated with standard $KMnO_4$ at 5° C. A separate sample was used for the determination of SiO_2, Fe_2O_3, Al_2O_3, CaO, and MgO. The sample was dissolved as above and the insoluble residue filtered off; this residue was examined microscopically and proved to be quartz in all samples and is therefore reported as SiO_2. Antimony was removed by precipitation with H_2S. The iron and aluminum were then precipitated with NH_4OH. The iron was determined colorimetrically and the Al_2O_3 value obtained by difference. The calcium was determined as oxalate and the magnesium as phosphate. The Penfield method was used to determine H_2O+. Duplicate analyses were run on all samples. The results of these chemical analyses are given in Table 2.

When the analyses in Table 2 are recalculated to atoms or ions per unit cell (as recommended by Hey, 1939), using a value of 10.27 Å for a_0 and the measured density for each sample (the analyses and densities of samples 4 and 9 being corrected for an estimated admixture of 10% valentinite) the figures in Table 3 are obtained. These figures have now

TABLE 2. ANALYSES OF STIBICONITE. ANALYST, M. E. COLLER

	4	9	16	18	23	24	29	30
Sb	73.4	67.0	63.4	62.5	56.2	55.3	51.0	51.9
O	21.3	20.4	20.9	19.6	18.6	17.0	16.3	16.9
CaO	1.79	5.77	9.63	8.56	13.5	13.1	13.9	11.9
H_2O-	0.61	0.66	0.28	0.77	0.96	1.77	4.42	2.64
H_2O+	1.98	4.13	3.04	3.67	5.65	5.83	8.82	8.73
SiO_2	1.03	1.51	0.76	3.65	2.81	6.41	5.20	7.19
Al_2O_3	0.05	0.08	0.99	0.07	0.23	0.94	0.11	0.33
Fe_2O_3	0.10	0.04	0.17	0.06	0.50	0.07	0.60	0.99
MgO	0.05	0.49	0.28	0.05	0.24	0.40	0.09	0.32
Total	100.3	100.1	99.5	99.6[2]	99.7[1]	100.8	100.4	100.9

[1] Includes Na_2O, 1.02%.

[2] Includes CO_2, 0.69%.

to be interpreted in terms of the pyrochlore structure.

The pyrochlore structure belongs in the space group *Fd3m*, which has two distinct sets of 16-fold lattice positions, one set of 48-fold positions, and one set of 8-fold positions. In the type substance pyrochlore, whose ideal formula is $Ca_2Nb_2O_6F$, there are eight formula groups in the unit cell (i.e. $Ca_{16}Nb_{16}O_{48}F_8$), and the atoms are distributed as follows:

TABLE 3. ANALYSES OF STIBICONITE, RECALCULATED IN ATOMS PER UNIT CELL

	4	9	16	18	23	24	29	30
Sb^{5+}	17.5	15.8	17.1	13.9	12.7	10.1	9.5	10.0
Sb^{3+}	4.2	1.3	—	1.8	—	2.1	0.6	0.3
Ca	1.3	3.6	5.6	4.2	7.1[1]	6.2	6.0	5.1
O, OH, H_2O	55.9	53.2	54.0	48.0	47.7	43.3	42.3	42.4

[1] Includes Na, 0.5.

16 Ca in 16 (*d*)
16 Nb in 16 (*c*)
48 O in 48 (*f*)
8 F in 8 (*b*)

Many substances crystallize in this structure, and it has been shown that the 16 (*d*) positions may be occupied by Ca, Na, Sb^{3+}, Pb, Ag, K and many other elements with an ionic radius of about 1Å or greater; the 16 (*c*) positions may be occupied by Nb, Ta, Sb^{5+}, Al, Ti and other elements with an ionic radius of 0.5Å to 0.8Å; the 48 (*f*) and the 8 (*b*) positions may be occupied by oxygen, hydroxyl, and fluoride ions, or water molecules. Pabst (1939) has given a useful summary of the characteristics of the pyrochlore structure and emphasizes the occurrence of defect lattices among substances of this type. He cites examples illustrating that both the 8 (*b*) and 16 (*d*) positions can be partly or wholly unoccupied. The figures in Table 3 show that this situation is usual in antimony ocher; the 16 (*d*) positions are only partially occupied by Sb^{3+}, Ca, and (in no. 23) Na, and the 8 (*b*) positions are completely occupied only in no. 4. In addition the 16 (*c*) positions, occupied by Sb^{5+}, are also not entirely filled in some specimens (18, 23, 24, 29, 30). It is believed that the slight excess of Sb^{5+} above 16 atoms per unit cell shown by the analyses of no. 4 and no. 16 is apparent rather than real, being due to error in the oxygen determination, which is the least precise of the analytical data. Similarly, the deficiency in (O, OH, H_2O) below 48 in nos. 24, 29, 30 is not believed to reflect empty lattice points in the 48 (*f*) positions, but to be due to part of the considerable amount of $H_2O(-)$ in these specimens being constitutional. The role of water in the antimony ochers, whether present as adsorbed water, as water molecules occupying lattice positions, or as hydroxyl ions, is difficult to evaluate; probably all three forms are present in greater or less quantity in most specimens.

The structural and chemical data thus indicate that analyses of homogeneous material of antimony ocher should be interpreted in terms of the following formula: $(Sb^{3+}, Ca)_ySb_{2-x}(O, OH, H_2O)_{6-7}$. From the nature of the pyrochlore structure it is conceivable that y, i.e. total (Ca, Sb^{3+}), might rise as high as 2 in the general formula. In the analyzed stibiconites, however, this total does not exceed 1 and is usually less. The value of x can be zero, or can range towards 1.

At first glance, it is remarkable that the variability in cell content is not accompanied by changes in the size of the unit cell. Our measurements show that most specimens have a value for a_0 between 10.26 Å and 10.27 Å. Admittedly only a few samples gave powder photographs with sharp back-reflection lines from which accurate lattice dimensions could be calculated, but the less legible photographs showed a close correspondence with the measured ones. However, as Pabst points out, the pyrochlore structure is characterized by the presence of a large amount of oxygen. On account of the large size of the oxygen anion the volume of the unit cell is determined almost entirely by the anions alone, and as a first approximation the structure may be regarded as consisting of a rigid framework of oxygen, in the interstices of which the cations are situated.

PHYSICAL PROPERTIES

As may be expected from the variability in chemical composition, the physical properties also vary greatly. The density ranges from about 3.3 up to a maximum of about 5.5 (when allowance is made for the approximate content of valentinite present in the densest specimens). A marked correlation exists between density and hardness. Specimens of high density are quite hard and generally cannot be scratched with a knife blade; the maximum hardness is about the same as that of quartz. With decreasing density the hardness falls off rapidly, and although the hardness of the more earthy specimens cannot be readily evaluated, it appears to be from 3 to 4 on Mohs scale. The usual color of most specimens of antimony ocher is chalky white to pale yellow, but orange, brown, gray, and black are not uncommon. The depth of color shows a distinct correlation with the amount of iron in the specimen, and brown or black colors often signify the presence of admixed tripuhyite (iron antimonate). In material from El Antimonio gray colors generally indicated admixed bystromite (magnesium antimonate).

In the literature the statement sometimes appears that cervantite is found as acicular orthorhombic crystals. Many specimens of this type were seen, but in every case the crystals were clearly pseudomorphs after stibnite. Under the microscope, all the material proved to be exceedingly fine-grained, with no trace of crystal outlines. Mr. T. B. Rhinehammer of the Chemistry Department of this university kindly examined some of our material under the electron microscope. He reports that even under the highest magnifications most of the material appeared to be structureless aggregates; a few grains, however, showed square cross-sections. *X*-ray powder photographs of antimony ochers sometimes have broadened and diffuse lines, indicating that the crystal size is very small; this is especially the case with the more hydrated specimens.

Optical Properties

The optical study of all the specimens was done in immersion oils. In general the mineral grains vary from highly turbid to translucent. Occasionally some clear glassy isotropic grains were found intermixed with the turbid grains. The refractive index of the clear grains was similar to that of the more turbid material in all cases.

Most of the material examined has irregular fracture. A few notable exceptions are the platy material with vicinal faces in no. 27 from Poggio Fuoco, Italy, and fibrous material in specimens from the Argentina Mine, El Antimonio, Sonora, Mexico, and in no. 4 from the Yucunani Mine, Oaxaca, Mexico.

Impurities consisted of original antimony minerals, chiefly incompletely replaced valentinite and stibnite; quartz in a number of specimens, and gypsum (?) in specimen no. 1, from Borneo. Iron oxide is the most common impurity and occurs in many of the specimens examined.

Under the microscope the color ranges from white (as in the Milton Canyon and Broken Hills specimens), through yellow (massive material, Siena, Italy), yellow-brown (Losacio, Spain), to dark brown (Piedra Azul Mine, El Antimonio, Mexico). Although mainly isotropic, many of the fragments, especially where turbid, show pinpoints or aggregates of doubly refracting material in a thin band around the edge of the grains.

The refractive index of the specimens examined ranged from 1.621 to 2.047. The majority of the specimens were homogeneous. Some gave a single refractive index value, while others exhibited a range of index of refraction. In no. 31 (Mexico) the refractive index ranged from 1.701 to 1.725 with a few grains slightly higher than 1.725. In no. 18 (Paletos district, Durango, Mexico), the refractive index of the majority of the grains is 1.728 with a few grains ranging from 1.710 to 1.740. Generally no relationship between n and other physical properties was apparent where a range of refractive index was found. No. 23 (Pachecho, Zacatecas, Mexico) was an exception. This was a white ocher with a yellow tinge. As the refractive index decreased the yellow tinge became stronger. In some heterogeneous specimens, composed of turbid and clear fragments, there is little or no variation in n between the different component parts, e.g. specimen no. 1 (Borneo) microcrystalline phase $n=2.045$, acicular phase $n=2.047$. A sample of heterogeneous material, which gave a considerable difference in the n of the separate fractions, was no. 29 (Wadley, San Luis Potosi, Mexico); fraction A, $n=1.621$ and fraction B, n slightly less than 1.649.

Qualitatively the refractive index (and density) shows a direct relationship to the antimony content and an inverse relationship to the water content. These relations are not linear, however, evidently because of the complex variability of the chemical composition coupled with a greater or less degree of defectness in the structure. Hence it is not possible to establish the chemical composition of a particular specimen from a measurement of refractive index or density.

Differential Thermal Analysis

Differential thermal analyses were made on all specimens for which complete chemical analyses were available. The thermal equipment and techniques used in determining the behavior of the antimony ochers are essentially similar to those described by Kerr, Kulp and Hamilton (pp. 7–11). The major difference is that but one sample can be determined during each furnace run. Preliminary runs at ordinary sensitivity yielded curves with small indistinguishable exothermic peaks and no visible endothermic peaks. All samples were then rerun with the D.C.

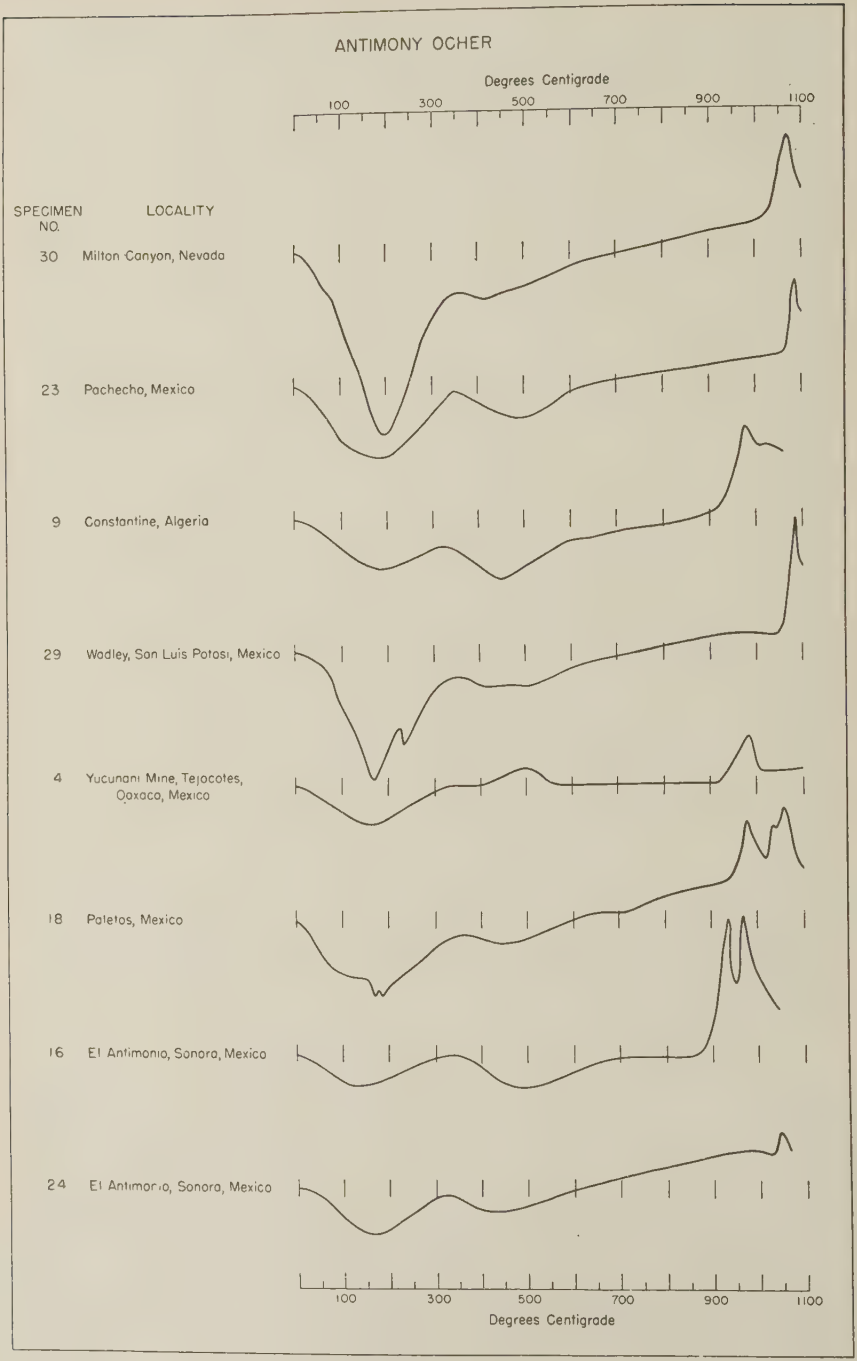
ANTIMONY OCHER
Degrees Centigrade
100
300
500
700
900
1100
SPECIMEN NO.
LOCALITY
30 Milton Canyon, Nevada
23 Pachecho, Mexico
9 Constantine, Algeria
29 Wadley, San Luis Potosi, Mexico
4 Yucunani Mine, Tejocotes, Oaxaca, Mexico
18 Paletos, Mexico
16 El Antimonio, Sonora, Mexico
24 El Antimonio, Sonora, Mexico
100
300
500
700
900
1100
Degrees Centigrade

FIG. 1

microvolt pre-amplifier in the circuit between the furnace and the recorder. The specimens were all run at a pre-amplifier scale of 50, the lowest possible magnification obtainable with the pre-amplifier in the circuit.

The resulting thermal curves (Fig. 1) show a change in composition and structure resulting in almost all instances when the specimens were heated to 1100° C. The curves for all the specimens are similar in the lower temperature ranges. A large endothermic peak representing dehydration occurs in samples nos. 30, 23, 29 and 18; and a somewhat smaller one in samples 4, 9, 16, and 24. The temperature at which the peak occurs varies slightly in each sample, but does not go above 200° C. The cause of the double peak in 29 and 18 is unknown. All the samples except no. 4 show an exothermic dome between 425° C. and 490° C. This is probably the result of a slight rearrangement of the crystal lattice. It was noted that all the thermal curves except no. 4 from the Yucunani Mine, Mexico, showed a very gradual return to the zero line after the peak representing the expulsion of H_2O. It was suspected that this might indicate gradual rather than rapid loss of H_2O in the antimony ocher. This was verified by making heat loss determinations on several specimens. These were heated up to 850° C., with weight determinations at regular intervals. Weight loss continued up to 750° C., at which temperature the last of the water had evidently been expelled. Finally, a strong exothermic peak occurs above 925° C. in all of the samples. This represents a change of phase. *X*-ray powder photographs were made on all the samples tested in the thermal apparatus. Comparison of the patterns before and after thermal analysis demonstrated the inversion to $CaSb_2O_6$ (hexagonal) at the exothermic peak temperature in all samples except no. 4. Sample 9 had, in addition to the $CaSb_2O_6$ lines on the powder photograph, a few weak lines which possibly could be attributed to unchanged stibiconite. Sample 4 remained essentially unchanged. A rerun of sample 29 to 950° C., a temperature just below the exothermic peak for this sample, showed that no change of phase had occurred as yet. On this basis it is believed that the phase change in all the specimens occurs at the exothermic peak temperature.

X-RAY DATA

The measurements of a powder photograph of a sample of pure stibiconite are reproduced in Table 4. This photograph was selected for measurement because of the purity of the sample and the sharpness of the lines. In many powder photographs of stibiconite the α_1 and α_2 lines of the back reflections are not resolved, and when the lines become very diffuse many of the weaker ones no longer appear and the strong reflections at 3.09 and 2.96 may almost coalesce. Although not the strongest line, the innermost reflection at 5.9 is useful for characterizing stibiconite, since it is extremely weak or absent in other antimony minerals with the pyrochlore structure, such as bindheimite. The strong reflection at 3.09 practically coincides with the strongest line for valentinite (3.13), which makes it difficult to recognize admixture when this mineral is present in amounts less than 10%. The best clue is a change in the relative intensities of the second and third lines in the stibiconite pattern; if the second line becomes equal to, or greater in intensity than the third, admixed valentinite is probably present.

Table 4. *X*-ray Powder Diffraction Data for Stibiconite (Cu—K$_\alpha$ Radiation; Intensities Estimated by Visual Inspection)

d	*I*	*hkl*	*d*	*I*	*hkl*
5.93	90	111	1.15	40	840
3.09	70	311	1.13	10	753 911
2.96	100	222	1.08	10	931
2.57	40	400	1.05	20	844
2.36	10	331	.987	20	666 10.22
1.98	30	511 333	.908	10	880
1.81	80	440	.897	10	955, 971, 11.31
1.74	30	531	.868	30	10.62
1.57	20	533	.855	20	884 12.00
1.55	60	622	.847	10	777 11.51
1.48	30	444	.824	10	975 11.53
1.44	30	711 551	.811	20	12.40
1.34	30	731 553	.785	10	993, 11.55, 11.71, 13.11
1.28	20	800	.783	20	10.66
1.18	40	662	.774	20	12.44

The powder photograph of stibiconite indexed in Table 4 is essentially identical with or similar to powder photographs of a number of antimony compounds indexed in the card file of *x*-ray diffraction data published by the *A.S.T.M.* (American Society for Testing Materials). For the convenience of those using this card file, the relevant cards are enumerated in Table 5. We believe that in effect all these cards index the same phase, the discrepancies between different cards being due partly to differences in technique (camera radius, radiation used, etc.), and partly to the nature of the material from which the powder photographs were made (poor crystallinity, admixture of foreign material). The photograph indexed in Table 4 was selected as the best of many taken during the course of this investigation, and the material from which it was made was carefully checked for homogeneity. We therefore believed that the data in Table 4 are the most reliable yet published for stibiconite and artificial antimony oxides with the pyrochlore structure.

TABLE 5. CARDS CORRESPONDING TO STIBICONITE IN THE A.S.T.M. FILE OF *X*-RAY DIFFRACTION DATA

Description	No. in 1950 ed.	Three strongest lines		
Antimony pentoxide	0363	6.0	3.10	2.97
Stibiconite	2364	2.92	1.80	1.53
Stibiconite	2480	2.88	1.42	1.79
Lewisite	3723	1.81	1.55	2.96
Romeite	3724	1.81	1.54	1.18
Stibiconite	3726	1.81	1.54	1.03
Hydroromeite	3725	1.80	1.54	1.17
Antimony tetroxide	3810	1.55	2.96	1.18
Antimony pentoxide hydrate, $Sb_2O_5 \cdot 3H_2O$	3815	1.55	1.81	1.18
Calcium antimony oxide, $2CaO \cdot Sb_2O_5$	3822	1.55	1.05	1.82
Antimony pentoxide	3831	1.54	1.81	1.17
Antimony pentoxide hydrate, $Sb_2O_5 \cdot H_2O$	3832	1.54	1.81	1.14
Hydroromeite	3833	1.54	1.79	1.15

STIBICONITE OR CERVANTITE?

The data presented in this paper indicate that the naturally occurring antimony oxides comprise three minerals: senarmontite, valentinite, and a third compound which we have referred to as antimony ocher. The latter compound is variable in composition and includes both stibiconite and cervantite. Which of these names should be adopted for this mineral? Since the name stibiconite (1832) antedates cervantite (1850) we suggest that the rule of priority is applicable and that stibiconite be adopted and cervantite relegated to the synonymy. Additional grounds for this procedure are that the name cervantite is false in significance. It was expressly applied by its author to the anhydrous compound Sb_2O_4, and all our analyses of antimony ocher show constitutional water. We believe that the few analyses of cervantite in the literature which show no water are unreliable, and that anhydrous Sb_2O_4 does not occur as a mineral.

We would therefore provide the following definition for stibiconite: an isometric mineral with the pyrochlore structure and the general formula $(Sb^{3+}, Ca)_y\, Sb_{2-x}\, (O, OH, H_2O)_{6-7}$. The only objection to this definition is that it is perhaps too wide, since it can include the mineral romeite, whose formula may be written $Ca_{1\frac{1}{2}}Sb_2(O, OH)_{6-7}$. If mode of occurrence were sufficient grounds for the naming of different minerals both names could be retained, since stibiconite is always found as a supergene alteration product whereas romeite is a mineral of metamorphosed ore deposits. The question is one which we prefer to leave to individual choice until such time as a clear formulation of what constitutes a mineral species has been generally accepted.

SYNONYMY

A number of names have appeared in the literature for antimony oxide minerals supposedly distinct from senarmontite, valentinite, and stibiconite. We have endeavored to obtain authentic specimens for as many of these as possible, in order to compare them with our own material, and to establish whether or not they are valid species. The results are enumerated in the following section.

Hydroromeite. The name hydroromeite was introduced by Natta and Baccaredda (1933), who applied it to specimens of "antimony ocher" from Higueras and Villafranca in Spain. Their analyses are comparable with those of stibiconite presented in this paper and the material had the pyrochlore structure with $a = 10.25$ Å. Natta and Baccaredda expressed the analyses in the formulas $CaO \cdot Sb_2O_5 \cdot 3H_2O$ and $3CaO \cdot 2Sb_2O_5 \cdot 8H_2O$, which are special cases of the general formula for stibiconite suggested in the preceding section. Under these circumstances we suggest that the name hydroromeite be dropped in favor of stibiconite.

Volgerite. The name volgerite was applied by Dana (1854) to an analyzed antimony ocher from Constantine in Algeria. The analysis is similar to those of stibiconite. A specimen labelled "Volgerite, Constantine, Algeria" (Harvard 83283) proved to consist of stibiconite with some admixed valentinite (no. 9, Table 1).

Arsenostibite (*arsenstibite*). Arsenstibite was introduced as a mineral name by Adam (1869) for a hydrous oxide of antimony and arsenic, with the Sb:As ratio about 3:1. The only other oxide of antimony and arsenic mentioned in the literature is that from Varuträsk, Sweden, described by Quensel (1937). The analysis of this material resembled that of arsenstibite, and Quensel revived this name for it, modifying it to arsenostibite for the sake of euphony. Professor Quensel kindly supplied us with a small portion of the type material from Varuträsk. It gave the characteristic *x*-ray powder photograph of the pyrochlore type, and arsenostibite is evidently structurally identical with stibiconite. Arsenostibite is a stibiconite with about one-quarter of the antimony replaced by arsenic, and in accordance with the nomenclature adopted in the seventh edition of "Dana's System of Mineralogy" it may be considered a variety of this mineral and referred to as arsenian stibiconite.

Stibianite. Stibianite was described by Goldsmith (1878) as an alteration product of stibnite from Victoria, Australia. Goldsmith's material is preserved in the museum of the Academy of Natural Sciences of Philadelphia, which kindly supplied a specimen (no. 2032) marked "Stibianite (type)" for examination. It proved to be stibiconite admixed with quartz.

Stibioferrite. Stibiaferrite (the name was changed to stibioferrite by Dana) was also described by Goldsmith (1873). Two specimens were available for study, one from the museum of the Academy of Natural Sciences of Philadelphia (no. 18562, from the Vaux Collection, labelled "Stibioferrite from California, E. D. Brown, 1918"), the other from the U. S. National Museum (no. R1769, labelled "Stibioferrite, Santa Clara County, California"). The curator of the mineral collection of the Philadelphia Academy of Natural Sciences informs us that the specimen supplied is the only one of stibioferrite in the collection, and its history is unknown. This specimen agrees with Goldsmith's description, showing small yellow crystals in yellow to brownish-yellow earthy material, the whole being enclosed in a matrix of vein quartz. It is a gross mixture; the small yellow crystals are wulfenite, the yellow to brownish-yellow material is bindheimite admixed with jarosite. The specimen from the U. S. National Museum consisted of similar brownish-yellow material in a quartz matrix without the yellow crystals. The brownish-yellow material on this specimen consisted entirely of jarosite; traces of antimony were detected spectrographically. It must be concluded that stibioferrite is not a valid species.

Rivotite. Rivotite was described by Ducloux in 1874 as a massive yellowish-green mineral disseminated through a yellowish white limestone on the west side of the Sierra del Cadi, province of Lerida, Spain. The following analysis was given: Sb_2O_5 42.00, Ag_2O 1.18, CuO 39.50, CO_2 21.00; total 103.88. Several specimens of rivotite from the type locality were available for study, all of which tallied closely with the description of Ducloux. *X*-ray powder photographs of all three were similar, and were found to correspond to malachite, with a few weak and diffuse lines of stibiconite. Dilute HCl dissolved the malachite and left a reddish colored residue which gave the stibiconite pattern alone. Under the microscope a few particles could be recognized as malachite but most grains consisted of submicroscopic aggregates, were turbid to opaque due to inclusions, and no diagnostic data could be obtained from them. To confirm our diagnosis of rivotite as a mixture of malachite and stibiconite we had a partial analysis made, with the following results: SiO_2 3.64, Al_2O_3 0.90, Fe_2O_3 5.86, CaO 1.74, Sb_2O_5 14.4, CuO 47.6, Ag_2O 1.03, CO_2 13.6, $H_2O(-)$ 1.29, $H_2O(+)$ 7.43. The proportions of CuO, CO_2, and $H_2O(+)$ in this analysis correspond closely with those required for malachite. The original analysis quoted by Ducloux is evidently erroneous. Rivotite is a mixture and the name can therefore be deleted.

Barcenite: Barcenite was described by Mallet (1878) as an antimonate of mercury occurring as pseudomorphs after livingstonite from Huitzuco, Guerrero, Mexico. Apparently no further data on this mineral has been published since Mallet's original description. A sample of barcenite, agreeing in all respects with Mallet's description, was obtained from the U. S. National Museum (no. 94243). Spectrographic analysis showed that the major metallic constituents were antimony, mercury, and calcium, in agreement with the published analysis. *X*-ray powder photographs gave a strong pattern of stibiconite accompanied by a weaker pattern of cinnabar. It is therefore concluded that barcenite is not a homogeneous mineral but an intimate mixture of stibiconite and cinnabar.

OCCURRENCE

Stibiconite typically occurs as an alteration product of stibnite, and is often clearly pseudomorphous after this mineral. The lead antimony sulfides, such as bournonite and jamesonite, generally alter to bindheimite rather than stibiconite. Stibiconite is an important ore of antimony, especially in China and Mexico. Indeed, a major part of the antimony produced in North America comes from Mexican stibiconite. Many of the Mexican deposits consist entirely of this mineral, and the derivation from stibnite is not obvious. In the El Antimonio district of Sonora, one of the larger producers of antimony ore, the stibiconite occurs as irregular masses in quartz veins, and no stibnite has ever been found in most of the mines (White and Guiza, 1949). However, it is probable that stibnite was the primary mineral.

An interesting feature is the common occurrence of valentinite intimately intermixed with stibiconite. This valentinite is often undetectable microscopically, and can only be recognized in *x*-ray powder photographs. On this account we are dubious as to whether the analyses of stibiconite and cervantite in the literature can be interpreted as representing homogeneous material. Our experience indicates that intimate admixture of stibiconite and valentinite is as common as pure stibiconite. It is intriguing that the common form of Sb_2O_3 as a mineral is valentinite, not senarmontite, which is the stable form at ordinary temperatures. The only senarmontite which we have seen is from the type locality at Hamimat near Constantine in Algeria; none of the specimens of antimony ocher which we examined contained this mineral, although many contained valentinite. Bloom (1939) showed that the formation of valentinite is favored by the presence of foreign ions, and this is confirmed by our data. Spectrographic analyses of senarmontite from Hamimat showed that it was as pure or purer than reagent grade Sb_2O_3; apart from antimony it contained a trace of arsenic and a slight trace of magnesium. Spectrograms of valentinite, however, always had numerous lines of elements other than antimony.

ACKNOWLEDGMENTS

In addition to the acknowledgments made in the body of this paper, we would like to express our thanks to the following persons for the gift or loan of specimens: Dr. G. M. Cardoso, who provided us with material from Spain; Dr. Mario Fornaseri, for specimens from Poggio Fuoco in Italy; Mr. H. M. Battey of the Auckland Museum, New Zealand; Dr. Henrich Neumann of the Mineralogisk Museum, Oslo, Norway; and Dr. Charles Milton of the U. S. Geological Survey.

REFERENCES

ADAM, M. (1869), Tableau minèralogique (no. 347).

BEUDANT, F. S. (1832), Traite elementaire de minèralogie, 2nd edition, vol. **2**, p. 616.

BLOOM, M. C. (1939), The mechanism of the genesis of polymorphous forms: *Am. Mineral.*, **24**, 281–292.

DANA, J. D. (1850), The System of Mineralogy, 3rd edition.

DANA, J. D. (1854), The System of Mineralogy, 4th edition.

DUCLOUX, X. (1874), Note sur une nouvelle espèce minèrale de la province de Lerida: *Comptes rendus*, **78**, 1471–1473.

DUFRENOY, A. (1845), Traite de minèralogie, vol. **2**.

GMELIN, L. (1949), Handbuch der anorganischen Chemie, 8th edition, vol. **18**.

GOLDSMITH, E. (1873), Stibiaferrite, a new mineral from Santa Clara County, California: *Proc. Acad. Nat. Sci. Philadelphia*, 366–370.

GOLDSMITH, E. (1878), Stibianite, a new mineral: *Proc. Acad. Nat. Sci. Philadelphia*, 154–155.

HEY, M. H. (1939), On the presentation of chemical analyses of minerals: *Mineral. Mag.*, **25**, 402–412.

KERR, P. F., KULP, J. L., AND HAMILTON, P. K. (1949), Differential thermal analyses of reference clay mineral specimens: Preliminary Report No. 3, *Am. Petrol. Inst. Project* **49**.

MALLET, J. W. (1878), On barcenite, a new antimonate, from Huitzuco, Mexico: *Am. J. Sci.*, **16**, 306–309.

MELLOR, J. W. (1929), A Comprehensive Treatise on Inorganic and Theoretical Chemistry, vol. **9**.

NATTA, G., AND BACCAREDDA, M. (1933), Tetrossido di antimonio e antimoniate: *Zeits. Krist.*, **85**, 271–296.

PABST, A. (1939), Formula and structure of ralstonite: *Am. Mineral.*, **24**, 566–576.

QUENSEL, P. (1937), Minerals of the Varuträsk pegmatite III. Arsenostibite, a hydrous oxidation product of allemontite: *Geol. Fören. Stockholm Förh.*, **59**, 145–149.

SCHREWELIUS, N. (1943), Studier över antimonat, hydroxoantimonat och fluoantimonat: Dissertation, University of Stockholm.

WHITE, D. E., AND GUIZA, R. (1949), Antimony deposits of El Antimonio district, Sonora, Mexico: *U. S. Geol. Surv., Bull.* **962-B**.

Manuscript received April 14, 1952.

CHEMICAL COMPOSITIONS OF HYPERSTHENE AND PIGEONITE IN EQUILIBRIUM IN MAGMA

HISASHI KUNO, *Geological Institute, Tokyo University,
Tokyo, Japan*

AND

KŌZŌ NAGASHIMA, *Tokyo University of Agriculture and
Technology, Tokyo, Japan*

ABSTRACT

Hypersthene and pigeonite occurring as microphenocrysts in the groundmass of hypersthene-olivine andesite from Hakone volcano were analyzed. They are almost identical in composition except that the pigeonite contains 4.06% CaO whereas the hypersthene contains 2.67% CaO. The mode of occurrence of these pyroxenes indicates that this difference in CaO content corresponds to the difference in composition across the inversion interval between the two pyroxenes in the magma. The unusually high CaO content of the hypersthene is discussed.

INTRODUCTION

Microphenocrysts of hypersthene and pigeonite, both from 0.1 to 0.7 mm. long, occur in basic andesite and basalt from Izu, Hakone, and other regions of northeastern Japan. They are characteristic of rocks free from augite phenocrysts (hypersthene andesite and hypersthene-olivine andesite), and are regarded by Kuno (1950*b*) as formed in a magma from which phenocrysts of hypersthene were separated prior to those of augite. The sequence of crystallization of pyroxenic phases in these rocks is as follows:

Intratelluric stage		During or just before extrusion		Effusive stage
Hypersthene phenocyrsts	→	Hypersthene and/or pigeonite microphenocrysts	→	Small crystals of subcalcic augite (pigeonitic augite of Kuno)

This sequence is seen also in pyroxenes of many dolerite and gabbro intrusions. The orthopyroxene occurring in the lower part of the dolerite sheets and the pigeonite (the early pigeonite of Walker and Poldervaart, 1949) in the upper part of the same sheets correspond respectively to the microphenocrystic hypersthene and pigeonite in the volcanic rocks. The pigeonite is interpreted as formed in place of the orthopyroxene when the magma crossed the clinopyroxene-orthopyroxene inversion curves (Hess, 1941; Edwards, 1942; Walker and Poldervaart, 1949; Kuno, 1950*b;* Poldervaart and Hess, 1951). The relation is illustrated by

Figs. 1 and 2. During the crystallization of magma, the orthopyroxene changes its composition until point *a* of both figures is attained. At this point, the orthopyroxene changes to pigeonite of the composition represented by point *b*. The distance between points *a* and *b*, namely the inversion interval, can be determined by analyzing the two pyroxenes associated in a single rock.

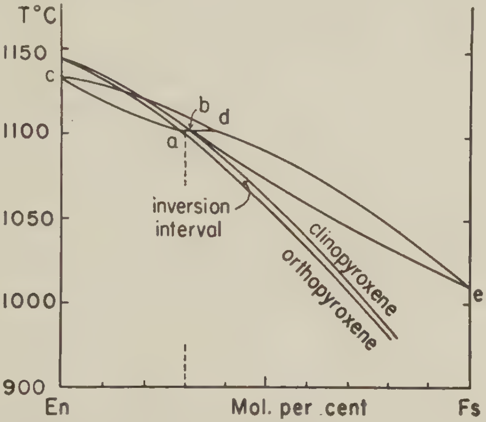

FIG. 1. Binary diagram En-Fs showing solidus (*c-a-b-e*) and liquidus (*c-d-e*) curves of crystallizing magma postulated by Kuno (1950*b*) and inversion curves given by Bowen and Schairer (1935). The inversion interval is shown schematically.

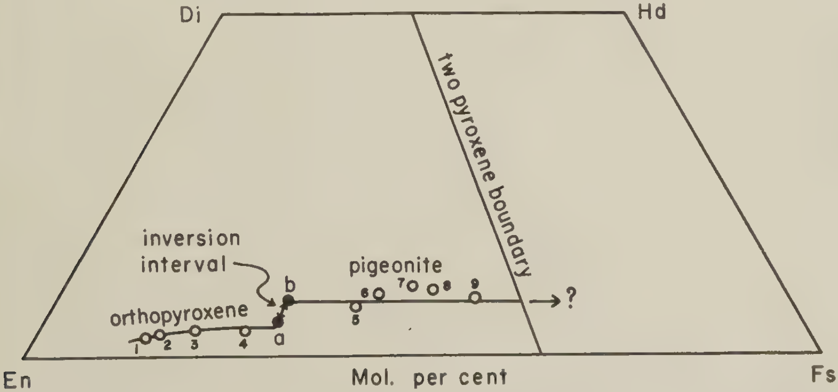

FIG. 2. The lower part of ternary diagram Wo-En-Fs showing the course of crystallization of orthopyroxene and pigeonite (after Poldervaart and Hess, 1951). Selected analyses of pyroxenes are plotted in the diagram. 1 is the orthopyroxene from Great Dike, South Africa, and 2–4 are those from Stillwater Complex, Montana (all unpublished analyses of Hess). *a* and *b* are orthopyroxene and pigeonite, respectively, described in this paper. 5 is pigeonite from Hakone (unpublished analysis of Kuno). 6, 7, 8, and 9 are pigeonites Nos. 41, 43, 42, and 44, respectively, in the table of analyses given by Hess (1949).

The separation of the two pyroxenes in dolerite and gabbro is extremely difficult, if not impossible, because part or all of the pigeonite has inverted again to orthopyroxene with exsolved blebs or plates of augite upon further cooling. However, the microphenocrystic pyroxenes can be separated from their mother rocks.

The microphenocrystic pyroxenes were separated by one of the writers (H. K.). The materials were analyzed by the other writer (K. N.). The former is responsible for the optical examination and interpretation.

Mode of Occurrence of the Pyroxenes

The hypersthene and pigeonite microphenocrysts occur either independently in different rocks or side by side in the same rock. In the latter case, some of the crystals form parallel intergrowths, the pigeonite being always outside the hypersthene.

At the base of the lava flow exposed on the eastern caldera wall of Hakone volcano, just below the horizon of basalt lava and agglomerate, there are several successive flows of basaltic andesite.* These flows are mostly scoriaceous and blocky, and are nearly identical to each other in mineral composition. The phenocrysts are plagioclase, olivine, and hypersthene. The microphenocrysts of hypersthene and/or pigeonite are set in a fine-grained groundmass consisting of plagioclase, clinopyroxene with 2V about 40° in the {010} plane, magnetite, glass, and cristobalite.

Two specimens were collected from a single lava flow exposed at an elevation of 450 m. on the northeastern wall of a valley named Tengu-zawa, southeast of Hatazyuku. One of them contains microphenocrysts of hypersthene alone whose optical properties are shown in No. 1 of Table 1. The other contains microphenocrysts of both hypersthene and pigeonite with optical properties shown in No. 2*a* and No. 2*b*, respectively.

A lava exposed at an elevation of 440 m. on the southwestern wall of a small valley named Usugoya-zawa, about 900 m. west of the former locality, is probably a continuation of the same flow. A specimen from Usugoya-zawa contains microphenocrysts of pigeonite alone whose optical properties are shown in No. 3 of Table 1.

Table 1 shows almost complete agreement between the optical properties of the hypersthenes Nos. 1 and 2*a* and between those of the pigeonites Nos. 2*b* and 3. This indicates the close proximity of their compositions.

It may be inferred that during the crystallization of these microphenocrysts the temperature of the magma was very near the inversion

---

* Lettered O_2 in the geologic map by Kuno (1950*a*).

TABLE 1. OPTICAL PROPERTIES OF THE PYROXENE MICROPHENOCRYSTS FROM HAKONE

No. 1 Hypersthene from Tengu-zawa	No. 2*a* Hypersthene from Tengu-zawa	No. 2*b* Pigeonite* from Tengu-zawa	No. 3 Pigeonite* from Usugoya-zawa
$\alpha=1.687$–1.695	2V=62°(−)	$\alpha=1.693$ (min.)	$\alpha=1.693$–1.698
$\beta=1.695$–1.703		2V=33°–8°(+)	$\beta=1.696$–1.701
$\gamma=1.699$–1.707		(O.P.$\perp$010)	$\gamma=1.720$–1.725
2V=64°–62°(−)			2V=27°–0°(+)
$r>v$			(O.P.$\perp$010)
Average:			→5°
$\alpha=1.691$			(O.P. in 010)
$\beta=1.699$			$r>v$
$\gamma=1.703$			$c\wedge Z=42^\circ$
2V=63°			
			Average:
			$\alpha=1.695$
			$\beta=1.698$
			$\gamma=1.722$
			2V=14° (O.P.$\perp$010)
			Z=Y=very pale green
			X=pale brown

* Showing zonal structure from less calcic core to more calcic margin.

temperature of hypersthene to pigeonite, and that a slight variation of temperature or composition in different parts of the magma has resulted in the difference of the pyroxenic phases. The pyroxenes Nos. 2*a* and 2*b* represent the hypersthene and pigeonite approximately in equilibrium with one another across the inversion interval. However, this interval was determined by analyzing the pyroxenes Nos. 1 and 3, instead of Nos. 2*a* and 2*b*, in view of the difficulty of separating the two pyroxenes within the same rock.

CHEMICAL COMPOSITIONS

Special care was taken in obtaining pure materials for chemical analysis. The olivine phenocrysts in these rocks are entirely altered to chlorite and a carbonate mineral. The porphyritic hypersthene is almost negligible in quantity. The rocks were first crushed to a powder with grain size a little larger than the microphenocrysts but smaller than the hypersthene phenocrysts. After passing through the electromagnetic separator, it was found that most of the hypersthene phenocrysts entered into the less magnetic fraction, whereas the pyroxene microphenocrysts were attracted to the more magnetic fraction owing to adhering grains of the groundmass magnetite. Next the more magnetic fraction was crushed to a powder with grain size a little smaller than the microphenocrysts but much larger than the groundmass grains of clinopyroxene and magnetite. After the electromagnetic treatment, a mixture of plagioclase and microphenocrystic pyroxenes free from groundmass pyroxene and magnetite was obtained from which the plagioclase was entirely removed by heavy liquids.

The materials thus separated still contained minute dust of an opaque mineral, probably hematite, but no lime bearing impurity. Repeated analyses were made which gave almost the identical results. The estimated amounts of the hematite impurity were subtracted from the analyses as shown in Nos. 1 and 3 of Table 2.

TABLE 2. CHEMICAL COMPOSITIONS OF THE PYROXENES FROM HAKONE

	No. 1	No. 3		Numbers of metal atoms on the basis of 6 oxygens			
				No. 1		No. 3	
SiO_2	53.17	52.84	Si	1.958	1.987	1.956	1.981
Al_2O_3	0.45	0.44	Al	0.022		0.018	
Fe_2O_3	1.32	1.06	Al	—		—	
FeO	17.18	16.89	Ti	0.007		0.007	
MgO	23.81	23.51	Fe'''	0.035	2.028	0.031	2.049
CaO	2.67	4.06	Fe''	0.528		0.522	
Na_2O	0.47	0.19	Mn	0.015		0.018	
K_2O	0.00	0.00	Mg	1.315		1.305	
H_2O+	n.d.	n.d.	Ca	0.104		0.160	
H_2O-	0.21	0.22	Na	0.031		0.013	
TiO_2	0.22	0.22					
P_2O_5	n.d.	n.d.	Ca	5		8	
MnO	0.48	0.56	Mg	66		64	
SrO	0.00	0.00	$Fe''+Fe'''+Mn$	29		28	
Total	99.98	99.99					

No. 1. Hypersthene in hypersthene-olivine andesite (HK49032901*b*) from Tengu-zawa, eastern caldera wall of Hakone volcano. The analysis was corrected for 0.5% hematite impurity.

No. 3. Pigeonite in hypersthene-olivine andesite (HK47122401) from Usugoya-zawa, eastern caldera wall of Hakone volcano.

The analysis was corrected for 1% hematite impurity.

By comparing the analyses Nos. 1 and 3, it will be seen that each oxide, except CaO, varies within the limit of only 0.33%. The difference of CaO content is obviously more than the analytical error.

It may be concluded that the change from hypersthene to pigeonite during the crystallization of the magma involved an increase of CaO content of about 1.4% but no appreciable change in the contents of the other oxides, the ratio $Mg:Fe^{+2}+Fe^{+3}+Mn$ remaining nearly constant. This ratio is 70:30, agreeing exactly with the generalization by Hess and Poldervaart (1951). However, the change takes place at more iron-rich compositions in porphyritic pyroxenes (Kuno, 1950*b*).

The analyzed hypersthene shows the highest CaO content so far known for orthopyroxenes from volcanic rocks. The CaO content of orthopyroxene phenocrysts is less than 2% (Kuno, 1941, 1947, 1950*b*; Larsen and others, 1936, 1937, 1938; Taneda, 1946). According to Hess* the CaO content of orthopyroxenes of basic plutonic rocks is also less than 2%.

Two alternative explanations may be offered to account for the high Ca content of the hypersthene No. 1. (1) It is a metastable phenomenon caused by rapid cooling of the magma. (2) The high Ca content is normal for an orthopyroxene which is in equilibrium with pigeonite across the inversion interval. One of the writers (H. K.) prefers the second alternative. He expects that such a lime-rich orthopyroxene would be found commonly in dolerite and gabbro, if chemical analyses were made on crystals directly surrounded by the orthopyroxene with exsolved blebs or plates of augite (inverted pigeonite).

From the ratio $Mg:Fe^{+2}+Fe^{+3}+Mn$ of the two pyroxenes given in Table 2 and the diagram Fig. 1, the temperature of the lava at the time of extrusion can be determined approximately as 1100°C.

ACKNOWLEDGMENTS

The cost of the present study was defrayed by a grant from the Japanese Government Expenditure for Scientific Research which is greatly appreciated by the writers. They also wish to express their acknowledgments to Professor H. H. Hess of Princeton University and Professor A. Poldervaart of Columbia University for a critical reading of the manuscript and the use of unpublished analyses.

REFERENCES

BOWEN, N. L., AND SCHAIRER, J. F. (1935), The system $MgO\text{-}FeO\text{-}SiO_2$: *Am. Jour. Sci.*, 5th ser.: **29,** 151–217.

EDWARDS, A. B. (1942), Differentiation of the dolerites of Tasmania: *Jour. Geol.*, **50,** 451–480; 579–610.

HESS, H. H. (1941), Pyroxenes of common mafic magmas: *Am. Mineral.*, **26,** 515–535; 573–594.

——— (1949), Chemical composition and optical properties of common clinopyroxenes, Part I: *Am. Mineral.*, **34,** 621–666.

---

* Oral communication.

KUNO, H. (1941), Dispersion of optic axes in the orthorhombic pyroxene series: *Proc. Imp. Acad. Tokyo,* **17,** 204–209.

——— (1947), Two orthopyroxenes from the so-called bronzite-andesites of Japan: *Proc. Japan Acad.,* **23,** 117–120.

——— (1950 *a*), Geology of Hakone volcano and adjacent areas, Part I: *Jour. Fac. Sci. Univ. Tokyo,* Sec. II, **7,** 257–279.

——— (1950 *b*), Petrology of Hakone volcano and the adjacent areas, Japan: *Bull. Geol. Soc. Am.,* **61,** 957–1020.

LARSEN, E. S., IRVING, J., GONYER, F. A., AND LARSEN, E. S., 3RD. (1936, 1937, 1938), Petrologic results of a study of the minerals from the Tertiary volcanic rocks of the San Juan region, Colorado: *Am. Mineral.,* **21,** 677–701; **22,** 889–905; **23,** 417–429.

POLDERVAART, A., AND HESS, H. H. (1951), Pyroxenes in the crystallization of basaltic magma: *Jour. Geol.,* **59,** 472–489.

TANEDA, S. (1946), Hypersthene from Haruna volcano: *Jour. Geol. Soc. Japan,* **52,** 61–64.

WALKER, F., AND POLDERVAART, A. (1949), Karroo dolerites of the Union of South Africa: *Bull. Geol. Soc. Am.,* **60,** 591–706.

Manuscript received March 10, 1952.

CONE-AXIS DIFFRACTION PATTERNS

D. JEROME FISHER, *University of Chicago, Chicago 37, Illinois*

ABSTRACT

Cone-axis *x*-ray pictures have been described briefly by Buerger (1944). They are obtained when a lattice translation direction is given a precessing motion with respect to the direct beam, providing a flat film is placed in the holder of the precession camera which is normally occupied with the layer-line screen. The result is a series of diffracted spots which lie along concentric circles ("rings"), one for each level of the reciprocal lattice within range. A cone-axis photo bears about the same relation to a precession picture that a rotation film has to a Weissenberg.

While cone-axis photos are useful in determining the value of d^* in the direction of the precessing crystal axis, they have a number of other possible uses, as herein discussed. After a short introduction to the precession technique, the present paper outlines the methods for indexing the spots on these pictures. A number of features of cone-axis films are then discussed under miscellaneous remarks, after which the use of these patterns for orientation purposes is briefly described. The paper concludes with a section on the Laue streaks found on these films.

INTRODUCTION TO THE PRECESSION TECHNIQUE

The Buerger precession camera (here assumed to be set up for a fixed, collimated horizontal *x*-ray beam) consists basically of a bed carrying a pair of two-axis universal joints whose centers are offset by a distance F along a horizontal line which coincides with the undiffracted beam.[1] Each joint comprises a horizontal and a vertical axis, like an oarlock; oscillation about these is so coupled that the resultant movement of a chosen direction (a crystal axis) through the center of the joint is that of the generatrix of a cone whose axis is the undiffracted beam. In the same way when the handle of an oar on a rowboat is moved along a circular path, the oar itself (like the crystal axis) becomes the generatrix of a cone. Figure 13[2] shows a simple model which illustrates this condition. One end of the rod representing the precessing crystal axis is pointed; this fits in a groove in the end of a cylinder (whose axis coincides with the direct beam) so that this pointed tip may be moved about a circular path. The two wire grids represent fantastically-enlarged levels of the reciprocal lattice (as cut off by the sphere of reflection) normal to the precessing axis. On the precession camera the two universal joints are tied together through a parallel linkage in such fashion that they partake of identical motions.

---

[1] A photograph of the current model of this instrument (as made by Charles Supper) appears as Fig. 6 on p. 100 (Fisher, 1952 *b*). V_{x1} is the vertical axis through the crystal and V_{ca} is the one through the film cassette.

[2] The numbers here assigned to figures, tables and formulas are in continuation of those used for the same purposes in earlier papers (Fisher, 1952 *b*, *c*).

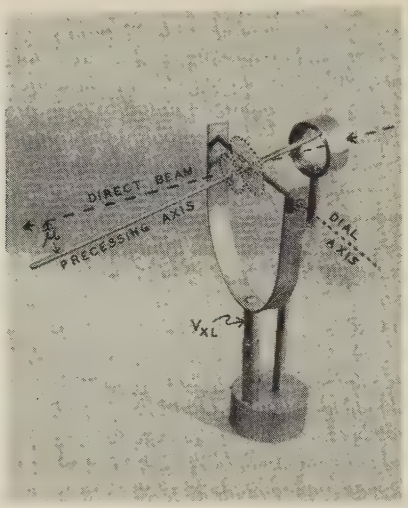

Fig. 13. Model to illustrate the first universal joint of the precession set-up. V_{xl} is the vertical axis through the crystal; the latter is also on the horizontal dial axis.

The crystal is mounted at the center of the first joint (at S, Fig. 14) so that its horizontal oscillation axis, called the dial axis, is parallel to a reciprocal axis (or any desired translation direction of the reciprocal lattice) of the crystal. The dial axis moves in a horizontal plane (as it oscillates back and forth on the vertical axis of the joint); the dial axis is thus normal to the direct beam at only two moments during a single

---

⋙→

Fig. 14. Vertical cross-section of the precession set-up (includes the direct beam and the $\bar{\mu}$-arc). This is a scale drawing to fit the sphalerite photo of Fig. 17, except that $s'=30.22$ mm.

Symbols

D—Distance, crystal to 0-level film measured normal to the film (SP_0).

F—Distance, crystal S to center Z_0 of 0-level film along the path of the undiffracted beam.

$\bar{\mu}$ (bar mu)—Angle between the direct beam and the normal to the reciprocal lattice levels (the precessing crystal axis).

$\bar{\nu}$ (bar nu)—Half apical angle of an n-level diffraction cone.

0—Points on the one-level film: 0_c=center; 0_0=0-level diffraction cone; 0_1=1-level diffraction cone.

P—Points on the precessing crystal axis: P_r=sphere of reflection; P_c=cone axis film; P_1=1-level film; P_0=0-level film.

R—Points in the reciprocal lattice: R_0=0-level (zero-point at R_0); R_1=1-level.

S—Center of crystal, at center of the sphere of reflection.

Z—Points on the zero-level film: Z_0=0-level diffraction cone (film center at Z_0); Z_1=1-level diffraction cone.

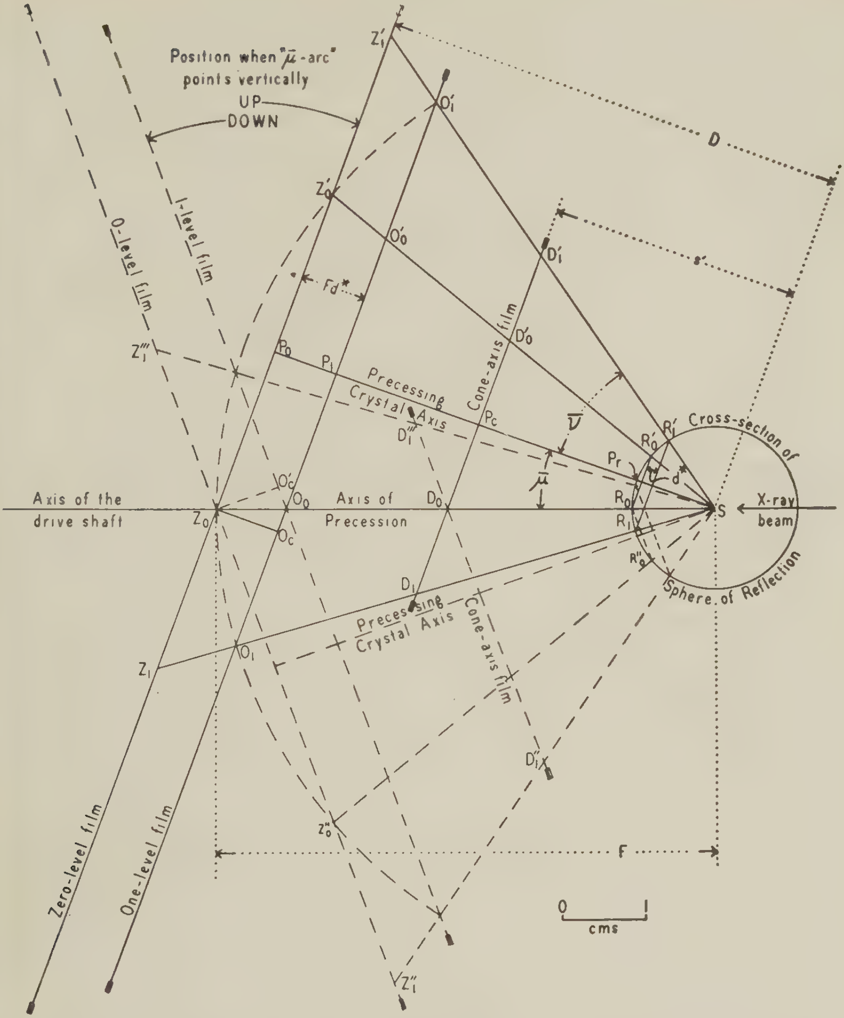

360° precession; these are the two positions of Fig. 14 (one shown by solid lines, the other with dashed lines); here the dial axis is normal to the paper through *S*. Mounted on the dial axis (and so partaking of a precessing motion identical with that of the crystal) is a bracket carrying the layer-line screen holder in which may be placed a plane layer-line screen (having an annular opening) at a distance *s* from the crystal, or a cone-axis flat-film cassette, with distance *s′* from crystal to film (measured normal to the screen holder). The layer-line screen is used when taking ordinary precession pictures, so that diffracted beams from but a single level of the reciprocal lattice can strike the film.

The plane film for taking a precession picture, which is an undistorted enlargement of a limited portion of some one level of the reciprocal lattice, is mounted in a cassette suspended in the second universal joint, whose center coincides with Z_0 (at a distance F from S, Fig. 14), the center of the zero-level film which lies on the undiffracted beam. For taking n-level precession pictures the cassette is moved towards the crystal a distance Fd^* along an axis normal to the film; n-level film is thus always parallel to that of the 0-level, but is closer to the crystal by a variable distance Fd,* where d^* is the spacing (measured in reciprocal lattice units) between adjacent levels of the reciprocal lattice measured along the precessing axis. The center of an n-level film is at O_c, which does not lie on the undiffracted beam during precession.

Since the crystal is mounted on the dial axis with a reciprocal lattice translation direction parallel this axis, levels of the direct lattice must lie normal to it. Thus the dial axis may be clamped at an azimuth position read on the dial such that a crystal axis (or some chosen translation direction of the direct lattice) lies in a horizontal plane (when the precessing position is 90° off that shown diagrammatically in Fig. 14)[3] and is normal to the dial axis. Under these conditions the crystal axis is set to undergo a precessing motion. The instrument is so designed that the angle (designated $\bar{\mu}$; read "bar mu") between the precessing crystal axis and the finely-collimated x-ray beam may be varied from 0° to about 30°; in Fig. 14, the value is 20°, one in common use. This setting is made by moving the "film-normal shaft" along the "$\bar{\mu}$ arc" attached to the front and of the horizontal drive shaft (the axis of which coincides with the undiffracted beam); the solid line part of Fig. 14 represents the condition where the $\bar{\mu}$ arc is up, and the dashed line part fits when this arc is down. The film-normal shaft is parallel to the precessing crystal axis, thus it is always normal to the dial axis, the $\bar{\mu}$-arc, and the film. When $\bar{\mu}=0°$, no precession occurs and so the crystal axis is parallel to the x-ray beam. Moreover with this angle set to 0° the instrument is suitable for taking flat film transmission Laue photos.

It is obvious that levels of the reciprocal lattice (R_0, R_1, etc. of Fig. 14) must lie normal to the precessing direction, since the latter is a crystal axis. These levels being planes cut the sphere of reflection in concentric circles whose common center is P_r (the point where the precessing crystal axis pierces the sphere of reflection). Thus the diffracted beams that "flash" out momentarily from any one level of the reciprocal lattice as the crystal undergoes its precessing motion must lie along a conical surface, the *diffraction* cone, whose axis is the precessing crystal axis, and whose half opening angle is designated $\bar{\nu}$ (read "bar nu"). Since the cone-axis film partakes of the same precessing motion as the crystal, and one identical with it (not offset from it, as is true for the various level precession films), the cones of diffraction for the various levels cut this film in a series of concentric circles or "rings." The diameters of these appear in Fig. 14 as D_0D_0' for the 0-level, D_1D_1' for the 1-level, etc.[4] A cone-axis picture is reproduced in Fig. 17*b*. Note from Fig. 14 that one generatrix for the 0-level diffraction cone (that from S to D_0) coincides with the undiffracted x-ray beam. Thus

---

[3] Actually the crystal is mounted when the $\bar{\mu}$-arc is set to 0°. Thus the chosen crystal axis is made horizontal (by adjusting the azimuth reading on the dial) without respect to any particular precessing position.

$$r_0 = s' \tan \bar{\mu} \tag{39}$$

where r_0 is the radius of the 0-level cone-axis ring. Since the instrument is set to a given $\bar{\mu}$ value, and r_0 can be measured from the film, this equation is convenient for computing s', the distance from the crystal to the film. Knowing this value and measuring r_1 (the radius of the 1-level cone-axis ring on the film) enables one to compute $\bar{\nu}_1$ (the half-apical angle for the 1-level diffraction cone), since

$$r_1 = s' \tan \bar{\nu}_1. \tag{40}$$

It will be noted that $\bar{\nu}_0 = \bar{\mu}$. Thus the latter symbol is employed for this angle, so that in general $\bar{\nu}$ can be used without a subscript when one is discussing some particular n-level. Of course if d^* is known, $\bar{\nu}$ can be computed from

$$\cos \bar{\nu}_n = \cos \bar{\mu} - d^* \qquad (41) \quad \text{[Buerger, 1944 (14)]}.$$

In making precession photos of the various levels, since the film cassette precesses off the universal joint centered at Z_0, offset by a distance F from the crystal, the diffraction cone from any one level shears over the film about a circular path, in contrast to the situation for the cone-axis film. Thus for cone-axis pictures the points D_1 and D_1' in one position of Fig. 14 go to the points D_1'' and D_1''' respectively in the other position; it will be noted that D_1 and D_1'' are the same distance from the bottom edge of the film. In similar fashion corresponding points Z_1 and Z_1' on the zero-level film in the "$\bar{\mu}$ arc up" position go to points Z_1'' and Z_1''' respectively in the other position, but it is clear that while Z_1 is only a short distance below the center of the film, Z_1'' is near the bottom edge. In short as the diffraction cone precesses, a larger *precession cone* is generated; the axis of this coincides with the undiffracted beam, and its half opening angle is $\bar{\mu}+\bar{\nu}$.

---

[4] In using Fig. 14 one should always remember that the sphere of reflection shown on it is purely schematic, and not drawn to the scale given. Thus its radius is unity; this may be thought of as 1 A (where λ is measured in A). Thus SZ_0 ($=F$, which is generally 6 cms.) is 600,000,000 times as great as SR_0!

INDEXING CONE-AXIS PICTURES

In indexing a cone-axis film it is first desirable that each level on it be converted to the same scale as the level precession film. Since each level of a series of precession pictures is photographed at a different distance from film to crystal (so that the resultant films can be superposed, with the reciprocal lattice grid developed on the same scale on each one), whereas the several levels appear on a single cone-axis film, it is clear that each cone-axis ring must be enlarged by a different factor to fit the proper level precession film. Of course this enlargement can be avoided by taking a series of cone-axis films at different s' values, one to fit each distance value of the various level precession films; but this technique is too time-consuming as well as expensive to be practicable.

While the scale of each level precession film may be reduced to fit that of the proper cone-axis ring, the reverse procedure is generally simpler, since it merely involves moving each spot on a given ring out radially a suitable distance. This is conveniently done by making a trace-o-film[5] copy of the spots of any ring, drawing radii through these, and adding another set of spots where these radii cut a newly-drawn circle of suitable radius r_D.

Taking first the n-level case, specifically the 1-level of Fig. 14, it is clear that the normal distance D from the crystal to the 0-level film is $F \cos \bar{\mu}$, and to the 1-level film is $D\text{-}Fd^*$. Thus from similar triangles the radius r_D of the 1-level cone-axis ring enlarged to the scale necessary to fit the 1-level precession pattern is given by (42), where r_D' is the radius of the 1-level ring measured on the cone axis film.

$$r_D = [r'_D(D - Fd^*)]/s'. \tag{42}$$

In Fig. 15 is given a copy of the 1-level precession photo of a sphalerite. Four circles are added to this as follows:

- P, the outcrop of the precession cone of radius r_P.
- D, the outcrop of the diffraction cone (its radius is r_D) at a given moment (when the center of its ring is at c_D).
- B, the area of no spots or blind area with radius r_B.
- G, the guide circle of radius r_G. While precession occurs, the precessing crystal axis (axis of the diffraction cone) moves along G.

It is obvious from the dotted line $tc_D = r_D$ of Fig. 15 that

$$r_G = r_D - r_B. \tag{43}$$

Referring to Fig. 14, it is clear that a circle with center S and radius F will intersect SZ_1 at O_1, since it is simply an F enlargement of the trace

---

[5] This is a .003″ thick colorless transparent cellulose acetate sheet with matte finish on one side obtainable in convenient rolls from The Lustro Co., 2455 S. Archer Ave., Chicago 16, Ill.

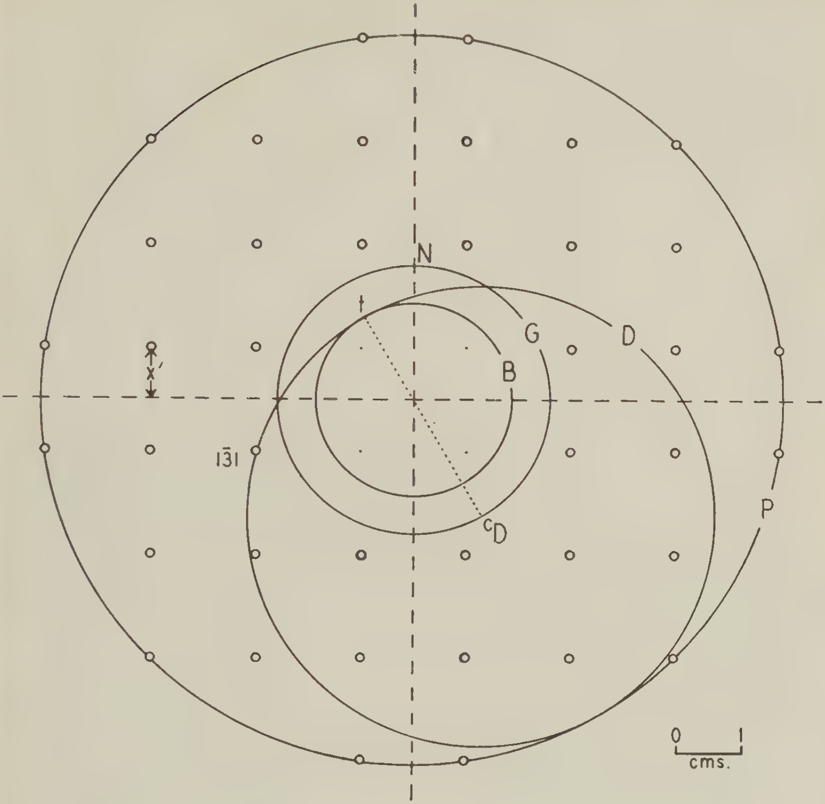

FIG. 15. Copy of 1-level precession photo along [a] of sphalerite ($a_0=5.401$; with $x'=0.7895$ cms. for MoK$_\alpha$ radiation where $F=6.000$ cms.; $\bar{\mu}=20°$).

of the sphere of reflection. Thus $SO_1=F$ and $\sin\bar{\nu}=P_1O_1/F$. But $r_B=O_cO_1=P_1O_1-P_1O_c$, and $P_1O_c=P_0Z_0$ (since Z_0O_c is parallel to the precessing crystal axis) $=F\sin\bar{\mu}$. Thus

$$r_B = F(\sin\bar{\nu} - \sin\bar{\mu}). \qquad (44)$$

Thus using the results of (42) and (44) to compute (43), one is able to draw the guide circle on the precession film or a copy traced from it (Fig. 15). If desired, the precession circle P may also be drawn, since $r_P=r_D+r_G$.[6]

---

[6] Circles B and P often show up as the mid-circles of shaded annular areas on n-level precession films. These areas mark where most of the scattered general radiation getting through the annular slot of the layer line screen strikes the film. The center for the circles bounding these shaded areas generally fails to coincide with the center of the film simply because the center of the layer line screen cannot be lined up exactly.

As precession is taking place, the circle D shears around so that it remains tangent to the outside of B and the inside of P, while its center c_D keeps on G. Under these conditions when D intersects a spot of the precession photo, such a point represents the location of a diffracted spot on the cone-axis ring D of the same index as the spot on the precession film; this is illustrated for $(1\bar{3}1)$ for the particular position of D given in Fig. 15. Assuming that one is looking in the direction of travel of the x-rays, if the drive shaft of the precession instrument rotates clockwise, then c_D (which represents the outcrop of the precessing crystal axis) moves about G in clockwise fashion also; in Fig. 15 a position of D is shown when c_D has moved 150° along G from the "north" position N (that represented by the solid lines of Fig. 14). It is instructive to think of Fig. 15 while watching a precession picture "in the making"; then c_D corresponds to the center of the layer-line screen (the point where the precessing crystal axis intersects the screen), and the "central circle" of the annular opening is represented by D.

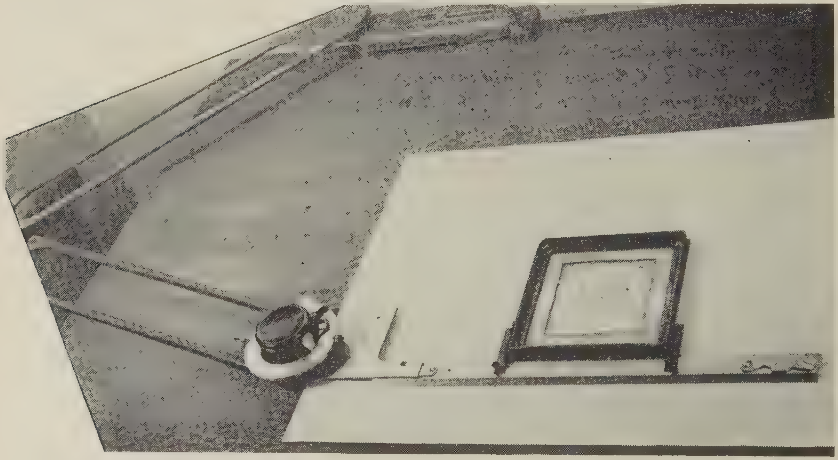

FIG. 16. Set-up for indexing the spots on a trace-o-film enlargement of a cone-axis ring.

All the spots on the trace-o-film enlargement of the 1-level cone-axis ring can be indexed quickly if it is mounted with Scotch tape on a simple hollow rectangular framework which is temporarily attached to one arm of a universal drafting machine as shown in Fig. 16. The latter is set so that the cardinal directions of the cone-axis ring enlargement always stay parallel the cardinal directions of the 1-level precession photo (or tracing thereof, which is attached to the drawing board) while c_D on the enlargement is moved about circle G drawn on the precession picture.

The 0-level case may be handled by using a simplification of (42) in which Fd^* is omitted, but it is easier to use

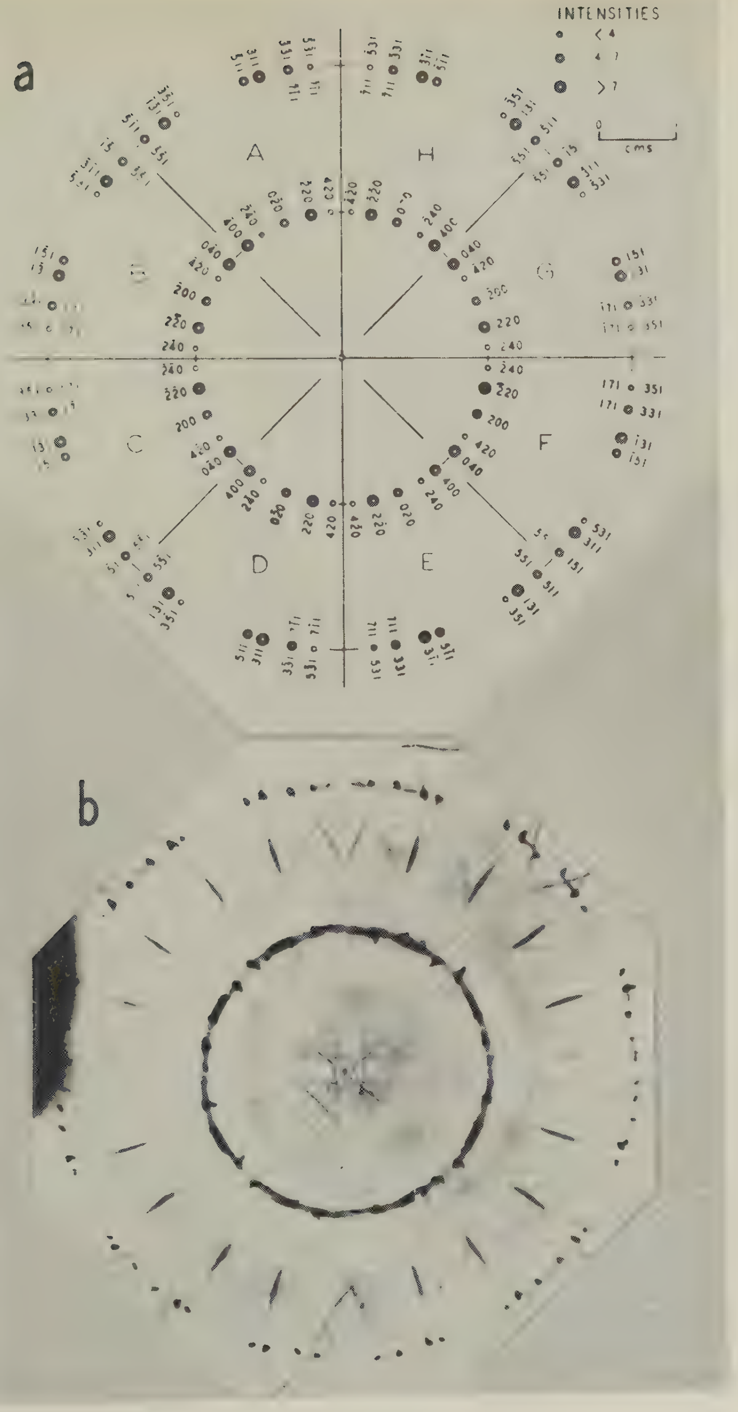

FIG. 17. Cone-axis picture of sphalerite with precession on [*a*] and dial axis [*a*.]
(*a*) Diagram to show spot-indices for 0- and 1-rings.
(*b*) The actual photo. MoK$_\alpha$ radiation, $\bar{\mu}=20°$, $s'=51.4$ mm.

$$r_D = F \sin \bar{\mu} \tag{45}$$

which is obvious from Fig. 14. Since for the 0-level $\bar{\nu}=\bar{\mu}$, equation (44) shows that $r_B=0$, and thus it follows from (43) that $r_D=r_G$.

Figure 17*a* is a copy of a cone-axis film of sphalerite with the spots for the 0- and 1-level rings indexed. A replica of the actual photograph appears as Fig. 17*b*.

An excellent exercise for students trying to visualize the precession technique consists in reversing the procedure just described. That is, the tracing of the spots of the 1-level precession photo is correctly mounted in the framework on the arm of the universal drafting machine and moved about over the proper enlargement of the 1-level cone-axis ring attached to the drawing board, so that some point of circle *G* drawn on the tracing of the precession photo is always above c_D, the center of

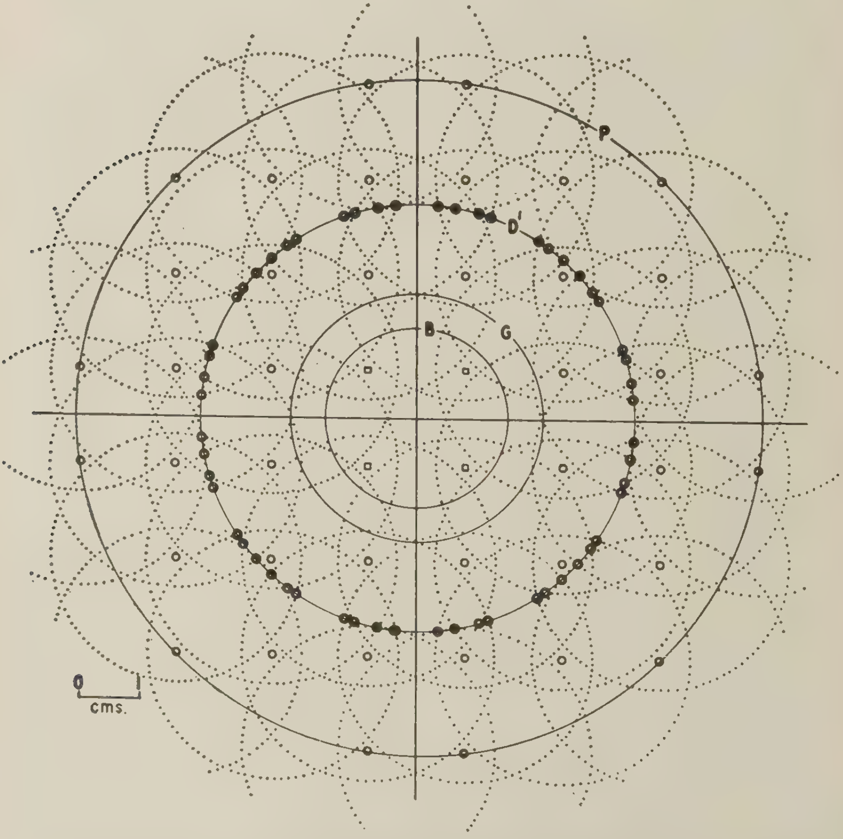

FIG. 18. Diagram to illustrate the method for indexing the spots of the 1-level cone-axis ring of sphalerite.

the cone-axis ring. Of course this is the same as saying that the center of the precession film should be moved about the circumference of a circle G drawn on the cone-axis enlargement. This gives the illusion that the 1-level grid of the reciprocal lattice is precessing through the base D of the calotte cut out of the enlarged sphere of reflection by the plane of the grid. Under these conditions whenever a point on the grid reaches circle D, this corresponds to a reciprocal lattice point cutting the sphere of reflection, and so angular and spacing relations are correct for diffraction to occur. This technique is not handy for actual indexing, since the sheet to be indexed is covered by the one having the spots of known index.

The procedure just described can be restated as follows. If the suitably enlarged 1-level cone axis ring D' is drawn with its center at the center of the 1-level precession grid (see Fig. 18), and if each point of this grid is made the center of a circle of radius r_G, then these circles (dotted in Fig. 18) will cut the circle D' at points marking diffracted spots on the enlarged cone-axis ring D'. This is illustrated in Figs. 18 and 19 for the 1- and 0-levels respectively of sphalerite, where the dotted circles have radius r_G with centers at the points of the level precession grid. In the absence of a universal drafting machine, this method will be of value.

In case of a non-orthogonal relationship between the various levels of the reciprocal lattice normal to the precessing crystal axis, the procedures just described need be modified only to allow for the shear between the grids of the various levels; for all levels the B, G, D', and P circles are centered at the (000)* point. This is illustrated by Fig. 20*a* for chalcanthite[7] (Fisher, 1952*b*) with [*b*] as the precessing axis, and $F=6.00$ cms. for the 1-level. This diagram shows enough of the reciprocal net grids for the 0- and 1-levels so that they can be completed if desired; also the B, G, and P circles can be added from the data given. It is clear that the 0-level grid is on a smaller scale than that of the 1-level; both grids are drawn proper scale to fit the respective cone-axis rings. Figure 20*b* is a reproduction of the actual cone-axis film, which also shows much of the 2-level ring; the light area along the upper left side marks where the film was shielded by a portion of the goniometer head; the light annulus about the 0-level ring is due to the direct beam-stopping cup, and the two light streaks extending to the right (and sloping down) from this are due to the arm supporting this cup. The spots on the 0-level ring are not very clearly discernible on the print because of the heavy general radiation reflection trail (Laue streak) that coincides with this ring; these spots are easily seen on the original film. Some of the elliptical Laue streaks associated with the 1-level shown in Fig. 20*b* are reproduced in Fig. 20*a;* these are discussed later.

---

[7] In Fig. 20*a* the spots on the 1-level ring are indexed as if they belonged to the $\bar{1}$-level. This is necessary in non-orthogonal situations if the 1-level reciprocal lattice grid is to correspond to the gnomonogram of morphology (Fisher, 1952*a*). This apparent anomaly arises since in precession work levels are taken as positive when going from near the surface of the sphere of reflection (the 0-level) towards the center, whereas in morphology the 0-level cuts the center of the unit sphere and the 1-level is near its surface.

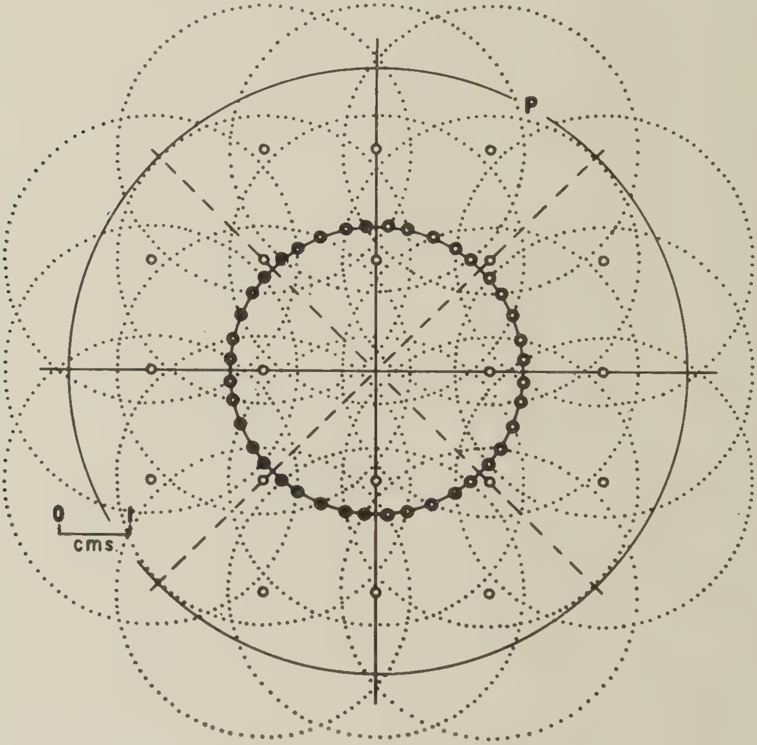

FIG. 19. Diagram to illustrate the method for indexing the spots of the 0-level cone-axis ring of sphalerite.

MISCELLANEOUS REMARKS

It will be noted that in general each spot on a given precession film is represented by two on the corresponding cone-axis ring. Diametrically-opposite spots on the 0-ring (which are present in all cases) have the same indices, but with all signs changed. The condition in this respect for the *n*-rings depends on the symmetry of the crystal. Thus the 0-ring condition is duplicated on the *n*-rings for sphalerite[8] (Fig. 17), but in

---

[8] Of course in the case of opposite spots on *n*-rings there is no change in sign for the index digit which corresponds to the precessing crystal axis.

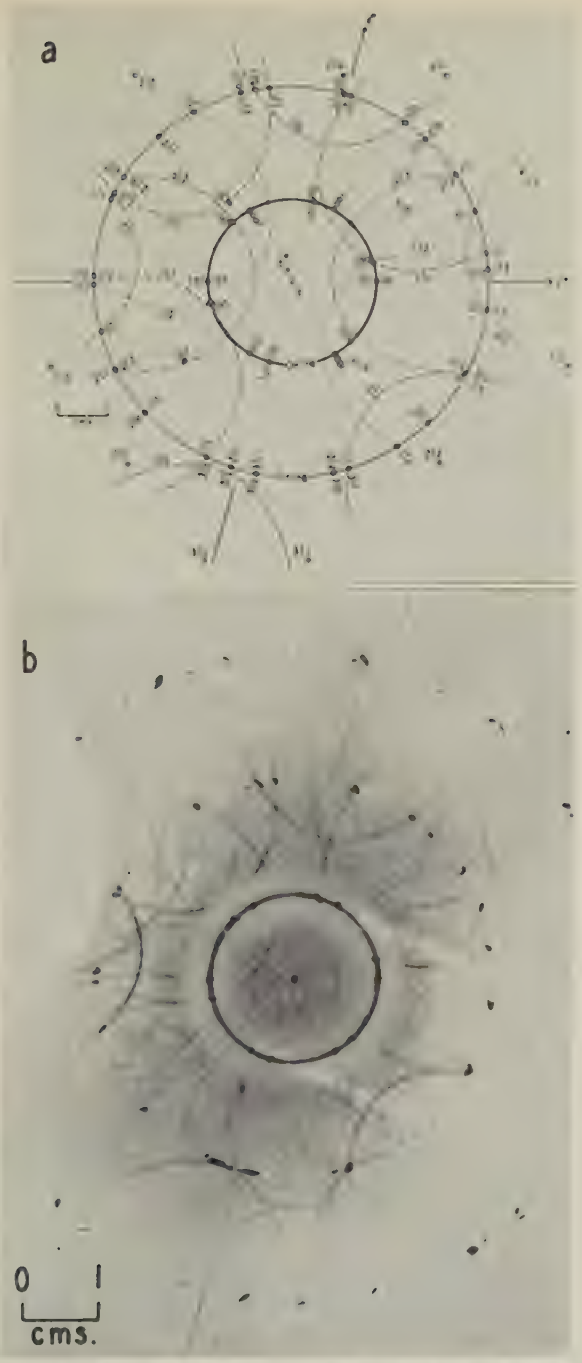

FIG. 20. Cone-axis picture of chalcanthite with precession on [b] and dial axis [c*]. (a) Diagram to show spot indices for 0- and 1-rings; also some of the Laue streaks through the spots on the 1-ring. (b) The actual photo (with some of the 0-ring spots touched up a bit). FeK$_\alpha$ radiation, $\bar{\mu}=20°$, $s'=30.5$ mm.

the case of chalcanthite (Fig. 20) the n-rings are not marked by diametrically opposite spots. This presence or absence of symmetry is also well shown by the n-level Laue streaks. This is particularly noticeable for the (110) streaks in Fig. 20; the one near the top cuts the $\bar{1}$-ring in pronounced fashion, whereas the one near the base barely misses it. Buerger (1944, p. 9) has called attention to the advantages of the use of cone-axis patterns (as compared to Laue photos) for the determination of diffraction symmetry.

Those interested in quantitative intensity studies from precession films might find it advantageous to use cone-axis photos. Each spot on a level precession negative is a composite made by two beams diffracted at different moments during a single 360° precession. Such a composite spot appears as two separate ones on a cone-axis ring; these two should be of equal intensity. If spots along any given ring are too thickly spaced for satisfactory intensity measurements, this situation can be remedied by any or all of the following three techniques: (1) decrease the $\bar{\mu}$-angle; (2) increase the wave-length of the x-rays; (3) increase the distance s' from crystal to film.

While the 0-ring is of no value in determining d^*, certain features of it are of interest. The radius of this ring depends solely on $\bar{\mu}$ and s', and is independent of λ. Thus a single 0-ring is obtained for both K_α and K_β radiation (this, of course, is not true for n-rings). Moreover, the 0-ring may be used to derive the geometrical constants of the crystal, just as is true for the 0-level precession film. This is illustrated in Fig. 21. It will be noted here that straight lines through the two $(002)^*$ spots and the two $(00\bar{2})^*$ spots, and lines through the two $(200)^*$ spots and the two $(\bar{2}00)^*$ spots, yield a network whose sides are $\perp c^*$ and $\perp a^*$ respectively. If parallel lines are run through $(000)^*$, a mesh at angle β^* is developed whose line "spacings" (see Fisher, 1952*b*, p. 100, footnote) are $t^*_{c^*}$ and $t^*_{a^*}$ respectively. From these values one can calculate a^* and c^* by using the following formulae:

$$a^* = t^*_{a^*}/(F\lambda) \quad \text{and} \quad c^* = t^*_{c^*}/(F\lambda). \tag{46}$$

Of course if γ and α are known, a and c may also be computed.[9] Note that the diagonal bisectors [through $(000)^*$] of this mesh yield reciprocal translation directions (in the case of Fig. 21) of $[101]^*$ and $[10\bar{1}]^*$.

It is a simple matter to compute the angle A (measured along the 0-ring) between a spot on this ring and the point where it is cut by a reciprocal translation direction on which the spot would lie on a 0-level precession photograph. Such a translation direction is the perpendicular bisector of a line joining two spots of the same indices on this ring. Thus

---

[9] Using (54′) and (56′) of Fisher, 1952 *c*, p. 698.

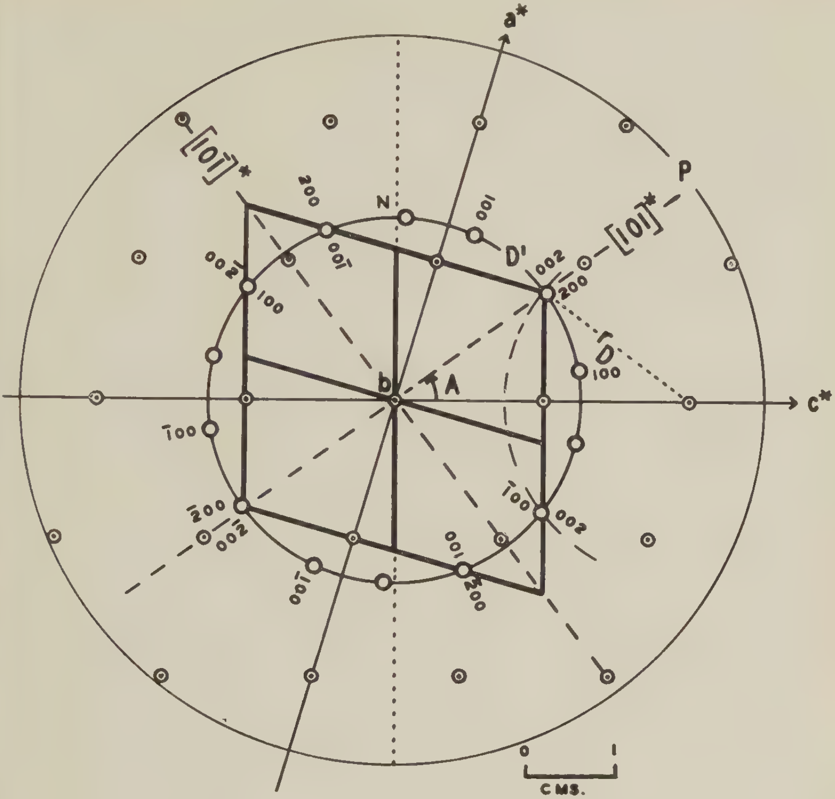

FIG. 21. Copy of an enlargement of the 0-ring of chalcanthite (same data as Fig. 20, except CuK$_\alpha$ radiation) to fit the $F=6.00$ cms. 0-level precession photo, copy of which is also shown.

for the two (002)* spots (where c^* is the given reciprocal translation direction):

$$\cos A_{(002)^*} = [(l/2)\cdot t^*_{c^*}]/r_D \qquad (47)$$

in which l is the value of l in the index $(00l)^*$, and $r_D = F \sin \bar{\mu}$. The two (002)* spots are thus an angle A of 37°17′ measured along the 0-ring off the point where it is cut by c^*. The corresponding angle for one of the (200)* spots is 35°50′; thus these two spots are practically superposed.

In similar fashion one can compute angle A for all the "pinacoidal" spots on the 0-level ring. These may be combined as in Table 9 in a form that gives an interesting picture of how diffraction occurs on the precession instrument for the case of Fig. 21. As one looks in the direction of travel of the direct x-ray beam, counting azimuth angles clockwise (taking 0° when the $\bar{\mu}$-arc is vertically up) diffraction occurs for each spot (also listing CuK$_\beta$ reflections which are not shown in Fig. 21) when the $\bar{\mu}$-arc is in the azimuth position noted. Thus (considering only K$_\alpha$ spots) when the $\bar{\mu}$-arc has moved clockwise 23°56′ from its up (north) position, the center point c_D of diffraction ring D (see Fig. 15) lies above the (001) point on the D' ring in the upper right quadrant of Fig. 21, and the other (001) point (*lower* right quadrant of Fig. 21) marks where the diffracted beam then strikes the film. All the other diffracted spots are formed in similar more or less complementary order from that in which they are met in going clockwise around the D' ring. Thus the next spot formed is the (002)* in the *lower* right quadrant (made when the $\bar{\mu}$-arc reaches an angle of 52°43′ off N); the third spot is the (200)* of the upper left quadrant; the last (sixteenth) spot is the (200)* of the upper right quadrant. The position of the $\bar{\mu}$-arc for other (non-"pinacoidal") spots could be computed in a like manner. In short a 0-level general radiation reflection streak (ring) is "painted" one spot at a time, more or less as each "ring" on a "powder" film is really composed of many spots representing directions along which diffraction occurred from a given set of planes $n(hkl)$ in all possible orientations at a constant glancing angle θ.

Table 9. Azimuth Angles for 0-Level Cone-axis Diffraction (Angles Measured Clockwise from N to Fit Conditions as Given for Fig. 21)

Angle	Spot		Angle	Spot		Angle	Spot		Angle	Spot	
	K$_\alpha$	K$_\beta$		K$_\alpha$	K$_\beta$		K$_\alpha$	K$_\beta$		K$_\alpha$	K$_\beta$
21-03		001	126-57		$\bar{1}00$	201-03		$00\bar{1}$	306-57		100
23-26	001		127-17	002		203-26	$00\bar{1}$		307-17	$00\bar{2}$	
45-55		002	129-18	$\bar{1}00$		225-55		$00\bar{2}$	309-18	100	
52-43	002		134-05		002	232-43	$00\bar{2}$		314-05		$00\bar{2}$
54-10	200		151-26		$\bar{2}00$	234-10	$\bar{2}00$		331-26		200
60-48		200	156-34	001		240-48		$\bar{2}00$	336-34	$00\bar{1}$	
82-56	100		158-04	$\bar{2}00$		262-56	$\bar{1}00$		338-04	200	
85-17		100	158-57		001	265-17		$\bar{1}00$	338-57		$00\bar{1}$

The position of the "pinacoidal" spots of the 0-level cone-axis ring in terms of the angle A is shown by the graph of Fig. 22. This gives all such spots for precession on [b] (upper curve, right ordinate scale) as in Fig. 21 (if rotated 180° on the dial axis), and also for precession on [a] (lower curve, left ordinate scale). The spots actually located in Fig. 22 fit CuK$_\alpha$ radiation. Thus the (001) spot with A of 66°34′ is shown in Table 9 at a complementary value, and the (100) spot with A of 66°49′ in Fig. 22 appears in Table 9 at an angle of this value plus $(90° - \beta^*)$. The positions

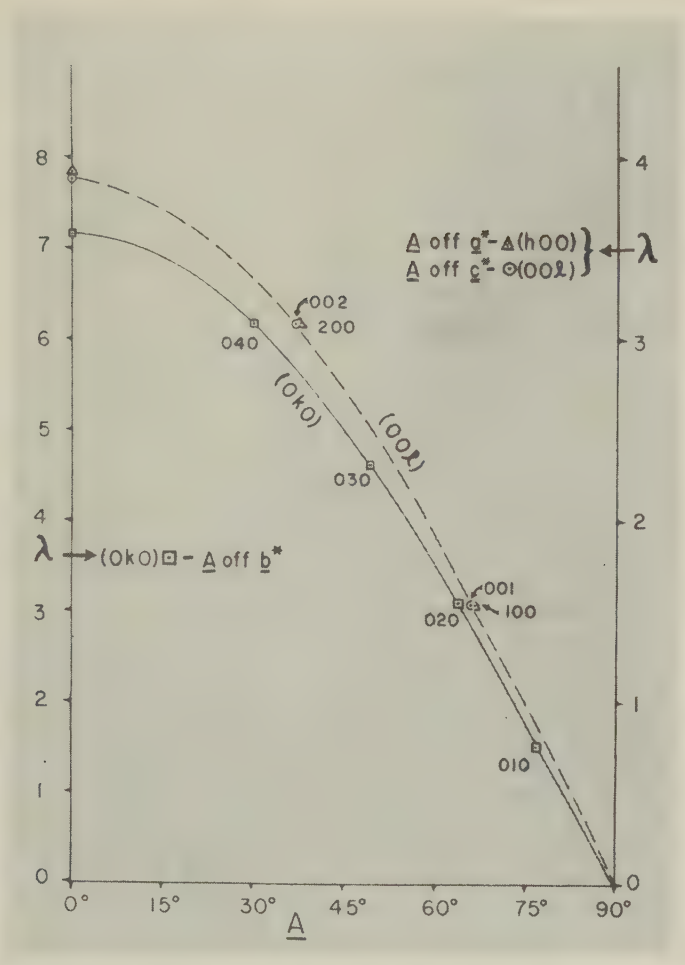

FIG. 22. Graph to show angle *A* for any "pinacoidal" spot of the 0-level cone-axis ring of chalcanthite for any possible radiation at $\bar{\mu}$ of 20° where the dial axis is [c^*].

of pinacoidal spots for radiation of any wave length can be read from Fig. 22 in similar manner. It can also be seen (left ends of curves) that the "unit pinacoid" spots of the 0-level ring would lie exactly on a reciprocal axis in the following cases:

(100) on a^* for $\lambda = 3.916$
(010) on b^* for $\lambda = 7.140$
(001) on c^* for $\lambda = 3.876$

These values are computed from equations (63), (59) and (65) of Fisher (1952*d*).

Knowing the positions of indexed spots for a 0-level ring also allows one to prepare a special layer-line screen useful in putting just a few calibration spots on any 0-level precession photograph. The writer has made such a screen for use with quartz ($\bar{\mu}=30°$; MoK_α radiation) precessing on [a^*] with [c] as the dial axis. This was finished by drilling small holes in a blank screen on a circle of $r=20$ mm. at angles A (measured off the dial axis) as follows: 2.°2 and 32.°5 for the (17) spots, and 60.°1 for the (30) spots. The center of the screen was found by letting the direct beam strike a small piece of fluorescent material fastened to it. In this way by keeping a quartz crystal accurately set on a goniometer head reserved for this purpose, one can make a double exposure on any 0-level precession photograph and thus have the quartz spots appear on it for purposes of calibration; by this scheme a large number of spots which

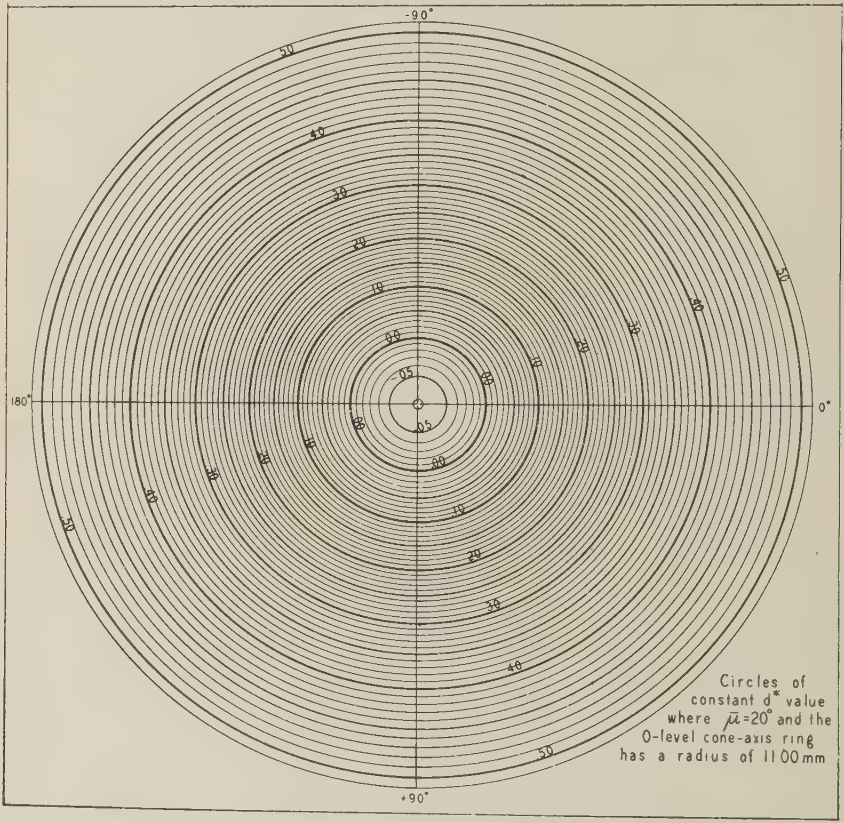

FIG. 23. Nomogram to furnish d^*-values from cone-axis photos where $\bar{\mu}=20°$; see text.

might cause confusion is avoided. Of course a similar screen could be made for use with a definite type of Laue photo from a given crystal.

The writer finds it convenient to take cone-axis photos at a distance s' of 30.22 mm. and $\bar{\mu}=20°$. Under these conditions no matter what the radiation the 0-ring has $r=11.00$ mm. If a glass positive is made from Fig. 23 so that the 0-ring has a radius of just 11.00 mm., then such a cone-axis film may be centered over the positive and the required spacing d^* (in reciprocal lattice units) for any n-level ring may be read directly from the graph.

Orientation from Cone-Axis Pictures

Cone-axis photos are normally not used for orientation with the precession camera, since it is ordinarily much more rapid to effect this by a technique described by Buerger (1944, 21–27) which employs unfiltered radiation and a small angle of precession. Under these conditions orientation can usually be reached quickly by adjusting the crystal until the Laue streaks (on the 0-level precession photograph made without a layer-line screen) radiating from the central spot are of equal lengths (see Fisher 1952*d*). However, the writer has been unable to employ this orientation technique in certain sulpho-salt work, whereas the cone-axis method yielded usable results.

When a translation direction of the direct lattice coincides with the precessing direction, a cone-axis photo may be obtained which yields diffraction spots along thin rings, one for each accessible level, if filtered radiation is employed. When the lattice translation direction deviates by a small angle from the precessing direction, the rings widen out into annular bands. Figure 24 shows a series of cone-axis photos of chalcanthite to illustrate this condition.

Figure 25 is a vertical cross-section through the cone-axis set-up to fit the case of Fig. 24*c* where the [*b*] axis of chalcanthite is off the precessing direction by 2° around the dial axis. In Fig. 25 the dashed lines represent the positions of the various reciprocal lattice levels drawn as they would be for perfect orientation; they are thus normal to the precessing direction and parallel the cone-axis film. The solid lines show the actual orientation of the levels normal to the [*b*]-axis; these are arranged in sheets, the thickness of each sheet corresponding to the shifting of that level due to the fact that it is not quite normal to the precessing direction. Thus when the $\bar{\mu}$-arc points vertically up, the 0-level lies along D_0K, the inner line (the one closer to the center of the crystal) of the 0-sheet; when it points vertically down, the 0-level lies along D_0K', the outer line of the 0-sheet. In between these two positions the 0-level lies at all possible intermediate (but parallel) positions. Thus as the precessing motion

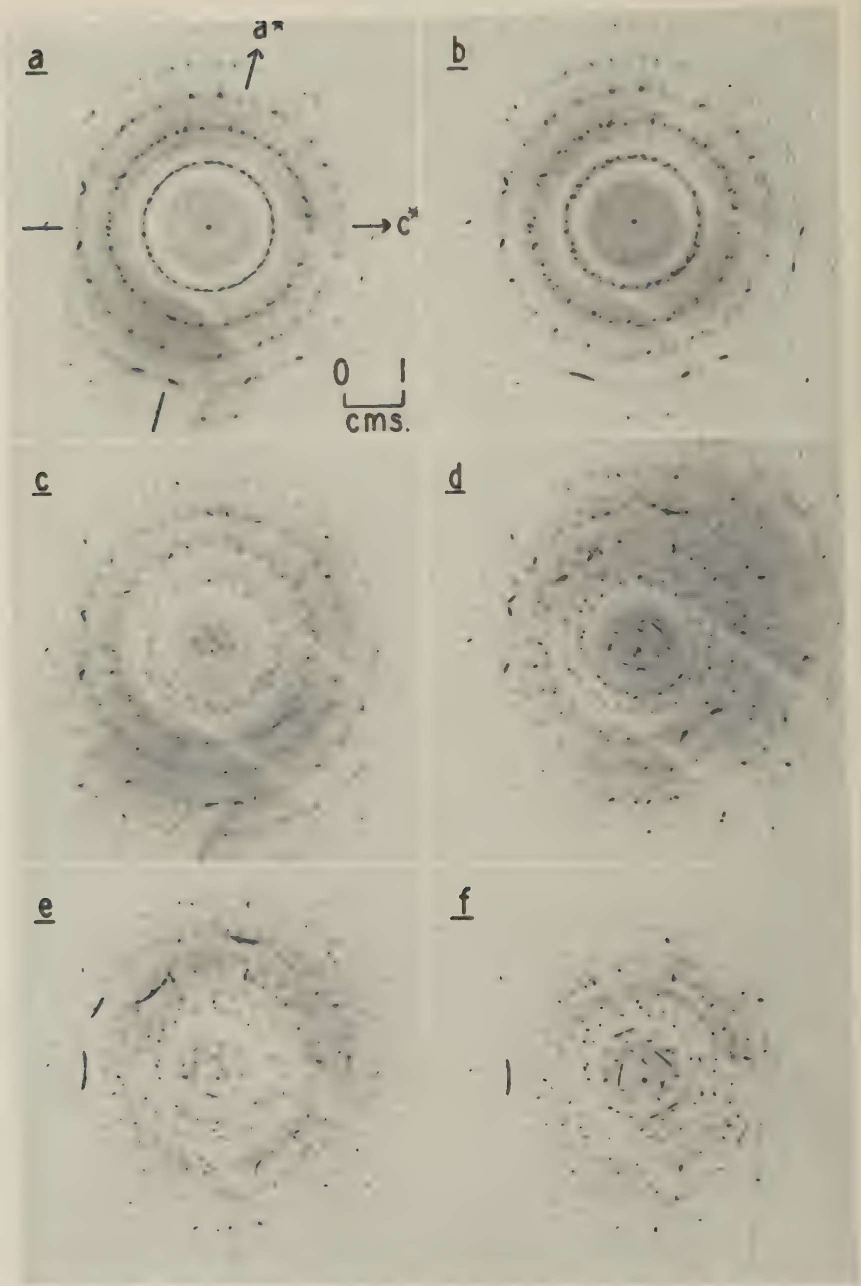

FIG. 24. Cone axis photos of chalcanthite. MoK$_\alpha$ radiation, $\bar{\mu}=20°$, $s'=30.22$ mm., [c^*] horizontal. Precessing direction is: (*a*) [*b*]; (*b*) 1/2° off [*b*] along dial (D) axis (parallel to [c^*]); (*c*) 2° off [*b*] along *D*; (*d*) 3° off [*b*] along *D*; (*e*) 3° off [*b*] along *D* and 1° off on vertical (*V*) axis; (*f*) 4° off [*b*] along *D* and 1° off on *V*.

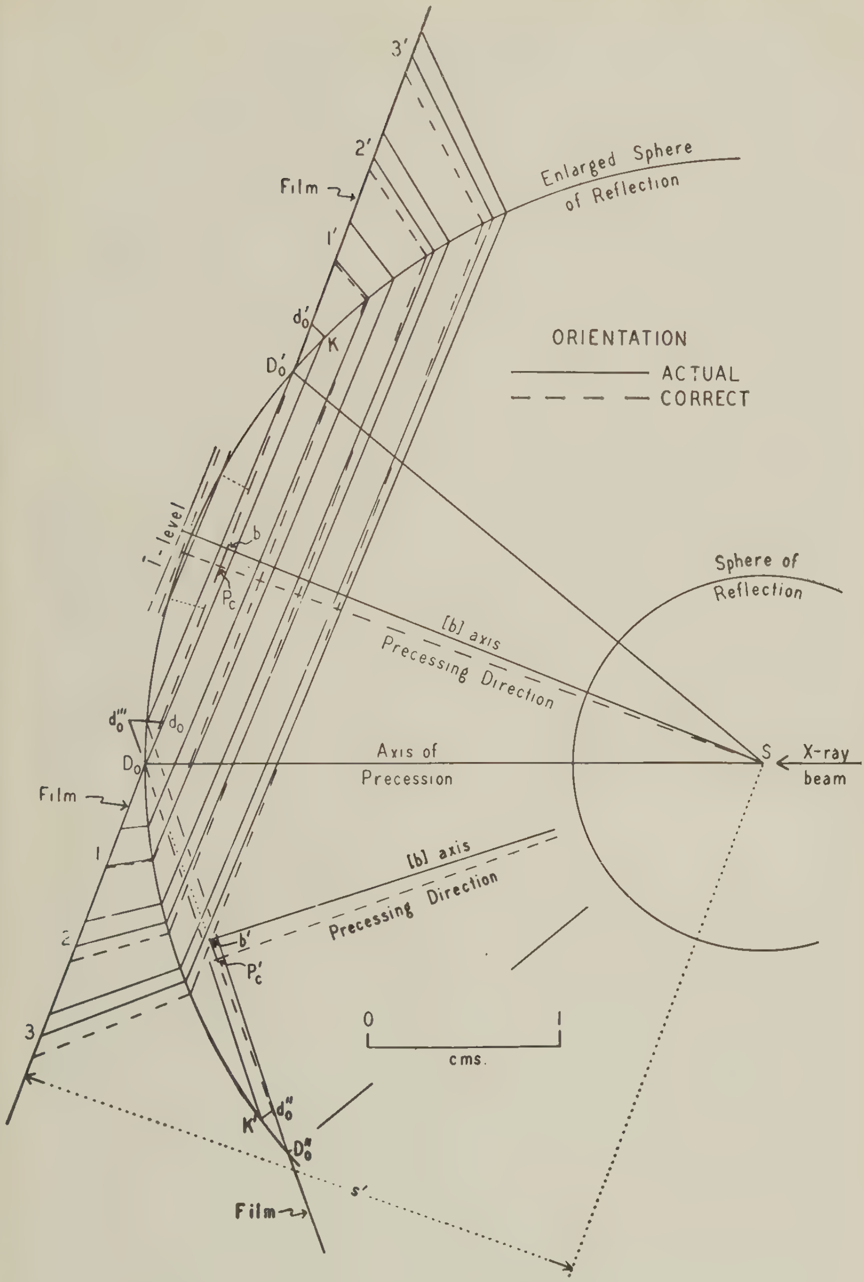

FIG. 25. Vertical cross-section through the cone-axis set-up to fit the case of Fig. 24*c*.

proceeds the 0-level moves in and out, sweeping over a spherical annulus of the enlarged sphere of reflection.

Thus the 0-level of the properly oriented crystal would give a sharp ring of spots on the film cutting through D_0 and D_0'. For convenience the enlarged sphere of reflection is drawn through these points. On the crystal oriented as shown in Fig. 25 with the $\bar{\mu}$-arc vertically up the 0-level ring forms an annulus of spots on the film through D_0d_0 and $D_0'd_0'$. This annulus is composed of spots which lie on near-circular ellipses; that is, the central projection of the various 0-level diffraction cones (whose axes coincide with [b], and not with the precessing direction) yields a series of near-circular ellipses on the flat film (which is normal to the precessing direction). After 180° precession, so that the $\bar{\mu}$-arc points vertically down, the annulus of spots goes through D_0d_0''' and $D_0''d_0''$. Thus the 0-level cone-axis annulus has a width of $D_0'd_0' = D_0d_0'''$ along a north (vertically up) radius through the central spot P_c, and a width $D_0d_0 = D_0''d_0''$ along a south radius. In short the annulus will be a trifle wider on the north radius, since the [b]-axis is outside of the precessing direction. Nevertheless one can find the center of the annulus along a north-south diameter through the central spot, and this gives the approximate location of b (the point where the b-axis cuts the film). Thus from film measurements one can readily get a value for the distance P_cb. The result obtained by this simplified method will be a trifle too large, and this error increases as the orientation gets worse. The approximate angular error of setting along the dial axis (e_D) can then be obtained since

$$\tan e_D = P_cb/s'. \tag{48}$$

Using this formula with the value of P_cb obtained from the film of Fig. 24*c* gave $e_D = 2°18'$, whereas the true value was 2°, an error of 15%.

If the setting is also off on a vertical axis, one may use the same method and formula to compute e_V, providing measurements for the location of b are made along an east-west diameter through the central spot P_c. The result obtained by this technique for the film of Fig. 24*e*, was 0°45′, which is too small by 25%. Since this last value is too small, whereas the above formula should lead to too large a result, it seems reasonable to suppose that any error inherent in the simplified formula is considerably less than the errors of measurement of the edges of the annulus.

LAUE STREAKS

Laue streaks (general radiation reflection trails) which appear on ordinary cone-axis films may be used for obtaining quite a precise orientation of a suitable single crystal, providing its symmetry is not too low grade. Although most of the cone-axis photographs here reproduced were made with filtered radiation, enough polychromatic radiation was present to yield pronounced Laue streaks. As is well known any Laue streak represents the locus of Bragg reflections marked out by where a central row of the reciprocal lattice [that is, a line joining $n(hkl)^*$ points to $(000)^*$] cuts the sphere of reflection. In effect, as the radiation becomes of shorter wave length than that characteristic of the target metal, the translation values in the reciprocal lattice decrease. Just as any point on the reference band of a 0-level Weissenberg photo may be taken to represent $(000)^*$, and the Laue streaks on such a photo head towards this band, making an angle of 63°26′ with it if the instrument has an undistorted scale, so any point on the 0-ring of a cone-axis photo may be taken to represent $(000)^*$. This ring is characterized by a heavy circular Laue streak. In analogous fashion the 0-level line of a rotation photo may be marked by a pronounced Laue streak.

The easiest way to explain these Laue streaks on precession pictures seems to be in terms of movement of the levels of the reciprocal lattice. Thus in Fig. 14 as the wave length of the x-rays varies, the position of the 0-level plane R_0R_0' remains constant, but the spacing d^* between this and the adjacent parallel plane varies directly; that is, with shorter wave length get smaller d^*, and vice versa. Thus with shorter wave length points R_1 and R_1' move along the surface of the sphere of reflection towards R_0 and R_0' respectively. Note also that under these conditions a $\bar{1}$-level (regarding R_1R_1' as the $+1$-level) moves in close enough to R_0R_0' so that it will eventually cut the sphere of reflection; see Fig. 26. For any given wave length there is a symmetrical relationship between these two 1-levels across the 0-level. Thus the general radiation reflection trails often trace out paths from an n-level ring spot $x(hkn)^*$ across the 0-level ring [at a "spot" corresponding to $(000)^*$] towards some $\bar{n}$-level ring spot $x(hk\bar{n})$.*

Such streaks may be seen tracing out conic sections through spots on the n-rings. Thus in Fig. 20*b* the $n(1\bar{1}\bar{2})^*$ elliptical streak, shown as a dotted line in the upper left part of Fig. 20*a*, quite pronouncedly goes through the two $(1\bar{1}\bar{2})^*$ spots on the $\bar{1}$-ring and cuts across the 0-ring [at points which can be regarded as $(000)^*$ spots] heading towards the $(11\bar{2})^*$ spots of the 1-ring. The latter ring does not appear in the photo. Also pronounced is the $n(1\bar{1}0)^*$ Laue streak in Fig. 20*b* which appears near the top of Fig. 20*a* as the elliptical dash-dot line. On the original film of Fig. 20*b* this streak clearly goes through a pair of spots on the $\bar{2}$-ring whose indices should be $(2\bar{2}0)^*$. The corresponding $(\bar{1}\bar{1}0)^*$ streak shown near the base of Fig. 20*b* does not quite reach the $\bar{1}$-ring of the film, but it does cut the two $(\bar{2}\bar{2}0)^*$ spots.

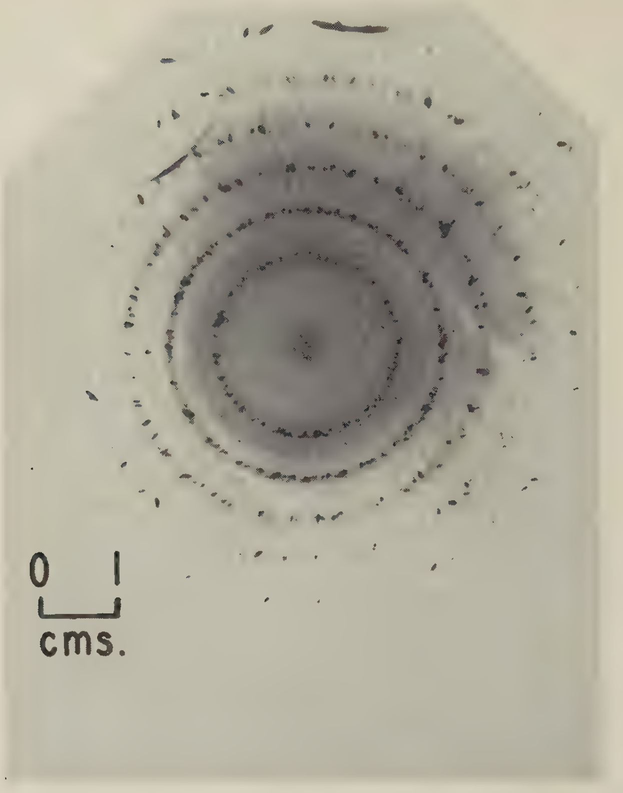

FIG. 26. Chalcanthite cone-axis photo. Same data as Fig. 24*a* except $\bar{\mu}=30°$. As usual the 0-ring is marked by a circular Laue streak. Inside it the $\bar{1}$-ring shows up very well; the central spot is hidden by Laue streaks associated with the $\bar{2}$-ring. Except for these, the most pronounced streaks on the original film are those just inside the 1-ring associated with spots on this ring.

As the wave length decreases, although the position of the 0-level (R_0R_0' of Fig. 14) remains constant, the translation units of the reciprocal net of this level (and of all others, too) also become smaller. Thus for non-characteristic radiation as the smaller-mesh 0-level grid shears through the sphere of reflection during precession, new directions of Bragg reflection are obtained along the 0-level cone of diffraction. This explains the pronounced circular Laue streak marking the 0-level cone-axis ring.

Of course the position of the 0-level R_0R_0' of Fig. 14 can be changed by altering the $\bar{\mu}$-angle; with decreasing angle R_0' moves along the sphere towards R_0. This yields a 0-level cone-axis ring which is smaller; moreover it also has fewer characteristic radiation diffraction spots on it, since a smaller part of the 0-level grid then precesses through the sphere of reflection.

Figure 27 shows a series of cone-axis photos, all of which were made exactly like that of Fig. 20 except for the $\bar{\mu}$-angle. The Laue photo of Fig. 27*d* may be regarded as a special case of a cone-axis photo where $\bar{\mu}=0°$. Some of the zone-ellipses and spot-indices of this are indicated by the tracing of it shown as Fig. 27*f*. Here the major axes of the [011] ellipses mark $[c]^t$, and of the [110] ellipses is $[a]^t$. Also $[c^*]$ is tangent to [100] through *b*, and $[a^*]$ is tangent to [001] through *b*. Figure 27*e* is a print showing the combination of Figs. 27*c* & *d*. It will be noted that each spot of *d* lies near the inner focal point (the one closer to the center of the figure) of a Laue streak ellipse of *c*. If *d* (or better a trace-o-film copy of *f*) is similarly superposed on *a* or *b*, the same is found to be true. Thus it is fitting that the general radiation reflection trails of *a*, *b*, & *c* be called Laue streaks. Indeed the spots of Fig. 27*d* become in the cone-axis photos Laue streaks which are elliptical with major-axes[10] of lengths equivalent to $2\bar{\mu}$. The 1- and 2-rings are indicated on these cone-axis photos, and it is easily seen that many elliptical Laue streaks cut these without giving rise to spots. Of course only those streaks belonging to a Bragg reflecting plane of the proper level can yield spots on any given cone-axis ring.

TABLE 10. INDICES OF CONE-AXIS SPOTS, Fig. 27*b* & *c*

Cone-axis spot		Quadrant			
		NW	SW	SE	NE
b	1-ring	—	$\bar{1}\bar{1}\bar{1}$ & $\bar{2}\bar{1}0$	$\bar{2}\bar{1}1$ & $\bar{1}\bar{1}2$	$0\bar{1}2$ & $1\bar{1}1$
	2-ring	$2\bar{2}\bar{1}$	$\bar{2}\bar{2}\bar{1}$	$\bar{2}\bar{2}2$	$1\bar{2}2$ & $2\bar{2}0$
c	1-ring	—	$\bar{1}\bar{1}\bar{1}$	$\bar{2}\bar{1}1$	$1\bar{1}1$
	2-ring	$2\bar{2}\bar{1}$	$\bar{2}\bar{2}\bar{1}$	$\bar{2}\bar{2}2$	$2\bar{2}0$

The indices of the spots (and associated Laue streaks) on the 1-ring (these are in circlets in Fig. 27*f*) and the 2-ring (these are in small squares in Fig. 27*f*) of the cone-axis photos of Fig. 27*b* & *c* are given in Table 10 (proceeding anticlockwise from the north position). The Laue streaks of Fig. 20*b* (the corresponding spots in Fig. 27*f* are in small triangles) are similarly indexed in Fig. 20*a*. It will be noted that Laue spots ($\bar{2}\bar{2}2$) and

---

[10] The major axis as well as the minor axis of each Laue streak ellipse is equivalent to $2\bar{\mu}$; the corresponding Laue spot is not at a focal point, but is a distance equivalent to $\bar{\mu}$ from each vertex.

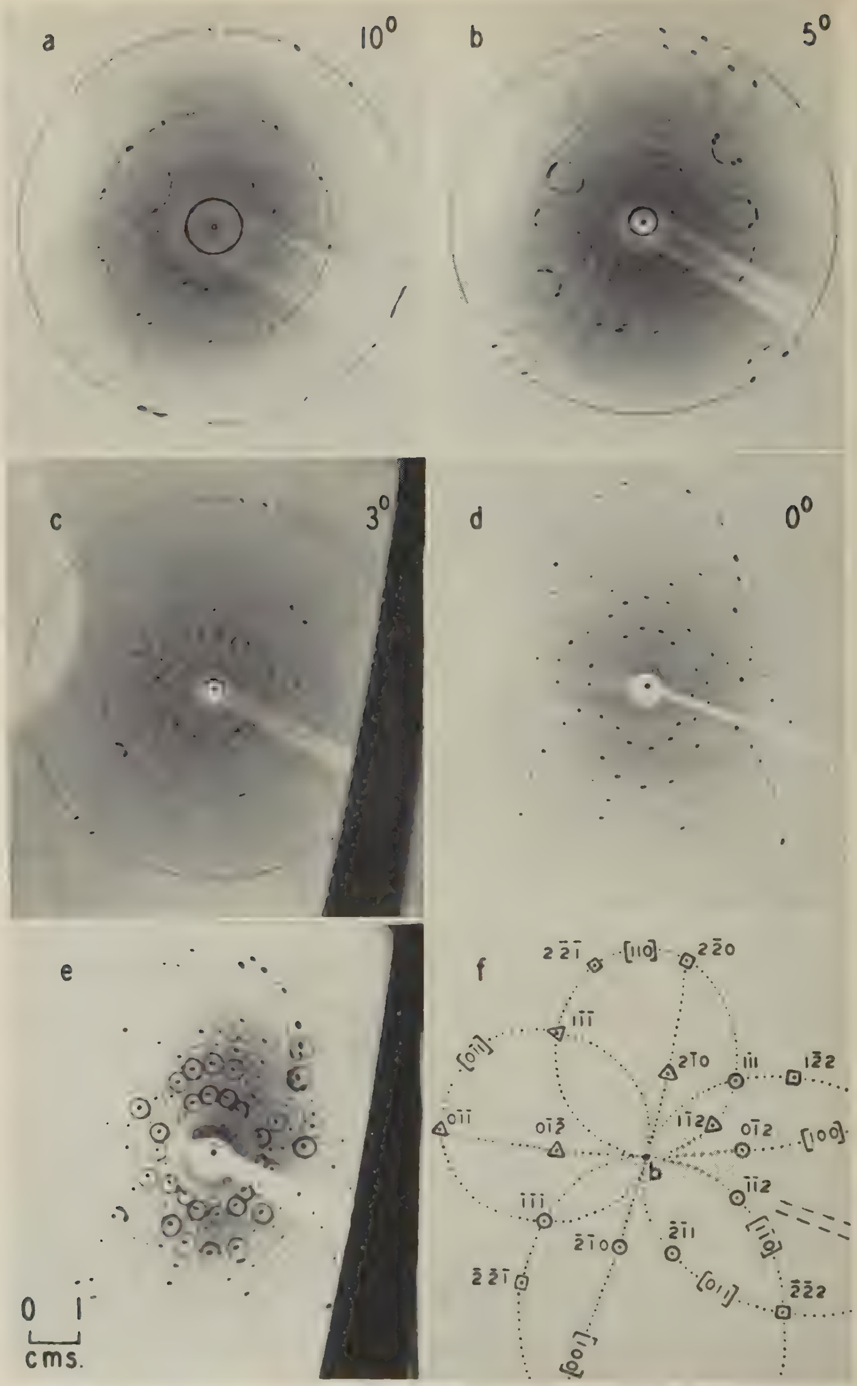

Fig. 27. Cone-axis and Laue photos of chalcanthite. Same data as Fig. 20 (except for $\bar{\mu}$ angles, which are given; also *b* and *d* were taken with *unfiltered* iron radiation). (*e*) is a composite print of *c* and *d*; (*f*) shows some of the spot and zone-ellipse indices of *d*.

$(2\bar{2}0)$ in Fig. 27*f* are given multiple indices. This is because they show up to have these values in Fig. 27*b* & *c* [though $(\bar{1}\bar{1}1)$ and $(1\bar{1}0)$ are present in Fig. 20]. It is obvious that the Laue streaks on a given cone-axis photo may be considered as representing the sum total of Laue photos which could be obtained by individual exposures from a non-moving crystal at each position of the $\bar{\mu}$-arc during a 360° precession.

In short the Laue streaks mark out conic sections on a cone-axis film. The axis of this general radiation cone (if the crystal is properly oriented) is normal to the film for the 0-ring spots, but is inclined in the case of *n*-level ring spots. If that generatrix of the general radiation cone which is most nearly parallel to the film is actually parallel to the film, the path traced is a parabola; if that generatrix is less inclined than this, the result is an ellipse; if more inclined, an hyperbola.

If a cone axis photo has well-developed Laue streaks cutting the 1-ring, it should be an easy matter to derive the reciprocal lattice net from it, and thus the spots could be indexed. For example one could take a suitably enlarged trace-o-film copy of the $\bar{1}$-ring of Fig. 20*b* and using each of the two spots on any one Laue streak as centers, draw circles of radius r_G (see Figs. 15 & 18) and find their points of intersection. One of these would mark a reciprocal lattice point. Given enough of these the grid could be prepared; some of the points of such a grid are shown in Fig. 20*a*. Thus from two cone-axis photos (one like Fig. 20*b*, another similar but with precession along [*a*]) one could derive all the geometrical constants of a triclinic unit cell (and the space group of a cell of higher symmetry), though one would hardly expect the results to be highly accurate.

Because of the low symmetry of chalcanthite the Laue streaks are not of help in orienting the crystal. In the case of sphalerite (Fig. 17*b*) however, certain trails are of great value in this connection. In particular the streaks which appear inside the 0-ring outlining a sort of lozenge (these show up very well on the original film) serve to give a very delicate check on the orientation, since the distances of these trails from the central spot vary quite perceptibly with but a tiny change in angular relations between the lattice planes and the direct beam. Similar trails of value in checking accurate orientation appear in the cone-axis photos of Fig. 28. Here in (*a*) the portions of the four streaks cutting the 1-ring which show up well inside this ring are of this character (the one at the lower left has been touched up a bit; it is perfectly clear on the original film). In (*b*) there are several valuable streaks inside the 0-ring; also the streaks along the horizontal (dial) axis inside the 2-ring. In (*c*) valuable streaks appear inside the 0-ring and also nearly tangent to the 1-ring in the NE & SW quadrants and cutting the 2-ring in the NW & SE quadrants.

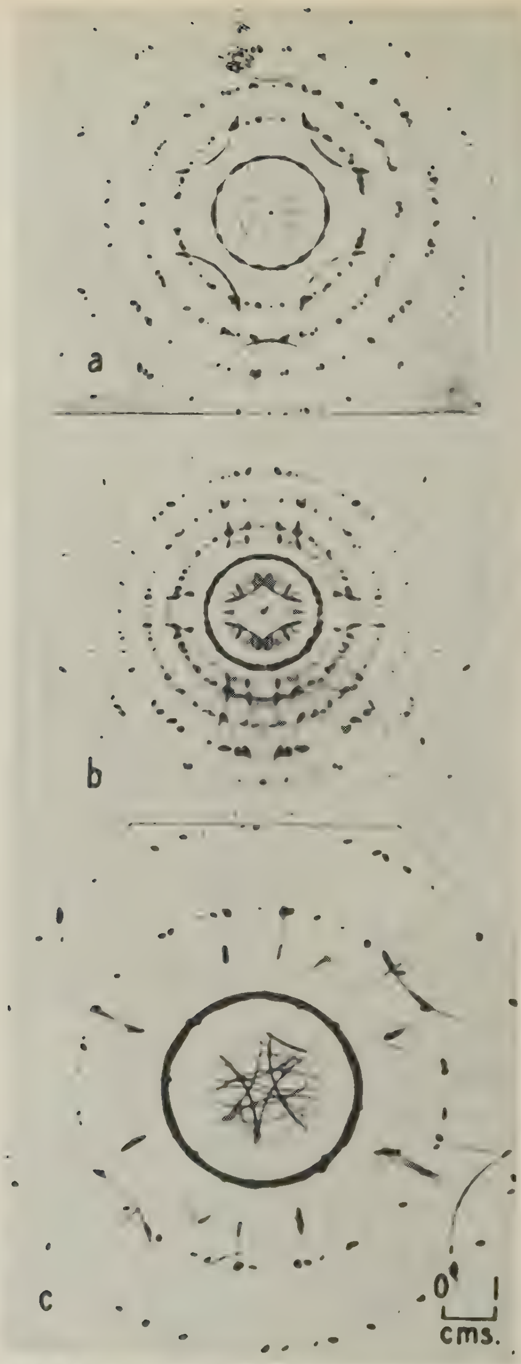

FIG. 28. Cone-axis pictures with $\bar{\mu}=20°$. (a) Quartz (hexagonal), precessing axis $(P)=[a^*]$, $D=[c]$, MoK_α radiation, $s'=30.22$ mm. (b) Natrophilite (orthorhombic, 0.60:1:0.47) Branchville, Conn. $P=[b]$, $D=[c]$, MoK_α, $s'=29.4$. (c) Adularia (monoclinic) Butte, Mont. $P=[b]$, $D=[a]$, CuK_α, $s'=50.0$.

ACKNOWLEDGEMENTS: W. F. Schmidt did the photography (other than the *x*-ray work), and F. A. Johnson and F. L. Koucky helped with the drawings.

REFERENCES

BUERGER, M. J. (1944), The photography of the reciprocal lattice: *Amer. Soc. X-ray & Electron Diffraction* (now *American Crystallographic Association*), *Monogr.*, No. **1**, 37 pp.

FISHER, D. J. (1952*a*), Triclinic gnomonostereograms: *Am. Mineral.*, **37**, 83–94.

——— (1952*b*), The lattice constants of synthetic chalcanthite, etc., *Ibid.*, **37**, 95–114.

——— (1952*c*), Triclinic calculations, *Ibid.*, **37**, 697–699.

——— (1952*d*), *X*-ray precession techniques, *Ibid.*, **37**, 1036–1054.

Manuscript received July 23, 1952.

X-RAY PRECESSION TECHNIQUES

D. JEROME FISHER, *University of Chicago, Chicago 37, Illinois*

ABSTRACT

Herewith is described a modified technique for taking orientation photos and evaluating them with some precision. Also are discussed for the triclinic case: (1) the identification of non-axial precessing directions; (2) the indexing of non-axial precession photos; and (3) the computation of reciprocal lattice spacings in non-axial directions. The paper concludes with simplified charts for determining the setting of the various layer-line screens.

PRECESSION ORIENTATION PICTURES

Orientation photos of single crystals with the precession camera are 0-level pictures taken by omitting the layer-line screen and using unfiltered radiation. The precessing angle is generally kept small, so that the 0-level Laue streaks are limited to the blank *n*-level area. The theory and practice of the technique are briefly described in Buerger (1944, 21–27).

X-ray photos herewith are all of the triclinic chalcanthite with copper radiation at $F=6.00$ cms., unless otherwise stated. In all cases the pictures are oriented as they appear in the cassette looking in the direction of travel of the direct beam with the dial axis $[c^*]$ horizontal. Unless otherwise indicated all reproductions are at natural scale. The exposures were unduly long for purposes of illustration.

A correctly-oriented crystal on the precession instrument has a reciprocal translation direction (generally a reciprocal axis) parallel to the dial axis, and a direct-lattice translation direction (generally a crystal axis) as the precessing direction. Such a crystal yields a diffraction pattern (Fig. 29),[1] the central part of which consists of radiating 0-level Laue streaks whose ends lie along the circumference of a circle, the circle of precession. One set of these streaks is horizontal and is parallel to the dial axis; these and the other streaks radiate in the direction of (what would appear on a 0-level precession film as) spots of simple indices. If the precessing angle ($\bar{\mu}$) is not too small, some of the 0-level spots will appear along the streaks; thus in Fig. 29 near the end of the east streak appears the K_β spot for $(001)^*$ and along the near-north and near-south streaks (marking $[b^*]$) are shown both K_α and K_β spots for $(0\bar{1}0)^*$ and $(010)^*$ respectively; the K_β spot of the latter is almost cut out by the direct beam-stopping cup.

As the various central lines of nodes of some one 0-level of the reciprocal lattice undergo a precessing motion, they slide or shear over the base of the calotte which they cut out of the sphere of reflection. While this results in a set of spots which unite into a 0-level cone axis ring as described in the previous paper, they form a series of radiating Laue streaks on the orientation film. In short a precession orientation photograph of a correctly set crystal appears the same as a 0-level precession photograph made at the same $\bar{\mu}$-angle taken with unfiltered radiation, except that the former also carries some higher-level diffractions. However, if the crystal is not approximately correctly oriented, any layer line screen present will cut off the ends of some of the 0-level streaks.

---

[1] The numbers here assigned to figures, tables and formulas are in continuation of those used in the preceding paper (Fisher, 1952 *b*).

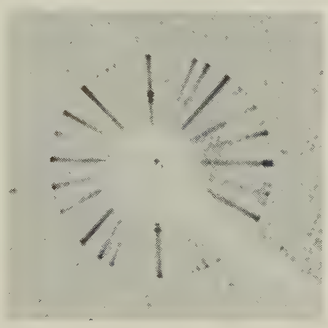

FIG. 29. Central portion of a precession orientation photo of chalcanthite, precessing on [a], $\bar{\mu}=7°$.

ORIENTATION PROCEDURE

In working with a reasonably well-developed subhedron, time will generally be saved if preliminary orientation is obtained with the optical goniometer. If the substance is unknown, one can proceed by standard Goldschmidt methods to locate the crystal axes. If the substance is monoclinic or triclinic, the stereographic technique (Fisher, 1951) is handy for setting a reciprocal axis as the dial axis.

If one is dealing with an unknown anhedron of a non-opaque material, it may be well to obtain optical data on the universal microscope (Fisher, 1952 *c*) to establish the crystal division (and the crystal system if biaxial). For any crystal neither isometric nor triclinic this would set up one or more axial directions. If the anhedron is opaque, one must proceed by trial and error *X*-ray methods of orientation, unless cleavage or some similar "directions" are exhibited.

Having reached the stage where a precession orientation picture showing a Laue streak diffraction pattern outlining a suitable circle of precession has been obtained, the procedure will vary with different situations. A suitable circle of precession may be taken as one which contains enough

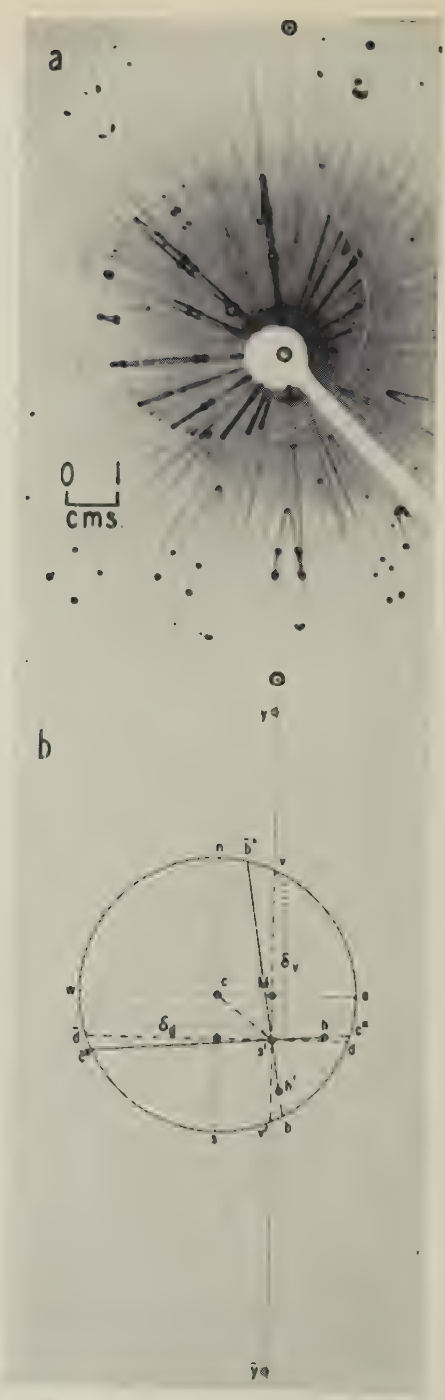

FIG. 30 (a) Precession orientation photo of chalcanthite. Same data as Fig. 29, except $\bar{\mu} = 10°$ and the orientation is a few degrees out of kilter. (*b*) diagram to explain *a*.

sufficiently pronounced radiating 0-level Laue streaks to indicate that one is dealing with a precessing direction that is either a true crystal axis or some translation direction of the direct lattice whose normal is a plane of the reciprocal lattice which is relatively thickly studded with nodes.

If the orientation shown by this picture is in error, it will more or less resemble Fig. 30*a*, which may be used as an illustrative example.[1a] Working above a light box put scratches along two pronounced streaks nearly at right angles (such as $\bar{c}^*$ and $\bar{b}^*$ of Fig. 30*b*) which establishes the direct beam spot s'. Let the scratch along that streak which it is desired to make parallel to the dial axis ($\bar{c}^*$ in Fig. 30*b*) extend to the edges of the film. If the circle of precession is not well marked (due to a short exposure), its outline may be indicated by a few India ink dots. It should be noted that unless the orientation error is quite small, the radial streaks whose ends mark the circle of precession will be shortened on the direct beam side of the center of the circle of precession. Thus h and h' of Fig. 30*b* mark the end points of certain Laue streaks. Place the film above a light box topped with a glass positive made from metric polar coordinate paper.[2] The center of the circle of precession c is made to coincide with the center of the net, and this is marked by a needle prick. Now with s' above the center of the net, make a scratch through it above the vertical axis of the net when the latter is parallel to a line through the two cassette dots y and $\bar{y}$.[3] Also scratch a line through s' above the dial (horizontal) axis of the net. Scratch the circle of precession, establishing d and $\bar{d}$ on the dial axis, and v and v' on the vertical scratch. Use is made of only one d and one v point; the ones farther from s'. Measure (in mm.) $\delta_v = s'v$ and $\delta_d = s'\bar{d}$. Measure angle $\bar{d}s'\bar{c}^*$ (using the polar net). From the graph (Fig. 31) it is seen that for $\bar{\mu} = 10°$ the value of δ_v ($= 31.3$ mm.) corresponds to a dial error of $4.°78 = 4°47'$. This graph also shows that δ_d($= 34.1$ mm.) corresponds to an error of $5.°95$ along a "horizontal" arc (one the plane of which is parallel the x-ray beam) of the goniometer head. The angle $\bar{d}s'\bar{c}^*(= 4\frac{1}{4}°)$ measures the approximate error along a

---

[1a] Having obtained such a picture, unless one of the arcs of the goniometer head would be approximately parallel the direct beam when the dial is set correctly, it is often time-saving to take another picture before proceeding further. In doing this, first set the dial to the approximately correct reading; then loosen the set-screw that holds the brass rod (which supports the crystal) in the goniometer head. Now holding this rod tightly with a pair of tweezers, rotate the dial until one of the arcs is parallel the direct beam collimator.

[2] If the film is put on this light box after it has been in the fixer for only a few seconds, the radii and circles of the polar net will be imprinted on it.

[3] On more recent cassettes the two dots mark the dial axis. In this case scratch the horizontal line first, running it through s' parallel to a line through the two dots. The vertical line joining the two cassette dots in Fig. 30 could be made to run through s' by moving the cassette 0.4 mm. to the right along its horizontal axis.

"vertical" arc (one the plane of which is normal to the x-ray beam). These corrections are to be applied as shown in Table 11.

Angle $\bar{d}s'\bar{c}^*$ measured as $4\frac{1}{4}°$ from the film of Fig. 30 is always less than the true angle needed to correct the "vertical" arc, as long as the axis of the cone of precession (marked by c) does not coincide with the direct beam (shown by s'). It is desired that the direction marked by c (Fig. 30) be made to lie at s' and the direction $\bar{c}^*s'$ be made the dial axis. We may think of moving c to M by adjusting the "horizontal" arc and then from M to s' by adjusting the dial. Then the "revised" direction $\bar{c}^*s'$ is made the dial axis by adjusting the "vertical" arc. Instead of trying to compute these corrections exactly, it is more practical to adjust the "vertical" arc reading by a *positive* percentage factor. Since the radius of the circle of precession of Fig. 30 is 25.4 mm. which corresponds to an error ϵ of 8.°4 (see graph, Fig. 32), one may use *twice* this value as a rough percentage factor of *increase* as shown in Table 11.

TABLE 11. INTERPRETATION OF FIG. 30

	Setting when the film was taken	Corrections (ϵ values)	New setting	Correct setting[6]
Dial	291°08	4°47′	286°21′	286°18′
S arc[4]	6.°22*l*[5]	5.°95(cos 7°) − factor 13.0% = 5.°14	1.°08*l*	1.°13*l*
L arc	0.°01*l*	$4\frac{1}{4}$°(cos 7°) + factor 16.8% = 4.°93	4.°94*l*	4.°97*l*

In similar fashion the correction obtained for the "horizontal" arc from the δ_d value leads to a high result (for reasons brought out later), and it is practical to adjust this by a *negative* percentage factor of *twice* the arc value of $cM[=8.°4 \sin 51°(=\text{angle } cs'M)=6.°5]$. It can be seen from the last column of Table 11 that these correction values are adjusted by percentage factors that are somewhat too small. This is immaterial, since it is impossible to get an exactly correct setting from a single picture; the results obtained by the method described are satisfactory for proceeding with the next step in the orientation process.

Using the "new setting" values of Table 11, take a picture which is a double exposure with dial values 180° apart. The two exposures may be differentiated by giving one of them but half the exposure time of the

---

[4] The plane of the *S* (small) arc is parallel to the direct beam when the dial reads $298\frac{1}{2}°$ (that is, about 7° off the setting used).

[5] *l* (left) or *r* (right) are recorded while looking from the crystal towards the goniometer head (Fisher, 1951, 125).

[6] Correct setting (for precession on [*a*] with [*c**] as the dial axis) determined by methods described ahead.

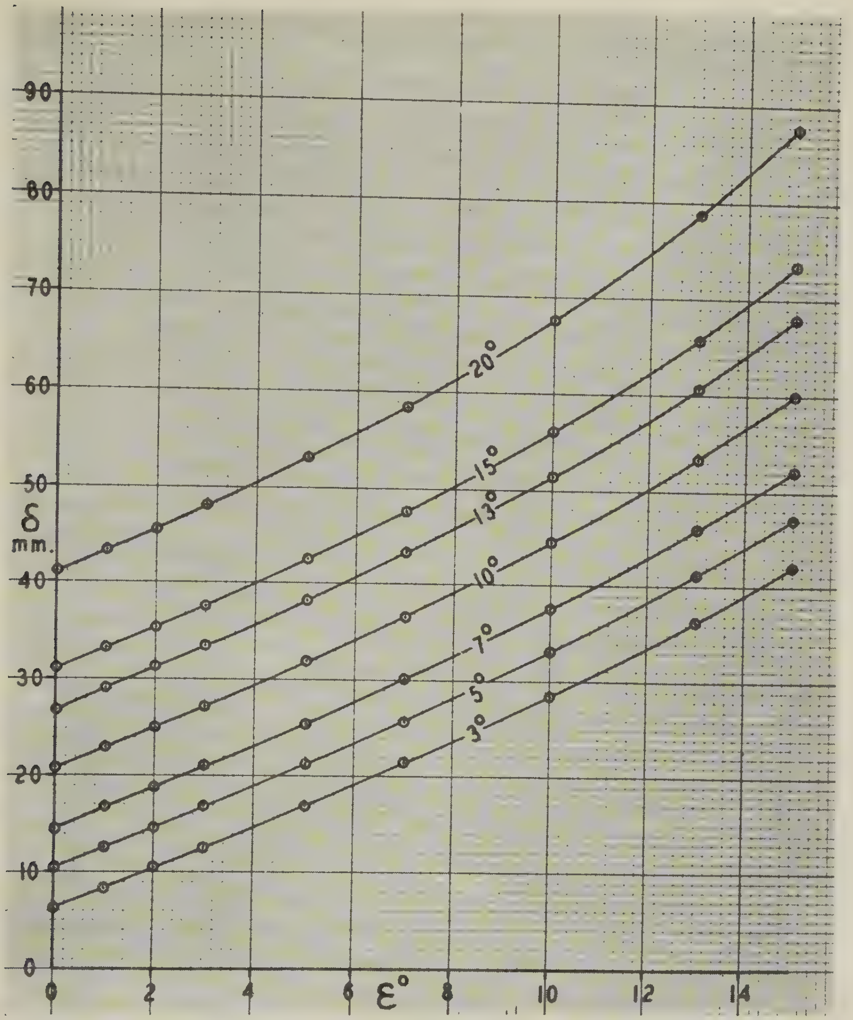

FIG. 31. Graph showing variation in δ (in mm.) with ϵ (in degrees) for various values of $\bar{\mu}$ (the figures on the curves) where $F = 60.00$ mm.

other, but it is quicker to keep the times the same and vary the $\bar{\mu}$ value. Moreover since the orientation will be nearly correct, it simplifies things to add the layer-line screen. This amounts to taking ordinary 0-level precession pictures with unfiltered radiation. Since such pictures cannot be taken[6a] on the ordinary precession camera with $\bar{\mu}$ less than 20°,

---

[6a] Unless one has a layer-line screen with an opening of $r < 15$ mm. Thus with an $r = 7$ mm. screen, such pictures could be taken with $\bar{\mu} = 15°$ ($s = 26.1$ mm.), 13° ($s = 30.3$ mm.), or 10° ($s = 39.7$ mm.).

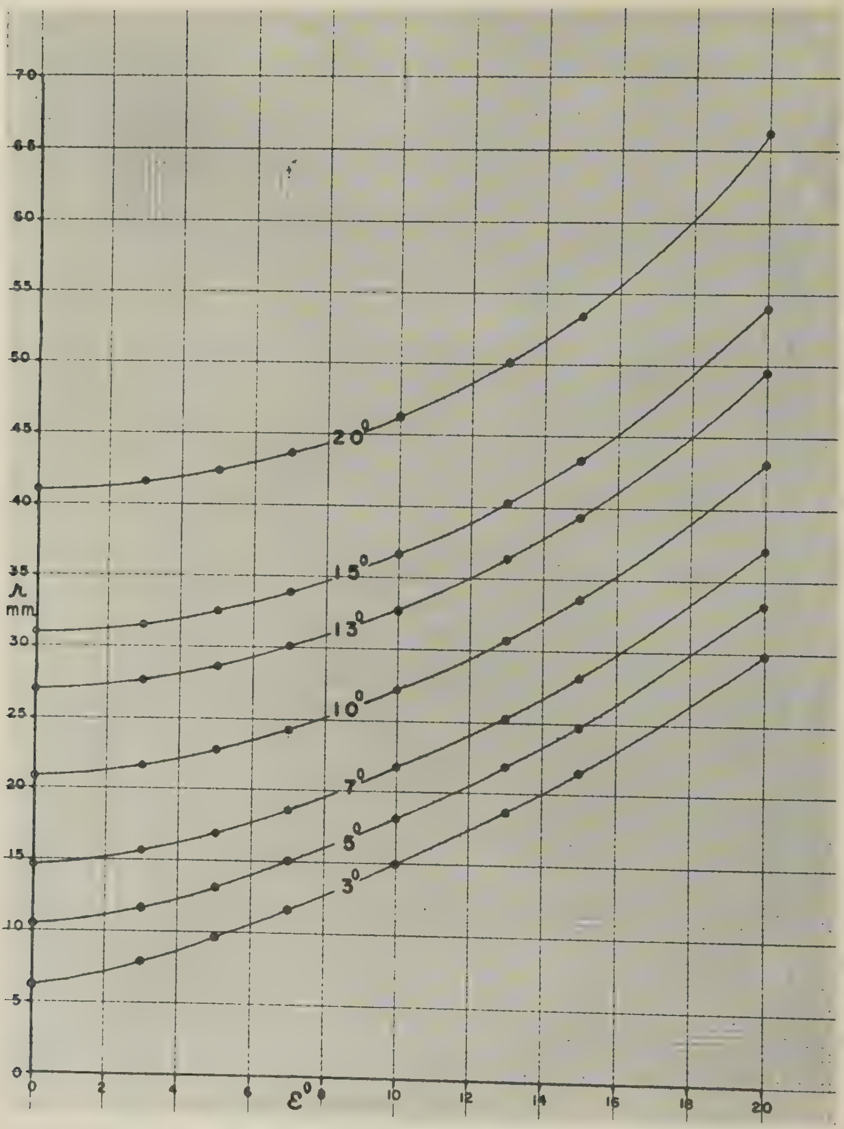

FIG. 32. Graph showing variation in r (in mm.) with ϵ (in degrees) for various values of $\bar{\mu}$ (the figures on the curves) where $F=60.00$ mm.

it is expedient to use precessing angles of 20° and 25°. Such large angles are perhaps unusual for orientation work, but nevertheless they are desirable in the final steps of the orientation procedure to insure satisfactory accuracy.

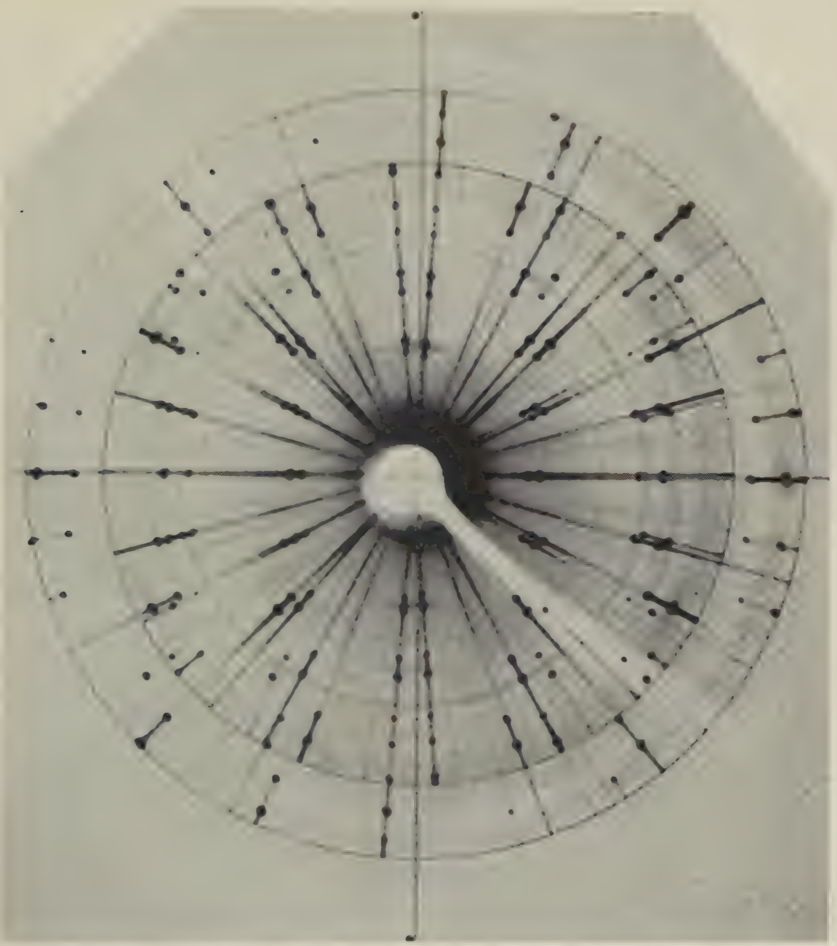

FIG. 33. Precession orientation photo of chalcanthite. Same data as Fig. 29 except a double exposure (with $\bar{\mu}$ values of 20° and 25° at dial readings 180° apart) and a 0 level layer line screen added.

Figure 33 is such a photograph, which may be interpreted as follows. Locate the direct beam spot s' by suitable scratches; the one which marks the dial axis should extend to the right and left edges of the film, using a mean position of the two dial axis streaks. Place the film above the polar net and establish the centers (c and C) of the two circles of precession; also make a vertical scratch normal to the dial axis going through the mean position of these centers (if c and C are not practically together, scratch ticks along vertical lines through both of them) which intersects the proper circle of precession at n & s for the smaller circle and N & S

for the larger circle. Now scratch the two circles of precession; inspect these under a hand lens to make sure they go exactly through the ends of the streaks; if they do not, make suitable allowances in the following measurements.

The error ϵ (in minutes) of the dial axis reading is found by measuring the difference g or G (in mm.) between the length of $c'\ n$ & $c'\ s$ and of $C'N$ & $C'S$, whence:

$$60g/4.494 = \epsilon \quad (\text{where } \bar{\mu} = 20°) \tag{49}$$

$$60G/4.625 = \epsilon \quad (\text{where } \bar{\mu} = 25°). \tag{50}$$

The denominators of these equations represent the difference in north-south streak lengths (in mm.) for dial orientation errors of 1° at the $\bar{\mu}$ values given (as is shown in Table 12).

The correct "horizontal" arc setting for a camera in perfect adjustment may be obtained from the difference in lengths between values of $s'c'$ and $s'C'$ (c' and C' are points on the dial axis scratch where it is cut by vertical scratches through c and C.). Since in Fig. 33 c' and C' are both to the right of s', it is clear that if the crystal setting were perfect, c' and C' would coincide (they would also coincide with c and C if the dial readings were just right) at a point 0.8 mm. to the right[7] of s'. Call this point O', the center of precession for the film. If the points where the dial axis scratch cuts the circles of precession be designated d (right side) and $\bar{d}$ (left side), where $\bar{\mu}=20°$, and D and $\overline{D}$ (where $\bar{\mu}=25°$), then the difference j or J (in mm.) between the length of $O'd$ & $O'\bar{d}$ and of $O'D$ & $O'\overline{D}$ supplies the error ϵ (in degrees) in the arc settings according to the following formulae:

$$j \cos I/4.494 = \epsilon \quad (\text{where } \bar{\mu} = 20°) \tag{51}$$

$$J \cos I/4.625 = \epsilon \quad (\text{where } \bar{\mu} = 25°) \tag{52}$$

where I is the angle between the plane of the "horizontal" arc and the direct x-ray beam.

It is not satisfactory to get the correction for the "vertical" arc setting by attempting to measure the angle between the two dial streaks of Fig. 33. Instead rotate on the dial axis until another crystal axis is in precessing position; now the other arc of the goniometer head is more or less "horizontal" and another double exposure picture may be taken. From this the desired angle of correction may be computed by the method just outlined.

---

[7] For perfect adjustment a precession camera must have its dial axis normal to and intersecting V_{vl} (the "vertical" axis through the crystal; see Fig. 6 on page 100 of Fisher 1952 a). Their point of intersection 0 is the center of precession for the crystal. Also the cassette holder must have its horizontal axis normal to and intersecting V_{ca} (the "vertical" axis of the cassette); their point of intersection 0′ is the center of precession for the film. And lastly the direct x-ray beam should cut both 0 and 0′!

Explanation of the Two Charts

The graphs of Figs. 31 and 32 are based on data given in Table 12. The derivation of these data may be explained in terms of a special case, Fig. 34*a*. It will be noted that all three orientation circles of precession indicated here have a common chord; namely, the direction which marks

Table 12. Values of δ, D, and r in mm. and of τ in °′ where $F = 60.00$ mm. for Various Values of $\bar{\mu}$ and ϵ

$\bar{\mu}$ \ ϵ		0°	1°	2°	3°	5°	7°	10°	13°	15°	20°
3°	δ	6.28	8.39	10.50	12.63	16.97	21.46	28.57	36.35	42.05	59.02
	τ	45-00	36-50	30-54	26-26	20-18	16-19	12-24	9-48	8-30	6-05
	D	—	4.20	8.42	12.63	—	—	—	—	—	—
	r	6.28	6.55	7.13	7.88	9.65	11.65	14.98	18.73	21.50	29.84
5°	δ	10.46	12.57	14.70	16.87	21.25	25.81	33.10	41.14	47.08	65.00
	τ	45-00	39-46	35-26	31-48	26-13	22-04	17-32	14-16	12-32	9-08
	D	—	4.21	8.42	12.68	21.25	—	—	—	—	—
	r	10.46	10.64	11.07	11.68	13.20	15.02	18.20	21.90	24.70	33.34
7°	δ	14.62	16.74	18.89	21.06	25.52	30.17	37.76	45.99	52.19	71.18
	τ	45-00	41-08	37-45	34-37	29-49	25-52	21-10	17-39	15-39	11-37
	D	—	4.22	8.46	12.71	21.33	30.17	—	—	—	—
	r	14.62	14.76	15.11	15.61	16.95	18.63	21.71	25.32	28.14	37.09
10°	δ	20.84	22.98	25.15	27.36	31.93	36.73	44.53	53.35	60.00	80.84
	τ	45-00	42-12	39-39	37-18	33-08	29-34	25-05	21-20	19-09	14-27
	D	—	4.26	8.52	12.81	21.51	30.44	44.53	—	—	—
	r	20.84	20.94	21.21	21.61	22.76	24.28	27.14	30.74	33.62	43.10
13°	δ	26.99	29.16	31.37	33.66	38.31	43.29	51.46	60.84	68.01	91.08
	τ	45-00	42-47	40-43	38-44	35-10	31-57	27-41	23-56	21-39	16-31
	D	—	4.30	8.61	12.98	21.75	30.81	45.14	60.84	—	—
	r	26.99	27.07	27.30	27.65	28.66	30.06	32.81	36.41	39.36	49.54
15°	δ	31.06	33.25	35.49	37.78	42.55	47.66	56.11	65.91	73.48	98.30
	τ	45-00	43-03	41-12	39-26	36-07	33-06	28-58	25-14	22-55	17-32
	D	—	4.34	8.69	13.07	21.96	31.12	45.65	61.64	73.48	—
	r	31.06	31.13	31.33	31.66	32.61	33.95	36.65	40.27	43.31	54.06
20°	δ	41.04	43.33	45.62	48.02	53.07	58.55	67.83	78.91	87.71	118.16
	τ	45-00	43-27	41-58	40-31	37-43	35-02	31-11	27-29	25-05	19-09
	D	—	4.49	8.94	13.44	22.61	32.11	47.31	64.31	77.14	118.16
	r	41.04	41.10	41.27	41.55	42.41	43.66	46.33	50.13	53.46	66.21

Following are $\delta = r$ values where $\epsilon = 0°$ for various values of $\bar{\mu}$ not given above:

$\bar{\mu}$	δ or r	$\bar{\mu}$	δ or r	$\bar{\mu}$	δ or r	$\bar{\mu}$	δ or r
4°	8.40	9°	18.77	14°	29.03	18°	37.08
6°	12.54	11°	22.90	16°	33.08	19°	39.07
8°	16.70	12°	24.95	17°	35.08	25°	50.71

For $\bar{\mu} = 25°$ and $\epsilon = 1°$ have; $\delta = 53.06$; $\tau = 43°42'$; $D = 4.63$; and $r = 50.77$.

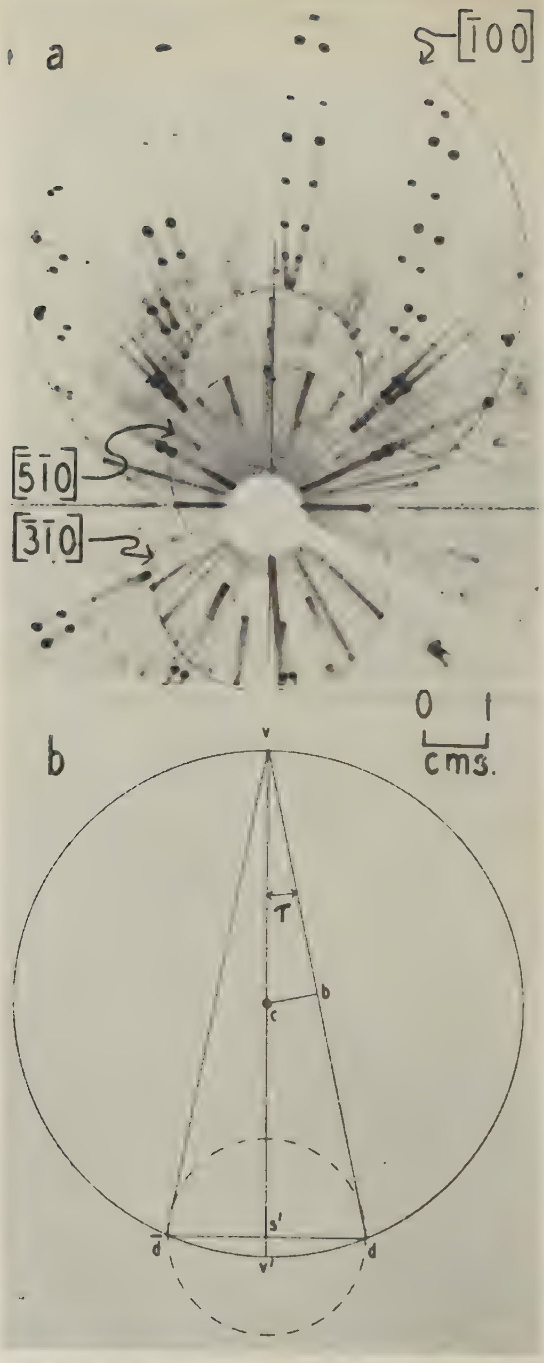

FIG. 34*a*. Precession orientation photo of chalcanthite. Same data as Fig. 29 except the precessing direction is 20°32′ off [*a*] about the dial axis. Circles of precession are indicated for three zone axes. (*b*) Diagram based on the [100] circle of precession of *a*.

the dial axis. This chord has a length of 29.25 mm., the diameter of a correctly oriented $\bar{\mu}=7°$ circle of precession (see Table 12). Thus as these circles of precession get farther and farther off the correct orientation [that where the center of any given circle coincides with s' (Fig. 34*b*) which represents the precessing direction], they get larger and larger. The method of indexing these circles of precession is given in the next section. The orientation error ϵ of any one of them may be determined from its radius r by using Fig. 32.

A diagram showing the geometry of the largest circle of precession of Fig. 34*a* appears as Fig. 34*b*. Here let $s'd=r_0$, the radius of a correctly oriented ($\epsilon=0°$) circle of precession (in this case where $\bar{\mu}=7°$). Of course

$$r_0 = 2F \sin \bar{\mu} \tag{53}$$

as is evident from Fig. 14 of the previous paper. Buerger [1944, p. 25, (23) and 23′)] gives:

$$\Delta = \frac{\sin 2\epsilon}{\cos (2\epsilon + \bar{\mu})} \quad \text{and} \quad \Delta' = \frac{\sin 2\epsilon}{\cos (2\epsilon - \bar{\mu})}.$$

In the terminology of this paper,

$$\delta = r_0 + F\Delta \quad (54) \qquad \text{and} \qquad \delta' = r_0 - F\Delta' \quad (54');$$

where δ' represents the shorter streak ($s'v'$ of Fig. 30*b*), just as δ stands for the longer streak ($s'v$ of Fig. 30*b*). Thus one can compute δ, δ', and also:

$$D = \delta - \delta' = F\Delta + F\Delta' \tag{55}$$

where D is the difference in length of the north & south streaks. It is clear from Fig. 34*b* that

$$\tan \tau = r_0/\delta \tag{56}$$

where $\tau = \angle s'vd$ and $\delta = s'v$. Similarly the radius r of an incorrectly oriented circle of precession is given by (57) or (58). Note in Fig. 34*b* that $r=cv$; and since cb is normal to vd, it follows that $vb=bd$.

$$r = (2vb)/(2 \cos \tau).$$

But

$$vd = \delta/\cos \tau.$$

Thus

$$r = \delta/(2 \cos^2 \tau). \tag{57}$$

Substituting in here the value of δ from (56) gives:

$$r = r_0/\sin 2\tau. \tag{58}$$

The data of Table 12 were computed from these equations.

In Fig. 35 are shown the central portions of two precession orientation photos taken under identical conditions, except in the case of (*b*) the film was 2.00 cms. closer to the crystal than was true for (*a*). Fig. 35*b*

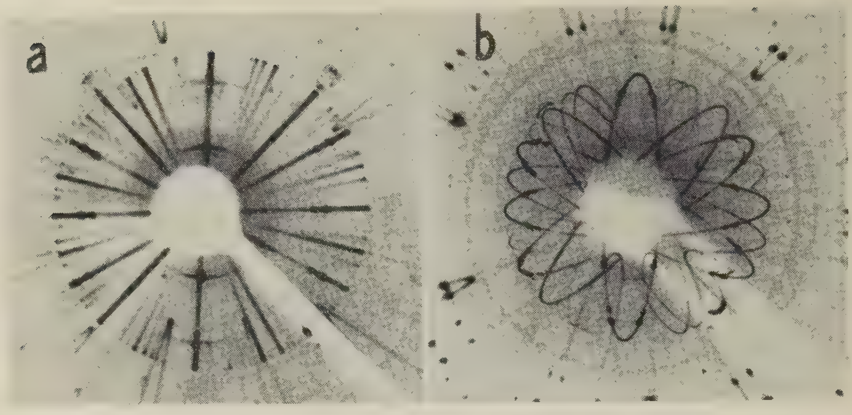

FIG. 35. Precession orientation photos of chalcanthite, precessing on $[\bar{a}]$ with $\bar{\mu}=10°$. (*a*) $F=6.00$ cms. (*b*) Same, except film cassette moved 2.00 cms. closer to the crystal.

is of minor interest, since it shows that where the center of the film is off the center of the second universal joint, the Laue streaks [which are straight lines in (*a*)] split apart into parentheses-like forms. Of course the circle of precession is smaller in (*b*) than in (*a*).

IDENTIFYING NON-AXIAL PRECESSING DIRECTIONS

Non-axial precessing directions can be identified readily by graphical means. Prepare a cross-section of the reciprocal lattice network through its origin and normal to the dial axis. If the dial axis is a reciprocal axis (which is generally the case), the network consists of lines making an interaxial angle (α, β, or γ) with each other. The apparent translations of such a network may be obtained from equations (59) to (70). These are derived from equations like those given in an earlier paper [Fisher 1952*a*, (30) to (35)]. Figure 36[8] shows such a network for chalcanthite with dial axis $[c^*]$. Here $\gamma=77°26'$, $G=0.884$, and $J=1.553$ cms.; note that G & J are defined in (59) & (63) below. Then $[\bar{1}\bar{1}0]$ is normal to a line through the origin and the point marked $(\bar{1}10)$; $[\bar{3}\bar{1}0]$ is normal to a central line through the point marked $(\bar{1}30)$, etc. The directional indices may be obtained by cross-multiplication, the standard zonal procedure, providing one first replaces the nought of the final digit of the index by unity. From the graph an ordinary protractor suffices to measure the angle between the non-axial precessing direction (such as $[\bar{1}\bar{1}0]$ or $[\bar{3}\bar{1}0]$) and $[\bar{a}]$ or $[\bar{b}]$, and thus its identification is readily accomplished.

---

[8] This diagram has $-[c^*]$ at the center because it was prepared to illustrate an actual working case looking from the dial towards the crystal, and it was assumed that $+[c^*]$ in the crystal extended from the mounted end of the crystal *away from* the goniometer head.

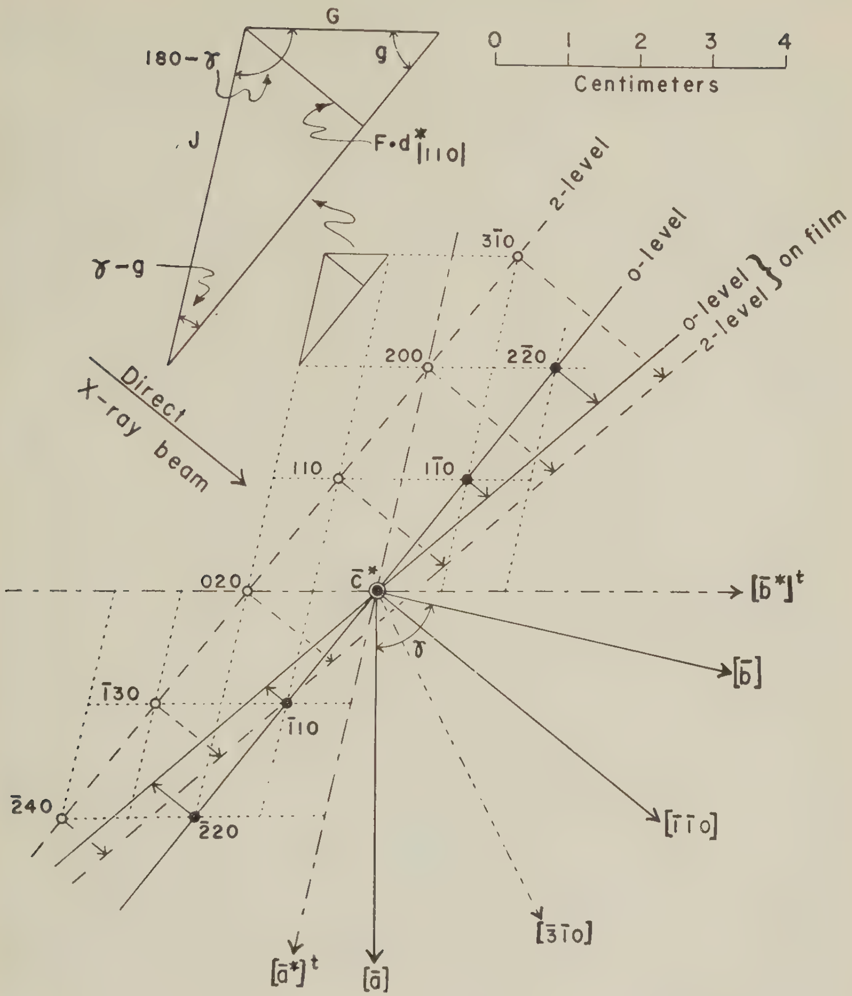

FIG. 36. Cross-section of the reciprocal lattice network of chalcanthite normal to [c^*] on a scale to fit copper radiation at $F = 60.00$ mm. Note that no nodes of the reciprocal lattice (except the one at its origin) lie in the plane of this cross-section.

An example is shown in Fig. 34.

Precession on [a]

$G = b^* \sin \alpha^* F\lambda$ (59) where $G = t^*_{\perp c^*}$ and D (dial axis) $= c^*$

$G = F\lambda/(b \sin \gamma)$ (60)

$H = c^* \sin \alpha^* F\lambda$ (61) where $H = t^*_{\perp b^*}$ and $D = b^*$

$H = F\lambda/(c \sin \beta)$ (62)

Precession on $[b]$

$J = a^* \sin \beta^* F\lambda$ (63) where $J = t^*{\perp_c}^*$ and $D = c$

$J = F\lambda/(a \sin \gamma)$ (64)

$K = c^* \sin \beta^* F\lambda$ (65) where $K = t^*{\perp_a}^*$ and $D = a^*$

$K = F\lambda/(c \sin \alpha)$ (66)

Precession on $[c]$

$M = a^* \sin \gamma^* F\lambda$ (67) where $M = t^*{\perp_b}^*$ and $D = b^*$

$M = F\lambda/(a \sin \beta)$ (68)

$N = b^* \sin \gamma^* F\lambda$ (69) where $N = t^*{\perp_a}^*$ and $D = a^*$

$N = F\lambda/(b \sin \alpha)$ (70)

From the above one can derive:

$$G \sin \gamma = N \sin \alpha; \qquad G \sin \gamma^* = N \sin \alpha^*. \tag{71}$$

$$H \sin \beta = K \sin \alpha; \qquad H \sin \beta^* = K \sin \alpha^*. \tag{72}$$

$$J \sin \gamma = M \sin \beta; \qquad J \sin \gamma^* = M \sin \beta^*. \tag{73}$$

COMPUTING RECIPROCAL LATTICE SPACINGS

Buerger (1942, 365) lists "Conditions B" which he states are essential in choosing a reciprocal cell corresponding to the reduced primitive triclinic cell. These conditions may be stated more simply as follows providing one assumes the $c<a<b$ rule:

$$d^*_{|100|} > d^*_{|010|} > d^*_{|1\bar{1}0|} > d^*_{|110|}$$

$$d^*_{|001|} > d^*_{|100|} > d^*_{|101|} > d^*_{|10\bar{1}|}$$

$$d^*_{|001|} > d^*_{|010|} > d^*_{|011|} > d^*_{|01\bar{1}|}$$

The computation of the necessary reciprocal spacings in directions other than those normal to "reciprocal pinacoidal" planes may be carried out by means of equations (74) to (85). The derivation of these may be illustrated for (82) & (83) by the triply-enlarged "diagonal half-mesh" of the reciprocal lattice shown in the upper left corner of Fig. 36.

Dial axis $[a^*]$

To compute $e = \perp[011] \wedge [c^*]^t$, use the tangent law:

$$\tan\left(e - \frac{\alpha}{2}\right) = \left(\tan \frac{\alpha}{2}\right)\left(\frac{N - K}{N + K}\right) \tag{74}$$

and

$$Fd^*_{|011|} = K \cdot \sin e. \tag{75}$$

To compute $e' = \perp[01\bar{1}] \wedge [c^*]^t$, the tangent law yields;

$$\tan\left(90 - \frac{\alpha}{2} - e'\right) = \tan\left(90 - \frac{\alpha}{2}\right) \cdot \left(\frac{K - N}{K + N}\right) \tag{76}$$

and

$$Fd^*_{|01\bar{1}|} = K \cdot \sin e'. \tag{77}$$

Dial axis $[b^*]$

To compute $f = \perp[101] \wedge [a^*]^t$, use the tangent law:

$$\tan\left(f - \frac{\beta}{2}\right) = \left(\tan\frac{\beta}{2}\right)\left(\frac{H - M}{H + M}\right) \tag{78}$$

and

$$Fd^*_{|101|} = M \cdot \sin f. \tag{79}$$

To compute $f' = \perp[10\bar{1}] \wedge [a^*]^t$, the tangent law gives:

$$\tan\left(90 - \frac{\beta}{2} - f'\right) = \tan\left(90 - \frac{\beta}{2}\right) \cdot \left(\frac{M - H}{M + H}\right) \tag{80}$$

and

$$Fd^*_{|10\bar{1}|} = M \cdot \sin f'. \tag{81}$$

Dial axis $[c^*]$

To compute $g = \perp[110] \wedge [b^*]^t$, use the tangent law:

$$\tan\left(g - \frac{\gamma}{2}\right) = \left(\tan\frac{\gamma}{2}\right)\left(\frac{J - G}{J + G}\right) \tag{82}$$

and

$$Fd^*_{|110|} = G \cdot \sin g. \tag{83}$$

To compute $g' = \perp[1\bar{1}0] \wedge [b^*]^t$, the tangent law yields:

$$\tan\left(90 - \frac{\gamma}{2} - g'\right) = \tan\left(90 - \frac{\gamma}{2}\right) \cdot \left(\frac{G - J}{G + J}\right) \tag{84}$$

and

$$Fd^*_{|1\bar{1}0|} = G \cdot \sin g'. \tag{85}$$

Note. The two sides of equations (74), (80), and (84) turn out to be negative in the case of chalcanthite. Of course they could be put in positive fashion, but it seems better to keep the equation triplets with similar forms, even though the signs may then become negative. The sign can be determined easily from a graphical check of angles e, f, and g.

INDEXING PRECESSION PHOTOGRAPHS

Precession photos where a crystal axis is the precessing axis are indexed on inspection. This is illustrated in an earlier paper (Fisher, 1952 *a*, Figs. 7 and 8). Where some other direction of precession is chosen, a simple graphical procedure suffices. Thus Fig. 37*a* is a precession picture of chalcanthite (0- and 2-levels on a single film) where $[\bar{1}\bar{1}0]$ is the precession axis and $[c^*]$ is the dial axis. If a trace-o-film copy of Fig. 37*a* is made and placed *upside down* above Fig. 36 so that $[c^*]$ on the trace-o-film lies above the $[\bar{1}\bar{1}0]$ direction of Fig. 36, with the (000) points of the two coinciding, it will be found that the spots on the $[1\bar{1}0]^*$ direction of the trace-o-film (for both 0- and 2-levels) will lie above the tips of the arrows shown along these two "film" levels in Fig. 36. Once these spots are indexed, since those along $[c^*]$ may be indexed on inspection, it is simple to index all the spots on the picture (see Fig. 37 *b*). The explanation of this procedure is obvious if one holds the sheet of trace-o-film

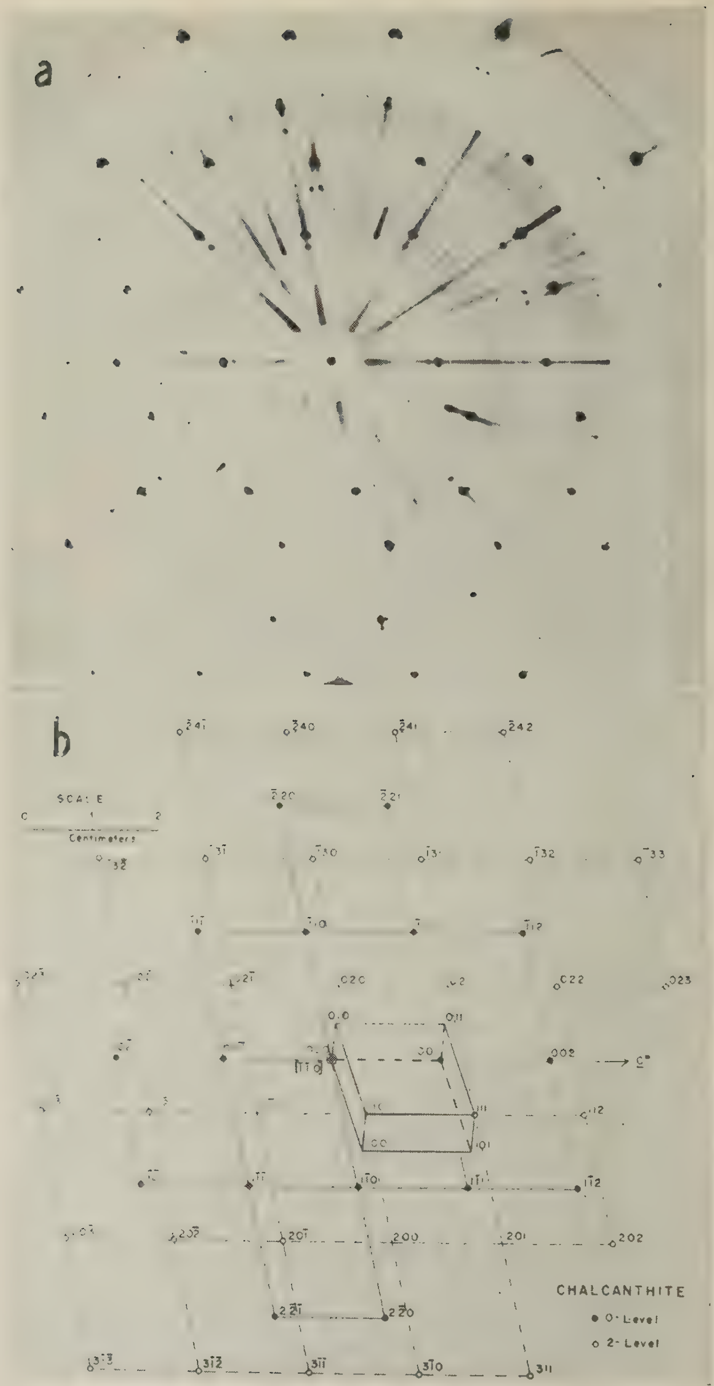

FIG. 37*a*. Precession photo of chalcanthite, 0- and 2-levels, precessing on $[\bar{1}\bar{1}0]$. $F = 6.00$ cms., $\bar{\mu} = 20°$, Cu K_α radiation. (*b*) Reciprocal lattice projection to fit *a*.

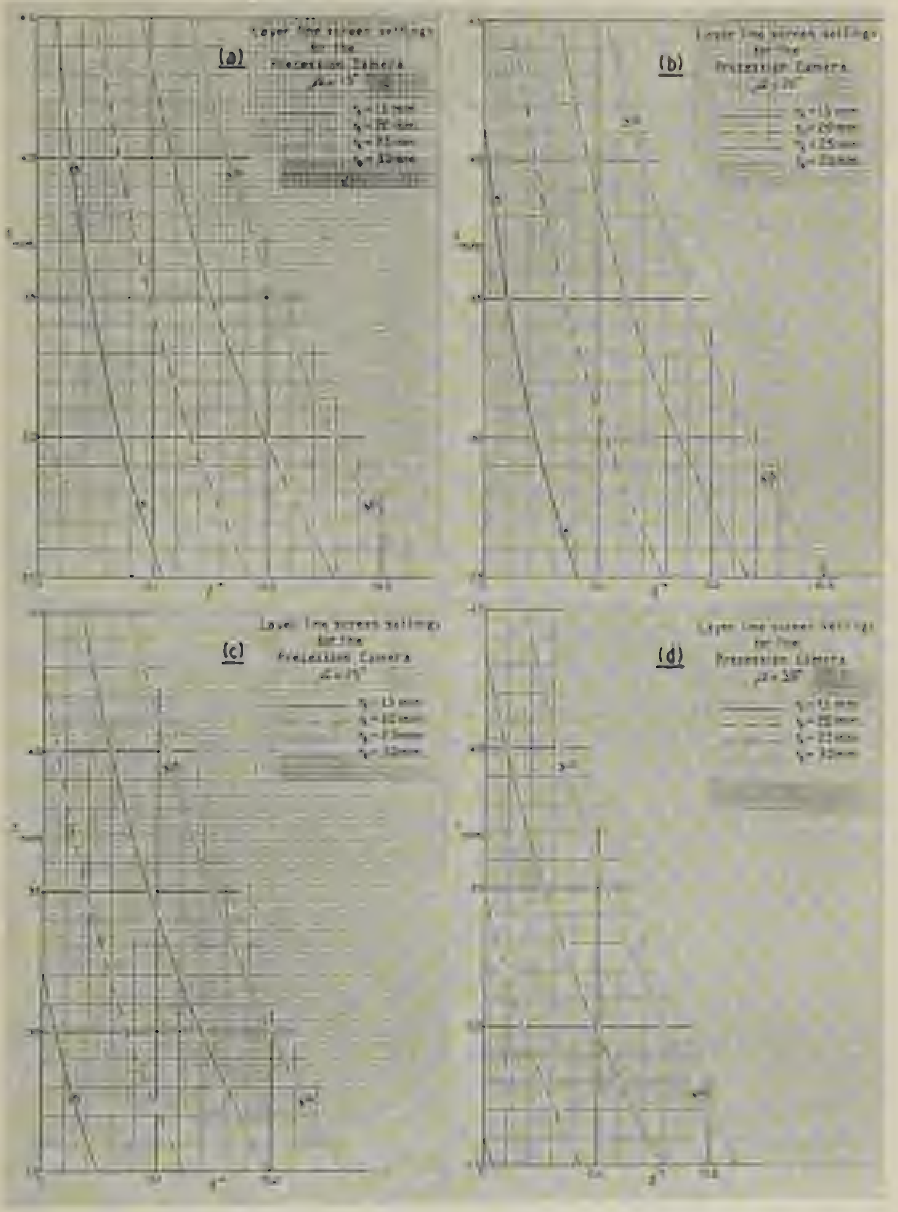

FIG. 38. Charts for determining s-settings of the various layer line screens ($r=15$, 20, 25, or 30 mm. shown by different types of lines).

(*a*) $\bar{u}=15°$; (*b*) $\bar{\mu}=20°$; (*c*) $\bar{\mu}=25°$; (*d*) $\bar{\mu}=30°$.

above Fig. 36 normal to the arrow marked "Direct X-ray Beam" (with the marked side of the trace-o-film towards this arrow and $[c^*]$ pointing *downwards* at the center of the figure) and imagines the (000) point on the trace-o-film coincides with the center of the figure.

CHARTS FOR SETTING LAYER-LINE SCREENS

In the original publication, Buerger (1944, p. 7) presented a simple graph for setting layer-line screens of $r = 15$ and 30 mm. where $\bar{\mu} = 20°$. Similar graphs covering screens of $r = 15$, 20, 25, & 30 mm. and $\bar{\mu}$-values of 15°, 20°, 25°, & 30° are given in Fig. 38. The writer has these on a single sheet in his laboratory, using different colors for different $\bar{\mu}$-values. Nomograms to accomplish the same end have been published by Evans *et al.* and by Tavora.

REFERENCES

BUERGER, M. J. (1942), *X*-ray crystallography, New York.

——— (1944), The photography of the reciprocal lattice: *Amer. Soc. X-ray & Electron Diffraction, Monogr.* No. **1**, 37 pp.

EVANS, H. T., TILDEN, S. G., AND ADAMS, P. (1949), New techniques applied to the Buerger precession camera for *x*-ray diffraction studies: *Rev. Sci. Instr.*, **20**, 155–159.

FISHER, D. J. (1951), Setting a given direction parallel to the axis of a goniometer head: *Am. Mineral.*, **36**, 123–128.

——— (1952*a*), The lattice constants of synthetic chalcanthite, etc. *Ibid.*, **37**, 95–114.

——— (1952*b*), Cone-axis diffraction patterns: *Ibid.*, **37**, 1007–1035.

——— (1952*c*), New universal microscope goniometer: *Ibid.*, **37**, 289 (abstract).

TAVORA, E. (1951), A new chart for setting the Buerger precession camera: *Acad. Brasil. de Ciencias*, **23**, 113–118.

Manuscript submitted July 23, 1952.

NOTES AND NEWS

STABILITY OF CHRYSOTILE ASBESTOS

Bartholomew Nagy and Thomas F. Bates, *The Pennsylvania State College, State College, Pa.*

Recent investigations have been conducted on the group of minerals, commonly referred to as the serpentine group, which possesses the general chemical formula $3MgO \cdot 2SiO_2 \cdot 2H_2O$ and the kaolinite type crystal structure. These studies have shown that chrysotile has the lowest chemical and thermal stability of the group.

On the basis of theoretical considerations Pauling (1930) came to the conclusion that if serpentine had a kaolinite type crystal structure, it would have a tendency to curve because of the misfit of the octahedral and tetrahedral layers of the unit cell. After Warren and Hering (1941) established a kaolinite type crystal lattice for chrysotile, Bates, Sand and Mink (1950) and Noll and Kircher (1950) decided on the basis of electron microscope studies, that the fibers of chrysotile asbestos are hollow tubes formed by the curvature of the kaolinite type layers. Bates and Mink (1950) attributed the flaky morphology of antigorite to replacement of the Mg^{++} ions of the octahedral layer by trivalent ions (chiefly Al^{+++} and Fe^{+++}), resulting in the disappearance of the size difference between the octahedral and tetrahedral layers.

The investigations just completed have shown that chrysotile has a higher solubility in hydrochloric acid than antigorite. The effects of chemical attack have been studied by *x*-rays, differential thermal analysis and electron microscopy.

Figure 1 shows the percentage weight loss of Thetford, Quebec, chrysotile and Unionville, Pennsylvania, antigorite plotted against various concentrations of HCl. The two curves are similar with the exception that the sudden increase in the solubility of chrysotile appears between 1 and 5 normal HCl, in contrast to the case of antigorite where 5 to 10 normal HCl is required to produce the same effect. Furthermore it was observed that treatment in low concentrations of HCl and in distilled water dissolves more chrysotile than antigorite.

In the *x*-ray diffraction diagrams the effect of acid treatment was to lower the intensities rather than shift the position of the reflections. In the case of chrysotile the reflections disappeared completely after treatment in 1 normal HCl, whereas disappearance of the antigorite peaks did not take place until concentrated HCl was used.

Differential thermal analysis showed that 1 normal hydrochloric acid treatment did not affect the antigorite pattern but changed the chrysotile curve into a nearly straight line exhibiting only one endothermic reaction

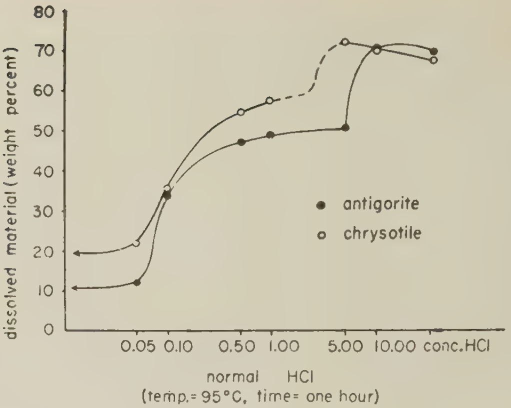

FIG. 1. Percentage weight loss of chrysotile and antigorite during acid treatment for one hour at 95° C.

at 125° C. due to the loss of the water adsorbed on the surface of the particles and a small exothermic peak at 830° C.

The result of 1 normal HCl treatment on the morphology of chrysotile is shown in Fig. 3. Those features of the chrysotile fibers which indicate a tubular morphology disappear causing the fibers to look like flat laths (*A*) having serrate and pitted surfaces (*B*). The untreated fibers are shown in Fig. 2, where (*A*) indicates a single chrysotile tube, (*B*) several tubes and (*C*) concentric tubes. In order to achieve a three dimensional effect Figs. 3 and 4 were prepared by enlarging from superimposed negative and positive plates which had been shifted very slightly with respect to each other. This procedure results in the accentuation of some of the details of the pictures but the loss of some of the fine structure

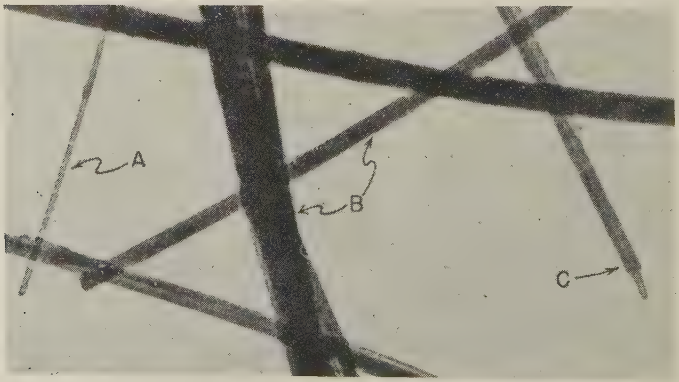

FIG. 2. Untreated chrysotile fibers, Thetford, Quebec. 46,000×.

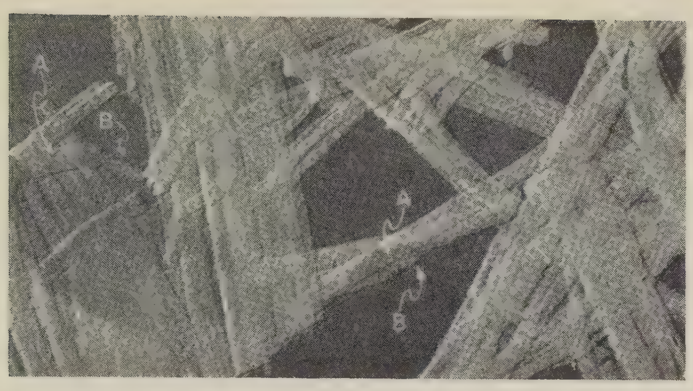

FIG. 3. One normal hydrochloric acid treated chrysotile fibers. 61,000×.

and therefore could not be used in the case of the untreated chrysotile. One normal HCl treatment did not produce any noticeable changes in the morphology of antigorite.

It was also observed that chrysotile has a relatively low thermal stability compared to other hydrous silicate minerals. The heat of the electron beam causes a very rapid change in the morphology of the fibers, and prolonged exposure to electron bombardment results in complete disintegration of the material, as reported by Noll and Kircher (1952). Figure 4 shows fibers which were subjected to electron bombardment for two minutes, whereas for figures 2 and 3 a fifteen second bombardment took place. Figure 4 indicates that although the outer surface of the tubes is "fused" resulting in rounded edges (*A*), in many cases the tubular morphology of the still unaffected tubes can be observed inside this "fused" coating (*B*). The chrysotile fibers are so sensitive to the heat of the electron beam that the "unfused" tubes can be observed only if

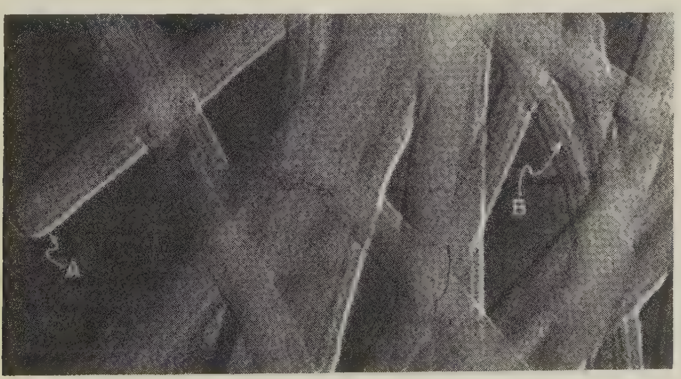

FIG. 4. Chrysotile fibers subjected to two minutes of electron bombardment. 75,000×.

the sample is subjected to the electron beam for not longer than about 30 seconds at a magnification of approximately 5700 times and very low electron beam intensity.

These results indicate that the stability of chrysotile is relatively low in comparison to that of antigorite and other hydrous silicate minerals. Surface area measurements using the B.E.T. gas adsorption method yielded a value of 7.24 m^2/gm for the chrysotile sample used in the experiments and 11.40 m^2/gm for the antigorite sample. The similarity in magnitude of these values indicates that the difference in the stability cannot be attributed to different surface areas. A possible explanation of the lower stability of chrysotile may be related to the strain that is believed to exist in the tubes. Bates, Hildebrand and Swineford (1950) pointed out that theoretically the unstrained portion of the endellite tubes is only one unit cell thick in the *c* direction and that with increase or decrease in radius of curvature the strain in the other layers also increases. Noll and Kircher (1951) used the same line of reasoning in discussing the morphology and structure of chrysotile.

REFERENCES

1. Bates, T. F., Hildebrand, F. A., and Swineford, Ada (1950), Morphology and structure of endellite and halloysite: *Am. Mineral.*, **35**, 463–484.
2. Bates, T. F., and Mink, J. F. (1950), Morphology and structure of the serpentine minerals antigorite and chrysotile: (abstract), *Geol. Soc. Am. Bull.*, **61**, (12), 1442.
3. Bates, T. F., Sand, L. B., and Mink, J. F. (1950), Tubular crystals of chrysotile asbestos: *Science*, **111**, 512–513.
4. Noll, W., and Kircher, H. (1950), Zur Morphologie des Chrysotilasbestes: *Naturw.*, **37**, 540–541.
5. Noll, W., and Kircher, H. (1951), Über die Morphologie von Asbesten und ihren Zusammenhang mit der Kristallstruktur: *Neues Jb. Mineral., Mh.* **10**, 219–240.
6. Noll, W., and Kircher, H. (1952), Veränderungen von Chrysotilasbest im Electronenmikroscop: *Naturw.*, **39**, 188.
7. Pauling, L. (1930), The structure of the chlorites: *Proc. Nat. Acad. Sci.*, **16**, 578–582.
8. Warren, B. E., and Hering, K. W. (1941), The random structure of chrysotile asbestos: *Phys. Rev.*, **59**, 925.

SECOND OCCURRENCE OF BAYLEYITE IN THE UNITED STATES

T. W. Stern and Alice Dowse Weeks, *U. S. Geological Survey, Washington, D.C.*

Bayleyite, $Mg_2UO_2(CO_3)_3 \cdot 18H_2O$, is one of three new uranium minerals first described from the Hillside mine, Yavapai County, Arizona, by Axelrod, Grimaldi, Milton, and Murata (1951). The minerals occurred at the 300-ft level of the mine and the authors state (1951, p. 2) that "In the mine, bayleyite crystals are sharp and well faceted. In the drier atmosphere of Washington, [D. C.] they soon become dull, losing their luster and finally disintegrate to a yellow powder." Branche, Chervet, and Guillemin (1951) who described bayleyite from Morocco, the only foreign locality for this mineral, also noted that the crystals disintegrated rapidly, but they ascribed this property to the humidity of their laboratory.

In July 1951 T. W. Stern collected a yellow efflorescent crust of a highly radioactive mineral from Hideout No. 1 mine on Deer Flats, along the north side of White Canyon, San Juan County, Utah, when the authors visited the mine with L. B. Riley and W. E. Benson also of the U. S. Geological Survey. Fortunately this material did not dehydrate as the Arizona and Morocco samples had, for when it was studied nine months later it was found to be fully hydrated bayleyite. The Hideout mine is thus the second bayleyite locality in the United States.

The Hideout No. 1 mine, not much more than a prospect in July 1951, is in a copper-uranium deposit in the Shinarump conglomerate (Triassic). The chief minerals observed were chalcocite, bornite, chalcopyrite, brochantite, malachite, and azurite, which replace fossil wood and impregnate coarse arkosic sandstone. Bayleyite and schroeckingerite are the only uranium minerals so far identified from this mine. They occur in the adit less than 100 feet from the cliff face, in contrast to the Arizona specimens which were collected from the 300-ft level. The massive pieces of copper sulfide replacing wood show some radioactivity with the Geiger counter, but no uranium mineral can be seen under a binocular microscope.

The bayleyite specimen from Hideout No. 1 mine is translucent, light yellow, and occurs in thin crusts that break away easily from the underlying rock. The bayleyite consists of microscopic, bladed or prismatic crystals (Fig. 1) with terminal faces on the upper surface of the crust. The optical properties determined in white light are similar to the type and Moroccan materials, with $\alpha = 1.454 \pm 0.003$, $\beta = 1.492 \pm 0.003$, and $\gamma = 1.502 \pm 0.003$, the extinction angle between X and the c axis is 14°, and Z is parallel to the b axis. It is not possible to obtain an acute bisectrix interference figure because the cross section of the blades is too small. The mineral is faintly pleochroic with pale pink in the X direction and light yellow to greenish yellow in the Y and Z directions.

Bayleyite is water-soluble and it effervesces vigorously and quickly dissolves in cold dilute hydrochloric acid. A semiquantitative spectrographic analysis, made by C. S. Annell of the Geological Survey, shows:

U	>10 per cent
Mg, Ca (low)	1.0 to 10 per cent
Al	0.1 to 1.0 per cent
Si, Sr	0.01 to 0.1 per cent

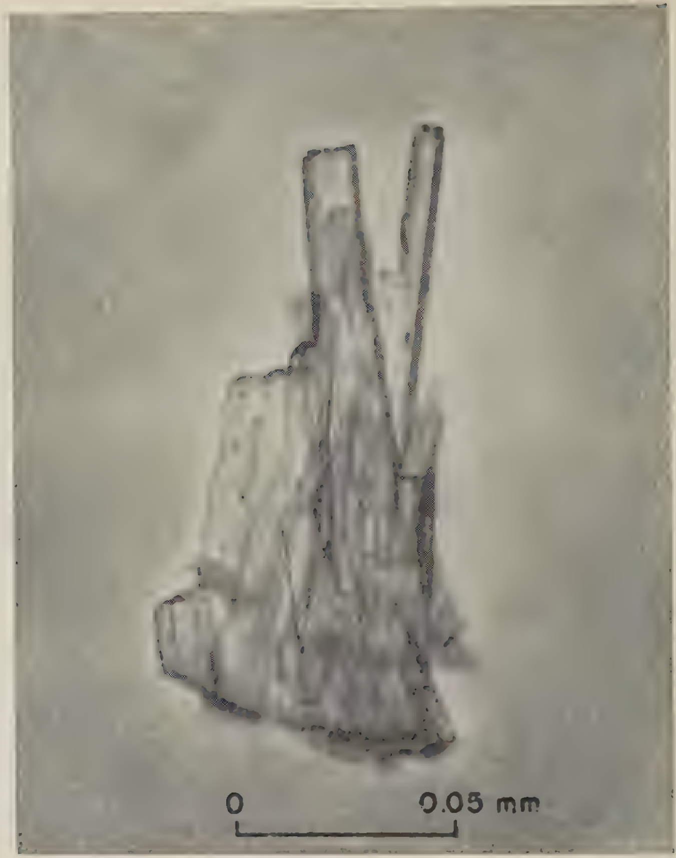

FIG. 1. Prismatic bayleyite crystals from Hideout No. 1 mine, San Juan County, Utah.

The calcium is probably due to a little gypsum and schroeckingerite that occur with the bayleyite. The schroeckingerite is in fine-grained greenish-yellow flakes on the under side of the bayleyite. When activated with long wavelength fluorescent light (3663 Å) the schroeckingerite fluoresces vivid yellow green and the bayleyite fluoresces faintly whitish green. The schroeckingerite gives the superficial appearance of the dehydrated bayleyite described by Axelrod, Grimaldi, Milton, and Murata (1951, p. 2), but an *x*-ray diffraction powder pattern shows only schroeckingerite lines and no metabayleyite lines. The bayleyite gives an *x*-ray pattern identical to that of the Arizona material.

REFERENCES

AXELROD, J. M., GRIMALDI, F. S., MILTON, C., AND MURATA, K. J. (1951), The uranium minerals from the Hillside mine, Yavapai County, Arizona: *Am. Mineral.*, **36**, 1–22.

BRANCHE, G., CHERVET, J., AND GUILLEMIN, C. (1951), Nouvelles espèces uranifères françaises: *Soc. franç. mineralogie et cristallographie Bull.*, **74**, 458–461.

GUADARRAMITE DISCREDITED[1]

George Switzer, *U. S. National Museum, Washington, D.C.*

A supposedly new radioactive mineral from Monte de Lagasca (in the Sierra de Guadarrama), near San Rafael, Segovia, Spain, was first mentioned by Munoz del Castillo (1906). Later that same year he described it more fully and named it guadarramite (Munoz del Castillo, 1906*A*).

Guadarramite was described as resembling ilmenite, but possessing strong radioactivity. A chemical analysis gave TiO_2 50.94%, FeO 38.49, MnO 3.71, SiO_2 5.80, undet. 1.06; sum 100.00. It was found as tabular black crystals on feldspar and mica, in the soil above a pegmatite outcrop.

Guadarramite is listed in Spencer's 6th list of new mineral names (*Min. Mag.*, **16**, 361) as a radioactive variety of ilmenite, and in the same way in Dana's *System of Mineralogy*, 6th edition and 7th edition. The original material has never been reexamined.

The U. S. National Museum recently received a specimen of guadarramite (U.S.N.M. Cat. No. 106159) from the type locality, from Sr. José Melgar, of Madrid, Spain. This specimen, consisting of tabular black crystals on a weathered feldspar matrix, is radioactive as a whole, as shown by a geiger counter. However, a purified sample of the guadarramite is not radioactive. A spectrographic analysis of the purified material, made by Helen W. Worthing of the U. S. Geological Survey, gave Fe, Ti$>$10%; Mn 1.0–10; Si, Al 0.1–1.0; Mg, Nb, Pb 0.01–0.1; Sr, Ca, Ni, Ba, V 0.001–0.01; Cr, Y, Yb, Ag, Cu 0.001–0.0001. The *x*-ray powder pattern of guadarramite is identical with that of ilmenite from Miask, Ural Mts., U. S. S. R.

The feldspar matrix contains small reddish-brown crystals of monazite. A polished section containing both guadarramite and matrix was placed in contact with the emulsion of a nuclear-track plate (Ilford L-2) and exposed for five days. The radioactivity as shown by alpha particle tracks on the developed and fixed plate is associated with the nonmetallic phase (monazite).[2]

In summary, guadarramite is not radioactive, the supposed radioactivity being contributed by the associated monazite. The name should, therefore, be dropped.

References

Munoz del Castillo, José (1906), Nuevos Minerales radioactivos de San Rafael de El Espinar (provincia de Segovia): *Bol. real Soc. Espanola Hist. Natur.*, **4**, 163–166.

——— (1906*A*) La Guadarramita: propuesta de una nueva individualidad mineralogica radioactiva: *Bol. real. Soc. Espanola Hist. Natur.*, **4**, 479–481.

---

[1] Published by permission of the Secretary, Smithsonian Institution, Washington, D. C.

[2] Personal communication from T. W. Stern, U. S. Geological Survey.

REVISED GLOSSARY OF URANIUM- AND THORIUM-BEARING MINERALS ISSUED

A publication, entitled "A glossary of uranium- and thorium-bearing minerals," by Judith Weiss Frondell and Michael Fleischer, is issued as Geological Survey Circular 194. Copies may be obtained without charge from the Director, Geological Survey, Washington 25, D. C.

The glossary, intended as a guide to the nomenclature of these minerals, was prepared as part of the work on radioactive minerals undertaken by the Geological Survey on behalf of the United States Atomic Energy Commission. It contains a list of minerals and their chemical formulas, together with information as to series relationships collected from laboratory work and scientific literature.

This second edition contains 350 entries comprising 182 species. The minerals listed in the glossary are divided into four groups, as follows: *A*, minerals containing uranium and thorium as major constituents; *B*, minerals containing minor amounts of uranium and thorium; *C*, minerals which, if investigated by modern analytical methods, might show uranium or thorium content; and *D*, minerals that are nonuranium- or nonthorium-bearing, but that have been reported to contain impurities or intergrowths of uranium, thorium or rare-earth minerals.

AGI REPORT NO. 6 TEMPORARILY OUT OF PRINT

Report No. 6, *Departments of Geological Science in Educational Institutions of the U. S. and Canada*, Shepard W. Lowman, Editor, is now being revised for re-issue as soon as possible this fall. Definite availability date cannot be announced at this time, but orders received from now on are being held for earliest possible delivery.

The Societa Mineralogica Italiana held its 9th National Congress of Mineralogy in Florence from Sept. 29 to Oct. 3, 1952. The Societa welcomes subscriptions from American mineralogists; the membership fee is $1.75 a year and members receive each year the *Rendiconti Soc. Ital. Mineral.* which includes abstracts and papers given at the annual meeting. Those interested should write to Prof. G. Carobbi, Instituto di Mineralogia, Univ. Firenze, Piazza S. Marco 4, Florence, Italy.

Professor Duncan McConnell, a member of the department of mineralogy staff at Ohio State University since October, 1950, has been appointed chairman of the department. He succeeds Professor William J. McCaughey, who retired this summer after 40 years of service on the faculty, and has now been named professor emeritus.

The vacancy on the staff of the department left by the retirement of Professor McCaughey will be filled by Dr. W. R. Foster of Detroit, a member of the research laboratory staff of the Champion Spark Plug Co. of that city.

The Austin Flint Rogers Research Fellowship in Mineralogy has been established at Stanford University. This fellowship is open to graduate students who intend to undertake research in the field of mineralogy and preference may be given to those who have had a year of graduate work. The emolument will be $2000 and teaching duties will not be required of the Fellow.

Further inquiries should be made to Professor C. Osborne Hutton, School of Mineral Sciences, Stanford University, Stanford, California.

Dr. Clarence S. Ross of the Geochemistry and Petrology Branch of the U. S. Geological Survey was one of the recipients to receive the "Distinguished Service Honor Award" at the ninth Honor Awards Convocation of the United States Department of the Interior at Washington, D. C., on Tuesday, September 23, 1952.

ERRATA

RESETTING A TRICLINIC UNIT-CELL IN THE CONVENTIONAL ORIENTATION:

J. D. H. DONNAY, *The Johns Hopkins University, Baltimore, Md.*

Corrections

While re-orienting a large number of triclinic substances for a forthcoming determinative table based on unit-cell dimensions, I had occasion to use the transformation matrices given in my paper of 1943 (*Am. Mineral.*, **28**, 507–511). This is how, to my dismay, I discovered the first mistake corrected below. The second mistake, which originated in a misprint in the literature, was kindly pointed out to me by Dr. H. T. Evans, Jr.

Page 510, Table 1: The transformation matrices printed in pigeon holes E, F, G, H should appear in pigeon holes K, L, M, N, respectively, and *vice versa*.

Page 511, under (S): Delete the second example (copper sulfate pentahydrate) and footnote 4. The value of a, 5.12, taken from the literature, should have read 6.12; transformation C is applicable.

MINERALOGICAL SOCIETY (LONDON)

A meeting of the Society was held on Thursday, June 12th, 1952, at 5 P.M., in the apartments of the Geological Society of London, Burlington House, Piccadilly, W.1 (by kind permission).

EXHIBIT

Latiumite (a sulphatic calcium potassium aluminium silicate), a new mineral from Albano, Italy: by Prof. C. E. Tilley and Dr. N. F. M. Henry.

PAPERS

The following papers were read:

(1) THE MINERALOGY OF THE ANTIMONY OXIDES AND ANTIMONATES.

By Dr. Brian Mason and Dr. Charles J. Vitaliano.

Apart from the polymorphs of Sb_2O_3, these minerals fall into two structural groups, a cubic group with the pyrochlore structures and a tetragonal group with the trirutile structure. When the antimony is associated with large cations the pyrochlore structure is stable; with smaller cations the trirutile structure is the stable form. Defect lattices are usual in these minerals, resulting in great variability of chemical composition and in physical and optical properties within the individual species.

(2) THE UNIT CELL AND SPACE GROUP OF ALAMOSITE ($PbSiO_3$).

By Dr. A. L. Mackay.

Alamosite was found to have a unit cell of space-group $P2/c$ with dimensions $a=11.28$, $b=7.03$, $c=13.06$ Å, and $\beta=120°$. Z=12. It is not isomorphous with monoclinic wollastonite as might appear from its morphology.

(3) A RE-EXAMINATION OF TOBERMORITE.

By Dr. G. F. Claringbull and Dr. M. H. Hey.

Type specimens of tobermorite have been examined by x-ray methods and shown to be a valid independent species identical with calcium silicate hydrate (I). A new chemical analysis is in close agreement with Heddle's.

(4) RIVERSIDEITE AND CRESTMOREITE: MINERALOGICAL AND CHEMICAL COMPOSITION.

By Dr. H. F. W. Taylor.

Neither of the substances until now characterized by their optical properties and x-ray data as riversideite ($CaO.SiO_2.\frac{1}{2}H_2O$) or crestmoreite ($CaO.SiO_2.H_2O$) is a true mineral species. The former consists of wilkeite closely intergrown with calcium silicate hydrate (I). Two crestmoreite samples consisted chiefly of hydroxyapatite, with only small amounts of silicate minerals. No evidence was obtained for the presence of a distinctive hydrated calcium silicate in either sample, although it appears that some other samples of crestmoreite may be identical with the riversideite studied here.

(5) AN IMPROVED POLARIZING MICROSCOPE. V. THE ORE MICROSCOPE.

By Dr. A. F. Hallimond and Mr. E. Wilfred Taylor.

A robust stand is provided with a stage rack and attachable substage for transmitted light work. A new system for obtaining homogeneous polarization over the whole aperture of the objective gives very complete extinction and has improved the sensitivity for small path differences (ellipticity). Since the whole of the back of the objective is equally effective there is considerable improvement in the ease of adjusting the illumination.

(6) NINETEENTH LIST OF NEW MINERAL NAMES.

By Dr. L. J. Spencer.

The following papers were taken as read:—

(1) MANGANESE-IRON GARNET FROM OTJOSONDU, SOUTH-WEST AFRICA.

By Mr. F. H. S. Vermaas.

Two garnets rich in iron and manganese from the manganese field of Otjosondu, S.W.A., are described mineralogically. They contain 54 and 35 per cent calderite by weight with $a=11.819$ and $a=12.000$ Å resp. Refractive indices (n_D) 1.872 and 1.901 resp., specific gravities 4.08 and 3.96, resp. Calculated specific gravities from x-ray data agree very well with experimental values. The presence of excess atoms in the unit cell of one of these garnets is discussed. The specific gravity of pure calderite is calculated.

(2) NACRITE FROM GROBY, LEICESTERSHIRE.

By Dr. G. F. Claringbull.

X-ray powder photographs show that a white mineral associated with quartz veins in syenite in the shatter zone of the main fault of Sheet Hedges Wood quarry, Groby, Leicestershire, is nacrite. This is believed to be the first British record of the mineral.

(3) A NEW OCCURRENCE OF NACRITE FROM HIRVIVAARA, NORTHERN KARELIA, FINLAND

By Mr. O. von Knorring, Dr. G. W. Brindley and Mr. K. Hunter.

Single crystal and powder analyses prove conclusively that the kaolin mineral from Hirvivaara, Finland, is nacrite: the six-layer structure discovered by Hendricks is confirmed. The powder diagram is resolved in somewhat greater detail than has previously been recorded. The lattice parameters are $a=8.91$, $b=5.14$, $c=7.16$ kX. Hendrick's value for β has not been modified (β 90° 20′).

(4) THE TRACHY-OPHITIC TEXTURE IN CARBONIFEROUS BASALTS.

By Dr. R. B. Elliott.

In the Langholm district of Dumfries there is an intrusion of olivine basalt of Jedburgh type in which flow-aligned felspars are enclosed in augite plates. The felspars are Ab_{42}—An_{58}, the augite is Fe 20, Ca 44, Mg 36. The enclosure of euhedral and oriented felspars within augite indicates that the latter mineral formed after the formation of felspar laths and after the production of the flow-structure. The sequence of events indicated is as follows: the formation of the felspar laths, the production of the flow structure and the crystallization of the augite. It is felt that this texture, which has also been recorded elsewhere, deserves a precise name and "trachy-ophitic" is proposed.

(5) KALSILITE FROM SAN VENANZO, ITALY.

By Dr. F. A. Bannister, Prof. Th. G. Sahama, with
chemical analyses by Mr. H. B. Wiik.

Presents new optical, chemical and x-ray diffraction data for kalsilite and leucite from a potash-rich lava.

(6) SYNTHETIC SODA-FREE AND GALLIUM-BEARING THOMSONITES.

By Mr. J. R. Goldsmith.

Artificial preparations of sodium-free thomsonite, one gallium bearing, crystallized at 245° C. give the same x-ray powder pattern as thomsonite from Table Mt., Colorado.

BOOK REVIEWS

GESTEINE UND MINERALLAGERSTÄTTEN. II, Exogene Gesteine und Minerallagerstätten by Paul Niggli with the collaboration of Ernst Niggli. Verlag Birkhäuser, Basel, Switzerland. 557 pp., 181 figures, 67 tables. 1952. 49.40 Swiss francs ($11.48)

This is Volume II of the projected three-volume work on rocks and mineral deposits. Volume I (*Am. Mineral.*, **34,** 128, 1949) presented basic principles of chemical and physical mineralogy; Volume II deals with sedimentary rocks (in the broadest sense) and their mineral deposits (exogenous rocks and deposits). Volume III will be concerned with endogenous rocks (igneous and metamorphic), described as the main research field of the authors. As the first volume, this book, too, is conceived and executed on a grand scale, encompassing considerably more information and delving into much greater detail than one ordinarily expects to encounter in a work on rocks and mineral deposits. So many data, so much information is crammed between the covers that one gains the impression that the authors were sincerely reluctant to omit mention of anything at all pertinent to their subject. Indeed the factual material comes so thick and fast that only the most careful reading can ferret out the critical interpretations of the accumulated data. And to many Americans this careful reading will be a hardship, for the German of Niggli has been remarked upon for its complexity of style and difficulty of disentanglement. Several generations of geology students have already shared this inherited knowledge and have, unfortunately, successively avoided this author's works in attempting to pass their German examinations successfully.

Those, however, who are seeking a most nearly complete and well integrated description of the products of weathering and sedimentation with many rich diversions on their sources, formations and environments will be amply rewarded by a careful reading. The book is for reference and for the further enlightenment of the advanced worker; it will confound the beginner and may well confuse the intermediate. The following summary of the contents may be useful in outlining not only the general scope of the work but also in sampling some of its remarkable detail.

The two major parts are: I, Autochthonous rocks and mineral deposits formed by weathering ("residual sedimentary" rocks and associated deposits); II, Sediments. Discussion of the autochthonous rocks opens with a consideration of weathering under (1) the weathering process: mechanical factors, chemical factors, oxidation, hydration, hydrolysis and silicates formed by weathering; (2) migration of colloidal and dissolved substance in the weathering zone; (3) classification of weathering residua; mineralogical and chemical characterization, profile of weathering, laterite, bauxite, kaolin, etc., silicification and desilicification; and (4) the solutions of weathering. Section two of Part I considers soils under such topics as: their formation, profiles, arid and humid types, soil erosion, soils and man, springs and groundwater.

Part II on the sediments describes them by the groups: *A*, clastic sediments—psephites and psammites; *B*, clayey pelites, sapropelites and humites (including peat, coal, petroleum and natural gas), sulfosapropelites and Fe-Mn-Si-hydrogelites; *C*, carbonate rocks—limestones and dolomites; *D*, phosphatic sediments—guano, insular phosphorite, bone phosphate and bedded phosphorites; *E*, evaporites—sulfates, chlorides, etc.; and *F*, snow and ice. Each rock or deposit type is described chemically, physically, mineralogically, and petrographically. Usually there are also included accounts of textures, structures, sources, transportation, deposition, consolidation, theories of genesis and economically significant characteristics and varieties. The final 14 pages discuss sedimentary petrographic provinces.

From the American viewpoint the chief defect of the book appears to be in the mechanisms and devices adopted for the presentation of data. For example, the unfamiliar Niggli semi-structural formulae of minerals again appear (*Am. Mineral.*, **34**, 128, 1949); all analyses also are computed in terms of the Niggli numbers and chemical changes in weathering are expressed by the Niggli-Grosser ray diagrams. In truth the book contains many Niggli-isms, with which a large number of American petrographers have chosen to remain unfamiliar. The European slant also is evident in the usage of a very large number of varietal rock and mineral names as well as many freshly minted complex textural terms, which must first be learned or deciphered before the textual meaning can be determined.

However, despite these shortcomings, no advanced researcher in sedimentary processes or products can afford to avoid this book. It is outstanding in most every way, and the difficulties attendant the assimilation of its contents should not deter the determined reader.

E. Wm. Heinrich,
University of Michigan, Ann Arbor, Michigan

RADIOCARBON DATING by Willard F. Libby. 124 pp., 11 figures, 2 appendixes; The University of Chicago Press, $3.50, 1952.

Willard F. Libby, who is Professor of Chemistry at the Institute for Nuclear Studies of the University of Chicago, and his associated workers for the last few years have pioneered research leading to the dating of fossil material by means of radiocarbon, or Carbon 14. In this concise work Professor Libby presents the first book on the method and its achievements, bringing under one cover details on principles, sample preparation and measurement and a list of dates obtained by the technique. The book is clearly and carefully written and will do much to advance knowledge of this means of age determination among many branches of science. Chapter I discusses principles fundamental to the method, Chapter II presents data on the worldwide distribution of radiocarbon and Chapter III discusses determination of the half-life of radiocarbon. Techniques are dealt with in Chapter IV, Preparation of the sample for measurement, and Chapter V, Measurement of the sample. Chapter VI is a listing of radiocarbon dates including the sample number of the Institute, a brief description of the type of material, source and location together with any archeological date and reference and finally the age by Carbon 14. The samples are listed by foreign countries and under U.S.A. by groups of states. Many collaborators are enumerated under the various groups in which are included all datings completed prior to September 1951. The last Chapter, Chapter VII—The Significance of the dates for Archeology and Geology has been prepared by Frederick Johnson of the Robert S. Peabody Foundation for Archeology. The work concludes with two appendixes; *A* —Special equipment and chemicals for the C^{14} sample preparation apparatus, giving item and source; *B*—Special materials for screen-wall counter, giving item, source and type. The indexes are three—by subject, name and sample.

Undoubtedly the book will be indispensable to workers in some branches of paleontology and paleobotany, in archeology, geomorphology, glaciology and geochemistry.

E. Wm. Heinrich,
University of Michigan, Ann Arbor, Michigan

THEORETICAL PETROLOGY, A textbook on the origin and the evolution of rocks, by Tom F. W. Barth. John Wiley and Sons. 387 pp., 146 figures, 75 tables. 1952. $6.50.

If *Theoretical Petrology* can be considered representative of Professor Barth's petrological credo and if the reviewer has correctly interpreted it, then it would appear that the author is both a magmatist as well as a transformationist, that he regards sedimentary rocks and processes to be of subordinate interest to petrologists, that metamorphism is generally metasomatic, and that migmatites are not hybrid rocks but products of metamorphic differentiation. For these and other interesting, if sometimes extreme, views the book is alone worth a careful reading.

The book is in four parts: I, Physics and chemistry of the earth; II, Formation of sedimentary rocks; III, Igneous Rocks; and IV, Metamorphic Rocks. Part I (36 pages) is woven largely of standard materials—origin of the earth, earth heat and strength, earth shells, thermodynamics in calculating earth structure, lithosphere composition and geochemical cycles. Part II on sediments is so short (23 pages) that one is tempted to believe that the author was in a hurry to get it over with and out of the way in order to hasten on to subjects of greater interest (to him). Indeed many petrologists might take exception to the statement p. 37, that, " . . . many of the sedimentological problems are of no general interest for the understanding of the rock-forming processes on the earth."

Part III is subdivided into four sections: *A*, Descriptive classifications; *B*, Physical chemistry of the minerals; *C*, Magmas and their locales; and *D*, Rocks as products of defined processes. Under classification are discussed mineralogical classification, chemical composition (the Daly averages are repeated), Niggli values, and his molecular norm, *C.I.P.W.* norm and Barth's standard cell of a rock. Section *B* includes a statement of the phase rule and reviews the crystal chemistry of the silica minerals, feldspars, feldspathoids, melilites, olivines, pyroxenes and the crystallization history of various combinations of these. Other topics are the reaction principle, crystallization of basaltic magma and the "residua" system of petrogeny. Magmas and their locales has as its chief topics liquid immiscibility, silicate-water systems, vapor phase and hydrothermal differentiation, viscosity and temperature of magmas, pyroclastic rocks and magma tectonics. Section *D* presents a survey of magmatic differentiation, descriptions of variation diagrams and rock series and discussions of the genesis of oceanic basalts, continental basalts, alkalic rocks, calcitic igneous rocks, potassic rocks, pegmatites, monomineralic rocks and granitic rocks.

Part IV on metamorphic rocks describes metamorphic minerals (including many generally of hydrothermal origin), applicable thermodynamic principles, metamorphism of minerals, contact metamorphism, metasomatic processes, structures of metamorphic rocks, recrystallization (illustrated by evaporites), metamorphic diffusion and differentiation, facies, regional metamorphism and finally, migmatites.

Lists of references are given only for Part II, Formation of sedimentary rocks, and for the section on Granite and granitization. Otherwise the sources are embodied in the text (or less commonly in footnotes) and if an article is used more than once, only the author and date are noted, which causes no end of frustration to the persevering reader in his attempts to recover the original citation. The figures and tables, although adequately illustrative, vary considerably in style of preparation and somewhat in quality; e.g., errors in table 35 and figures 16 and 188 and over-reduction in the legend of figure 79. The author, despite a cogent criticism against the overproduction of rock names (p. 1), abets the cause of stockpiling "excess-baggage" nomenclature by using or repeating such terms as phlebite, leptologic, hypermelanic, aorite, holoblast, ectect and entect.

The courses served up in Professor Barth's book make for rich and varied fare, but together they hardly constitute an organized petrologic meal or a well-balanced petrogenetic diet. After concluding that the work is neither sufficiently objective for a textbook nor sufficiently complete for a reference, the reviewer decided the book may perhaps best be classed as a related series of petrogenetic essays, all of which deserve the careful reading of critical petrologists. Obviously much thought has been expended in its preparation and many of its challenging ideas will provoke much further thought and discussion.

E. Wm. Heinrich,
University of Michigan, Ann Arbor, Michigan

INTRODUCTION TO GEOPHYSICAL PROSPECTING, by MILTON P. DOBRIN. McGraw-Hill Book Company, Incorporated: New York, 1952, 1st edition; 435+xi pages.

This book attempts to describe and explain the most commonly used methods of geophysical prospecting to a reader whose knowledge of mathematics is, to quote the preface, no "more advanced than that generally required of students entering upon graduate work in geology." There is also the tacit assumption that the reader has had an elementary college physics course. Dr. Dobrin has succeeded quite admirably.

There are those who maintain that you cannot teach geophysics to students who do not have a stronger background of mathematics and physics than called for above. With this the reviewer agrees. However, there are a great many geologists, both in school and out, who want, and need, to know something about geophysics, and for them this book will be very useful. They and the professors who teach them from this book, must remember, however, that it will not make them geophysicists.

After an introductory chapter the book takes up in order, gravity, magnetic, electric, seismic, and electrical prospecting methods in some 300 pages. The remainder of the book includes a chapter on prospecting for radio-active minerals, a very good chapter on case histories, and chapters on well-logging methods and radio location methods for geophysical surveys. Throughout the treatment is kept at a very consistent level and is put together very smoothly.

Books on physical and mathematical subjects written for non-professionals are likely to contain loosely worded statements that annoy professionals. The reviewer was pleased to find very few of these in this one.

The book is very adequately illustrated with good line drawings and well chosen halftones.

JAMES T. WILSON,
University of Michigan, Ann Arbor, Michigan

IMPERFECTIONS IN NEARLY PERFECT CRYSTALS, prepared by an Editorial Committee, consisting of W. Shockley (chairman), J. H. Hollomon, R. Maurer, and F. Seitz. 1952, John Wiley and Sons, Inc., xii+490 pp. Price $7.50.

Imperfections in Nearly Perfect Crystals is a collection of papers arising from a conference on "Lattice Imperfections" held in 1950, under the sponsorship of the National Research Council and the Office of Naval Research. The book consists of 17 articles by 20 authors.

The book is divided into four parts. Part I is introductory and is concerned with the description of the various kinds of imperfections, namely, phonons (vibrations), electrons and holes, excited atoms, vacancies and displaced atoms, foreign atoms, and dislocations; plus transient imperfections. The article by Seitz defines and classifies the imperfections, and discusses their interactions. Read and Shockley develop the geometry of dislocations, and reduce all dislocations to standard forms or their combinations.

Parts II, III, and IV are reports of experimental data, which are interpreted on the basis of the theoretical foundation laid down in Part I.

Part II discusses the types of dislocations associated with various deformations of crystals. Dislocations due to quenching strains, cold work, and plastic flow are treated. A rather elaborate Fourier analysis of distribution functions for cold-worked metals is given by Warren and Averbach. The effect of impurities on the ease of dislocation is discussed. Koehler computes and measures the dissipation of vibrational energy by dislocations.

Part III deals with diffusion and the mobility of particles and imperfections within the crystal. The dielectric and photoelectric properties of ionic crystals are investigated and related to defects in the crystal. The diffusion of atoms and vacancies in alloys is examined statistically and thermodynamically.

Part IV is concerned with the properties and effects of surfaces and boundaries in the crystal. Surface and intergrain boundary tensions are discussed by Fisher and Dunn. Read and Shockley continue with a treatment of the geometry of boundaries, and boundary energy. Smith examines interphase energies, and concludes with the topology of interfaces. Mosaics and fine structures are also discussed. The book concludes with a discussion of the properties, physical and chemical, of grain boundaries, and diffusion effects near the boundaries.

On the whole, the book gives a well unified picture of the somewhat heterogeneous knowledge collected to date. A lesser amount of confusion of nomenclature and diversity of belief is evident than might be expected in a collection of essays. Of course, the authors actually worked together at the symposium; the differences of opinion which do exist are included as reproductions of the discussions which took place at the conference.

The book assumes considerably more knowledge of metallurgy and the theory of solids than the average mineralogist possesses. It fails in several small instances where a very slight amount of reorganization or additional information would make the book more understandable.

In the first place, the book looks at crystal imperfections from a different viewpoint from any previously held. The nomenclature and classification of crystal defects is not entirely new, but will be unfamiliar to mineralogists. Principally, the difficulty is that one of the authors assumes another has already explained the unfamiliarity. The term "F-center" is used several times with ominous import; finally about midway through the book it is grudgingly admitted what it is. In another case, we find twice the mention of "holes attached to vacancies." The meaning is obscure, even when one knows what the terms mean.

The paper on geometry is short and difficult, though the geometry of dislocations forms the basis for description of all subsequent distortions in crystals. A system of ill-defined and obscure vector mathematics is used to describe dislocations. The illustrations fail to clarify the text. The chapter is possibly a satisfactory refresher for one versed in the concepts used, but is abstract and unsatisfying for the mineralogist.

The most significant article is the first, by Seitz. His tentative unification of crystallography, metallurgy, and physics into a new science of solids should appeal to most readers. Seitz points to the hazy outline of a unified theory of solids which seems sure to come in the future.

The book presents a concise picture of most of the important experimental and theoretical work done on solids in recent years, and furnishes a wealth of references. The editors cheerfully admit that the experimenters and interpreters have barely started to integrate their findings; the book will be of greatest value if it stimulates others to enter the field. It is highly recommended to all who are interested in crystals and solids.

E. H. Poindexter,
University of Michigan, Ann Arbor, Michigan

NEW MINERAL NAMES

Gunnbjarnite

O. B. Bøggild, Gunnbjarnite, a new mineral from East Greenland. *Medd. om Grønland*, Bd. **142,** No. 8, 1–11 (1951) (in English).

The mineral occurs with calcite in veins cutting a basalt dike at Mt. Steensby. It is dark brown to nearly black, streak very light brown. Luster pearly on the basal cleavage.

Cleavage basal micaceous, the flakes flexible and elastic in one direction, easily broken in the other. A second cleavage, taken as {010}, is strongly developed so that ribbon-like fragments are formed. Hardness 2–2½, sp. gr. variable (depending on hydration?); measurements using Thoulet solution gave 2.025 to 2.134. Optically negative, axial plane (010), with indices variable, $\beta=1.540$ to 1.571, $\gamma=1.561$ to 1.593, 2V ca. 60°.

Analysis by A. H. Nielsen gave SiO_2 43.15, TiO_2 none, Al_2O_3 3.29, Fe_2O_3 14.57, FeO 1.06, MnO 0.13, MgO 12.98, CaO 3.66, H_2O^+ 7.19, H_2O^- 12.17, CO_2 not detd.; sum 98.20%. (Presumably the sample contained calcite M.F.). A dehydration curve is given; 9.47% was lost to 110°, 11.3% to 206°, 12.4% to 300°. The mineral rehydrates rapidly in the air. Nearly infusible before the blowpipe; very thin splinters fuse to a black, magnetic mass. Easily decomposed by HCl with separation of amorphous silica, which shows double refraction.

The mineral is a member of the nontronite group, differing from many similar materials in its high content of MgO and Fe_2O_3.

NAME: For the Norseman Gunnbjørn Ulfsson who is generally regarded as the discoverer of Greenland (ca. 900).

DISCUSSION: Study by *x*-ray, electron microscope, and differential thermal analysis would be highly desirable.

MICHAEL FLEISCHER

Dalyite

R. VAN TASSEL, Dalyite, a new potassium zirconium silicate, from Ascension Island Atlantic. *Mineralog. Mag.*, **29**, 850–857 (1952).

The mineral occurs as a rare accessory, about 0.2% of the rock, in medium-grained, pinkish-gray alkali granites mainly composed of microperthite and quartz with aegirine and an amphibole. It is in colorless crystals 0.05 to 0.5 mm. in size with short prismatic habit and vitreous luster. Hardness 7½. Sp. gr. 2.84±0.02. Dalyite is optically biaxial negative with $\alpha=1.575$, $\beta=1.590$, $\gamma=1.601$, all ±0.002, 2V 72°, $\alpha:c=7°$. Dispersion very weak with presumably $v<r$.

Goniometric measurements of 23 crystals showed 16 forms with $\{\bar{1}01\}$, {100}, $\{1\bar{1}0\}$, {110}, and $\{\bar{1}11\}$ most common. Cleavages {101} and {010} good, {100} less distinct. Twinning was observed with (100) as composition plane. Weissenberg photographs show dalyite to be triclinic, with $a=7.51$, $b=7.73$, $c=7.00$Å, $\alpha=106°$, $\beta=113\frac{1}{2}°$, $\gamma=99\frac{1}{2}°$. Space group $P\bar{1}$. Goniometric data agree with the cell constants from *x*-rays. The unit cell contains $K_2ZrSi_6O_{15}$. *X*-ray powder data are given.

A microchemical analysis by M. H. Hey on 22 mg. gave SiO_2 61.85, ZrO_2 21.70, K_2O 14.60, Na_2O 1.75, Fe_2O_3 0.37, H_2O 0.64; sum 100.91%, corresponding to $(K,Na)_2O:ZrO_2:SiO_2=2.11:1.01:5.95$, or $K_2ZrSi_6O_{15}$. Dalyite is unaffected by warm concentrated HNO_3, but is attacked slowly by cold HF, readily dissolved by hot HF. The name is for Reginald Aldworth Daly, Emeritus Professor of Geology, Harvard University.

M. F.

Hanléite

LEWIS LEIGH FERMOR, On a new chrome-garnet. *Geological Magazine*, **89**, 145–147 (1952).

A description is quoted from F. R. Mallet, *Mem. Geol. Survey India*, **5**, 153–172 (1866) of material from near the Hanlé Monastery, in Rupshu, Kashmir. Here chromite is cut by thin seams, both sides of which are coated with very minute crystals of a brilliant emerald-green color. Analyses are quoted by Mallet of (*a*) by Komonen, (*b*) on a minute amount of material by Mr. Tween.

	(*a*)	(*b*)
Silica	37.11	41.2
Cr_2O_3	22.54	33.5
Al_2O_3	5.88	24.2
FeO	2.44	
MgO	1.10	
CaO	30.34	—
H_2O	1.01	1.1

On this basis, Fermor believes it likely that the material of analysis (*b*) is mainly $Mg_3Cr_2(SiO_4)_3$ probably with some $Fe_3Cr_2(SiO_4)_3$, and suggests the name hanléite for the locality. The type material can not be found and the locality is very inaccessible.

Discussion: Inadequate basis for giving a new name.

M. F.

Sinhalite

G. F. Claringbull and Max H. Hey, Sinhalite ($MgAlBO_4$), a new mineral. *Mineralog. Mag.*, **29,** 841–849 (1952).

A brown cut gemstone labelled olivine was found by George Switzer of the U. S. National Museum to give an *x*-ray photograph differing from that of olivine. Examination of 22 such stones in England showed 2 to be olivine, 20 to be a new mineral. The color is yellow to dark brown and greenish-brown. The mineral is biaxial, negative with *ns* (Na): $\alpha = 1.6667$ to 1.6765 (19 samples), $\beta = 1.6966$ to 1.7038 (18 samples), $\gamma = 1.7048$ to 1.7121 (20 samples), $\gamma - \alpha = 0.036$ to 0.0383, sp. gr. 3.47 to 3.50 (15 samples). The hardness is close to that of olivine. Weissenberg photographs showed sinhalite to be orthorhombic with $a = 4.328$, $b = 9.878$, $c = 5.675$ Å, $a{:}b{:}c = 0.4381{:}1{:}0.5745$. The unit cell contains $4MgAlBO_4$. Calculated sp. gr. 3.446. The following space groups are possible:

$$D_{2h}^5 - Pbmm,\ C_{2v}^2 - Pb2_1m,\ \text{and}\ C_{2v}^4 - Pbm(2).$$

Further study is in progress. *X*-ray powder data are given. Analysis of 6.4 mg. gave B_2O_3 24.2, Al_2O_3 41.01, Fe_2O_3 2.0, MgO 32.3, H_2O 0.3; sum 99.8%. Sinhalite is insoluble in or only slightly attacked by acids other than HF. Four of the 20 samples are known to be from Ceylon; the others are from unknown sources. The name is for Sinhala, the Sanskrit name for Ceylon.

M. F.

Sanderite, Leonhardtite

Waldemar Berdesinski, Sanderit, Leonhardtit, Allenit und Hexahydrit, neue Mineralien der marinen Kalisalzlagerstatten. *Neues Jahrb. Mineral., Monatsh.* 1952, No. 1, 28–29.

J. Leonhardt and W. Berdesinski, Über die Effloreszenzen des Kieserits in Salzbergwerken: *Z. anorg. Chem.*, **265,** 284–287 (1951).

Efflorescences on kieserite in the 601 m. level of the "Hansa I" shaft, Empelde, and the 675 m. level of the "Niedersachsen" shaft near Wathlingen are shown by *x*-ray powder photographs to be mixtures of $MgSO_4 \cdot 2H_2O$ (Sanderite), $MgSO_4 \cdot 4H_2O$ (Leonhardtite), $MgSO_4 \cdot 5H_2O$ (Pentahydrite, here called Allenite, see *Am. Mineral.*, **36,** 641 (1951), and $MgSO_4 \cdot 6H_2O$ (Hexahydrite). Approximate optical data are given for some of the mixtures. Sanderite is named for Professor Bruno Sander, Innsbruck, Austria; leonhardtite for Prof. J. Leonhardt of Kiel.

Discussion: As pointed out by Berdesinski, the name leonhardtite (Blum, 1843) has long been used for a variety of laumontite.

M. F.

DISCREDITED MINERALS

Milanite (=Halloysite)

DUŠAN STANGAČILOVIČ, Milanite—the Serbian mineral: *Geol. Vesnik*, **9**, 271–274 (1951), (in English 272–274).

X-ray study of material from Majdanpek, Yugoslavia, previously called milanite (Tietze, 1870), kaolinite, allophane, and halloysite, shows it to be halloysite.

M. F.

Built for ROUGHING IT!

World's finest 3-dimensional microscope . . . with wider fields than ever before!

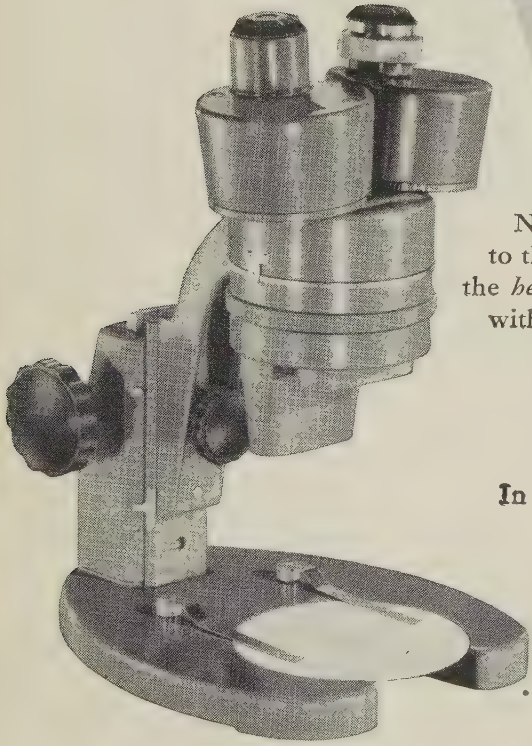

No time lost sending specimens back to the laboratory for analysis. You take the *heart* of your lab right into the field with you—your B&L Stereomicroscope. Sturdily built to take all the punishment you're ever likely to give it. Prisms and nosepiece are completely dustproof.

In field or lab, your B&L Stereomicroscope gives you largest-area critical focus . . . with the finest optics ever produced for wide field work. No other stereomicroscope gives you so many exclusive advantages . . . in so many phases of your work.

Prompt delivery, of course.

WRITE **FOR NEW CATALOG, D-15, JUST OFF THE PRESS.**
Bausch & Lomb Optical Co., 67611 St. Paul St., Rochester 2, N.Y.

Bausch & Lomb Stereomicroscopes

IN SCIENCE, INDUSTRY, EDUCATION

the trend is to AO

Stereoscopic Microscopes

● The natural, three-dimensional image is large and clear... the specimen is seen right side up... all movements appear in their actual directions. These unique characteristics of AO Stereoscopic Microscopes have made them increasingly popular for examining gross specimens, for inspecting precision mechanical parts, for maintaining purity in food products, for many delicate operations such as manufacturing and assembling minute precision parts or dissecting biological specimens.

No other optical instrument is so versatile. Ask to see an AO Stereoscopic Microscope soon . . . you'll undoubtedly get ideas for using one effectively in *your* work.

American Optical
COMPANY
INSTRUMENT DIVISION • BUFFALO 15, NEW YORK

THERE'S AN
AO STEREOSCOPIC
FOR EVERY NEED

MODERATELY PRICED
NO. 21 MICROSCOPI
A simple instrument
for use with
opaque specimens.

NO. 23
MICROSCOPE FOR
LARGE SPECIMENS

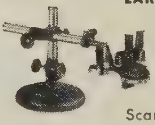

Scans a 4 foot circle,
vertical surfaces;
or specimens in deep
receptacles.

STEREOSCOPIC SHOP
MICROSCOPE
Mounts on machinery
for observing
precision operations.

NO. 25 MICROSCOPE
Has removable
horseshoe base and
glass stage
for both opaque
and transparent
specimens.

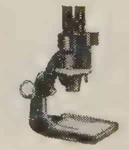

NO. 26 MICROSCOPE
For examination
by reflected light.
Readily converted for
other uses.

NO. 28 MICROSCOPE
Combines advantages
of No. 25 and No. 23.
Takes opaque
and transparent
specimens.
Scans large areas.

Widening the use of your polarizing microscope

Leitz UNIVERSAL STAGES

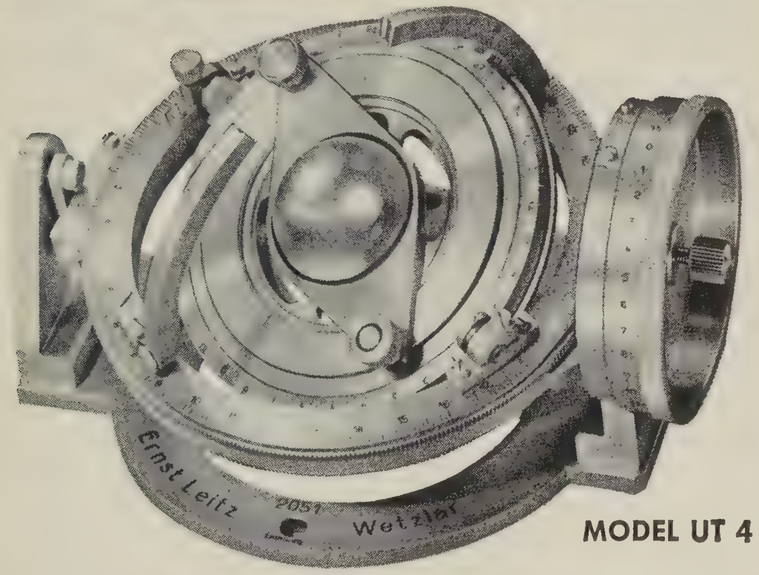

MODEL UT 4

Making your polarizing microscope even more versatile, Leitz Universal Stages permit accurate and rapid determination of the optical properties and orientation of crystal plates and fragments. In addition they embody several vital improvements which enable you to change the slide rapidly and to orient it easily onto the point of junction of the rotating axis.

Several models are available, offering two, four or five axes of rotation. Stages are designed for use with the following Leitz microscopes: Models AM, SY, CMU, IIIM, MOP and PANPHOT.

Four special UM objectives for universal stage methods are now available. Each of the four is equipped with iris diaphragm and corrected for the same free working distance with respect to the segments.

Another fine accessory for the famous Leitz Microscopes—recognized everywhere as the finest microscopes made anywhere.

For details, write Dept. 102A

E. LEITZ, Inc., 304 Hudson Street, New York 13, N. Y.

LEITZ MICROSCOPES • LEITZ SCIENTIFIC INSTRUMENTS
BINOCULARS • LEICA CAMERAS AND ACCESSORIES

New American

PEAT AND MARL SAMPLER

The instrument embodies the essential features of a design by Professor Davis of the Geographical Survey. It consists of a jacketed plunger with a sharpened end. As the instrument is pressed into the ground, it remains closed. When the proper depth has been reached for taking the sample, the instrument is drawn up about 6 or 8 inches; at this point an internal locking device holds the plunger fast in the upper part of the jacket. This instrument is again forced downward, cutting and retaining the desired sample. Complete with illustrated head, 9 four foot lengths of extension rod and case; catalog number 76-432 sells for $65.50.

Eberbach CORPORATION
SCIENTIFIC INSTRUMENTS & APPARATUS
ANN ARBOR, MICH.
ESTABLISHED 1843

W. HAROLD TOMLINSON
Petrographic Laboratory
260 N. ROLLING RD., SPRINGFIELD, PA.
ROCK SECTIONS ORIENTATED MINERAL SECTIONS

CRYSTALLOGRAPHY
Specializing in choice crystals, singles, groups, from world wide sources. Catalog free.
V. D. HILL
Complete Gem & Mineral Establishment
5450-F Portland Road, Salem, Oregon

Good Quality
Rapid Service
THIN SECTIONS
Dr. H. S. Armstrong
Department of Geology
McMaster University
Hamilton, Ontario

New . . . 1952
ALLEN REFERENCE SETS For MICROSCOPICAL STUDIES in MINERALOGY and PETROLOGY

MINERALS, POWDERED (100 mesh)		
Selected for microscopical study	Set of 60	$40.00
MINERALS AND GLASSES of known refractive index;		
Range of Index: 1.34 to 2.4. Intervals of 0.01 throughout most of this range.	Set of 60	45.00
COMMINUTED COMMON MINERALS Mounted in Balsam.		
One elementary set, 25 slides		16.00
Two advanced sets, 25 slides each		
	Per set	20.00
	Both advanced sets	40.00
PETROGRAPHIC SLIDES		
Type minerals and rocks for demonstration of optical characteristics.	Set of 25	35.00

Two to five sets on one order—5% discount.

Six sets as listed above, complete (Priced separately at $176.00) 149.90

Write for Leaflet RA-AM

Other Cargille Products for Mineralogists and Petrologists

Shillaber's Certified Index of Refraction Liquids.	Code # 52-A-AM
Shillaber's Immersion Oil, for Microscopy	52-B-AM
Reagents for Chemical Microscopy For use with Chamot and Mason's Handbooks	52-C-AM
Heavy Liquids for determination of sp. gr. New type liquid up to 7.5 sp. gr.	52 D-AM
Transparent Plastic Specimen Boxes For Storing and Exhibiting small specimens	52-E-AM
Sample Storage Sets For keeping small specimens in glass vials for quick reference.	52-F-AM

Inquiries Solicited

R. P. CARGILLE

117 Liberty Street
New York 6, N.Y.

Announcing the Publication of the
lithoprinted edition of
A Manual for Geometrical Crystallography
by
Caleb Wroe Wolfe, Boston University

Approximate date of publication, Feb. 1, 1953

Selling price—$3.00

GEOPUBLISHING COMPANY
171 School Street, Watertown, Mass.

MINERALS UNLIMITED

•

Suppliers of high quality minerals to students and research organizations. Catalogues available on request.

Our firm is interested in obtaining unusual massive or crystallized minerals in quantity, as well as single examples of fine crystallization, collections being of particular interest. Either purchase or exchange is welcome.

•

MINERALS UNLIMITED
1724 University Avenue **Berkeley 3, California, U.S.A.**

COOKE

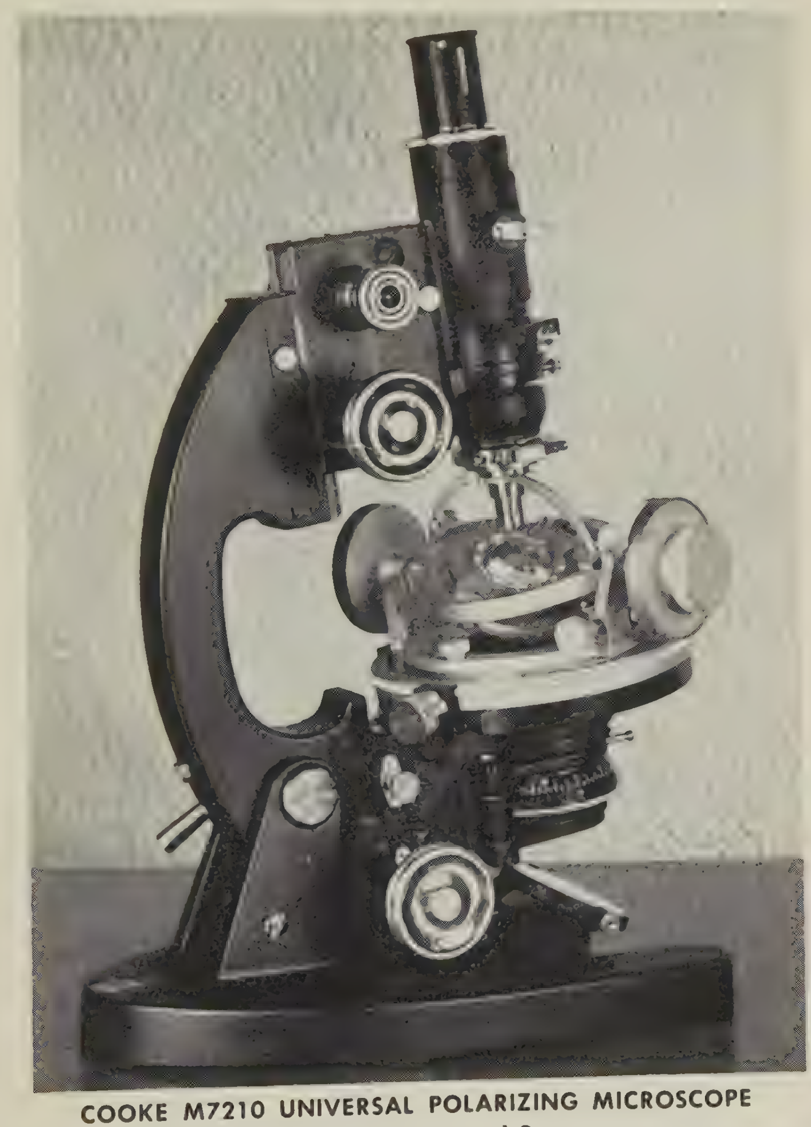

COOKE M7210 UNIVERSAL POLARIZING MICROSCOPE
with Cooke Universal Stage

Complete catalog of Cooke Polarizing Microscopes available from:

THE R. Y. FERNER CO., INC.
110 PLEASANT STREET
MALDEN 48, MASS.

In Canada: Cooke Troughton and Simms, Ltd., 61 College St., Toronto

OPTICAL INSTRUMENTS ZEISS WINKEL SINCE 1857, GOTTINGEN, ALLIED ZONE

RADICALLY NEW STYLE
POLARIZING MICROSCOPE with
INCLINED OBSERVATION TUBE

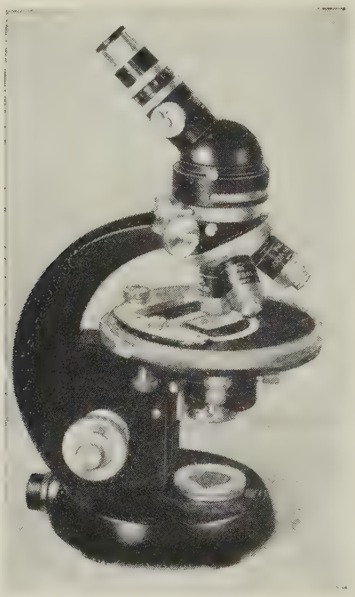

- Inclined observation tube with adjustable *Amici-Bertrand* lens, iris diaphragm extensible eye-piece sleeve.
- Dust-proof integral tube analyser with degree scale, rotating about 180°, coated Telan lens system to establish telecentric pencil of rays and eliminate astigmatism.
- Filter polarizer and filter analyser of great light-transmission; neutral grey tint.
- Ball-bearing, rotating stage, graduated into 360° with vernier reading to 0.1°, with clamping screw, fine rotation adjustment and click-stop device to click-stop at 45°-intervals at any desired points.
- Low position, co-axial coarse and fine motions, controlled from either side.
- Objectives furnished in eccentric mounts for quick and accurate alignment.
- May be equipped with integral illuminator permitting illumination by the Koehler principle.

write for literature

CARL ZEISS, INC., 485 FIFTH AVE., NEW YORK 17, N.Y.

Guaranteed Uninterrupted Repair Service

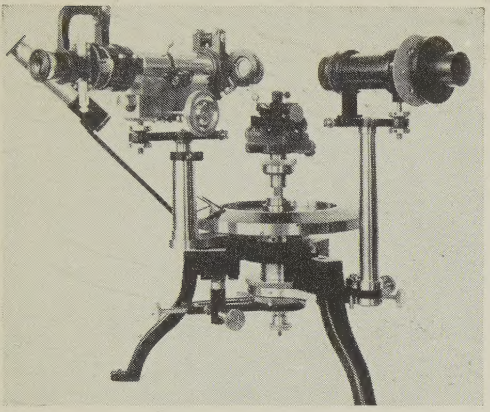

Stoe-Heidelberg one and two circle reflection goniometers, X-ray gonio heads are available from us.

Also Fuess Sphere Refractometer

B & S Pulfrich (Critical Angle) Refractometers

New Zeiss-Winkel Pol. Microscopes with built-in illumination.

C. A. BRINKMAN & CO.
261 Great Neck Road
GREAT NECK, N.Y.

INDEX MEDIA

LIQUID IMMERSION MEDIA—Original series, colorless, odorless, stable, exact specified indices, range Nd 1.41 to 1.65, steps of .01, in twenty-five 1-ounce applicator vials, with cabinet $27.50

Set of thirty-eight Immersion Media Nd 1.41 to 1.78 in steps of .01, in ⅛ fl. oz. each, applicator vials with cabinet $40.00

J. T. Rooney, Chemist, P.O. Box 358, Buffalo, N.Y.

"Supplying dependable index media to petrographers for more than 25 years"

ARTICLES TO APPEAR IN EARLY ISSUES OF THE AMERICAN MINERALOGIST

●

Observations on the distribution of trace elements in the perthite pegmatites of the Black Hills . . . by Riad A. Higazy

Chinoite, a new mineral . . by Carl W. Beck and David B. Givens

Prehnitization of albitite . . . . by K. D. Watson

Crystal chemistry and differential thermal effects of dolomite . . . . by W. F. Bradley, J. F. Burst, and D. L. Graf

Fluid inclusions in beryl and quartz from pegmatites of the Middletown District, Connecticut . . . . by Eugene N. Cameron, Robert B. Rowe, and Paul L. Weis

The genesis of pegmatites I. Occurrence and origin of giant crystals . . . . by Richard H. Jahns

Quantitative analysis of endellite, halloysite and kaolinite by differential thermal analysis . . . . by Leonard B. Sand and Thomas F. Bates

A lath shaped non-expanded dioctahedral 2:1 clay mineral . . . . by Charles Edward Weaver

Crystal geometry of some alkali silicates . . . . by Gabrielle Donnay and J. D. H. Donnay

Beryllium minerals in the Victorio Mountains, Luna County, New Mexico . . . . by William T. Holser

Allophanes from Lawrence County, Indiana . . . . by W. Arthur White

Faheylite, a new phosphate mineral from the Sapucaia pegmatite Mine, Minas Gerais . . . . by Marie Louise Lindberg and K. J. Murata

Crystallized Native Gold

Every collection, whether private or museum, requires an exceptionally fine NATIVE GOLD specimen. It should be large enough to command attention, showy enough to make visitors gasp and rare enough to be desired.

GOLD has always remained one of the most looked for minerals!

We are pleased to list several specimens of crystallized NATIVE GOLD that meet all of the above requirements.

No. 1. A superb bright crystallized NATIVE GOLD with very little quartz matrix attached. Size 3½″ x 4″. Price $400.00. This is a truly magnificent NATIVE GOLD specimen.

No. 2. An irregular shaped arborescent-type NATIVE GOLD with numerous small octahedron crystals present. Very showy. Size 2⅝″ x 3¼″. Price $400.00.

No. 3. A well crystallized arborescent-type NATIVE GOLD with octahedron crystals present. Very desirable. Size 1¼″ x 2⅜″. Price $250.00.

No. 4. A bright mass of minute crystals and crystallized wires of NATIVE GOLD matted to form a showy specimen. Size 1¾″ x 2⅛″. Price $150.00.

No. 5. An irregular shaped crystallized NATIVE GOLD with very little quartz present. Size 1⅛″ x 1½″. Price $100.00.

Any of the above specimens will be submitted for approval to seriously interested parties furnishing a deposit of one-half or more of the stated prices.

If you have not received our recent bulletins
FLUORESCENT MINERALS
and
BOOKS FOR THE MINERAL COLLECTOR
send for your copies today. They are free.

SCHORTMANN'S MINERALS
6 and 10 McKinley Avenue
Easthampton, Massachusetts

MINERALS FROM OUTOKUMPU, FINLAND

Chromite. Crude crystals in massive gray dolomite 2 x 3″, $1.00; 3 x 4″, $1.50; 4 x 4½″, $2.00; 5 x 6″, $3.50; 6 x 8½″, $6.00

Chrome Diopside. Bright green crystals and crystalline masses in milky quartz. 2 x 2″ to 2 x 3″, $1.50, $2.00; 4 x 4″, $3.50; 4 x 5″ to 4 x 6″, $4.50, $5.00; 4 x 10″, $7.50

Chrome Tremolite. Bright green crystalline masses. 2 x 3″, $1.50; 3½ x 5″, $3.00, $4.00; 4 x 6″, $5.00; 7 x 9″, $12.50; Xline in pyrrhotite, 4 x 6″, $5.00

Siliceous Calcite (South Dakota)

Spectacular groups of calcite crystals enclosing sand. 2 x 3″ to 3 x 4″, $2.00, $2.50; 3 x 4″ to 4 x 5″, $3.00, $3.50, $4.50, $5.00; 4 x 5″ to 5 x 7″, $5.00, $6.00; 6 x 7″ to 6 x 11″, $10.00; 4 x 7″ to 6 x 8″, $7.50

Supplies for Blowpipe Analysis

The Ward Blowpipe Kit SP 43. A moderately priced kit, newly designed to meet the needs of the mineralogical laboratory or the field prospector $14.95

The Smith Blowpipe Kit SP 41. A standard set of materials to be used with O. C. Smith's "Identification and Qualitative Chemical Analysis of Minerals," ($7.50) or any other good text on mineral analysis $40.00

The Smith Blowpipe and Chemical Kit. A more elaborate assemblage than the preceding $60.00

Complete descriptions of the above available on request.

Prices are list at Rochester, N.Y.

Recent Price Lists

Geological Collections. A description of collections especially designed for students and collectors. Price list No. 352.

Supplies and Equipment for the Geologist. A listing of popular and essential equipment for the field and laboratory.

CM 4a. Fluorescence Supplies.

U-7 Uranium and Thorium Minerals.

S-9 Selected Materials for Cutting and Polishing.

FM-5 Fine mineral specimens.

Meteorite Price List.

WARD'S NATURAL SCIENCE ESTABLISHMENT, INC.
3000 RIDGE ROAD EAST · ROCHESTER 9, N.Y.